



Λίμνη Καδούλα, Μεσσηνία



ΕΛΛΗΝΙΚΗ  
ΕΠΙΣΤΗΜΟΝΙΚΗ  
ΕΤΑΙΡΕΙΑ  
ΕΔΑΦΟΜΗΧΑΝΙΚΗΣ  
& ΓΕΩΤΕΧΝΙΚΗΣ  
ΜΗΧΑΝΙΚΗΣ

# Τα Νέα

62

## της Ε Ε Ε Ε Γ Μ

### ΣΥΜΜΕΤΟΧΕΣ ΕΛΛΗΝΩΝ ΓΕΩΜΗΧΑΝΙΚΩΝ ΣΕ ΠΡΟΣΦΑΤΑ ΣΥΝΕΔΡΙΑ ΓΕΩΤΕΧΝΙΚΟΥ ΕΝΔΙΑΦΕΡΟΝΤΟΣ

Το τελευταίο τρίμηνο του παρελθόντος έτους διεξήχθησαν διεθνή και ελληνικά συνέδρια ενδιαφέροντος γεωμηχανικού.

Το διάστημα 2 - 5 Σεπτεμβρίου 2013 διεξήχθη στο Παρίσι το 18<sup>th</sup> International Conference on Soil Mechanics and Geotechnical Engineering "Challenges and Innovations in Geotechnics" με εξαιρετικά μεγάλη επιτυχία. Η ΕΕΕΕΓΜ συμμετείχε με 9 ανακοινώσεις μελών της, οι οποίες παρουσιάζονται σε αυτό το τεύχος. Επίσης το μέλος μας Γιώργος Γκαζέτας παρουσίασε την Ishihara Lecture κατά την εναρκτήρια συνεδρία, ενώ το μέλος μας Κυριαζής Πιπιλάκης προήδρευσε της συνεδρίας που διοργανώθηκε από την TC 203 - 1 «Experimental characterization and analysis of soil behaviour under earthquake loads», καθώς και της εργομηγύρεως «Workshop TC 203 Geotechnical Issues in the Recent World Earthquakes: Lessons and Mitigation Measures» (μαζί με τον Α. Ansal).

Το διάστημα 23 - 26 Σεπτεμβρίου 2013 διεξήχθη στο Wroclaw, Πολωνίας το EUROCK 2013 International Rock Mechanics Congress. Στο συνέδριο παρουσιάστηκαν 4 άρθρα μελών της ΕΕΕΕΓΜ, τα οποία παρουσιάζονται σε αυτό το τεύχος, ενώ το μέλος μας Αλέξανδρος Σοφιανός προήδρευσε της συνεδρίας S7 «Constitutive modeling & Computer simulation». Η σχετική έκθεση παρουσιάζεται επίσης στο τεύχος αυτό.

Το διήμερο 7 και 8 Νοεμβρίου 2013 διεξήχθη στην Αθήνα το 2<sup>ο</sup> Πανελλήνιο Συνέδριο Φραγμάτων και Ταμιευτήρων. Στο συνέδριο παρουσιάστηκαν 53 άρθρα, ένας μεγάλος αριθμός των

Αρ. 62 – ΜΑΡΤΙΟΣ 2014



## Π Ε Ρ Ι Ε Χ Ο Μ Ε Ν Α

Συμμετοχές Ελλήνων γεωμηχανικών σε πρόσφατα συνέδρια γεωτεχνικού ενδιαφέροντος	1	
18 <sup>th</sup> International Conference on Soil Mechanics and Geotechnical Engineering Challenges and Innovations in Geotechnics”	3	
- The December 29 <sup>th</sup> 2010 Xerolakka Municipal Solid Waste landfill failure	4	
- Effects on adjacent buildings from diaphragm wall installation	8	
- Reliability analysis of empirical predictive models for earthquake-induced sliding displacements of slopes	12	
- Stability and movements of open-pit lignite mines in Northern Greece	17	
- Interaction of stone column and surrounding soil during its construction: 3D numerical analysis	21	(συνέχεια από την πρώτη σελίδα)
- Residual shear strength behavior of swelling soils	25	οποίων αφωρούσε σε θέματα γεωμηχανικής.
- Effect of Grout Bleed Capacity on the Engineering Properties of Cement Grouted Sands	29	Το διάστημα 11 – 15 Νοεμβρίου 2013 διεξήχθη το 6 <sup>ο</sup> Πανελλήνιο Συνέδριο Λιμενικών έργων, με ορισμένο αριθμό άρθρων γεωτεχνικού ενδιαφέροντος.
- Effectiveness of In-soil Seismic Isolation taking into account of Soil-Structure Interaction	33	Τέλος, στις 16 Σεπτεμβρίου 2013 ο καθηγητής του Georgia Institute of Technology Carlos Santamarina παρουσίασε διάλεξη με τίτλο «ENERGY GEOTECHNOLOGY: The Role of Geotechnical Engineers in the Energy Challenge» και στις 24 Οκτωβρίου 2013 η Chief Civil Engineer της Tensar International Χάϊδω Δουλαλά – Rigby παρουσίασε διάλεξη με τίτλο «Μελέτη και κατασκευή οπλισμένων επιχώσεων αντιστήριξης».
- Bridge foundation on very soft alluvia with stone column ground improvement	37	
The 2013 ISRM International Symposium EUROCK 2013	41	
- Rock engineering design and the evolution of Eurocode 7	42	
- Rockfall: Scaling factors for the Coefficient of Restitution	47	
- Influence of rock mass creep on tunnel loading	52	
- Tunnel behavior and support in molassic rocks. Experience from 12 tunnels in Greece	57	
- Elastic response of laterally loaded rock sockets using 3D finite element analyses	63	
2 <sup>ο</sup> Πανελλήνιο Συνέδριο Φραγμάτων & Ταμειυτήρων : Σχεδιασμός · Διαχείριση · Περιβάλλον	69	
6 <sup>ο</sup> Πανελλήνιο Συνέδριο Λιμενικών Έργων	72	
Διάλεξη Carlos Santamarina “ ENERGY GEOTECHNOLOGY - The Role of Geotechnical Engineers in the Energy Challenge ”	74	
Διάλεξης Χάϊδως Δούλαλα – Rigby “Μελέτη και κατασκευή οπλισμένων επιχώσεων αντιστήριξης”	74	



## 18<sup>th</sup> International Conference on Soil Mechanics and Geotechnical Engineering “Challenges and Innovations in Geotechnics”

The 18th International Conference on Soil Mechanics and Geotechnical Engineering (18 ICSMGE), which took place from 2 to 6 September 2013 at the Palais des Congrès de Paris (France) and was organized by the French Society for Soil Mechanics and Geotechnical Engineering (CFMS), was a very successful event. It was preceded by the 5th International Young Geotechnical Engineers' Conference (iYGEC 2013) held on the 31st of August and 1st of September at the Ecole des Ponts at Marne-la-Vallée (which brought together 164 participants from 57 countries – see report by Yu-Jun Cui, Chair of the iYGEC OC in the ISSMGE Bulletin, Volume 7, Issue 6, December 2013).

On Sunday 1st of September, the 80 Member Societies attending or being represented elected the new President of the International Society for Soil Mechanics and Geotechnical Engineering (ISSMGE) for four years: Professor Roger Frank (Ecole des Ponts, France) was elected, and he thus succeeds Professor Jean-Louis Briaud (Texas A&M University, Texas, USA). Of course, the CFMS, which had nominated him, congratulates him and will support him in his work throughout the four years. At the same meeting, the host city of the next International Conference in 2017 was decided: it is Seoul (South Korea).

The participation in the 18th ICSMGE was a success: there were 2081 participants in total, 179 accompanying persons and 87 exhibitors, including four partners, one Platinum sponsor and 15 Gold sponsors. In particular, 1875 participants were registered for the scientific sessions. A big thank to all of them, as they made the Conference possible. The 12 plenary sessions on Monday and Tuesday brought together up to 1650 participants. The important implication of the Technical Committees (TCs) of the ISSMGE created a strong mobilisation in the 55 parallel sessions held on Wednesday and Thursday consisting of 28 discussion sessions, 19 workshops and 8 special sessions (there were on average 800 participants during each of the seven time slots).

The four volumes of the Proceedings of the 18th ICSMGE (3486 pages, plus the table of contents and the index of authors) contain the Terzaghi Oration, the Honour Lectures, and the Special Lectures, followed by the written contributions presented according to the relevant TC and introduced by the TC General Reports. More than half of the 772 written contributions were presented orally during the discussion sessions (173) or during the poster sessions (230). The proceedings will soon be available online, free of charge, through the website of the CFMS ([www.geotechnique.org](http://www.geotechnique.org)) and the website of the ISSMGE ([www.issmge.org](http://www.issmge.org)). Many pictures taken during the sessions and breaks are already available on the Conference website ([www.issmge2013.org](http://www.issmge2013.org)).

The 7 technical visits on Friday brought together about 133 participants. The Francophone event, which took place at the Conservatoire National des Arts et Métiers (CNAM) on Friday afternoon, gathered 64 participants on "Francophone Geotechnics: education and sharing of knowledge".

From the financial point of view, the high participation in Paris 2013 should allow benefits which the CFMS will spend to

promote geotechnical engineering and geotechnical engineers in countries which need financial support.

The Geotechnical Exhibition "Underneath ground", organised inside the museum of CNAM and which opened 2 months before the Conference, will go on for some 5 years more. It is a great success with many young visitors: it aims at attracting young talents towards the ground engineering professions in our country (and in other countries too!). A virtual visit of the Geotechnical Exhibition will be uploaded soon.

Philippe Mestat, IFSTTAR, President of the CFMS, Chairman of the 18th ICSMGE

Jacques ROBERT, ARCADIS, Vice President of CFMS



Opening session of Paris 2013 Conference in the great amphitheatre of the Palais des Congrès de Paris



Poster presentation in the corridors leading to the parallel sessions



Gala dinner at the Pavillon Dauphine

Τα άρθρα των μελών της ΕΕΕΕΓΜ παρουσιάζονται στις επόμενες σελίδες (με αλφαβητική σειρά του πρώτου συγγραφέα).

# The December 29<sup>th</sup> 2010 Xerolakka Municipal Solid Waste landfill failure

## La 29<sup>th</sup> Décembre 2010 l'échec d'enfouissement Xerolakka

George Athanasopoulos  
Prof., Dept. of Civil Engineering, University of Patras, Greece,  
gaa@upatras.gr

Dimitrios Zekkos  
Asst. Prof., Dept. of Civil and Environmental Engineering,  
University of Michigan, Ann Arbor, USA

Vasileios Vlachakis  
Doctoral student, Dept. of Civil Engineering, University of  
Patras, Greece

George Spiliotopoulos  
Head of Technical Division, Patras Municipality, Greece

**ABSTRACT:** On December 29th 2010, a 30 m high slope failed at the Xerolakka Municipal Solid Waste landfill in Greece. The failure resulted in temporary interruption of the landfill disposal activities and closure of the landfill access road; it also received significant media attention. A reconnaissance of the landfill slope instability was performed a few hours after the failure. Subsequent data collection, field investigations and numerical analyses were performed to better characterize the causes of the instability. Data collection included review of available data regarding the landfill design and the waste material at the Xerolakka landfill. Field investigations included Lidar surveying to closely map the post-failure geometry, as well as shear wave velocity measurements that were used as a basis for characterization of the MSW material and comparison with data available in the literature. Numerical analyses included limit equilibrium as well as finite element analyses. The results of the investigation indicate that the failure was caused by a combination of factors, including, inappropriate waste disposal practices, inadequate compaction, leachate and gas pressure generation and increased steepening of the landfill slopes.

**RÉSUMÉ:** Le 29 Décembre 2010, une pente de 30 m de haut a échoué à la mise en décharge des déchets Xerolakka solides municipaux en Grèce. L'échec a entraîné une interruption temporaire des activités de mise en décharge et la fermeture de la route d'accès à la zone d'enfouissement et d'élimination ont reçu une attention médiatique importante. Une reconnaissance de l'instabilité de la pente d'enfouissement a été réalisée quelques heures après l'échec. Après la collecte des données, enquêtes sur le terrain et des analyses numériques ont été réalisées afin de mieux caractériser les causes de l'instabilité. La collecte des données comprenait un examen des données disponibles concernant la conception de la décharge et les déchets à la décharge Xerolakka. Les enquêtes de terrain incluent Lidar arpentage de près cartographier la géométrie post-rupture, ainsi que les mesures de vitesse de cisaillement d'ondes qui ont été utilisées comme base pour la caractérisation de la matière MSW et comparaison avec les données disponibles dans la littérature. Des analyses numériques incluent équilibre limite ainsi que des analyses par éléments finis. Les résultats de l'enquête indiquent que la panne a été causée par une combinaison de facteurs, y compris, les mauvaises pratiques d'élimination des déchets, le compactage insuffisant, le lixiviat et la génération de la pression du gaz et l'augmentation accentuation des pistes d'enfouissement.

**KEYWORDS:** Municipal solid waste, landfill, slope failure, shear wave velocity

### 1 INTRODUCTION

To protect public health and the environment, Municipal Solid Waste (MSW) landfill slopes need to be stable. Unfortunately, numerous landfill slope failures have been documented in the literature (e.g. Eid et al. 2000, Hendron et al. 1999, Kavazanjian and Merry 2005, Huvaj-Sarihan and Stark 2008) and

many more remain undocumented. Although such failures are undesirable, it is important to learn from them so that similar occurrences are avoided in the future.

This paper presents the field observations from a reconnaissance study performed within hours after the December 29th 2010 Xerolakka landfill slope failure, as well as subsequent field measurements and stability analyses that were executed to better understand the causes of the failure.

### 2 THE XEROLAKKA LANDFILL

The Xerolakka landfill is one of the nine MSW landfills in the Region of Western Greece, located 5 km east of the City of Patras. It is a canyon landfill at the foothills of the Panachaikon Mountain. It started receiving waste in September 1993 and presently receives 300 tn of waste daily (Sufalnet, 2006).

The site is located on a geologic sequence of Pleistocene and Pliocene claystone, marls and siltstones with lenses of sandstones that are generally considered intact. The groundwater table fluctuates seasonally significantly.

A topographic map of the landfill is shown in Fig. 1. The first cell of the landfill was geomembrane-lined. Subsequently the use of geosynthetics was discontinued because of the presence of impermeable geologic formations (Seisakis and Rousos, 1994). Due to strong public opposition, new cells were not constructed, as anticipated in design. In the absence of an alternative waste management solution, the landfill continued to receive waste. Thus, a waste mound with increasing height and slope inclination was formed (shown in the south-east side of Fig. 1) which partially failed on December 29th 2010.

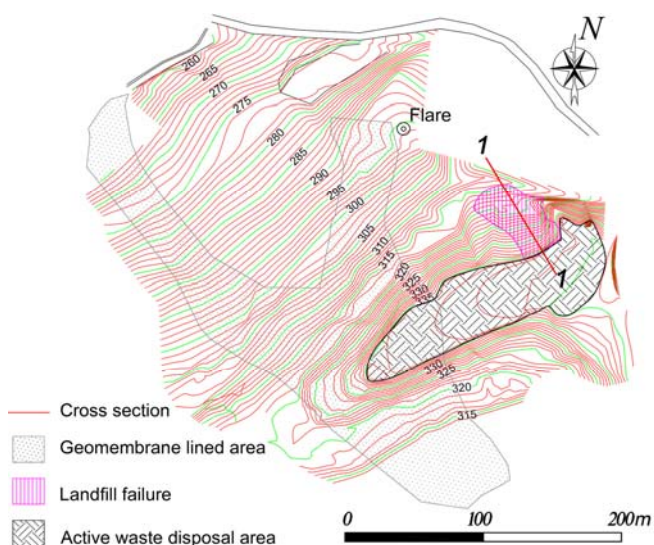


Figure 1. February 2011 topographic map of the Xerolakka canyon landfill.

### 3 FIELD OBSERVATIONS

On December 29<sup>th</sup> 2010, early in the morning (around 08:00 am), a failure of one of the landfill slopes occurred in the active waste disposal area. The authors performed on-site reconnaissance at 14:00. The waste slide had plan dimensions of 50 m by 30 m and its crest was located at the top of the landfill (absolute elevation of +340 m) whereas its toe reached the access bench 27 m below. The volume of the slided waste mass is estimated to be equal to 12,000 m<sup>3</sup>. The waste slide debris covered one of the landfill benches that was used as access road to the active waste disposal area, thus disrupting landfill disposal operations. During the reconnaissance visit, the waste that covered the access road was

already partially removed and pushed downhill. A view of the slide from the West is shown in Fig. 2 and a view of the slide from its toe after removal of the waste from the landfill access bench is shown in Fig. 3.



Figure 2. Waste slide view from the western side of the MSW landfill.



Figure 3. Waste slide view from the access bench located at the toe of the slide.

The waste slide is located adjacent to the graded canyon slopes with the Northeast portion of the slide exposing the native rock mass (also shown on the left side of Fig. 3). Precipitation on the steep canyon slopes in the vicinity of the waste slide drains towards the waste mass due to the absence of surface water cutoff drainage ditches and percolates in the waste.

The uppermost layer of MSW in the active waste disposal area (i.e., the landfill crest) was not compacted and did not include any daily soil cover. The compaction of waste had reportedly ceased for at least a year prior to the failure and daily soil cover was not used for many months, possibly years. The absence of daily soil cover on the top waste layers can be seen at the right side of Fig. 2. In addition, the gas collection system was not operational.

The crest of the landfill was not graded properly to manage surface water runoff due to precipitation and in the vicinity of the failure slide mass, rainfall water was found to be ponding. Leachate was observed to pour from the toe of the waste slide whereas an interceptor trench that was built next to the landfill bench was also found to contain leachate. Media photos from earlier in the morning of the 29<sup>th</sup> of December indi-

cate a large wet area in the vicinity of the failure, apparently from liquids that came out of the waste mass.

The December 29<sup>th</sup> 2010 failure occurred four days after a rainfall event. A weather station located in the Port of Patras at a distance of 4.5 km away from the landfill and at an absolute elevation of +6 m, recorded approximately 11 mm of precipitation for that event and a total of 16.5 mm in the five days prior to the failure. Ten days earlier, another event with a precipitation of 20 mm occurred. This amount of precipitation is lower than the corresponding amount of rainfall in the past two years; however, the geometry (height and inclination) of the landfill slopes had changed in the last year, adversely affecting its stability. The complete absence of surface water management system and daily soil cover, would have allowed for the rainfall water to easily percolate in the waste mass.

#### 4 FIELD MEASUREMENTS

A high-resolution 3-D topographic map of the landfill area was generated by performing terrestrial LIDAR (Light Detection and Ranging) measurements, in addition to conventional geodetic survey. The measurements utilized land-based laser scanning technology and allowed a reliable definition of the failed waste mass. Field measurements of the in situ shear wave velocity ( $V_{S0}$ ) were also performed. Shear wave velocity is a critical parameter that has been used to characterize the MSW (Zekkos, 2011). In this project,  $V_{S0}$  was used to characterize the MSW and assist in the selection of values for MSW material properties. Shear wave velocity profiles were also explicitly used for the performance of seismic stability analyses that are not described herein.

The small strain shear wave velocity of waste material was evaluated as a function of depth by applying the Spectral Analysis of Surface Waves (SASW) and Refraction Microtremor (ReMi) techniques. The application of these techniques is preferred in the case of landfills due to their non-intrusive nature (Matasovic et al., 2011). The  $V_{S0}$  vs. depth profile is shown in Fig. 4.

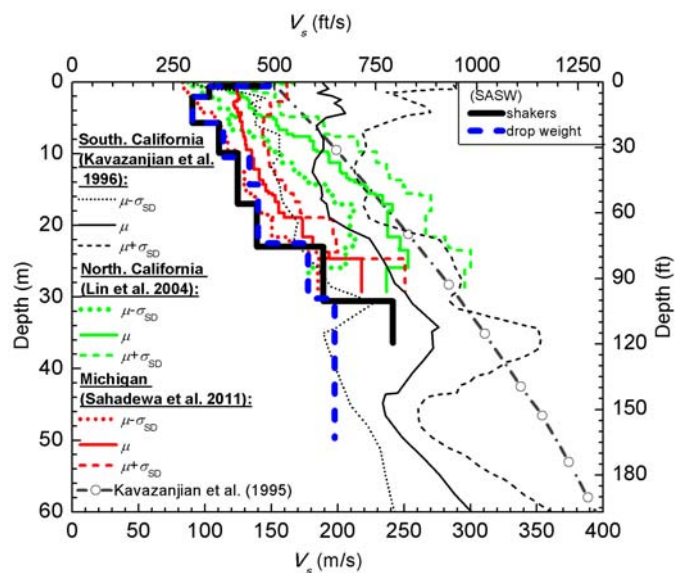


Figure 4. Comparison of  $V_{S0}$  vs depth profile at Xerolakka landfill with other published cases of landfills.

Fig. 4 compares the  $V_{S0}$  vs depth profiles measured at Xerolakka landfill with the data available in the literature. The mean and mean±sigma  $V_{S0}$  curves are shown for MSW in three geographic regions, specifically southern California (Kavazanjian et al. 1996), northern California (Lin et al. 2004) and Michigan (Sahadewa et al. 2011). It is observed that the in situ data from Xerolakka are in the lower range of the literature  $V_{S0}$  data. This difference may be attributed to a number of factors including waste composition, but more

importantly the absence of waste compaction and daily soil cover. It should be mentioned that, following the waste slide, the placement of waste (from Dec. 2011 to May 2012) was carried out in a single thick lift (~8 m), overlain by a soil cover ranging from 1 to 3 m.

## 5 PROPERTIES OF MUNICIPAL SOLID WASTE

No site specific data was available on the MSW that was disposed of at the Xerolakka landfill. Thus, for the performance of the limit equilibrium and finite element stability analyses, the measured  $V_{s0}$  was used to guide the selection of MSW properties. For the performance of the analyses the unit weight, shear strength, deformation modulus (for the finite element analyses) and Poisson's ratio of MSW are required and were selected as follows:

**Unit Weight:** The selection of the MSW unit weight has an impact on the stability of the waste mass. On the basis of the available landfill information and the Zekkos et al. (2006) recommendations, for the 30 m thick waste mass, an average unit weight value of 12 kN/m<sup>3</sup> was used. This value is also consistent with the unit weight value used for the design of the landfill facility (Koronis 1995).

**Shear Strength:** The selection of appropriate shear strength parameters is critical in evaluating the stability of the waste mass. Bray et al. (2009) recommended a generic MSW shear strength envelope. The recommended strength envelope was the mean fit to a large dataset, however, various factors such as waste composition and unit weight may result in variations from this envelope. For example, the unit weight has an important impact on the shear resistance of MSW. As reported by Zekkos et al. (2010), for waste with the same waste composition, a reduction in unit weight by 2kN/m<sup>3</sup> results in an approximate reduction in shear strength by 20%. Considering the absence of compaction and daily soil cover as well as the particularly low measured shear wave velocity of the MSW, the shear strength of the Xerolakka landfill MSW was reduced by 20% from the shear strength envelope recommended by Bray et al. (2009).

**MSW elastic modulus and Poisson's ratio:** The large-strain elastic modulus  $E_{ref}$  is an explicit input parameter in finite element analysis. The value of  $E_{ref}$  impacts the calculated displacements, but does not influence significantly the calculated factor of safety. In the present study, it was assumed that the modulus is equal to 1/10 of the small-strain elastic modulus  $E_o$ , which was calculated from the measured small strain shear modulus  $G_o$ , whereas the Poisson's ratio value was assumed to be equal to 0.1, based on data available in the literature (Zekkos, 2005).

## 6 STABILITY ANALYSES

Stability analyses of the Xerolakka landfill slope failure were performed using both limit equilibrium (Geo-Slope 2007 – SLOPE/W) and finite element (PLAXIS, 2004) analyses and the material properties described earlier. Each analysis methodology has its strengths and limitations. In finite element analyses, there is no requirement to predefine candidate failure surfaces; instead, the failure surface with the lowest factor of safety is identified using the phi-c reduction methodology (PLAXIS, 2004). Another known advantage of the FEM is its ability to calculate displacements in every prescribed stage of calculation as well as its ability to model progressive failure. In limit equilibrium methodology, the factor of safety for a large number of failure surfaces is calculated and the one with the lowest factor of safety is the critical one. For the calculation of the factor of safety, the Spencer method (Spencer, 1967) is used. Limit equilibrium methods do not account for the presence of strain softening materials, since no consideration of strains or displacements is made.

It is important to note that, in the case of Xerolakka landfill, it is very difficult to evaluate the actual pore pressure regime

within the waste mass due to the unavailability of field data. Thus, stability analyses were performed for two cases: complete absence of leachate table (provided a leachate and gas collection system was operating properly) and for the case of a high leachate table resulting from the absence/non operative leachate and gas collection system. The leachate table used in the analyses was estimated on the basis of field observations, namely: 1) the presence of ponding water at the crest of the landfill (near the waste slide) and 2) observed seepage at the toe of the waste slide. The high leachate table is intended to account in a conventional manner for the presence, and possibly flow, of leachate and more importantly the generation of gas due to biodegradation. The amount of gas generated can be significant and for that reason, modern landfill facilities are equipped with a gas collection system that collects the gas and either combusts it using a flame or uses it to generate energy. There was no gas collection system in the active waste disposal area. Gas and leachate pressures would result in a reduction of the effective stress in the waste and a subsequent reduction in the factor of safety.

## 7 RESULTS OF ANALYSES AND DISCUSSION

Analyses were performed for the selected properties and the cross-section geometry at the location of the failure. The inclination of the slopes in the upper part of the landfill is as high as 1.2:1 (horizontal to vertical). In the case of absence of leachate table and gas pressure ("dry tomb" landfills), the results of analyses indicate a stable condition with a calculated factor of safety equal to 1.60, i.e., higher than the 1.50 typically required. Additional analyses were performed with the assumed leachate table, as shown in Fig. 5.

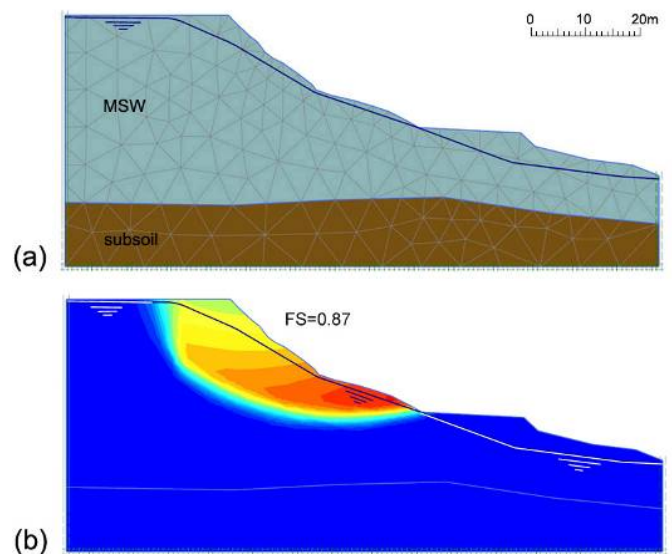


Figure 5. Finite element mesh (PLAXIS 8.6) of the critical failure surface with (a) soil stratigraphy and (b) critical failure surface for the estimated leachate table.

For these conditions, the factor of safety based on finite element analyses is calculated equal to 0.87, indicative of unstable conditions.

Analyses using the limit equilibrium method (Geo-Slope 2007 – SLOPE/W) resulted in similar critical failure surfaces for dry conditions and for the assumed leachate table (shown in Fig. 6). The factor of safety is equal to 1.60 for dry conditions and 0.96 for the assumed water table.

The results of the above and additional analyses indicate that the reduction in the factor of safety due to the presence of leachate is significant and much greater than the impact of other uncertainties, such as the unit weight of waste material.



## Effects on adjacent buildings from diaphragm wall installation

### Effets sur des bâtiments adjacents par l'installation de parois moulées

Emilios M. Comodromos & Mello C. Papadopoulou  
Dept. of Civil Engineering, University of Thessaly, Greece

Georgios K. Konstantinidis  
Manager, Attiko Metro S.A., Greece

**ABSTRACT:** A new approach for simulating the excavation and construction of subsequent panels is proposed to investigate the effects from the installation of diaphragm walls on the surrounding soil and adjacent buildings. The method has been combined with a 3-D nonlinear analysis and a constitutive law providing bulk and shear modulus variation, depending on the stress path (loading, unloading, reloading). The effects on an adjacent building have been investigated by applying a full soil-structure interaction analysis including the whole building. Contrary to lateral movements, which mostly take place at the panel under construction, it was found that the effect of settlements covers a larger area leading to a progressive settlement increase. The effect highly depends on the distance from the panel under construction. Settlement profiles and settlements at specific points as increasing with subsequent panels installation are given providing the ability of specific monitoring guidelines for the upcoming construction of the diaphragm wall in front of the building.

**RÉSUMÉ :** Une nouvelle approche pour simuler l'excavation et la construction des panneaux subséquents est proposé pour étudier les effets par l'installation de parois moulées aux bâtiments adjacents et au sol autour. La méthode a été associée à une analyse 3-D non linéaire et une loi de comportement qui permet la variation des modules de déformations en fonction des chemins des contraintes. Les effets sur un bâtiment adjacent ont été étudiés en appliquant une analyse d'interaction sol-structures pleine, qui inclut l'ensemble du bâtiment voisin. Contrairement aux mouvements latéraux, qui principalement prennent lieu à partir du panneau en cours de construction, il a été constaté que l'effet aux tassements couvre une plus grande région, conduisant à une augmentation progressive de tassements. Les effets dépendent fortement à la distance à partir du panneau en cours de construction. Les profils des tassements et tassements aux points spécifiques progressivement augmentant avec l'installation des panneaux sont donnés en face de l'immeuble où la paroi moulée est en train de construction.

**KEYWORDS:** diaphragm walls, soil-structure interaction, multi-stage analysis, buildings settlements.

#### INTRODUCTION.

It is widely accepted that the process of installing diaphragm walls can result in potentially significant soil displacements and cause substantial reductions in horizontal stress. Depending on the soil profile, the diaphragm wall configuration (length and construction sequence) and the close existence of adjacent buildings with poor foundations may render the effects of diaphragm wall installation considerable. Field monitoring confirms that ground movements resulting from diaphragm wall installation could be a significant component of the overall displacement (Burland and Hancock 1977, Tedd et al. 1984, Symons and Carder 1993), while centrifuge tests verified the development of the effect as well (Powrie and Kantartzis 1996). Recent field evidences recorded during the on going construction of subway stations in Thessaloniki demonstrated that the component of ground movements resulting from the diaphragm wall installation may be higher than 50% of the overall displacements. It is therefore evident that the simplistic assumption of a 'wished-in-place' wall (installation without any change in stress and cinematic field) commonly applied for design purposes is rather questionable.

The aim of the present paper is to investigate the effect of a diaphragm wall installation to adjacent buildings with relatively poor foundations. The sequential installation of each individual diaphragm wall panel installation was simulated by a substitution of the parameters of excavated elements with those corresponding to the bentonite slurry and later on by the concrete tremied into the panel. Valuable qualitative and quantitative conclusions regarding the variation of the effects to the adjacent building have been drawn.

#### 2 INSTALLATION PROCEDURE MODELLING

With the aim of minimising disturbance and increase stability during the excavation process, rotary drilling machines for slot excavation have been used in Thessaloniki's underground stations with poor soil conditions. Figure 1, on the left side, shows a rotary drilling machine equipped with cutting wheels and a reverse circulation system. On the right side of Figure 1 the numerical simulation of the excavation process is illustrated. The soil from the surface level down to the upper limit of the rotary wheels (line A), is replaced by a material simulating the bentonite slurry. Appropriate, very small values are attributed to the bulk and the shear modulus of the material. Within that zone the stresses are initialised to the values hydrostatically defined from the weight of bentonite slurry. This simulation process ensures that stresses within this zone remain always equal to the hydrostatic conditions no matter the deformation level. However, in the area occupied by the rotary cutters (area between line A and line B) the development of static hydrostatic pressure is not evident. For this reason, in that zone the stresses are not initialised hydrostatically and only internal gravitational stresses are considered. Within this zone the material (cuttings with bentonite slurry) has higher unit weight and is stiffer than bentonite slurry. The zone undertakes the pressure from the surrounding elements depending on the internal gravitational stresses, the stiffness and the shear resistance of the surrounding soil elements, and the arching developed around the trench. This complicated mechanism provokes a redistribution of stresses and the surrounding soil elements undergo some deformation. As a result horizontal displacements at the wall/soil interface are governed by the ability of the soil to move in response to the reduction in lateral stresses during the wall installation. The above mechanism leads to a temporary reduction of the horizontal stresses in the surrounding excavation faces, which however increase to the hydrostatic bentonite slurry pressure in the next stage of excavation. When the excavation of a panel is accomplished concrete is cast in place using tremie pipes. The same numerical process is applied to simulate the panel completion, i.e. appropriate values are attributed to the bulk and the shear modulus of the material simulating wet concrete, while, stresses are initialised to the values hydrostatically defined from the weight of wet concrete. When equilibrium is attained, regular concrete values are attributed to bulk and the shear modulus to the panel. The above simulation process is repeated over the entire depth of the panel.

The aforementioned simulation process reflects the construction of a single panel and is applied to all panels in a diaphragm wall. However, the response of each particular panel is greatly influenced by the construction sequence. Obviously when constructing a subsequent panel, with already completed adjacent panels, the effect of arching is strengthened due the high resistance of these elements. As a result a stress increase is observed not only at the adjacent soil, but also on neighbouring panels that have already been casted. Thus over the period of wall construction there will be a progressive transferring of load back and forth laterally, either from a primary panel to the adjacent soil or, as the wall progresses, from new panels to panels previously casted. It can be realised that when accurate prediction of displacements and stresses redistribution are demanded, a profound 3-D nonlinear multi-stage numerical analysis is required.

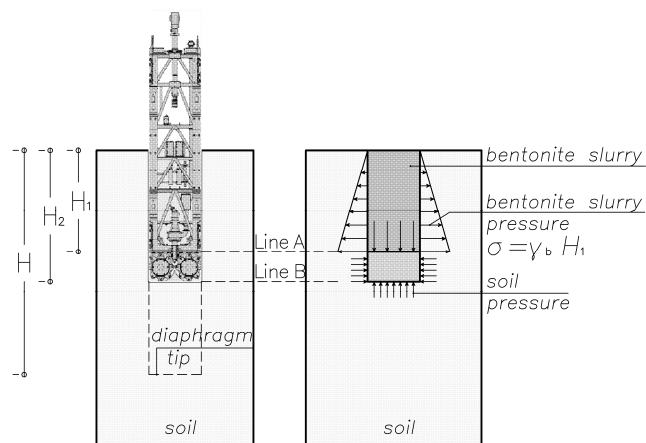


Figure 1. Schematic illustration of the proposed approach for simulating a single panel excavation

### 3 NUMERICAL SIMULATION

#### 3.1 Project description

The station of Anapisis, 210 m long and 16.4 m wide, is considered as one of the most critical of the underground of Thessaloniki. With the exception of the surficial layer the soil conditions are relatively good. However, the fact that the diaphragm wall is located very close to adjacent buildings with poor foundations, in many cases, renders the construction of the diaphragm wall extremely demanding. According to the guidelines of the German code DIN 4126, the critical zone around the trench excavation extends up to a distance of 70% of the pile length. For this reason a relatively small typical panel length  $L = 2.8$  m was applied and a rotary cutting machine was selected to perform the ongoing excavation of the panels. The thickness of the panels is  $t = 1.20$  m, its depth is  $H = 44.0$  m and the basement of the station is 28.0 m below the ground surface.

#### 3.2 Soil model and material properties

The ground conditions at the site together with the soil properties of each soil layer, derived from the carried out geotechnical investigation and the evaluation of in-situ and laboratory tests are presented in Table 1. The groundwater level was encountered at 5.0 m below the ground level. Pressure-meter tests were carried out at the area to assess the in situ horizontal stresses and, according to the evaluation of the results, a constant value of  $K_0 = 0.54$  has been adopted.

Bearing in mind the crucial effect and the necessity for settlements predictions to the adjacent buildings, a constitutive law with double yielding (FLAC 3D) has been applied in the present study. The model includes a volumetric yield cap surface in addition to Mohr-Coulomb shear and tensile failure envelopes. The cap surface is independent of the shear strength and it consists of a vertical line on a plot of shear stress vs mean stress with a trace on the mean stress axis defined as cap pressure  $p_c$ . Any violation of the cap surface produces volumetric plastic strain following a piecewise-linear law prescribed in a user-supplied table. The tangential bulk and shear moduli evolve as plastic volumetric strain takes place according to a special law de-fined in terms of a constant factor,  $R$ , which is the ratio of elastic bulk modulus,  $K_c$ , to plastic bulk modulus,  $K_t$ . The relevant values adopted are given in Table 1.

The concrete diaphragm wall behaviour was considered as an isotropic linear elastic. Linear elastic behaviour was attributed to the bentonite slurry with infinitesimal deformation values. The shear strength of bentonite slurry with unit weight of 11 kN/m<sup>3</sup> is of the order 50 Pa (DIN4126). A reasonable value for the slurry shear modulus is three hundred times the shear strength,  $G_{sl} = 15$  kPa, while the Poisson's ratio was taken

equal to 0.49. The application of these values to the analysis produced stresses within the bentonite computational domain equal to hydrostatic gravitational state, ensuring that appropriate hydrostatic pressures were developed at the trench faces. A higher value of unit weight (12.5 kN/m<sup>3</sup>) has been attributed to cutting products mixed with bentonite slurry and similarly the shear modulus has been taken equal to 25 kPa. Taking into account that the construction schedule, the time period between adjacent panels installation, particularly the primary panels, is quite enough for any excess pore dissipation an effective stress analysis was applied.

Table 1. Geotechnical properties of soil layers.

Layer	Fill	A1a	A1b	A1c	B
Depth (m)	0 – 3	3 – 10	10 – 35	35 – 40	40 – 60
Effective cohesion, $c'$ (kPa)	3	3	5	40	50
Effective angle of friction, $\phi'$ (deg)	30	25	25	25	25
Poisson's ration, $\nu$	0.3	0.3	0.3	0.3	0.3
Plastic bulk modulus, $K_t$ (kPa)	4,000	5,000	8,500	10,000	10,000
Ratio of elastic to plastic bulk modulus, $R$	5	6.5	10.5	12	12
Cap pressure, $p_c$ (kPa)	100	100	NC*	NC*	NC*

Remark: NC means that cap pressure is equal to the in-situ mean stress

#### 3.3 Simulation procedure

The effective numerical simulation of typical construction procedure for a cast in situ diaphragm wall must reflect the stages and the mechanisms developed during the excavation and throughout the completion of the wall. The first step was to establish the in-situ state of stresses. The construction of a single panel was simulated in 22 stages during which the excavation was advanced in 2.0 m. Within each stage the soil in the excavation zone was replaced by cutting-bentonite, while the area above the zone being excavated was replaced by bentonite. The end of the excavation was followed by wet concrete placing and the value of  $E_{wc} = 1,000$  MPa was attributed to Young's modulus and  $\nu_{wc} = 0.49$  to Poisson's ratio. The last stage of analysis corresponded to concrete hardening. The same process was applied to all panels under consideration.

The most critical location in the area of the station corresponds to poor building foundation conditions very close to the diaphragm wall. The analysis is therefore focused on that. Prior to the currently presented full soil-structure interaction analysis including a 6-storey building, numerical analyses of a single panel construction and of a wall and an adjacent foundation verified the proposed simulation process as well as the constitutive law and the values for the parameters. Figure 2 shows the foundation plan of the adjacent building together with the location of the diaphragm wall and a curtain of micropiles used to minimize the effect of panels' installation. Further to the bay number of each panel the figure shows the panel type (primary, P, or secondary, S) and the order of installation in the circles on the right side of each panel. The foundation consists of individual footings connected with 0.20 m × 0.50 m reinforced concrete beams. The foundation level is at 3.0 m from the ground surface. The F.D. mesh included 89,000 3-D elements, 4,272 shell elements and 225 beam elements. The dead weight of the building has been explicitly introduced by the gravity of each element while a uniform load of 5 kPa has been applied to each slab to simulate all other permanent and variable loads. After the establishment of the initial stresses, the installation of the micropiles was introduced followed by the installation of the 9 panels ac-

According to the previously described approach. The sequence of installation is presented in Figure 3.

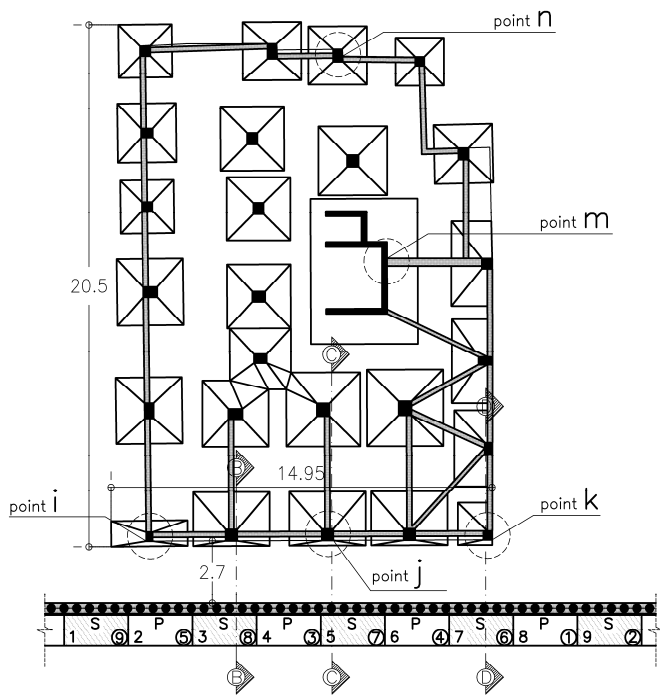


Figure 2. Individual footings of a 6-story building together with the diaphragm wall and the micropiles

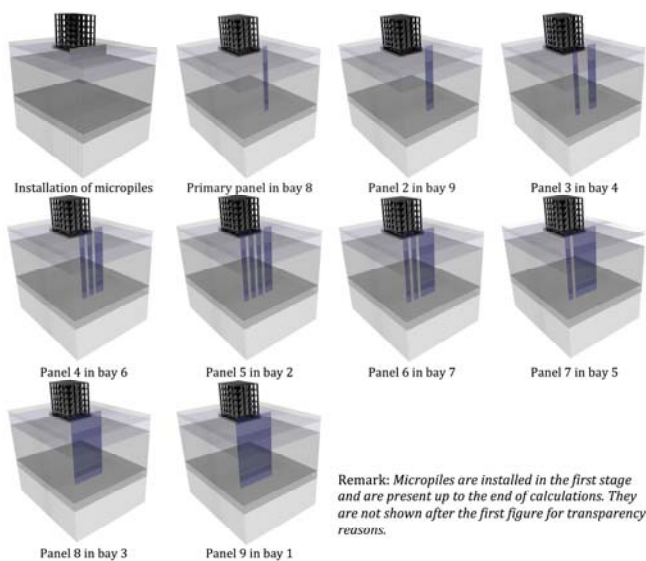


Figure 3. Sequence of panel installation

#### 4 NUMERICAL RESULTS

The contour values for soil settlements, the building floors' settlements and the axial forces of the building columns developed after the completion of the first element (element no 8) are illustrated in Figure 4. For visibility reasons the figure is given in a section at the building face and a cross section at the middle of the building. It can be seen that the maximum soil settlement is located around the excavated panel and is of the order of 2.4 mm. The maximum settlement of the building is located at its corner nearby the excavated panel and the contours show a uniform reduction with distance from that point.

The sequential construction of the next panels provokes the maximum effect in front of each panel, as it has been expected, but at the same time contributes to a progressive increase of settlements in a widespread zone. When the pri-

mary panels are installed, an increase of settlements to the value of 4.2 mm is occurred. The soil settlements progressively decrease with the distance from the diaphragm wall and are almost zero at the backside of the building. The completion of the wall with the rest 4 secondary panels does not encounter significant increase to the maximum value of the soil settlements. The final value of maximum settlement is 5.3 mm and the same value is developed at the external side of the building close to the diaphragm wall. From the comparison of the axial forces variation throughout the construction of the panel arises that the panels' installation does not practically affect them.

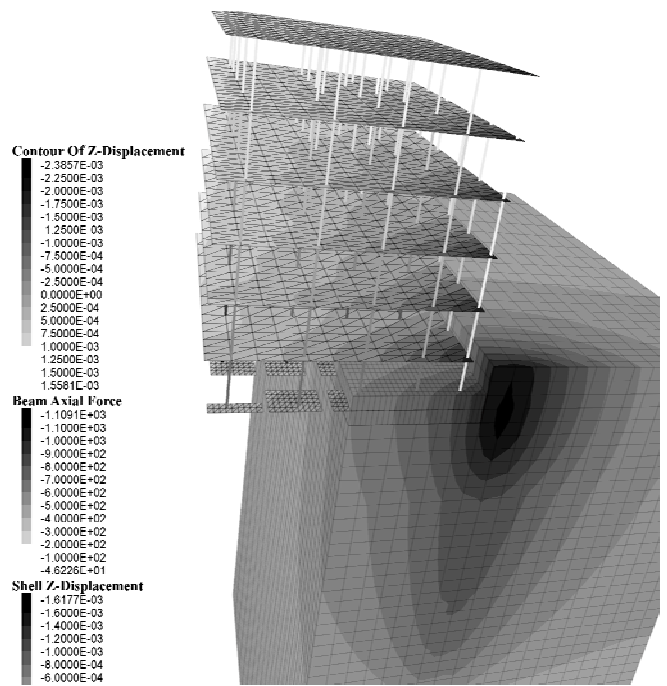


Figure 4. Soil and building settlement contours together with column axial forces after the completion of the first panel (bay no 8)

Figure 5a illustrates the variation of the horizontal displacements with depth below the external boundary of a footing at the front side of the building (cross section 'C-C'). The values are not exceeding the order of 1.0 mm and this is mainly due to the existence of the micropiles. The construction of the panels with bay no 8 and 9 (first and second in construction sequence) are relatively too far from that point and they do not provoke any horizontal displacement at the point under consideration. The panel with bay no 5 is just in front of the point and this explains the important movement of the displacement field during the construction of this panel. Similar are the results in the case of the point below the footing at the edge of the external footing at section 'D-D', Figure 5b.

The most important effect to the adjacent building is the anticipated settlements, the angular distortion that will develop to the foundation and if that last could be capable of provoking any notable bending moment to the foundation elements. Figure 6 illustrates the progressive increase of the settlements across the section 'C-C'. On the same figure the location of the diaphragm wall and the foundation of the building are shown. The construction of every panel contributes to a progressive increase of settlements, with the maximum influence experienced when the primary panel close to the cross section is installed. This explains the maximum difference observed when panel no 4 is in-stalled. The maximum settlement is developed at the end of the construction of all panels, its value is of the order of 5.5 mm and occurs at the front side of the building.

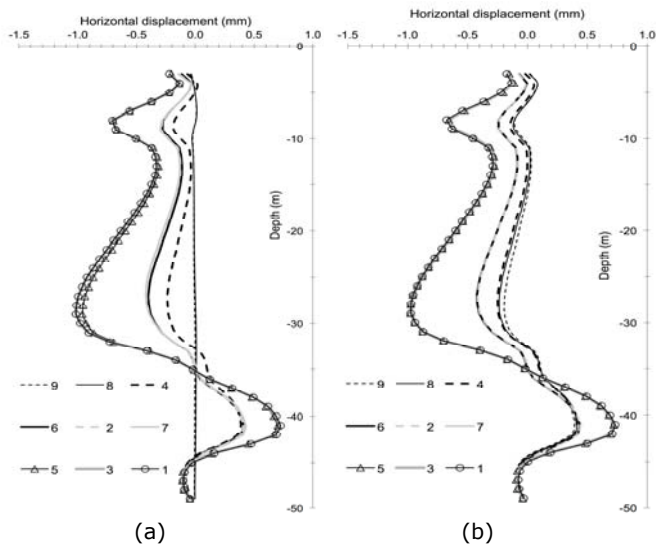


Figure 5. Profile of horizontal displacements below the external footing at (a) the mid-face, point j, and (b) the end-face of the building, point k

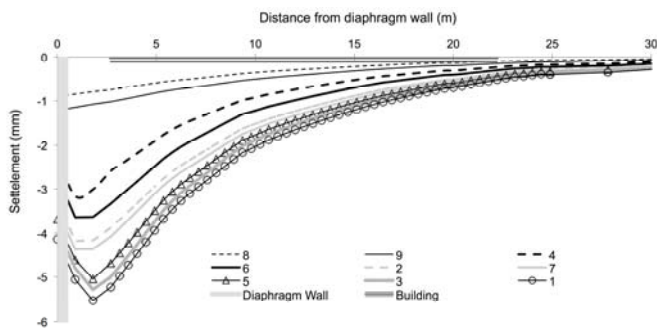


Figure 6. Development of settlement profile with panel sequence construction at cross section 'C-C'

It is worth noticing that the settlement values estimated from the 3-D analysis are leading to an angular distortion of 1:5,000. This value is considerably lower than the limits provided by CIRIA and the CFEM.

An effective design of complex retaining structures, with closely adjacent buildings, includes instrumentation and monitoring to ensure the safety of the construction and control the effect on the adjacent buildings. These data will be available when the diaphragm wall at this area will commence and histograms giving the contribution to cumulative settlements of each particular panel can be drawn. It is therefore extremely helpful to give these histograms resulting from the 3-D analysis and follow up the values as the wall is constructed. Figure 7 illustrates the numerically established cumulative settlements after the completion of each panel, at the characteristic points, i, j, k, m and n. The location of each panel corresponds to relative position from left to right, while the installation sequence is given on the top of the histograms.

It can be seen that the final settlements at the front face of the building (points i, j and k) are of the same magnitude and that the values provided for the points far from the diaphragm wall (points m and n) are drastically lower and with no practical effect on the building. It is clearly evident that Figure 7 can be efficiently used to compare settlements during the upcoming construction and provide alarm signal in case of significantly higher settlements values.

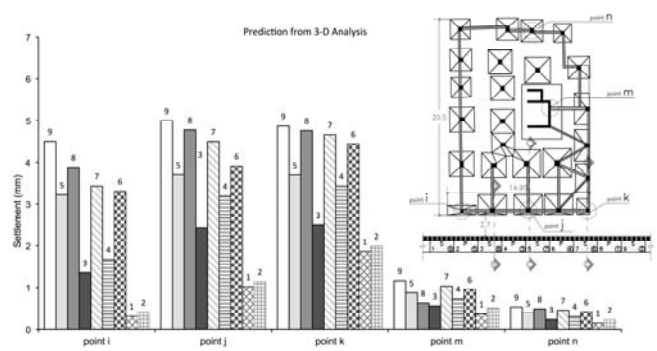


Figure 7. Predicted development of cumulative settlements at points i, j, k, m and n at the end of each panel construction

## 5 CONCLUSION

In this paper the effects from the installation of diaphragm walls have been investigated using a new approach for simulating the excavation and construction of subsequent panels. The method has been combined with a 3-D nonlinear analysis and a constitutive law providing bulk and shear modulus variation, depending on the stress path (loading, unloading, reloading). It has been observed that the most significant effect in front of a given panel occurs during the installation of that panel and that the effect on stress reduction and lateral movements in front of the subsequent panels is rather limited. The method has been used to estimate the effects on an adjacent 6-storey building by applying a full soil-structure interaction including the whole building. Progressively increased with subsequent panels installation settlement profiles are given along the building foundation. Moreover, settlements at specific points where leveling captures have been installed are given in cumulative form. The predictions indicate that the angular distortion of the building remains under the required limits of serviceability and at the same time provide the guidelines for the monitoring of the upcoming construction of the diaphragm wall in front of the building.

## 6 REFERENCES

- Burland J.B. and Hancock R.J.R. 1977. Underground car park at the House of Commons, London: geotechnical aspects. *Struct Engr* 55 (2), 87-100.
- Tedd P., Chard B.M., Charles J.A. and Symons I.F. 1984. Behaviour of a propped embedded retaining wall in stiff clay at Bell Common Tunnel. *Géotechnique* 34 (4), 513-32.
- Symons I.F. and Carder D.R. 1993. Stress changes in stiff clay caused by the installation of embedded retaining walls. *Retaining structures*. Thomas Telford, London.
- Powrie W. and Kantartzi C. 1996. Ground response during diaphragm wall installation in clay: centrifuge model tests. *Géotechnique* 46 (4), 725-39.
- DIN 4126. 1986. *Cast-in-situ concrete diaphragm walls*. Berlin.
- Itasca. 2009. *FLAC3D, Fast Lagrangian analysis of continua*, version 4.0: User's and theory manuals. Itasca Consulting Group, Inc. Minneapolis.
- CIRIA. 1983. *Settlement of structures on clay soils. Report 113*, London.
- Canadian Geotechnical Society. 1992. *Canadian foundation engineering manual*. British Publishers Ktd, Vancouver.

# Reliability analysis of empirical predictive models for earthquake-induced sliding displacements of slopes

## Analyse de fiabilité des modèles empiriques de prédiction des déplacements sismiques de pentes

S. Fotopoulou & K. Pitilakis

Department of Civil Engineering, Aristotle University, Thessaloniki, Greece

**ABSTRACT:** The goal of this study is twofold: (i) to identify the influence of the earthquake characteristics on the magnitude of the residual co-seismic slope displacements of a typical slope using different predictive analytical models and (ii) to compare the results of the analytical models with an exact fully dynamic non-linear analysis. In particular, three analytical models were used to predict the permanent slope displacements: the classical Newmark rigid block model (Newmark 1965), the decoupled Rathje and Antonakos (2011) model and the coupled Bray and Travarasou (2007) sliding block model. In addition, 2 dimensional fully non-linear numerical analyses were performed using the code FLAC (Itasca 2008) for idealized sand and clayey step-like slopes considering different real acceleration time histories as input motion. All three models predict displacements that are generally in good agreement with the numerical results for the sand slope case. On the contrary, for the clay more flexible slope the correlation is not so good. However it is shown that the some crucial parameters, like the frequency content of the input motion, are not always appropriately captured in all analytical models.

**RÉSUMÉ :** L'objectif de cette étude est (i) d'identifier l'influence des caractéristiques du tremblement de terre sur l'ampleur des déplacements co sismiques résiduels d'une pente, en utilisant différents modèles analytiques et (ii) de comparer les déplacements analytiques avec une analyse numérique plus élaborée. En particulier, trois modèles différents étaient utilisées pour estimer les déplacements permanentes : le modèle de base de bloc rigide de Newmark (Newmark 1965), le modèle découplé de Rathje et Antonakos (2011) et le modèle couplé de Bray et Travarasou (2007). L'analyse numérique a été effectuée sur la même pente avec le code FLAC (Itasca 2008) et pour les mêmes matériaux de sol (sable et argile). Dans le cas de pente sableuse les déplacements calculés par les trois modèles analytiques sont généralement en relativement bon accord avec les résultats numériques. La comparaison est moins bonne pour la pente argileuse. Néanmoins il a été démontré que tous les modèles analytiques ne tient pas en compte proprement quelques paramètres importants come la fréquence du mouvement fort des sol.

**KEYWORDS:** co-seismic slope displacements, Newmark-type displacement models, non-linear dynamic numerical analysis.

## 1 INTRODUCTION

It is common practice in geotechnical earthquake engineering to assess the expected seismic performance of slopes and earth structures by estimating the potential for seismically induced permanent displacements using one of the available displacement-based analytical procedures. Considering that (total and/or differential) displacements ultimately govern the serviceability level of a slope after an earthquake, the use of such approaches is strongly recommended. Typically, two different approaches of increased complexity are proposed to assess permanent ground displacements in case of seismically triggered slides: Newmark-type displacement methods and advanced stress- strain dynamic methods.

The sliding-block analog proposed by Newmark (1965) still provides the conceptual basis on which all other displacement-based methods have been developed aiming to yield more accurate estimates of slope displacement. This has

been accomplished by proposing more efficient ground motion intensity measures (e.g. Saygili and Rathje, 2008), improving the modeling of dynamic resistance of the slope characterized by its yield coefficient (e.g. Bray, 2007) and by analyzing the dynamic slope response more rigorously (e.g. Bray and Travarasou, 2007; Rathje and Antonakos, 2011). In terms of their assumptions to analyze the dynamic slope response, displacement based methods can be classified into three main types: rigid block, decoupled and coupled. A short description of the different types of Newmark-type displacement methods as well as recommendations for the selection of the most appropriate ones is given in Jibson (2011).

Advanced stress-deformation analyses based on continuum (finite element, FE, finite difference, FDM) or discontinuum formulations usually incorporating complicated constitutive models, are becoming recently more and more attractive, as they can provide approximate solutions to problems which otherwise cannot be solved by conventional methods e.g. the complex geometry including topographic and basin effects, material anisotropy and non-linear behavior under seismic loading, in situ stresses, pore water pressure built-up, progressive failure of slopes due to strain localization. Several investigators have implemented continuum FE or FD codes to evaluate the residual ground displacements of slopes using elastoplastic constitutive models (e.g. Chugh and Stark, 2006; Lenti and Martino, 2012 etc.).

In this paper we study the accuracy of three different Newmark-type based models i.e. the conventional analytical Newmark (1965) rigid block approach, the Rathje and Antonakos (2011) decoupled model and Bray and Travarasou (2007) coupled model, classically used to estimate the expected co-seismic slope displacements, with a more refined numerical approach, considering different earthquake input motions scaled to different PGA values and compliance of the sliding surface. For the purpose of this comparative study we selected a typical configuration of a 30° inclined sand and clayey slope.

## 2 IMPLEMENTATION OF NEWMARK-TYPE PREDICTIVE MODELS

The Newmark conventional analytical rigid block method is used to predict cumulative slope displacements obtained by integrating twice with respect to time the parts of an earthquake acceleration-time history that exceed the critical or yield acceleration,  $a_c$  ( $k_y \cdot g$ ) (e.g. threshold acceleration required to overcome shear soil resistance and initiate sliding). The second approach is a two-parameter vector (PGA, PGV) model proposed by Rathje and Antonakos (2011) applied herein to evaluate co-seismic slope displacements. This model is recommended for use in practice due to its ability to significantly reduce the variability in the displacement prediction. For flexible sliding,  $k_{max}$  (e.g. peak value of the average acceleration time history within the sliding mass) is used in lieu of PGA and  $k\text{-vel}_{max}$  (e.g. peak value of the  $k\text{-vel}$  time history provided by numerical integration of the  $k\text{-time}$  history) is used to replace PGV. The third one is the Bray and Travarasou (2007) model. In this model cumulative displacements are calculated using the nonlinear fully coupled stick-slip deformable sliding block model proposed by Rathje and Bray (2000) to capture the dynamic response of the sliding mass. They use a single intensity parameter to characterize the equivalent seismic loading on the sliding mass, i.e. the ground motion's spectral acceleration  $S_s$  at a degraded period equal to  $1.5T_s$ , which was found to be the optimal one in terms of efficiency and sufficiency (Bray 2007).

The first goal is to study the influence of the earthquake characteristics and the dynamic response of the slope on the magnitude of the residual slope displacements using the aforementioned three predictive models. In this respect, permanent displacements as a function of the critical acceleration ratio (e.g.  $k_y/k_{max}$  or  $k_y/PGA$ ) are computed using the three approaches considering different earthquake input mo-

tions and compliance of the sliding surface. Comparisons between the models allowed evaluating their reliability. Mean displacements were calculated using the Newmark rigid block model, as reference, whereas median values  $\pm 1$  standard deviation and median and 16<sup>th</sup> - 84<sup>th</sup> percentiles were derived for the decoupled and coupled approximations respectively.

The seismic input consists of two real acceleration time histories recorded at rock outcropping conditions and scaled at two levels of PGA, i.e. 0.3 and 0.7g. Table 1 presents the parameters describing some basic characteristics of the ground motions and the flexibility of the potential sliding surface. The displacements were computed for nearly rigid ( $T_s=0.032\text{sec}$ ) and relatively flexible ( $T_s=0.16\text{sec}$ ) sliding masses. The derived (mean or median) permanent displacements for the three different predictive models and for the different considered earthquake scenarios plotted as a function of the critical acceleration ratio,  $k_y/k_{max}$  or  $k_y/PGA$ , are illustrated in Figures 1a, 1b and 1c when considering the nearly rigid sliding surface. Moreover in Figures 3a and 3b we compared between them the three analytical models for the Pacoima 0.7g input motion for the nearly rigid and the relatively flexible sliding mass respectively.

Table 1. Parameters describing the characteristics of the ground motions and the dynamic response of the sliding mass

Earthquake record name	<i>Valnerina</i> 1979- <i>Cascia_L</i>		<i>Northridge</i> 1994- <i>Pacoima</i> <i>Dam_L</i>	
	<i>Cascia</i>		<i>Pacoima</i>	
Earthquake code	<i>Cascia</i>		<i>Pacoima</i>	
Moment magnitude ( $M_w$ )	5.9		6.7	
PGA (g)	0.15		0.41	
Fundamental period $T_p$ (sec)	0.23		0.48	
Mean Period $T_m$ (sec)	0.295		0.507	
Scaled PGA (g)	0.3	0.7	0.3	0.7
PGV (cm/sec)	10.3	30.9	14.6	43.9
Natural period of the sliding mass $T_s$ (sec)	0.16	0.032	0.16	0.032
$S_a(1.5T_s)/PGA_{scaled}$	2.93	1.07	2.26	1.03
$T_s/T_m$	0.54	0.11	0.32	0.06

The results prove the important role of the amplitude and frequency content of the earthquake as well as the compliance of the sliding surface on the magnitude of the computed displacements. As it should be expected, time histories scaled at 0.7g produce larger displacements compared to those scaled at 0.3g for the same critical acceleration ratios. For the Newmark and Rathje and Antonakos models the lower frequency input motion (Pacoima-  $f_p=2.1\text{Hz}$ ) generally yields larger displacements in relation to the higher frequency input motion (Cascia-  $f_p=4.4\text{Hz}$ ). For the Newmark model (see Fig. 1a) this trend becomes more pronounced with the increase of the critical acceleration ratio, whereas in Rathje and Antonakos (see Fig. 1b) this trend does not seem to be influenced by the critical acceleration ratio. Contrary to the previous models it seems that the importance of the frequency content is not taken into account in the Bray and Travararou coupled model, which predicts slightly larger displacements for the higher frequency input motion (see Fig. 1c). The latter model generally predicts larger displacements compared to Newmark rigid block and Rathje and Antonakos decoupled models. In particular, the difference in the displacement predic-

tion is by far more noticeable for the flexible (Fig. 2b) compared to the nearly rigid (Fig. 2a) sliding mass. Displacements computed using Rathje and Antonakos predictive equations are closer to the Newmark rigid block model. The comparison is even better for the higher frequency input motion and for the lower level of shaking.

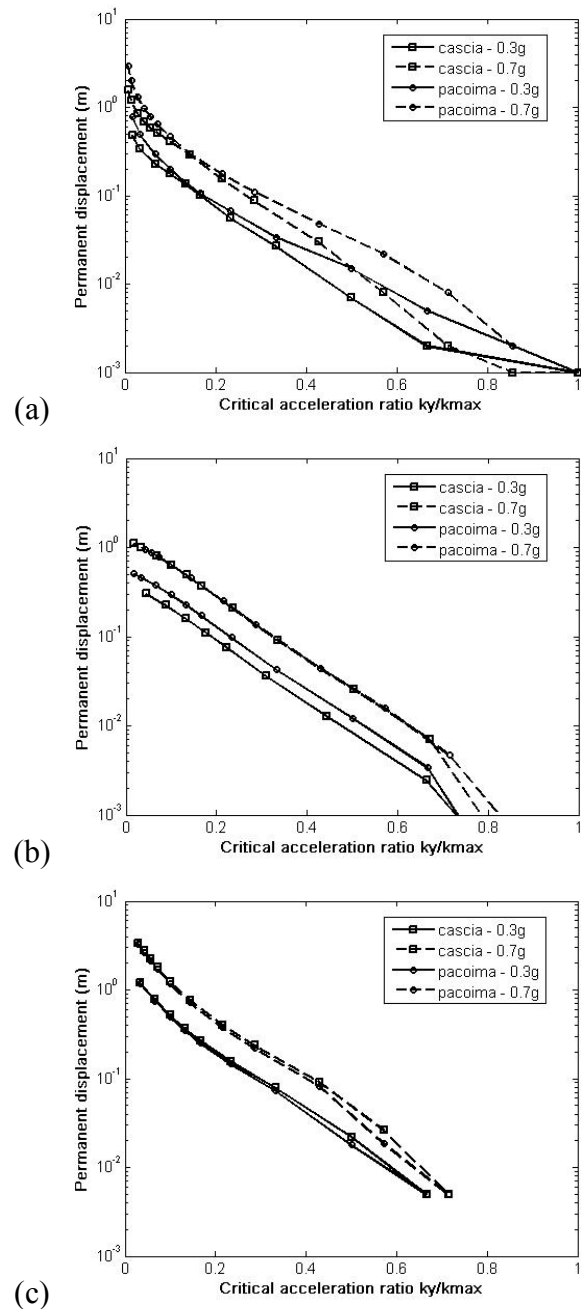
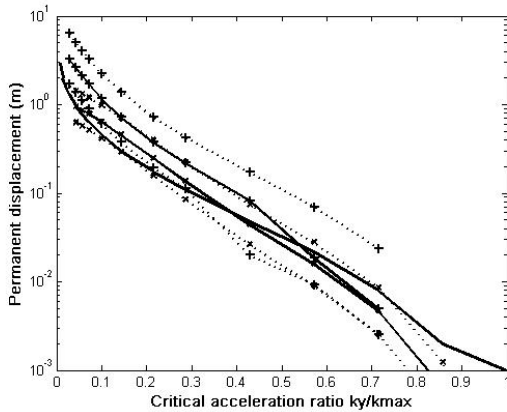


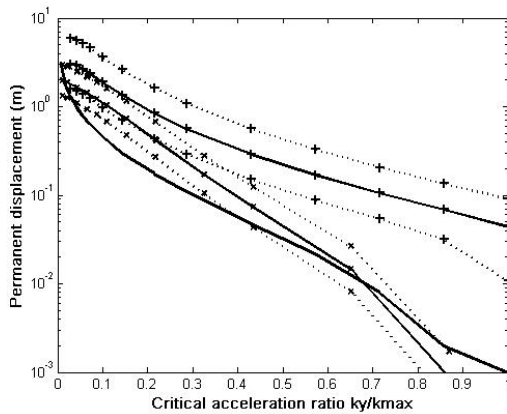
Figure 1. Newmark (a), Rathje and Antonakos (b) and Bray and Travararou (c) displacement versus  $k_y/k_{max}$  considering a nearly rigid sliding mass for different acceleration time histories (cascia, pacoima) scaled at different levels of PGA (0.3g, 0.7g)

### 3 COMPARISON WITH THE DYNAMIC NUMERICAL ANALYSIS

The second goal is to compare the Newmark-type analytical models with an a-priori more accurate numerical model. For this purpose a two-dimensional fully non-linear FLAC (Itasca, 2008) model has been used. The computed permanent horizontal displacements within the sliding mass for the two idealized step-like slopes, characterized by different flexibility of the potential sliding surface, are compared with the three Newmark-type models.



(a)



(b)

Figure 2. Comparison of the different Newmark-type models when considering a nearly rigid (a) and a relatively flexible (b) sliding mass for a certain earthquake scenario (Pacoima scaled at 0.7g)

The geometry of the finite slope is shown in Figure 3. The discretization allows for a maximum frequency of at least 10Hz to propagate through the grid without distortion. Free field absorbing boundaries are applied along the lateral boundaries whereas quiet boundaries are applied along the bottom of the dynamic model to minimize the effect of artificially reflected waves. The soil materials are modeled using an elastoplastic constitutive model with the Mohr-Coulomb failure criterion, assuming a non-associated flow rule for shear failure. Two different soil types are selected for the surface deposits to represent relatively stiff frictional and cohesive materials. The mechanical properties for the soil materials and the elastic bedrock are presented in Table 2.

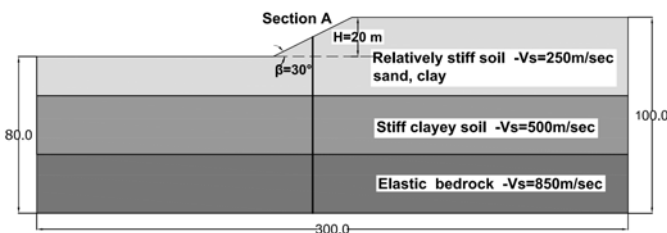


Figure 3. Slope configuration used for the numerical modeling

The initial fundamental period of the sliding mass ( $T_s$ ) is estimated using the simplified expression:  $T_s = 4H/V_s$ , where H is the depth and  $V_s$  is the shear wave velocity of the potential

sliding mass. The depth of the sliding surface is evaluated equal to 2m for the sandy slope and 10m for the clayey one by means of limit equilibrium pseudostatic analyses. The horizontal yield coefficient,  $k_y$ , is computed via pseudostatic slope stability analysis equal to 0.16 and 0.15 for the 30° inclined sand and clayey slopes respectively.

Table 2. Soil properties of the analyzed slopes

Parameter	Relatively stiff soil		Stiff soil	Elastic bedrock
	sand	clay		
Dry density (kg/m <sup>3</sup> )	1800	1800	2000	2300
Poisson's ratio	0.3	0.3	0.3	0.3
Cohesion c (KPa)	0	10	50	-
Friction angle $\phi$ (degrees)	36	25.0	27	-
Shear wave Velocity $V_s$ (m/sec)	250	250	500	850

The seismic input applied along the base of the dynamic model consists of a set of 7 real acceleration time histories recorded on rock outcrop (see Table 3) and scaled at PGA=0.7g. To derive the appropriate inputs for the Newmark-type methods that include the effect of soil conditions, and to allow a direct comparison with the numerical results, we computed the time histories at the depth of the sliding surfaces through a 1D non-linear site response analysis considering the same soil properties as in the 2D dynamic analysis. It is noticed that the 1D soil profile is located at the section that approximately corresponds to the maximum slide mass thickness of the slope (Section A in Figure 4). The bottom of the sliding surface is taken be consistent to the estimated fundamental period of the sliding mass ( $T_s$ ) that is different for the clay and sand slopes.

Table 3. Selected outcropping records used for the dynamic analyses

Earthquake	Record station	Mw	R(km)	PGA(g)
Valnerina, Italy 1979	<i>Cascia</i>	5.9	5.0	0.15
Parnitha, Athens 1999	<i>Kypseli</i>	6.0	10.0	0.12
Montenegro 1979	<i>Hercegnovi Novi</i>	6.9	60.0	0.26
Northridge, California 1994	<i>Pacoima Dam</i>	6.7	19.3	0.41
Campano Lucano, Italy 1980	<i>Sturno</i>	7.2	32.0	0.32
Duzce, Turkey 1999	<i>Mudurno_000</i>	7.2	33.8	0.12
Loma Prieta, California 1989	<i>Gilroy1</i>	6.9	28.6	0.44

Table 4 presents the computed numerical horizontal displacements together with those calculated using the different Newmark-type displacement methods. The average difference (%) of the Newmark-type models in the median (or mean) displacement estimation compared to the numerical displacement is shown in Figure 4a for both sand and clay

slopes. The dispersion of the corresponding differences is presented in Figure 4b.

Table 4. Comparison between numerical, Newmark (1965), Rathje and Antonakos (2011) and Bray and Travararou (2007) displacements for sand and clayey slope materials and for outcropping accelerograms scaled at 0.7g

Slope soil material	Earthquake code	Computed horizontal displacement (m)	Average Newmark (m)	Rathje and Antonakos Median (m)	Bray and Travararou Median (m)
sand	<i>cascia</i>	0.6	0.64	0.40	0.60
	<i>kypseli</i>	0.50	0.55	0.50	0.65
	<i>montenegro</i>	0.90	0.70	0.37	0.42
	<i>pacoima</i>	0.70	0.53	0.49	0.57
	<i>sturno</i>	1.70	1.38	0.83	0.81
	<i>duzce</i>	1.10	0.94	0.36	0.57
	<i>gilroy</i>	0.20	0.23	0.28	0.57
clayey	<i>cascia</i>	0.50	0.36	0.16	0.57
	<i>kypseli</i>	0.45	0.28	0.14	0.53
	<i>montenegro</i>	0.82	0.47	0.16	0.72
	<i>pacoima</i>	0.62	0.35	0.19	0.79
	<i>sturno</i>	1.40	0.90	0.25	0.71
	<i>duzce</i>	0.85	0.48	0.16	1.16
	<i>gilroy</i>	0.20	0.09	0.09	0.55

#### 4 DISCUSSION- CONCLUSIONS

In general the Newmark-type analytical models predict comparable displacements, at least in the order of magnitude, with the exact numerical analysis. The comparison is generally better for the sand slope case, while for the clayey more flexible slope the divergences are amplified. In particular Bray and Travararou model tend to predict generally larger displacements with respect to the numerical analysis, whereas Newmark and Rathje and Antonakos models underpredict the corresponding displacements.

Among the three methods, Bray and Travararou model was found to present the minimum average predictive error (%) in relation to the numerical analysis for both sand and clay slope cases. This is in line with the inherent coupled stick-slip assumption adopted in the method that offers a conceptual improvement over the rigid block and decoupled approaches for modeling the physical mechanism of earthquake-induced landslide deformation. However, Bray and Travararou model presents a very large dispersion in the median displacement estimation (up to 70% for both sandy and clayey slopes). Thus, the use of  $S_a(1.5 T_s)$  seems rather insufficient to fully describe the characteristics of the seismic loading (i.e. amplitude, frequency content and duration) for site-specific applications.

Newmark analytical approach shows the minimum dispersion in the displacement prediction (less than 10-20%) with respect to the numerical analysis results compared to the Bray and Travararou and Rathje and Antonakos models. This may be justified by the fact that Newmark analytical method uses the entire time history to characterize the seismic loading as

opposed to the Bray and Travararou and Rathje and Antonakos models that use one [ $S_a(1.5 T_s)$ ] and two (PGA, PGV) intensity parameters respectively. As such, uncertainties associated to the selection of the ground motion intensity parameters are lower in the Newmark analytical approach.

Overall, the differences in the displacement prediction between the three models are larger for the clayey slope. Thus, the compliance of the sliding surface in relation with the way that the frequency content of the input motion is taken or not into account may produce some important errors to the estimated earthquake-induced sliding displacements of slopes. It is suggested that a better framework is deemed necessary to account for the various uncertainties in the seismic displacements prediction.

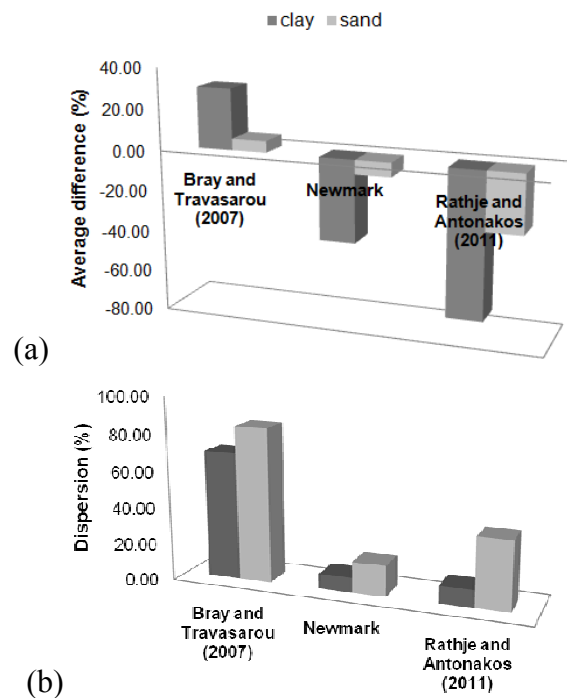


Figure 4. (a) Average difference (%) and (b) dispersion of the predictive models in the median displacement estimation compared to the corresponding numerical displacement considering nearly rigid (sand slope) and flexible (clayey slope) sliding masses

#### 5 REFERENCES

Bray J.D. 2007. Simplified seismic slope displacement procedures. Earthquake Geotechnical Engineering. K. D. Pitilakis Editor, 2007 Springer.

Bray J.D. and Travararou T. 2007. Simplified procedure for estimating earthquake-induced deviatoric slope displacements. Journal of Geotechnical and Geoenvironmental Engineering 133(4), 381-392.

Chugh A.K., Stark T.D. 2006. Permanent seismic deformation analysis of a landslide. Landslides 3(1), 2-12.

Itasca Consulting Group 2008. Inc. FLAC (Fast Lagrangian Analysis of Continua), ver. 6.0. Itasca Consulting Group, Inc., Minneapolis.

Jibson R.W. 2011. Methods for assessing the stability of slopes during earthquakes-A retrospective. Engineering Geology 122(1-2), 43-50.

Lenti L. and Martino S. 2012. The interaction of seismic waves with step-like slopes and its influence on landslide movements. Engineering Geology 126, 19-36.

Newmark N.M. 1965. Effects of earthquakes on dams and embankments. *Geotechnique* 15 (2), 139–159.

Rathje E.M. and Bray J.D. 2000. Nonlinear coupled seismic sliding analysis of earth structures. *Journal of Geotechnical and Geoenvironmental Engineering* 126(11), 1002–1014.

Rathje E.M. and Antonakos G. 2011. A unified model for predicting earthquake-induced sliding displacements of rigid and flexible slopes. *Engineering Geology* 122(1-2), 51-60.

Saygili G. and Rathje E.M. 2008. Empirical Predictive Models for Earthquake-Induced Sliding Displacements of Slopes. *Journal of Geotechnical and Geoenvironmental Engineering* 134(6), 790.

# Stability and movements of open-pit lignite mines in Northern Greece

## La stabilité et les mouvements des mines de lignite à pente ouverts en Grèce du Nord

M. Kavvadas

National Technical University of Athens, Greece

Z. Agioutantis

Technical University of Crete, Greece

P. Schilizzi

Public Power Cooperation, Greece

C. Steiakakis

General Consulting Ltd "ISTRIA", Greece



Figure 1. Southeast slopes of Mavropigi lignite mine.

**ABSTRACT:** This paper presents a case of a lignite mine in Northern Greece with excavated slopes exceeding 100-120 m in depth in which substantial movement is occurring, with an average rate 10-20mm/day. The Mavropigi mine is very important for the power supply of Greece and uninterrupted operation is often critical, meaning that excavation is taking place on moving soil masses. The stability of the moving southeast slope is investigated and the information developed from an extensive monitoring campaign, with survey prisms, inclinometers and piezometers is presented. The use of the investigation data to evaluate the type of movement, the geometry of sliding surface and the effectiveness of remediation measures are analyzed in detail. The procedure of assessing the stability and safe slope operation during production, even with high rates of movement and the effect of precipitation are presented. It is shown that there are situations that mine slopes can move several meters laterally and still be operational without catastrophic failures.

**RÉSUMÉ :** Cet article présente le cas d'une mine de lignite en Grèce du Nord avec des pentes excavées dépassant 100-120m dans lequel un mouvement important se produit, avec un taux moyen 10-20mm/day. La mine Mavropigi est très importante pour l'alimentation de fonctionnement ininterrompu Grèce et est souvent critique, ce qui signifie que les fouilles se déroule sur les masses en mouvement du sol. La stabilité de la pente sud-mobile est une enquête et l'information produite à partir d'une campagne de surveillance intensive, avec des prismes de l'enquête, inclinomètres et des piézomètres est présent. L'utilisation des données d'enquête pour évaluer le type de mouvement, la géométrie de la surface de glissement et l'efficacité des mesures d'assainissement sont analysés en détail. La procédure d'évaluation de la stabilité et le fonctionnement pen-te en toute sécurité pendant la production, même avec des taux élevés de mouvement et l'effet des précipitations sont présentés. On montre qu'il ya des situations que les pentes de mines peuvent se déplacer de plusieurs mètres latéra-lement et être toujours opérationnelles sans défaillances catastrophiques.

**KEYWORDS:** Slope movement, Coal open pit, Slope monitoring, Slope stability, Landslide.

### INTRODUCTION

The Public Power Cooperation (PPC) operates a number of large open pit lignite mines in Northern Greece (Amyntaio-Ptolemais Basin). The Mavropigi mine has been mined since 2003 and at present the excavated slopes have reached depths exceeding 100-120m. Since 2011, the southeast slopes have shown persistent large horizontal movements at an average rate of 10-20mm/day, at times reaching more than 40-50mm/day affected by increased precipitation. The moving mass was estimated around 6Mm<sup>3</sup>. This paper presents a case of significant movements that occurred at the southeast slope (Fig. 1), and details the monitoring, evaluation and mitigation measures taken to safeguard mining operations which had to be uninterrupted for production management purposes.

## 2 GEOLOGICAL AND GEOTECHNICAL CONDITIONS

The Mavropigi mine is in the sedimentary fill of the Ptolemais basin which includes terrestrial and lacustrine deposits of Miocene up to Pleistocene age, with abundant lignite horizons (Diamantopoulos, 2006). Near horizontal intercalations of Marls, Lignites, Stiff Clays and Sands are the predominant materials; from a geotechnical point of view they can be described as "Hard Soils - Soft Rocks". The main intercalations are Marl and Lignite. The Marl material is mostly classified as Elastic SILT or Organic SILT (MH-OH) per USCS (ASTM D2487). Locally in the Marl - Lignite intercalations, thin (few centimeters thick) beds of High Plasticity CLAY (CH) are found. These almost horizontal thin beds have very low residual shear strength and often act as slip surfaces. The mechanical properties of the different materials encountered in the area of Mavropigi are presented in Table 1. These parameters are assessed from triaxial, direct shear and ring shear tests performed on selected core samples and are used for the slope stability calculations of the Mine.

Table 1. Range of Geotechnical Properties of Mavropigi Mine Materials.

Parameters / Materials	Marl	Lignite	Clay (CH)
Unit weight $\gamma$ (kN/m <sup>3</sup> )	16-18	11-13	16-18
Effective Cohesion $c'$ (kPa)	50-150	150-200	5-50
Effective friction $\phi'$ (deg)	28-35	34-36	26-30
Residual Friction $\phi_r'$ (deg)	-	-	5-10

## 3 MONITORING OF SLOPE MOVEMENTS

At the end of 2010, tension cracks were observed at the crest of the Southeast mine slopes and visually observed horizontal transverse movements at the toe under prisms 5A3 and 6A4. Although this is usual in large and deep open pit mines, nevertheless, 20 prism monitoring stations, two inclinometers (KL-10, 11) and two piezometers (PM-10, 11) were installed on the slopes. The locations of the instruments are shown in Figure 2 together with the limits of the moving mass.

Prism measurement records were made available between January 2012 and up to the writing of this paper (Sept. 2012).

Initially the measurements were executed with a lower accuracy total station and only the "sloping distance" between the prism and the measurement base was evaluated. Due to the complexity and criticality of the situation, a new robotic total station of high accuracy (0.5cc) replaced the old one. With the new total station the movement vectors could easily be measured and evaluated. The use of the robotic total station eliminated the surveyor operation error and the high accuracy significantly reduced the horizontal and vertical angular measurement error.

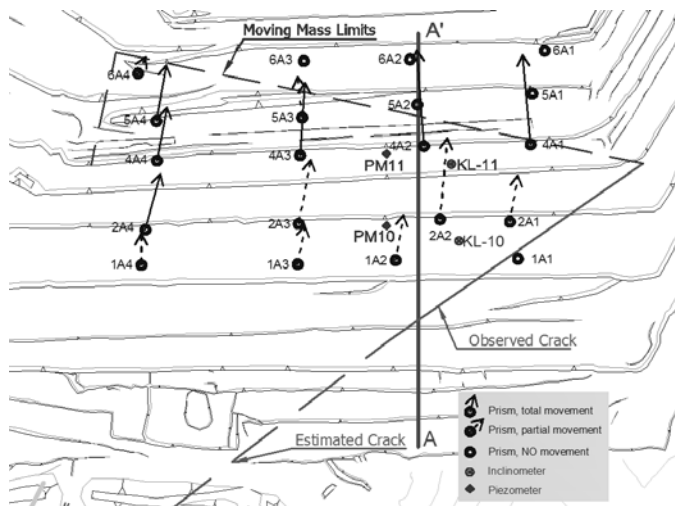


Figure 2. Monitoring equipment and trends on Southeast slopes

Due to the high rate of movement, few measurements were taken from the inclinometers before they were sheared off. From inclinometer KL-10, six measurements were obtained in a period of one month which recorded a total displacement 100mm at 27m depth from ground surface. Inclinometer KL-11 recorded only three measurements in a period of 11 days, with maximum displacement 150mm at 9m depth. The two piezometers could only be measured twice due to operational reasons and recorded water table elevation at 18.4m in PM-10 and 9.9m in PM-11. A precise water table could not be estimated based on the piezometer measurements because of the number of measurements and since the faces of the slopes were found dry. Piezometric conditions and water pressures are very difficult to model with a high degree of accuracy in mines (Sullivan, 2007) mainly due to the presence of multiple perched aquifers. Figure 3 shows a geological cross section with the monitoring equipment and the failure surface location (white line). Dark zones indicate the lignite beds.

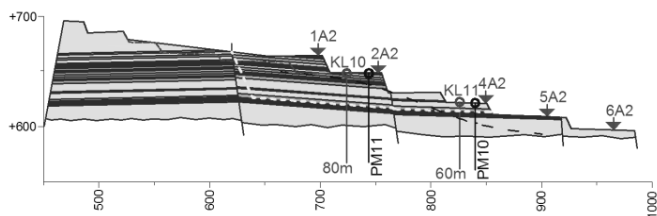


Figure 3. A-A' cross section with monitoring locations

#### 4 EVALUATION OF SLOPE MOVEMENTS

The operation of Mavropigi mine is very important for the power supply of Greece and uninterrupted operation is often critical. Mining operations may take place even in moving slopes, as long as safety of personnel and equipment is satisfied. Zavodni (2000) states that "mining operations can proceed safely with minimum interruption if failure mechanisms are understood and slopes are properly monitored" even in moving slopes. The way to assess if a "moving slope" can be mined safely is to determine if the slope movement is regressive or progressive. A regressive movement is cyclic decelerated while a progressive movement exhibits overall acceleration without appreciable deceleration intervals (Zavodni, 2000). In regressive movements, mining operation can continue after incorporating a monitoring system. If monitoring data indicate a progressive type of movement the operations are in danger of imminent collapse. The question posed to the Geotechnical Engineer is to determine the type of movement that characterizes each particular slope. The failure mechanism needs to be understood and a sufficient quantity of qualitative measurements is required. In the literature, most

case studies are analyzed after an incident and with adequate monitoring data and the type of movement is identified (Ryan & Call 1992). At the Mavropigi mine, decisions had to be made based on the day to day data becoming available without a priori having a large amount of data that could be used to determine the type of movement.

Initially, based on the geological model of the area, the visual observations of the cracks in the crest and the translational surface located by the inclinometers, a limit equilibrium model was analyzed to evaluate if the movement was possible and to back calculate the material properties of the shear surface. Based on back analysis (Figure 4) it was found that a sliding surface was possible with residual friction angle of  $\phi_r=7^\circ$  for the near horizontal surface and  $\phi_r=24^\circ$  for the back scarp. These values were considered to be the lower bounds since no water pressures were introduced and were in good agreement with the laboratory ones provided in Table 1 for the area.

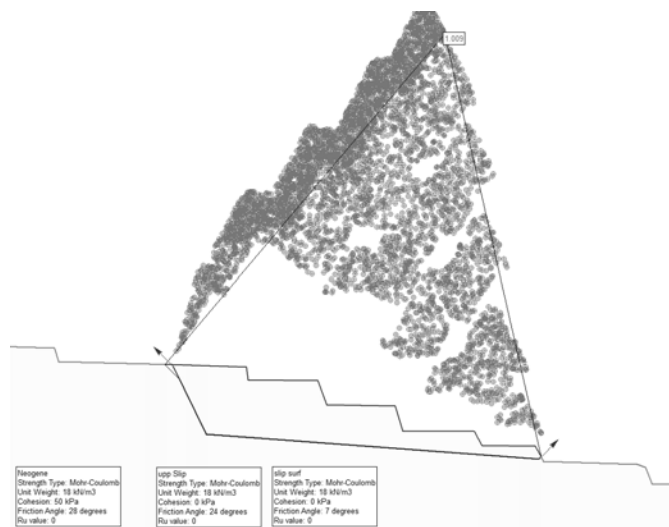


Figure 4. Back analysis of the sliding surface

From the geological model, the inclinometer readings and the back analysis it was found that the movement is taking place in a failure shear zone (thin high plasticity clay interlayer) with an inclination of about 4-5°. Based on this information an initial estimate was made that the movement could be of the regressive type based on the recommendations by (Zavodni and Broadbent, 1980), by which movements are deemed regressive when taking place on a surface with a lower angle in relation to the slope face inclination and the shear resistance (friction angle) of the material. Initial remediation measures consisting of excavating part of the top two benches were analyzed with the same data. Analysis showed that the FS became 1.06 which was considered positive for reducing the rate of movement. The slope stability analysis was considered only indicative due to the complex nature of the sliding mass (fig 2) and greater emphasis was placed on slope monitoring.

The data were further analyzed to verify the regressive type of movement and to identify a possible onset of a progressive type of movement, leading to failure. One method to evaluate monitoring data is the inverse velocity measurement versus time. Based on this method, as described by (Rose and Hungr, 2007), when the inverse velocity of slope movement is plotted against time, failure is imminent as the trend line approaches zero values (velocity increases asymptotically). In Figure 5 the inverse velocity versus time is presented for prism 2A4.

Figure 5 suggests that if this method is to be followed, at numerous times the mine slopes could be at imminent collapse. This is evaluated based on the extrapolation to zero of the regression lines for different time intervals (straight

lines). For example the first imminent collapse could have been evaluated to have occurred on 01/03/12, which did not happen.

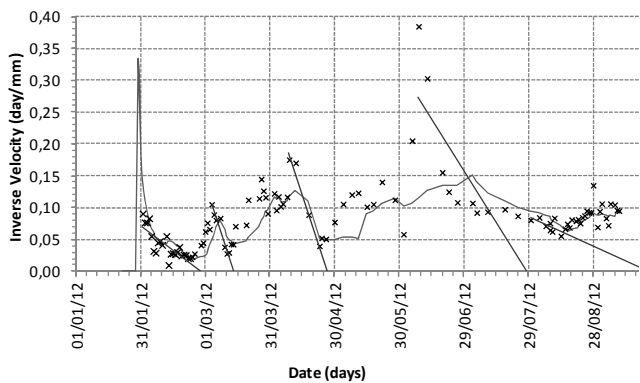


Figure 5. Inverse velocity versus time for prism 2A4

Figure 6 presents velocity versus time for all prisms of bench 2 while figure 7 shows the daily and cumulative precipitation for two weather stations. The mine is located in between these stations with a distance of about 7km. No precipitation data at the mine were available.

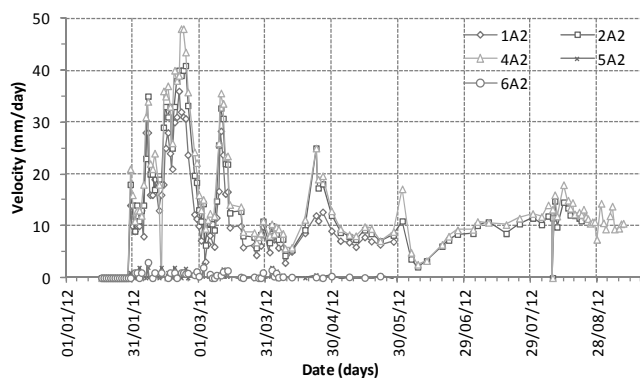


Figure 6. Velocity versus time for prisms of bench 2

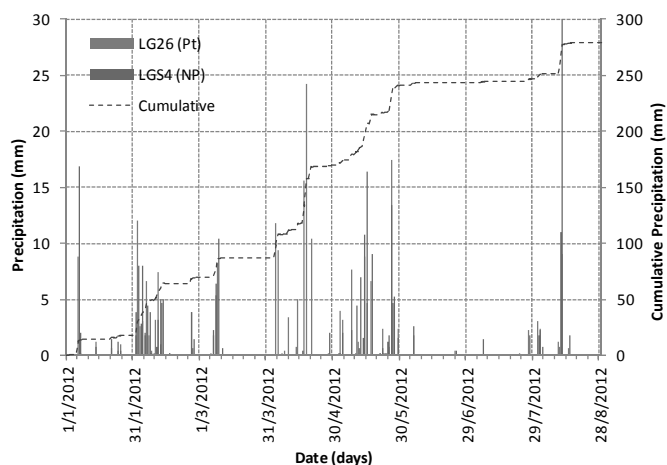


Figure 7. Precipitation versus time from two stations

Subsequently regression analysis presented times that failure could take place. This graph presents a situation where the method could not work properly without evaluating other critical factors such as precipitation or excavation unloading.

From the evaluation of figures 6 and 7, a strong correlation between the precipitation and the increase of velocity is observed. Further observation of figure 6 provides information of a stick – slip mechanism and a regressive type of movement in which the velocity does not increase or decrease at a constant rate but undergoes abrupt changes. During and af-

ter heavy precipitation the water filled tension cracks provide an increasing driving force. As displacement continues, the width of the cracks increase and the water level drops with a dissipation of water pressure. This is a repetitive situation which modifies the velocity of the sliding mass. Beginning of February 2012 limited (day shift) remedial excavation was executed on bench 1 and above to reduce the weight of the sliding mass. Such excavation increased after March 2012 being conducted on 24hour shifts. As a result movement velocities were reduced after that date.

In retrospect the movement was of the regression type (or behaved in this respect due to the excavation at the top of the slope) as can be seen from the displacement measurements at bench 4 presented in Figure 8. In this graph the displacement at the bench is plotted versus time for four different prisms in different locations transversally placed on the slope (Figure 2).

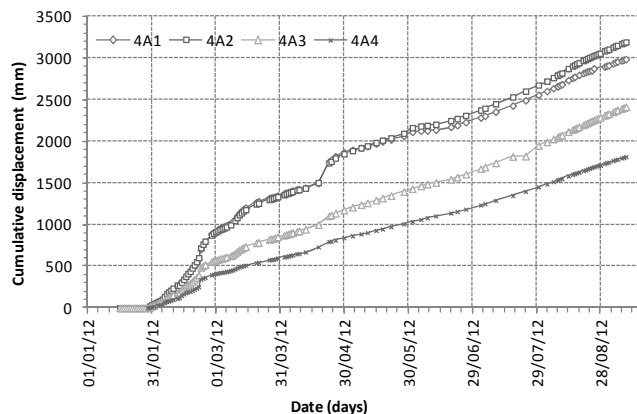


Figure 8. Cumulative displacement of prisms on bench 4

When the cumulative displacement becomes convex, movement acceleration is evident and a progressive type of movement can be inferred. When the cumulative displacement becomes concave then deceleration takes place. As can be seen from Figure 8 displacements “cyclically” change from convex to concave and back to convex meaning that this is of a mixed condition where the regressive type of movement prevails. Although the cumulative displacement for this slope for a period of 7 months is over 3m, they are still in a regressive type of movement and therefore mine operations continue.

## 5 GEOMETRICAL MOVEMENT INFORMATION

The dense grid of monitoring prisms together with the high accuracy of the robotic total station produced additional invaluable data for the moving mass. As can be seen from Figure 2 the vectors of motion are presented with arrows. The continuous arrows present monitoring information until the writing of this paper. The dashed arrows present monitoring data that were discontinued for operational reasons at different times. As can be seen from the arrows and the displacements at bench 4 (figure 8) the slope moves more to the east than to the west while both translation and rotation occurs at the same time. The reason for this complex movement can be explained taking into account the sloping surface geometry and the kinematic conditions of the adjacent southwest slopes.

The southwest slopes can be considered in a regressive moving condition as well. The movement there occurs at a very deep seated slip surface which is, partly formed on the schist bedrock probably on top of an old “inactive” fault and partly on the Neogene formation. The movement of that deeper slide may be generating lateral forces that are applied on the moving mass at the southeast mine slopes.

The complex movement of the southeast slope is also affected by the inclination of the sliding surface where the southeast slopes are moving on. As was shown previously in section A-A' the shear surface was found to have an unfavorable inclination of about 4-5°. This unfavorable situation is not continuous transversely across the slope. This can be safely stipulated after careful evaluation of the vertical - horizontal displacement of different prisms in the same bench (figure 9). In this plot the abrupt change of measurements is due to maintenance of the prisms.

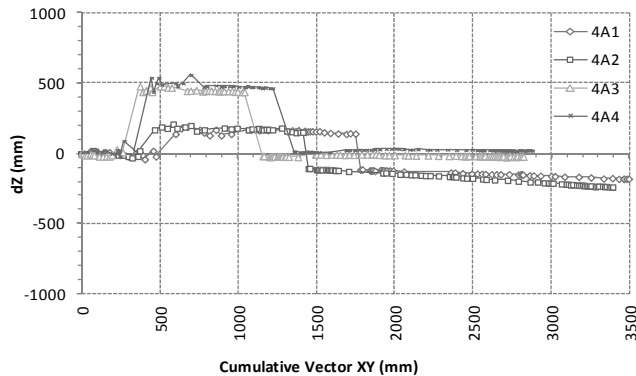


Figure 9. Vertical versus horizontal displacement

As can be seen from figure 9 and especially after about 1500mm of horizontal displacement, when no abrupt changes are recorded, the prisms at the east (4A1, 4A2) produce a downward movement with an angle of about 4-5°. The 4A2 prism which is located at cross section A-A' produces the same shear surface inclination as determined by the inclinometers. Further to the west the sliding surface becomes horizontal or even with slight favorable inclination. This sliding surface geometry is responsible for the increased movement to the east and the rotation of the moving mass.

This detailed evaluation of the moving mass could not be possible without the dense grid of measuring points and the high accuracy of the robotic total station. It is evident that with accurate monitoring data shear surface inclinations can be evaluated from surface measurements.

## 6 CONCLUSIONS

A case study of high horizontal movements recorded on operational surface mine slopes has been presented. The slopes have been moving with an average velocity of about 10-20mm/day and until today they have moved more than 3m.

The sliding mechanism was investigated and, based on back-analysis, it was determined that the southeast slopes of the mine are moving on top of a near horizontal shear surface with a residual friction angle of about 7°. As no water pore pressure was used in the analysis, this value is considered a lower bound, and coincides with values determined through lab experiments for similar material in the mine area. The slope stability analysis is considered only indicative due to the complex geometry of the moving mass. It is not possible to exactly model this mass with plain strain limit equilibrium methods.

Great emphasis was given in the monitoring program in which twenty prisms, two inclinometers and two piezometers were used. The surface monitoring of the prisms was greatly enhanced when a high accuracy robotic total station was used. With the high accuracy of the robotic total station, movement vectors could easily and accurately be measured.

The measurements presented a complex type of movement of the slopes which most of the time was of the regressive type. The slope movement has been found to be greatly affected by the periodic precipitation and the infilling of the tension cracks.

Based on the regressive type of movement, the mining operation could continue and at the same time remedial measures taken with excavation of the top benches for unloading. This remediation decreased but did not stop slope movements. Although the slopes have moved more than 3m horizontally, they are still in operation without significant problems. Movements were found to be very sensitive to external conditions such as precipitation.

The increased accuracy of the prism measurements allowed the identification of the sliding surface inclination along the mine slopes. It was found that the sliding surface changed inclination transversely.

High mine slopes can be in operation even if they produce high rates of movement, as long as the sliding mechanism type is identified and continuously monitored. Remedial measures can be incorporated in the mine plan in order to reduce movements.

## REFERENCES

- ASTM D2487-98. *Standard Practice for Classification of Soils for Engineering Purposes (Unified Soil Classification System)*. American Society for Testing and Materials.
- Diamantopoulos, A., 2006. *Plio-Quaternary Geometry and Kinematics of Ptolemais Basin (Northern Greece): Implications for the Intra-Plate Tectonics in Western Macedonia*. *Geologia Croatica*, 59/1, Zagreb.
- Rose, N.D, Hungr, O., 2007. *Forecasting potential rock slope failure in open pit mines using the inverse-velocity method*. *International Journal of Rock Mechanics & Mining Sciences*, Vol. 44, pp. 308-320.
- Ryan, T. M. & Call, R. D., 1992. *Applications of rock mass monitoring for stability assessment of pit slope failures*. *Rock Mechanics*, Tillerson & Wawersik (eds), Balkema, Rotterdam.
- Sullivan, T. D., 2007. *Hydromechanical Coupling and Pit Slope Movements*. *Slope Stability 2007*, Potvin (ed), Australian Center for Geomechanics, Perth
- Zavodni, Z. M. and Broadbent, C. D., 1980. *Slope failure kinematics*. *CIM Bulletin*, Vol. 73, No. 816.
- Zavodni, Z. M., 2000. *Time-Dependent Movement of Open-Pit Slopes*. Chapter 8, *Slope stability in surface mining*, Hustulid, McCarter, VanZyl (eds), Society for Mining, Metallurgy and Exploration.

# Interaction of stone column and surrounding soil during its construction: 3D numerical analysis

## Interaction d'une colonne ballastée et du sol environnant pendant sa construction :3D analyse numérique

Nikolaos S. Klimis

Associate Professor, Civil Engineering Department,  
Democritus University of Thrace (DUTH), Xanthi, Greece

Dimitrios D. Sarigiannis

Dr Civil Engineer AUTH, MSc DIC

**ABSTRACT:** This work deals with a simulation of a construction sequence of a stone column in two distinct stages: a) a one stage excavation and b) a multi-stage backfilling of the column stone excavation with crushed gravel at ascending steps of 1m. Simulation of this procedure is attempted using a 3D model which represents the stone column and the surrounding soil. Analysis is carried out using a numerical code, called FLAC3D, based on finite differences. The mathematical model incorporates geometry and boundary conditions of the problem, profile of soil layers with their physical, deformational and mechanical properties and their constitutive laws, as well as, initial conditions of stresses and deformations of subsoil stratum of the examined area. Special emphasis is given to simulation of an harmonically imposed vertical loading of the vibrating column, into an equivalent static vertical loading and subsequently into an equivalent radial pressure against internal wall of the cylindrical excavation of the constructed stone column. Results clearly denote that there is a strong interaction of the complex system in the kinematical and stress field, which satisfactorily justifies modification of the final diameter of the constructed stone column compared to the theoretical proposed diameter.

**RÉSUMÉ :** Ce travail se réfère à une simulation numérique de la séquence de construction d'une colonne ballastée, en deux étapes séparées : a) une étape unique d'excavation, et b) plusieurs pas successifs de remblayage de l'excavation cylindrique de la colonne ballastée, avec du matériau granulaire écrasé, à des pas montants de 1m. La simulation est effectuée à l'aide d'un modèle 3D qui représente la colonne ballastée et le sol environnant. Le code numérique utilisé est FLAC3D et il est basé sur le modèle des différences finies. Le modèle mathématique intègre la géométrie et les conditions limites du problème, le profil du sol avec leurs propriétés physiques, mécaniques et de déformation, ainsi que leurs lois de comportement et conditions initiales de la région examinée. On accentue sur la simulation d'un chargement harmonique, verticalement imposé par la colonne vibrante, à un chargement équivalent vertical statique, et par la suite, à une pression équivalente radiale qui charge l'intérieur de l'excavation cylindrique de la colonne ballastée construite. Les résultats démontrent clairement, l'interaction prononcée du système complexe, qui justifie aisément le grossissement du diamètre construit, par rapport au diamètre théorique, conçu lors du dimensionnement du projet.

**KEYWORDS:** stone column, excavation, multi-stage backfilling, Flac3D, interaction, complex system, diameter.

### 1 INTRODUCTION – SCOPE OF THE WORK

The present work focuses on the investigation of kinematic and strain interaction of a complex system consisting of a single column stone and the surrounding soil, during the excavation stage and the backfilling stage with crushed gravel.

The scope of this work is the investigation and a possible explanation of the problem concerning modification of the constructed stone column diameter, versus the theoretical (design) one, taking into account the procedure of the stone column construction, its geometrical characteristics and the

geotechnical model representing the surrounding soil and its physical, deformational and mechanical properties.

In the framework of this work, a summary of geological, geophysical, geotechnical and seismological data are presented in a succinct way in the following chapters, for the examined area, based on a number of corresponding projects performed in the recent past. After a short technical description of the stone column constructing procedure adopted for this project, the numerical model is determined and numerical analyses results are presented, in an attempt to explain the deduced discrepancy between "constructed" and "designed" stone column diameter. The examined area is located in the wide bed of a river in northern Greece, prone to liquefy, where a bridge is founded.

### 2 GEOLOGICAL AND SEISMOLOGICAL DESCRIPTION OF THE SITE

According to geological and geotechnical data, resulting from preceding investigation projects on this area, the surface is covered by deposits that belong to the Quaternary and is subdivided into: a) river deposits (RD) consisting of silty sands, clay-silty sands, gravels and locally cobbles of gneiss or marble, and b) alluvial deposits (AL), consisting mainly of sands with a largely fluctuating percentage of clays, silts and gravels, of a thickness ranging from 12 to almost 55m.

The geological bedrock of the examined site consists of rocks of the alpic age and belongs to the Rodopic Mass, consisting mainly of biotitic gneisses (gn) interpolated by amphibolites and marbles green-gray coloured. The upper part of the gneissic rockmass appears intensively weathered to totally weathered, consisting thus the weathering zone of 2 to 4m of thickness. The permeability of different geological formations is quite heterogeneous: the riverbed deposits, mainly gravel consisting (RDg) are a rather permeable soil formation ( $k \geq 10^{-3}$  m/sec), whilst alluvial deposits present a rather low permeability ( $10^{-7} \leq k \leq 10^{-5}$  m/sec).

As for the seismological data, the examined site belongs to zone I of low seismic hazard, with a horizontal free-field peak ground acceleration value:  $a_{max}=0.16g$ , according to the most recent Hellenic map of seismic zones, valid from 1/1/2004.

### 3 GEOTECHNICAL CHARACTERIZATION

According to the entity of the geotechnical and geophysical investigation programs performed on the broad area (geotechnical boreholes, CPTs and Cross-Hole tests), it results that the prevailing soil formation are alluvial deposits consisting of sands to silty sands, with a high degree of heterogeneity, characterized by USCS as SP, SW, SM, SM-SP, SM-SW. In some cases they appear as clayey sand (SC) to sandy clay (CL), whereas in other cases, they turn out to be gravel layers, such as: GP, GW, GM, GP-GM. According to the almost 200 SPTs performed, the mean value of blows was calculated about 23, with a standard deviation of  $\pm 11$ . The whole area, where the bridge is founded, has been initially divided into three sub-regions represented each by a different geotechnical design section (ITSAK & Gazetas 2003), and finally a design geotechnical section has been attributed to each bridge pier (Edafomichaniki 2007) used for dynamic analyses purposes.

From various simplified design geotechnical sections, each per bridge pier, it has been chosen one, for the needs of the present project, corresponding to a precise pier of the bridge, as being the most representative of the area, but not the most conservative one. The soil profile used in the present work, can be described as follows:

Layer  $S_{1A}$  (0 to 2m): loose to medium dense gravels with sand and sand or silty sand with local presence of gravels (GP, SW-SM, SP):  $N_{SPT} \cong 22$ ,  $\gamma = 20.5 \text{ kN/m}^3$ ,  $\phi' = 36^\circ$ ,  $c' = 3 \text{ kPa}$ ,  $E_s = 10 \text{ MPa}$ ,  $\nu = 0.33$

Layer S<sub>1B</sub> (2 to 5m): medium dense gravels with sand and sand to silty sand with local presence of gravels (GP, SW-SM, SP):  $N_{SPT} \cong 23$ ,  $\gamma=20.5\text{kN/m}^3$ ,  $\phi'=37^\circ$ ,  $c'=5\text{kPa}$ ,  $E_s=12\text{MPa}$ ,  $\nu=0.32$

Layer S<sub>2A</sub> (5 to 12m): medium dense gravels with silt and sand to silty sand with presence of gravels (GM-GP, SP-SM, SM):  $N_{SPT} \cong 25$ ,  $\gamma=21.0\text{kN/m}^3$ ,  $\phi'=39^\circ$ ,  $c'=6\text{kPa}$ ,  $E_s=16\text{MPa}$ ,  $\nu=0.31$

Layer S<sub>2B</sub> (12 to 19m): medium dense silty gravels, silty sand with presence of gravels to silty sand (GM-GP, SP-SM, SM):  $N_{SPT} \cong 28$ ,  $\gamma=21.0\text{kN/m}^3$ ,  $\phi'=40^\circ$ ,  $c'=8\text{kPa}$ ,  $E_s=20\text{MPa}$ ,  $\nu=0.30$

Layer S<sub>3A</sub> (19 to 23m) and layer S<sub>3B</sub> (23 to 35m): medium dense clayey sand-gravels mixture to sandy clay with gravels, or silty sand-gravels mixture (GC-GM, SM, CL):  $N_{SPT} \cong 26$ ,  $\gamma=21.2\text{kN/m}^3$ ,  $\phi'=37^\circ$ ,  $c'=12\text{kPa}$ ,  $E_s=15\text{MPa}$ ,  $\nu=0.31$ .

From 35 to almost 48m the weathering zone of the gneissic bedrock or highly weathered gneiss is met.

#### 4 METHODOLOGICAL APPROACH

The analysis was carried out with FLAC 3D numerical code of finite differences.

##### 4.1 Modeling Procedure

By considering the construction of a stone column in the above soil profile, simulation of two distinct stages of the construction of a stone column is attempted using a three-dimensional (3D) model which represents the stone column and the surrounding soil. Simulation of soil materials is realized by a 3-dimensional polyhedral grid with use of the finite difference method. The mathematical model adopted, incorporates geometry and boundary conditions of the problem, the profile of soil layers, physical, deformational and mechanical properties, constitutive laws for the geomaterials, as well as, initial conditions of stresses and deformations of the subsoil stratum of the area under study.

Geometry of the problem is simplified to axial symmetry. A vertical plane through stone column axis is a plane of symmetry for the analysis. Model grid is shown in figure (1). Coordinate axes are located with origin at the base of the grid, whereas y-axis is oriented along vertical column axis and upward. The initial grid is assigned by 5.0m and 50 units in x-direction, by 5.0m and 50 units in z-direction and by 28.0m and 56 units of in y-direction. A Mohr-Coulomb constitutive model elastoplastic behavior is assigned to all zones of soil surrounding stone column, whilst linear elastic one is assigned to stone column backfilling crushed material. Boundary conditions consist of roller boundaries along the external grid sides of column axis and a fixed base. Equilibrium conditions for initial stresses are based on earth pressure coefficient at rest  $K_0=\nu/(1-\nu)$ , where  $\nu$ : Poisson's ratio.

The modeling sequence consists of the following stages:

Stage I : Initial stresses

Establish equilibrium conditions to initialize stresses

Stage II : Excavation

Stone column excavation at full penetration depth was decided to be numerically simulated in one and only stage, since in reality, excavation was accomplished in about 30 min for a typical stone column of the project, and also, because no steps of excavation during its construction, could be discretized.

Stage III: Stone Column Construction

In reality, construction of cylindrical stone columns of the project with a theoretical diameter  $D=0.8\text{m}$  and a length  $L=23.0\text{m}$ , is realized by ascending steps of 0.5m; at each step, the crushed geomaterials are driven through the top of the stone column downwards (top feed method), and then, the vibrational torpedo is sunk into the excavated cyclic area, reaches the top of the crushed material and starts vibrating harmonically at a frequency of 30Hz, in order to achieve an harmonically applied normal stress of 30 to 35MPa. However, our choice of computational ascending steps to simulate stone column construction was of 1.0m, since an initial comparative study between 0.5m and 1.0m ascending steps, revealed no significant differences, whereas computational time difference was important. Therefore, Stage III is sub-divided in two distinct calculation steps, ever after named as "Sub-stage IIIa and IIIb"

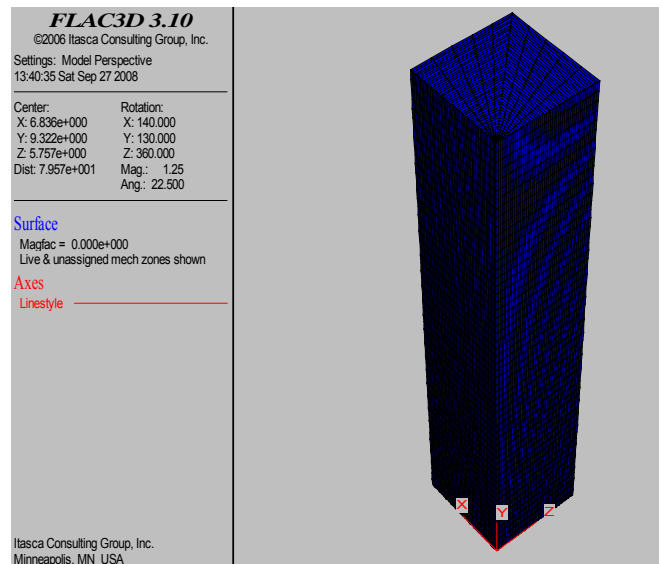


Figure 1. Model grid used for 3D numerical analyses.

Sub-stage IIIa : Simulation of Vibration and Compaction

Based on the construction procedure concerning the one stage of excavation of the stone column to be realized, which affects significantly the mechanical properties of the surrounding zone, a weak zone boundary has been created, by reducing  $\phi'$  &  $c'$ , in a distance of 0.60m surrounding column lateral sides, in order to simulate relaxation due to excavation. The width of the weak zone, the reduced values of the mechanical parameters and the elastic deformation modulus, resulted from a "trial and error" back calculating procedure, based on the quantity of the crushed material measured in situ, during the construction of a stone column of the project. Namely, we tried to match the increase of the "as built" diameter of the examined stone column, in agreement with the quantity of the crushed material used for the construction of the stone column, by adjusting the values of mechanical and deformational parameters of the disturbed zone. Vertical normal stress, harmonically applied on top of filling crushed material in order to compact the crushed fill material, per numerical ascending step of the stone column construction, is transferred as a lateral pressure "p" to simulate subjected compressive lateral loads of material due to gravel compaction, in terms of an "equivalent static" lateral (radial) pressure, as explained in the following paragraph.

Sub-stage IIIb : Simulation of Crushed Stone Material filling

This sub-stage simulates filling of the stone column crushed material taking under consideration the preceding compaction procedure. In order to maintain the shape of the "deformed diameter" per constructed step of the stone column, crushed fill material, considered as a linear elastic one, it has been attributed a very high modulus of elasticity, avoiding

thus a rebound of the plastic lateral displacements obtained from sub-stage IIIa.

#### 4.2 Assessment of equivalent lateral static loading

It is widely known in Mechanics, that a dynamic system responds to an harmonic external loading, according to the following equation:

$$u(f) = u_{st} \frac{1}{\sqrt{[1 - (f/f_1)^2]^2 + 4\zeta^2}} \quad (1)$$

where,  $u(f)$ : dynamic displacement,  $u_{st}$ : equivalent static displacement ( $=P/K$ ),  $\omega$ : frequency of the input motion,  $\omega_1$ : predominant frequency of the system (herein: the soil column overlying gneissic bedrock), and  $\zeta$ : damping ratio of the system.

From equation (1), it results that ratio  $u(f)/u_{st}$  is greater than 1.0 when  $f/f_1 < 1.0$ , and vice versa, when  $f/f_1 >> 1.0$ . In this last case, it results:

$$u(f)/u_{st} \cong 1/(f/f_1)^2 < 1 \quad (2)$$

Based on the aforementioned, in order to use an "equivalent static" loading instead of a dynamic or harmonic one, we need to use a coefficient  $b(f)$ , defined as in equation 2. As  $b(f)$  is proportional to  $u(f)/u_{st}$ , it is evident that it will be inversely proportional to loadings, i.e. the ratio  $P_{st}/P(f)$ . Therefore:

$$b(f) \cong \frac{P(f)}{P_{st}} = \frac{1}{\sqrt{[1 - (f/f_1)^2]^2 + 4\zeta^2}} \quad (3)$$

In the present problem, it can be assumed approximately, that:

$$f_1 \cong \frac{V_{La}}{4H} \cong \frac{3V_s}{8H} \quad (4)$$

where,  $V_{La}$ : wave velocity according to Lysmer ( $V_{La} \approx 1.5V_s$ ),  $V_s$ : shear wave velocity, and  $H$ : depth of the soil column overlying the gneissic bedrock.

Consequently, for the examined case, where a mean depth of the soil column is admitted as:  $H=30m$  and  $V_{S30} \approx 250m/sec$ , the predominant frequency of the system for vertically induced harmonic external loading, can be roughly approximated, as:

$$f_1 \approx \frac{3 \times 250m/s}{8 \times 30m} = 3 Hz \quad (5)$$

For input motion frequencies ranging from 20 to 35Hz (mean estimated value of 30Hz) and mean estimated value of damping ratio  $\zeta=20\%$  (Mylonakis et al 2006), equation (3) results  $b \approx 0.15$ , which represents a reductional coefficient due to the frequency of the input motion. It is estimated that due to a large number of uncertainties of the system, and also because the examined system is not a single degree freedom oscillator, it would be wiser to impose a factor of safety of 2.0, resulting thus to a design coefficient  $b_{design} = b \times 2 = 0.3$ . Accordingly, it results that  $P_{st} \approx 30\%P_{cyclic}$ .

Based on the above, vertical harmonic loading imposed by a hydraulic vibrating torpedo, can be calculated via cyclic normal stress (30 to 35MPa) applied through the edge of the vibrating column of a diameter  $d=0.40m$ . The vertical harmonic loading, is calculated, as follows:

$$P_{cyclic} = q_{cyclic} \frac{\pi d^2}{4} = 30x \frac{3.14x0.4^2}{4} = 3.768MN \quad (6)$$

providing thus an equivalent static vertical loading  $P_{st} \approx 30\%P_{cyclic} = 0.3 \times 3.768 \approx 1.13MN$ , and an equivalent vertical normal stress that is estimated to compact vertically the crushed fill material of the stone column at every step of construction:

$$\sigma_{z,st} = \frac{1130x4}{3.14x0.8^2} \cong 1777kPa \quad (7)$$

According to linear elastic theory, earth pressure coefficient at rest, equals to:  $k_0 = \nu/(1-\nu) = 0.3/(1.0-0.3) \approx 0.429$ , and then the equivalent radial (horizontal) static normal stress is estimated  $\sigma_h = 0.429 \times 1777 \approx 762kPa$ .

For the numerical analyses performed, for the deeper part of the stone column it was adopted a radial pressure of 750 to 800kPa, whereas, it has been progressively reduced as ascending steps of stone column construction were getting close to the head of the stone column at free surface until it has almost been nullified in the last step.

#### 5 NUMERICAL ANALYSIS IMPLEMENTATION & RESULTS

Developing a step by step simulation of a stone column construction (excavation, filling & compaction), analysis results are mainly concentrated to the plasticity limits of soil strength and to the outwards lateral displacement of the stone column excavated sides due to gravel compaction. Plasticity indicators for shear or tension are divided at a present plastic yield indicator with symbol (-n) or a past plastic yield indicator with symbol (-p). Outwards lateral displacement are being recorded at every depth level of the stone column, in different grid points with distance of 0, 30cm, 60cm and 100cm of the excavated sides of the stone column.

Figure (2) shows plasticity indicators generated due to the excavation at full penetration depth. It can be seen that one step column excavation, has no remarkable effect at inwards horizontal displacements. At this case, plasticity limits of soil strength developed in a distance of 0.20-0.40m surrounded excavated sides. Inwards horizontal displacements of the excavation are limited in a range of 4-5mm with maximum values appearing at deeper levels of excavation.

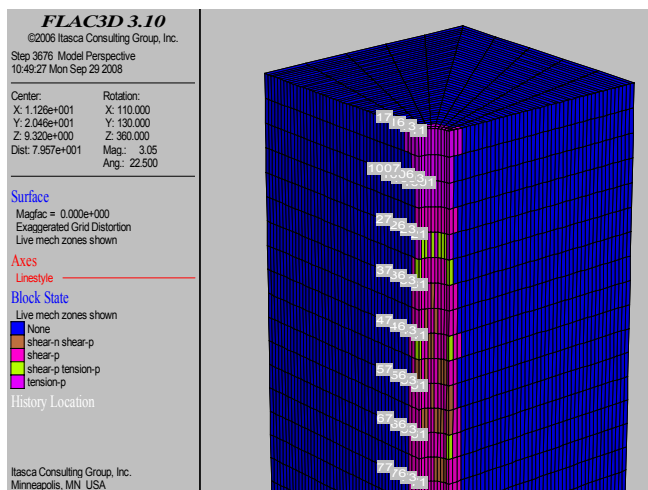


Figure 2. Plasticity zones during the one stage excavation of the examined stone column

Sub-stages IIIa & IIIb simulate the compaction/filling of crushed stone material and interaction of the above to surrounding soil. Figures (3) and (4) exhibit plasticity indicators for two different construction depths from 16m to 15m and from 1m up to the head of the stone column (free soil surface) respectively. Although, most of plastic indicators, reveal

a past plastic yield (indicator -p) in shear or tension, plasticity disturbance of the soil is generated in a remarkable distance of 1.0 to 1.2m surrounding column sides for the first example and in almost the entire surface area of the surrounding soil at the second one. Low initial stress state at free soil surface, leads to a remarkable plastic yield over limit close to the stone column head, even though equivalent static normal radial stress is very low. Concerning lateral outwards displacement of stone column excavated sides, due to gravel compaction/filling, shows that values between 10 and 20cm keep well at a distance of 100cm of the excavated sides. Indicatively, outwards radial displacement values (at excavated sides) for depths at 22.5m, 11.0m and 1.0m are in a size of 23cm, 12cm and 20cm respectively. In general terms, outwards horizontal displacements are eliminated at distances more than 60cm of excavated sides.

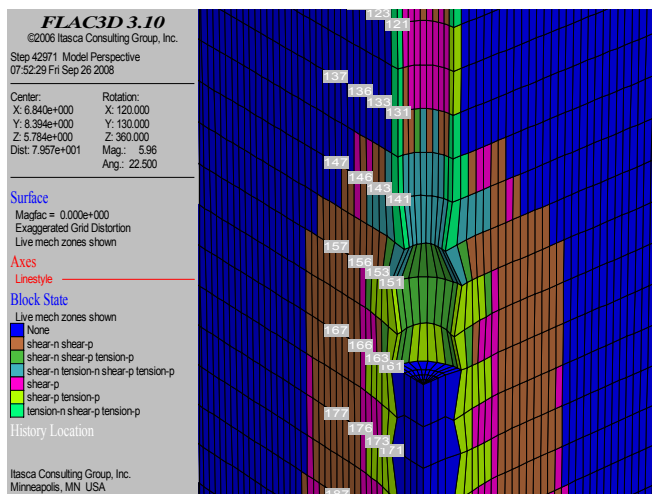


Figure 3. Plasticity zones during multi-stage filling of the stone column with crushed geomaterial at depth of 16 to 15m simulated by an equivalent static radial pressure (sub-stage IIIa, 8<sup>th</sup> ascending step of construction of the examined stone column)

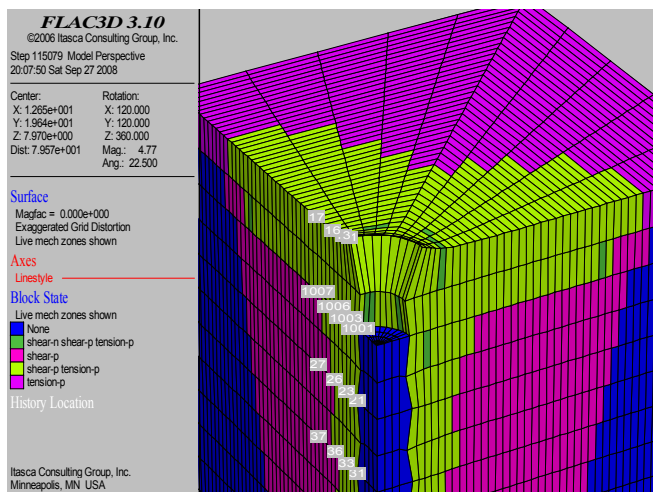


Figure 4. Plasticity zones during multi-stage filling of the stone column with crushed geomaterial at depth of 1m to head of the stone column, simulated by an equivalent static radial pressure (sub-stage IIIa, 23<sup>rd</sup> final ascending step of construction of the examined stone column)

## 6 CONCLUDING REMARKS

For the needs of the present project it has been decided to adopt a rather simple, yet representative, soil profile corresponding to a bridge pier, where typical stone columns of 0.8m diameter and 23m length are constructed, in order to improve foundation soil behaviour. The complex system consisting of a stone column and the surrounding soil is numeri-

cally analyzed with FLAC3D numerical code based on finite differences.

The numerical code used considered the procedure of construction, as well as, its effects on the surrounding soil, and simulated at its best, the physical procedure of the stone column construction, in a rational and well documented way.

Excavation stage is simulated in one and unique stage, whereas, construction of a stone column is simulated by a multi-stage complex procedure divided in two distinct calculating steps. Those are identified as two sub-stages per ascending step of construction: a) vibration and compaction, materialized by application of an equivalent radial pressure against the internal wall of the cylindrical excavation and b) stone column filling with a linear elastic geomaterial assigned a high elastic modulus of compressibility, due to the compaction procedure, preventing a rebound of the induced radial displacements of the first sub-stage.

Commenting the outcome of numerical analyses performed, the following points can be outlined:

1. after completion of excavation stage, the plastic zones developed around the cylindrical excavation are limited, same as horizontal displacements, ranging from some millimeters to only a few centimeters,
2. once excavation procedure is completed, it has been documented via a "trial and error" back calculating procedure, that a zone of about 60cm is seriously disturbed, affecting notably the mechanical and deformational parameters of the surrounding soil,
3. the stage of construction of the stone column has been simulated by a multi-stage procedure of ascending steps of 1m and application of an equivalent static radial pressure, as defined in §4.2, progressively reduced as ascending construction steps approached the head of the stone column at the free surface,
4. horizontal inelastic displacements in the limit of the side wall of the cylindrical excavation range between 10 and 20cm, resulting thus in an expansion of the constructed diameter, compared to the theoretical one as designed.

## 7 REFERENCES

- Edafomichaniki s.a. 2007. Egnatia Odos s.a., section of Nestos bridge and road access on it (14.1.2/14.2.1). Geotechnical Final Design Study (boreholes GT1 to GT5).
- Itasca Consulting Group Inc. FLAC3D v3.10 : Fast Lagrangian Analysis of Continua. User's Manual version 3.10.
- Itsak and Gazetas G. 2003. Study of seismic response and evaluation of liquefaction risk. *Issue 1*, pp 73.
- Mylonakis G., Nikolaou S. and Gazetas G. 2006. Footings under seismic loading: Analysis and design issues with emphasis on bridge foundations. *Soil Dyn. Earthquake Eng.*, 26(9), 824-853.

## Residual shear strength behavior of swelling soils

### Comportement de force résiduelle de cisaillement des sols gonflants

I.N. Markou

Democritus University of Thrace, Xanthi, Greece

**ABSTRACT:** Three clay soils from North-Eastern Greece, presenting "high" or "very high" swelling potential, were used in this investigation. The residual strength behavior of these soils was evaluated by performing ring shear tests on remolded specimens. The specimens were prepared either with the optimum water contents resulted from Standard compaction test (26% - 31%) or with higher water contents (46% - 47%), derived from the specimen moistures at the end of the preceding tests with optimum water contents. Ring shear tests were performed using a Bromhead apparatus, according to the procedures described in BS 1377 - Part 7. The results obtained from the consolidation stage of the ring shear tests conducted in swelling clays, do not present the typical form attained in ordinary clays. Although the failure envelopes in residual state present curvature in some cases, they can be considered as linear for effective normal stresses up to 250 kPa. The resulting values of residual friction angle do not exceed  $14^\circ$  and, in some cases, are affected by the water content of the specimens used in the tests.

**RÉSUMÉ:** Trois sols argileux provenant du Nord-Est de la Grèce et présentant un potentiel de gonflement «haut» ou bien «très haut», ont été utilisés dans le cadre de ce travail. Le comportement de la force résiduelle de cisaillement a été évalué à l'aide des essais de cisaillement annulaire sur des échantillons remués. Les échantillons étaient préparés, soit avec le pourcentage de contenu de l'eau optimal, résultant par l'essai de compactage standard (26% - 31%), soit avec des pourcentages de contenu de l'eau plus élevés (46% - 47%) qui dérivent par l'humidité des échantillons à la fin des essais précédents avec des contenus de l'eau optimaux. Les essais de cisaillement annulaire ont été réalisés à l'aide de l'appareil de Bromhead, selon la procédure décrite dans BS 1377-Partie 7. Les résultats obtenus par le stage de consolidation du cisaillement annulaire, conduits sur des argiles gonflants, n'atteignent point la forme classique des argiles ordinaires. Bien que, l'enveloppe de rupture présente une courbe dans quelques cas, elles peuvent être considérées comme linéaires pour des contraintes normales effectives allant jusqu'à 250 kPa. Les valeurs résultantes de l'angle de friction résiduelle, n'excèdent point  $14^\circ$ , et dans quelques cas, elles sont affectées par le contenu de l'eau des échantillons utilisés lors des essais.

**KEYWORDS:** soil behaviour, swelling soils, expansive clays, residual shear strength, laboratory investigation, ring shear tests

## 1 INTRODUCTION

The residual shear strength of cohesive soils plays a part in the stability of old landslips, in the assessment of the engineering properties of soil deposits which contain pre-existing shear surfaces, and in the assessment of the risk of progressive failure in stability problems in general. Extensive investigations on the residual strength have been carried out and directed towards: (a) developing suitable laboratory techniques for its measurement, (b) identifying the influence of geomechanical features on the residual strength, (c) understanding the basic mechanisms involved in the mobilization of shear strength during the residual stage of deformation and (d) establishing correlations with soil index properties. Although the residual strength has been studied in the laboratory using experimental techniques such as the triaxial test procedure proposed by Chandler (1966), the ring shear test and the multi-reversal direct shear test are widely used to measure the residual strength of soils. Published results (Lu-

pini et al. 1981, Skempton 1985) show that residual shear behavior changes significantly as the clay content of cohesive soil increases, and that a change in shearing mechanism also occurs. Apart from the clay fraction, the mineralogy of the clay also has an effect on residual strength, especially when the clay fraction is large (Kalteziotis 1993). A number of correlations between residual strength and clay fraction, plasticity index and liquid limit have been proposed (e.g. Skempton 1964, Lupini et al. 1981, Hawkins and Privett 1985, Skempton 1985, Mesri and Cepeda-Diaz 1986), but Lupini et al. (1981) suggested that all these correlations can not be general.

Soils containing expansive clay minerals, called swelling or expansive soils, have created problems of uplift and instability on many structures, because there is an opportunity for water to become available and thus facilitate the expansion (swelling) of the clay minerals. Swelling clays are often subject to extreme changes in shear strength because of extreme moisture changes. In addition to the strength factors related to the minerals involved, the interrelation of moisture, density and load plays an important part in the strength (Gibbs et al. 1960). Swelling soils also exist in Greece and have created a number of problems and/or failures in projects (Christodoulis and Gasios 1987, Stamatopoulos et al. 1989). Therefore, the properties and the swelling characteristics of swelling soils from Greece were investigated (Xeidakis 1993, Tsiambaos and Tsaligopoulos 1995, Kollaros and Athanasopoulou 1997), preventive and corrective measures against swelling were applied (Christodoulis and Gasios 1987, Stamatopoulos et al. 1989) and the treatment of swelling soils using various methods for reducing swell potential and increasing strength was examined (Stamatopoulos et al. 1992). It is, therefore, of merit to investigate the residual shear strength behavior of swelling soils. Toward this end, a laboratory investigation was conducted in order to evaluate the residual shear strength parameters of selected swelling soils having different moisture contents and the results obtained and observations made, are reported herein.

## 2 SOIL PROPERTIES

Three soils from the region of Thrace (North-Eastern Greece) were used in this investigation because of their swelling characteristics. According to the properties presented in Table 1, all three soils can be considered as clay soils since the clay fraction (grain sizes  $<0.002$  mm) ranges from 70% to 80%. The P1-S2 and P2-S2 soils are classified as CH, while the P2-S1 soil is classified as MH in accordance with the Unified Soil Classification System. The values of maximum dry unit weight,  $\gamma_{dmax}$ , and optimum moisture content,  $w_{opt}$ , were obtained by conducting compaction tests with standard compaction effort.

Table 1. Properties of soils.

Soil designation		P1-S2	P2-S1	P2-S2
Sampling depth (m)		1.5-3.0	0.0-1.6	1.6-3.0
Specific gravity $G_s$		2.82	2.68	2.73
Grain size analysis	Sand (%)	11.5	5.6	3.8
	Silt (%)	9.3	23.9	25.8
	Clay (%)	79.2	70.5	70.4
Atterberg limits	Liquid limit $w_L$	86	82	87
	Plasticity index $I_p$	63	42	55
Compaction characteristics	Maximum dry unit weight $\gamma_{dmax}$ (kN/m <sup>3</sup> )	13.80	13.95	14.27
	Optimum moisture content $w_{opt}$ (%)	31.2	27.0	25.8

All three soils present "high" or "very high" swelling potential, according to the known correlations of soil index properties with swelling characteristics (Papakyriakopoulos and

Koudoumakis 2001). One-dimensional swell tests (ASTM D4546, Method A) were conducted using laboratory-compacted specimens (ASTM D698) of these soils (Koudoumakis 2000). The results obtained from specimens with initial moisture contents similar to the optimum moisture contents of the soils (Table 1), are presented in Table 2. It can be observed that the swell pressure ranges from 170 kPa to 820 kPa and the free swell ranges from 11% to 19%. These values are indicative of the swelling potential of the soils used in this investigation.

Table 2. Typical results of one-dimensional swell tests.

Soil designation	P1-S2	P2-S1	P2-S2	
Initial moisture content $w_0$ (%)	30.63	31.13	24.02	27.48
Initial void ratio $e_0$	0.990	0.946	1.054	1.045
Initial degree of saturation $S_{r0}$ (%)	87.25	88.19	61.08	71.79
Dry unit weight $\gamma_d$ (kN/m <sup>3</sup> )	13.87	13.52	12.81	13.09
Swell pressure $P_s$ (kPa)	820	335	170	410
Specimen height increase $\Delta h$ (mm)	3.85	2.20	2.52	2.83
Free swell $\Delta h/h_0$ (%)	19.23	11.60	13.28	14.17

### 3 EXPERIMENTAL PROCEDURES

The residual shear strength behavior of the soils was evaluated by performing ring shear tests on remolded specimens. The use of remolded specimens allowed the adequate control of the specimen moisture content. The specimens were prepared with the moisture contents shown in Table 3. At first, the optimum moisture content, resulted from the Standard compaction test (Table 1), was used for each soil. The following specimens were prepared with larger moisture content, obtained for each soil as the average value of the specimen moisture contents at the end of the preceding tests started with optimum water content. The specimens were placed in the cell of the ring shear apparatus by kneading the soil with the desired moisture content evenly to fill the annular cavity between the confining rings of the cell, using a small spatula (BS 1377 – Part 7).

Table 3. Testing program.

Soil	Moisture content $w$ (%)	Effective normal stress $\sigma'_n$ (kPa)			
		25	75	250	800
P1-S2	31.2	25	75	250	800
	45.8	25	50	100	200
P2-S1	27.0	25	75	200	600
	47.1	25	50	100	200
P2-S2	25.8	25	75	200	600
	46.4	25	50	100	200

Ring shear testing was based on the procedure described in BS 1377 – Part 7. The tests were conducted using a Bromhead ring shear apparatus (Bromhead 1979) and annular specimens of 5 mm thickness with internal and external diameters of 70 mm and 100 mm, respectively. The specimens were consolidated for a period of 24 hours under the effective normal stresses,  $\sigma'_n$ , presented in Table 3 and, subsequently, were sheared at a constant rate of angular displacement equal to 0.048 degrees/min. The selection of this rate of angular displacement was dictated by the unconventional results of the consolidation stage of the tests, described in the next section, and was based on the fact that this rate has been found satisfactory for a large range of soils (BS 1377 – Part 7). One of the objectives of the present study was to investigate the residual strength behavior of the soils for a wide range of effective normal stresses reaching or even exceeding the values of swell pressure shown in Table 2. Although this goal was accomplished for the specimens prepared with the optimum moisture contents (Table 3), the use of effective normal stresses larger than 200 kPa was not

feasible in the tests performed with soil moisture contents ranging from 46% to 47% because of excessive specimen loss during testing.

### 4 RESULTS AND DISCUSSION

Typical “specimen length change” – “log time” curves obtained from the consolidation stage of ring shear tests conducted with optimum moisture content and with moisture content ranging from 46% to 47%, are shown in Figures 1a and 1b, respectively. It can be observed (Figure 1a) that, in several cases, the curves do not present the usual form attained in ordinary clays, either due to the expansion of specimens or because the consolidation was not completed within the predetermined period of 24 hours. It can also be observed (Figure 1b) that, in general, the classic type of curves appears in the test performed under the highest effective normal stress of each test series. The overall behavior of the three soils in the consolidation stage of the ring shear tests is summarized in Table 4. More specifically, the tests are divided in those exhibited specimen expansion and those demonstrated specimen compression during consolidation. It is evident that specimen expansion occurred almost in all series of tests and that the interchange of expansion and compression takes place at higher values of effective normal stress in the tests conducted with optimum water contents. This can be attributed to the denser condition of the specimens in these tests, since their values of initial dry unit weight,  $\gamma_{d0}$ , range from 1.24 gr/cm<sup>3</sup> to 1.59 gr/cm<sup>3</sup> and are larger than those ( $\gamma_{d0}=1.10$  gr/cm<sup>3</sup> – 1.27 gr/cm<sup>3</sup>) in the tests conducted with moisture contents ranging from 46% to 47%.

The residual shear stress,  $\tau_r$ , is the minimum constant value of shear stress, determined at the end of the shearing stage of each test and used in the drawing of the residual failure envelopes of soils. As typically shown in Figure 2a, the residual failure envelopes resulted from the ring shear tests conducted on specimens with optimum water contents are curved, in agreement with the observation of Stark and Eid (1994) that the non-linearity of failure envelopes is significant for soils with a clay fraction > 50% and a liquid limit between 60 and 220. The fitting of the same experimental data with a linear failure envelope is applied in Figure 2b, without considering the measurement corresponding to the maximum effective normal stress. As a result, a very high correlation coefficient,  $R^2$ , is obtained indicating that the failure envelopes of the soils with optimum water contents can be considered as linear for effective normal stresses up to 250 kPa. Typical residual failure envelope obtained from specimens prepared with moisture contents ranging from 46% to 47%, is also presented in Figure 2b. It can be stated with confidence that these failure envelopes are also linear because the resulting correlation coefficients range from 0.98 to 0.99. Linear residual failure envelopes were also obtained from ring shear tests conducted on Greek clayey soils with effective normal stresses ranging from 50 to 400 kPa (Kalteziotis 1993).

The values of the residual friction angle,  $\phi'_r$ , obtained in this investigation, are summarized in Table 5. These values are similar to those reported by other researchers (Bishop et al. 1971) and were determined after it was ascertained that the values of residual cohesion,  $c'_r$ , are negligible and can be set equal to zero. If the curvature of the failure envelopes for optimum water contents is not taken into consideration and all experimental data are fitted with a linear failure envelope (Figure 2a), the correlation coefficients are satisfactory ( $R^2 > 0.92$ ) but the resulting  $\phi'_r$  values are even by 30% lower than 0.92) but the resulting  $\phi'_r$  values are even by 30% lower than the values obtained for effective normal stresses up to 250 kPa (Table 5). The relatively low difference (7.7%) in P2-S1 soil is attributed to the not so pronounced curvature of its failure envelope. Xeidakis (1993) has reported that the residual friction angle decreases as the moisture content of swelling soils increases. This effect of moisture content on the

residual friction angle was verified in the present research only for P2-S2 soil (Table 5), probably because the variation of moisture content used, ranges from 14% to 21% and is low, compared to the variation of 35% used by Xeidakis (1993).

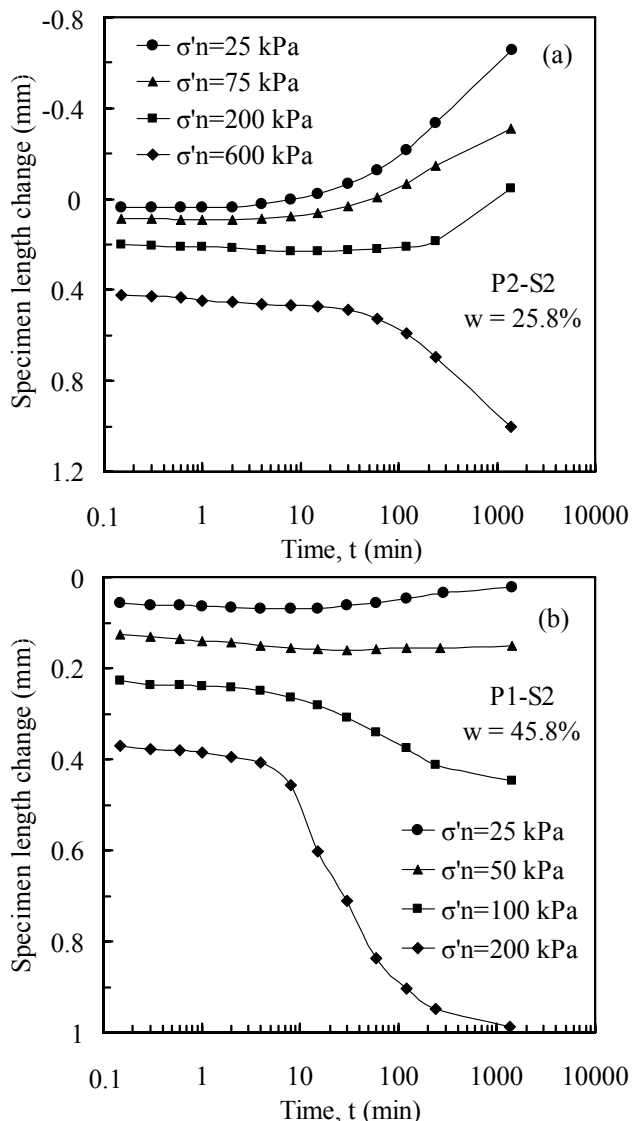


Figure 1. Typical results from the consolidation stage of ring shear tests.

Table 4. Soil behavior during the consolidation stage of ring shear tests.

Soil	Moisture content w (%)	Expansion	Compression
P1-S2	31.2	25, 75 <sup>a</sup>	250, 800 <sup>a</sup>
	45.8	25, 50	100, 200
P2-S1	27.0	25, 75, 200	600
	47.1	-----	25, 50, 100, 200
P2-S2	25.8	25, 75, 200	600
	46.4	25	50, 100, 200

<sup>a</sup> Values of effective normal stress  $\sigma'_n$  (kPa) used in the tests

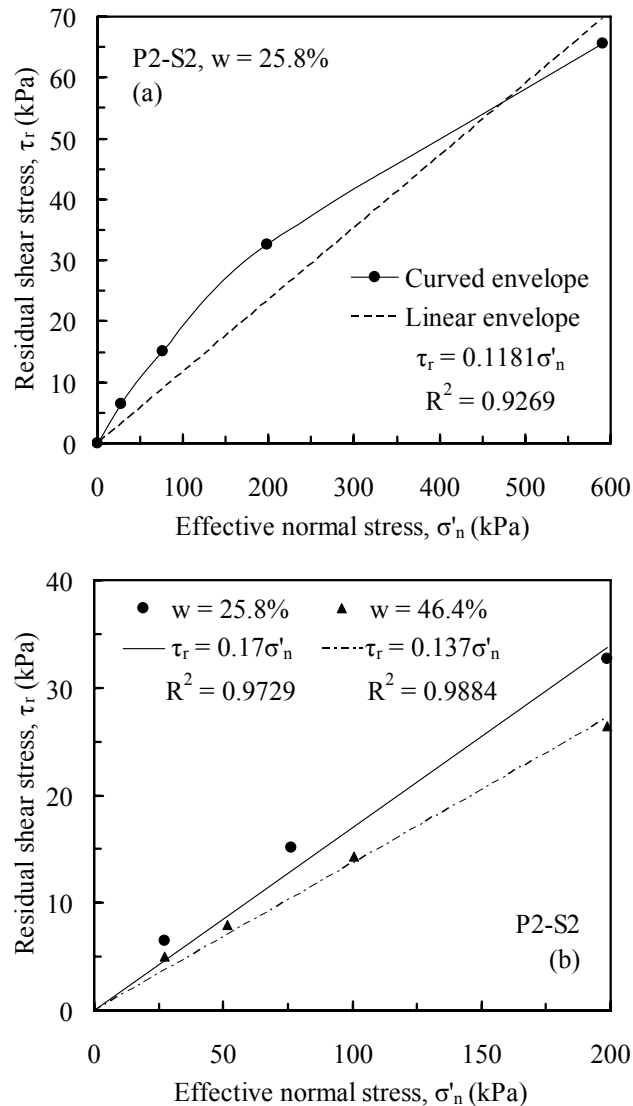


Figure 2. Typical residual failure envelopes from ring shear testing.

Table 5. Values of residual friction angle  $\phi'_R$  (degrees).

Soil	$W_{opt}$	$W_{opt}$	$w = 46\% - 47\%$	Difference (%)
P1-S2	7.3 <sup>a</sup>	8.8 <sup>b</sup>	8.8	17.0 <sup>c</sup> 0.0 <sup>d</sup>
P2-S1	8.4 <sup>a</sup>	9.1 <sup>b</sup>	8.7	7.7 <sup>c</sup> 4.4 <sup>d</sup>
P2-S2	6.7 <sup>a</sup>	9.6 <sup>b</sup>	7.8	30.2 <sup>c</sup> 18.8 <sup>d</sup>

<sup>a</sup> For all values of effective normal stress used in the tests

<sup>b</sup> For values of effective normal stress up to 250 kPa

<sup>c</sup> Between the two angle values determined for  $W_{opt}$

<sup>d</sup> Between angles determined for  $W_{opt}$  ( $\sigma'_n \leq 250$  kPa) and  $w = 46\% - 47\%$

The results of residual shear strength tests are often presented by plotting the values of residual friction coefficient,  $\tau_r/\sigma'_n$ , against the corresponding values of effective normal stress,  $\sigma'_n$ , (Lupini et al. 1981, Hawkins and Privett 1985). Thus, the "complete residual failure envelopes" (Hawkins and Privett 1985) can be obtained and the effect of effective normal stress on residual shear strength can be evaluated. The residual friction angle can be expressed as (Hawkins and Privett 1985):

$$\phi'_R = \tan^{-1} \frac{\tau_r}{\sigma'_n} \quad (1)$$

The results of ring shear tests conducted on specimens with optimum water contents were analyzed using Equation 1 and the resultant values of residual friction angle are presented in Figure 3. It is observed that the residual friction angle de-

creases with increasing effective normal stress and that P2-S2 soil presents the most pronounced curvature of failure envelope and, as a result, the maximum variation of residual friction angle. Finally, it appears that the "lowest constant residual strength" (Hawkins and Privett 1985) was not reached by the tested soils for the range of effective normal stresses used in this study.

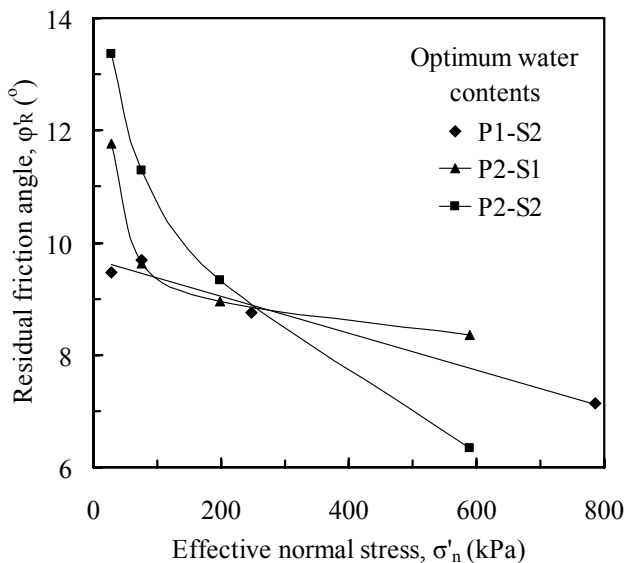


Figure 3. Complete residual failure envelopes of swelling soils tested with optimum water contents.

## 5 CONCLUSIONS

Based on the results of this investigation and within the limitations posed by the soils used and the number of tests conducted, the following conclusions may be advanced:

- The behavior of swelling soils in the consolidation stage of ring shear tests depends on the specimen moisture content and the effective normal stress used.
- The residual failure envelopes obtained for swelling soils, tested with the optimum moisture contents resulted from the Standard compaction test, are curved. Consequently, the residual friction angle decreases with increasing effective normal stress and does not attain a minimum constant value for the range of effective normal stresses used in this study.
- All residual failure envelopes obtained in this investigation can be considered as linear for effective normal stresses up to 250 kPa, regardless of the moisture content of soils.
- The residual friction angle does not always decrease as the moisture content of soil increases.

## 6 ACKNOWLEDGEMENTS

The ring shear tests described in this paper were conducted at the Soil Mechanics & Foundation Engineering Laboratory of Democritus University of Thrace by the students M. Georgiadou and Ch. Trigousi, whose careful work is acknowledged.

## 7 REFERENCES

ASTM D698 1998. Standard test method for laboratory compaction characteristics of soil using Standard effort (12,400 ft-lbf/ft<sup>3</sup> (600 kN-m/m<sup>3</sup>)). *Annual Book of ASTM Standards* 04.08 (I), 77-84.

ASTM D4546 1998. Standard test methods for one-dimensional swell or settlement potential of cohesive soils. *Annual Book of ASTM Standards* 04.08 (I), 663-669.

BS 1377 1990. *Soils for Civil Engineering Purposes – Part 7: Shear Strength Tests (Total Stress)*. British Standards Institution, London.

Bishop A.W., Green G.E., Garga V.K., Andresen A. and Brown J.D. 1971. A new ring shear apparatus and its application to the measurement of residual strength. *Géotechnique* 21 (4), 273-328.

Bromhead E.N. 1979. A simple ring shear apparatus. *Ground Engineering* 12 (5), 40-44.

Chandler R.J. 1966. The measurement of residual strength in triaxial compression. *Géotechnique* 16 (3), 181-186.

Christodoulis J. and Gasios E. 1987. Investigation on the motorway damage due to expansive soil in Greece. *Proc. 6th Int. Conf. on Expansive Soils*, New Delhi, 241-245.

Gibbs H.J., Hilf J.W., Holtz W.G. and Walker F.C. 1960. Shear strength of cohesive soils. *Proc. Research Conf. on Shear Strength of Cohesive Soils*, Boulder, 33-162.

Hawkins A.B. and Privett K.D. 1985. Measurement and use of residual shear strength of cohesive soils. *Ground Engineering* 18 (8), 22-29.

Kalteziotis N. 1993. The residual shear strength of some Hellenic clayey soils. *Geotechnical and Geological Engineering* 11, 125-145.

Kollaros G. and Athanasopoulou A. 1997. The character and identification of swelling soils in road construction projects. *Proc. Engineering Geology and the Environment*, Marinos et al. (eds.), Balkema, 187-192.

Koudoumakis P. 2000. *Personal communication*. Democritus University of Thrace, Xanthi, Greece.

Lupini J.F., Skinner A.E. and Vaughan P.R. 1981. The drained residual strength of cohesive soils. *Géotechnique* 31 (2), 181-213.

Mesri G. and Cepeda – Diaz A.F. 1986. Residual shear strength of clays and shales. *Géotechnique* 36 (2), 269-274.

Papakyriakopoulos P. and Koudoumakis P. 2001. Swelling soils in the area of Thrace. *Proc. 4th Hellenic Conf. on Geotechnical and Geoenvironmental Engineering* 1, Athens, 163-170. (in Greek)

Skempton A.W. 1964. Long-term stability of clay slopes. *Géotechnique* 14 (2), 75-101.

Skempton A.W. 1985. Residual strength of clays in landslides, folded strata and the laboratory. *Géotechnique* 35 (1), 3-18.

Stamatopoulos A., Gassios E., Christodoulis J. and Giannaros H. 1989. Recent experiences with swelling soils. *Proc. 12th Int. Conf. on Soil Mechanics and Foundation Engineering* 2, Rio de Janeiro, 655-658.

Stamatopoulos A., Christodoulis J. and Giannaros H. 1992. Treatment of expansive soils for reducing swell potential and increasing strength. *Quarterly Journal of Engineering Geology* 25, 301-312.

Stark T.D. and Eid H.T. 1994. Drained residual strength of cohesive soils. *Journal of Geotechnical Engineering* 120 (5), 856-871.

Tsiambaos G. and Tsaligopoulos Ch. 1995. A proposed method of estimating the swelling characteristics of soils: some examples from Greece. *Bulletin of the International Association of Engineering Geology* 52, 109-115.

Xeidakis G. 1993. Swelling soils in Thrace, Northern Greece: origins and properties. *Proc. Geotechnical Engineering of Hard Soils – Soft Rocks* 1, Anagnostopoulos et al. (eds.), Balkema, 863-870.

## Effect of Grout Bleed Capacity on the Engineering Properties of Cement Grouted Sands

### Effet de la capacité de ressuage de coulis de ciment sur les propriétés mécaniques des sables injectés

I.A. Pantazopoulos, D.K. Atmatzidis, V.G. Basas, S.K. Papageorgopoulou

Geotechnical Engineering Laboratory, Department of Civil Engineering, University of Patras, Greece

**ABSTRACT:** Grouts of three different cement types, each at four different cement gradations, with W/C ratios ranging from 0.6 to 3.0 and bleed capacities ranging up to 70% were injected into two different sands. Permeability, unconfined and triaxial compression and resonant column tests were conducted to investigate the influence of grout bleed capacity on the engineering properties of cement grouted sands. Cement grouting resulted in (a) permeability coefficient values as low as  $10^{-8}$ cm/s, (b) unconfined compressive strength in the range of 1MPa to 35MPa, (c) cohesion in the range of 100kPa to 1400kPa, (d) improvement of the internal friction angle by up to  $5^{\circ}$ , (e) higher shear modulus by up to 25 times and (f) improved damping ratio by up to 10 times. Bleed capacity is an indicator of sand void volume filled with solidified grout but its degree of correlation with the static and dynamic properties of the grouted sands ranges from very good to negligible.

**RÉSUMÉ :** On a injecté des coulis de trois types de ciments différents, chaque un avec quatre gradations différentes, ayant un rapport eau/ciment variant de 0.6 à 3.0, et une capacité de ressuage se situant jusqu'à 70% lorsque injectés, dans deux sables propres. On a effectué des essais de perméabilité, de compression simple et triaxiale et de colonne résonnante pour étudier l'influence de la capacité de ressuage des coulis sur les propriétés mécaniques des sables injectés. L'injection du ciment a résulté en: a) des valeurs de coefficients de perméabilité aussi bas que  $10^{-8}$ cm/s, b) une compression simple de 1MPa à 35MPa, c) une cohésion de 100kPa à 1400kPa, d) une augmentation de l'angle de frottement jusqu'à  $5^{\circ}$ , e) un module de cisaillement jusqu'à 25 fois plus élevé, f) une augmentation du coefficient d'amortissement jusqu'à 10 fois plus élevé. Le ressuage des coulis est un indicateur du volume des vides du sable remplis de coulis solidifié mais son degré de corrélation avec les propriétés statiques et dynamiques des sables cimentés varie de très bonnes à négligeables.

**KEYWORDS:** cement grout, bleed capacity, permeability, strength, shear modulus, damping ratio

## 1 INTRODUCTION

Improvement of the mechanical properties and behavior of soils by permeation grouting using cement suspensions is frequently required in order to assure the safe construction and operation of many structures. The grout water-to-cement ratio (W/C) and the maximum cement grain size ( $d_{max}$ ) are two important parameters controlling the cement grout bleed capacity and, consequently, the effectiveness of cement grouts in terms of the percentage of soil voids volume filled by grouting. Although the bleed capacity of cement grouts has been frequently quantified, its correlation with the engineering properties of the grouted sand has not been investigated so far.

Scope of this presentation is to provide some insights on the effect of grout bleed capacity on permeability, unconfined compressive strength, shear strength parameters and dynamic properties of ordinary and microfine cement grouted sands, in conjunction with the effect of the grout W/C ratio.

## 2 MATERIALS AND PROCEDURES

For the purposes of this investigation, a Portland, a Portland-composite and a pozzolanic cement (CEM I, CEM II/B-M and CEM IV/B according to Standard EN 197-1) were used. Each cement was pulverized to produce three additional cements with nominal maximum grain sizes ( $d_{max}$ ) of 40 $\mu$ m, 20 $\mu$ m and 10 $\mu$ m and average Blain specific surface values of 567, 720 and 928m<sup>2</sup>/kg, respectively. Cements with  $d_{max}$ =10 $\mu$ m can be considered as "microfine" according to Standard EN 12715 ( $d_{95}$ <20 $\mu$ m and specific surface over 800m<sup>2</sup>/kg). Also, cements with  $d_{max}$ =20 $\mu$ m have adequately small characteristic grain sizes to be considered, marginally, as "microfine". Typical gradations of these cements are presented in Figure 1.

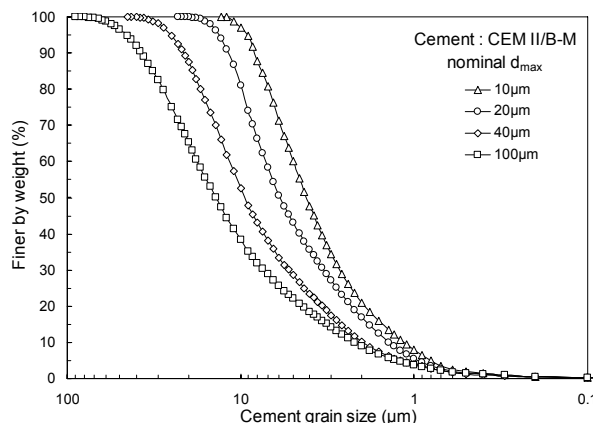


Figure 1. Typical cement gradations.

All suspensions tested during this investigation were prepared using potable water since it is considered appropriate for preparing cement-based suspension grouts. The W/C ratio of the suspensions was set equal to 0.6, 0.8, 1.0, 2.0 and 3.0 by weight, in order to test both stable and unstable suspensions in terms of bleed capacity. A superplasticizer (patented new generation of admixture based on polycarboxylate chemistry) at a dosage of 1.4 % by weight of dry cement was used to improve grout properties. All suspensions were prepared using high speed mixers. As recommended by the superplasticizer producer, the total amount of cement, 70 % of the water and the superplasticizer dosage were mixed for 5 min. Then, the rest of the water was added and mixing continued for another 5 min. Bleed capacity measurements were conducted for all cement suspensions used and the results are summarized in Table 1.

Table 1. Bleed capacity values (%) of all cement grouts

$d_{max}$	W/C				
	0.6	0.8	1.0	2.0	3.0
100 $\mu$ m	5-10	17-19	16-39	44-60	60-70
40 $\mu$ m	5-7	11-15	10-26	42-55	56-68
20 $\mu$ m	N/T	N/T	0-4	25-37	43-49
10 $\mu$ m	N/T	N/T	0-2	7-26	38-42

N/T: Not tested

According to Standard EN 12715, a suspension is stable when it has a bleed capacity of not more than 5 % after 120 min from preparation. It can be observed that a W/C ratio of about 0.6 was required to obtain stable suspension of the coarse cements ( $d_{max}$ =100 $\mu$ m and 40 $\mu$ m) while microfine cement suspensions were stable for a W/C ratio of 1.0

The soils used were clean, uniform, limestone sands with angular grains and were grouted at a dense (relative density approximately 90%) and dry state. Two different sand grada-

tions were used with grain sizes limited between sieve sizes (ASTM E11) Nos. 10-14 and 14-25 ( $d_{15}$  size of 1.5mm and 0.8mm, respectively) in order to allow grouting by both the coarse- and fine-grained suspensions. The angle of internal friction of the sands was  $42.2^\circ$  and  $42.6^\circ$ , respectively.

Laboratory equipment, similar to the arrangement described in ASTM D4320-84, was used to produce small-size grouted sand specimens, with a height of 112mm and a diameter of 50mm, ready for testing (Pantazopoulos et al. 2012). Injection was stopped when the volume of the injected grout was equal to two void volumes of the sand in the molds. After 24 h, the specimens were extracted from the split molds and cured in a humid room for 28 days before testing.

Grouted specimens were tested in unconfined compression at a displacement rate equal to 0.1%/min. Hydraulic conductivity tests were performed according to the procedure described by Head (1986) for permeability testing in a triaxial cell with two back-pressure systems. Drained triaxial compression tests were conducted under confining pressures of 100, 200 and 400kPa and axial strain rate equal to 0.1%/min, without initial saturation and consolidation. The dynamic properties of the grouted sands were investigated at confining pressures up to 400kPa by conducting torsional resonant column tests for a shear strain range,  $\gamma$ , of approximately  $5 \cdot 10^{-5}$  % to  $5 \cdot 10^{-2}$  %. Testing procedures and interpretation of raw data complied with well established methods (Pantazopoulos and Atmatzidis 2012). For comparison, similar tests were conducted on clean sands.

### 3 COEFFICIENT OF PERMEABILITY

The coefficient of permeability values of all grouted sands tested are presented in Figure 2 with respect to W/C ratio, bleed capacity and maximum cement grain size of the suspensions. The coefficient of permeability decreases considerably (by about 5 orders of magnitude) as the W/C ratio decreases from 3 to 0.6 and attains a value of about  $10^{-7}$  to  $10^{-8}$  cm/s indicating practically impermeable materials. The permeability of the grouted sands appears not to be affected by the cement grain size. Evaluation of the permeability of the grouted sands in terms of grout bleed capacity indicates a similar trend as with the W/C, but allows some observations to be made in terms of the effect of cement grain size. For cement grouts with  $d_{max}$  equal to 100 $\mu$ m and 40 $\mu$ m, the coefficient of permeability of the grouted sands attained values in the range of  $10^{-7}$  to  $10^{-8}$  cm/s and  $10^{-3}$  to  $10^{-4}$  cm/s, for grout bleed capacity ranging from 6% to 30% and from 48% to 68%, respectively. Sands injected with microfine cement grouts ( $d_{max}=20\mu$ m and 10 $\mu$ m) obtained, generally, higher coefficients of permeability, by half to one order of magnitude, compared to sands grouted with the coarser cement suspensions, for similar bleed capacities. This is reasonable and can be attributed to the increased amount of coarse-grained cement needed to obtain the same bleed capacity with suspensions of microfine cements. It should also be noted that (a) similar coefficient of permeability values ( $10^{-7}$  to  $10^{-8}$  cm/s) are obtained when injecting with stable or unstable suspensions for bleed capacity values up to 30% and (b) for higher bleed capacity values, the coefficient of permeability of the grouted sand decreases dramatically but remains in the range of  $10^{-4}$  to  $10^{-3}$  cm/s.

### 4 UNCONFINED COMPRESSION STRENGTH

The results presented in Figure 3 indicate that the unconfined compression strength of the grouted sands increases significantly with decreasing W/C ratio of the grouts, as verified by other research efforts (i.e. Dano et al. 2004) and seems not to be affected by cement grain size. However, the effect of cement grain size can be clearly demonstrated in terms of grout bleed capacity. The unconfined compression strength of the grouted sands is very well correlated with grout bleed capacity of both the coarse-grained cements ( $d_{max}=100$  and 40 $\mu$ m) and the microfine cements ( $d_{max}=20$  and 10 $\mu$ m) but, defi-

nately, microfine cement grouts with the same bleed capacity as cement grouts yield significantly lower grouted sand strength. As with permeability, this can be attributed to the increased amount of coarse-grained cement needed to obtain the same bleed capacity as microfine cement suspensions.

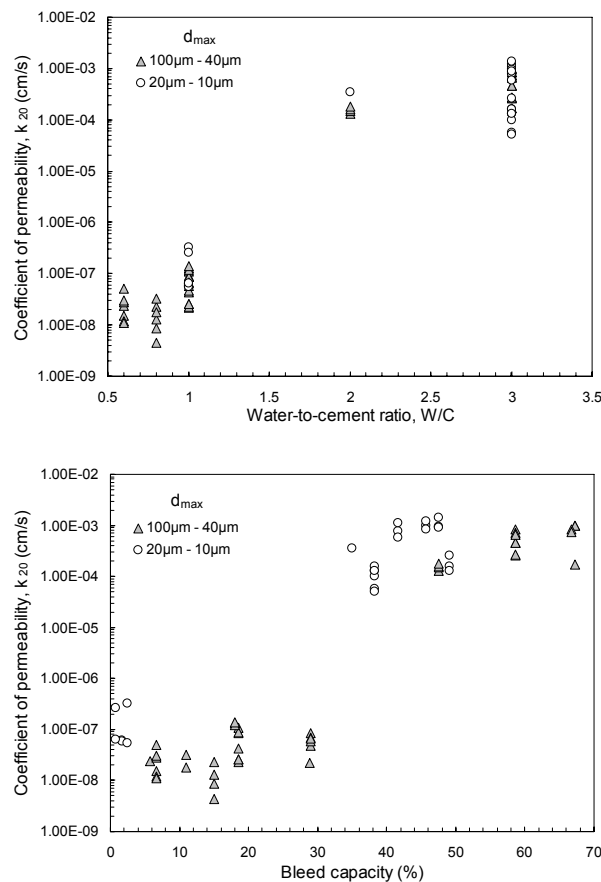


Figure 2. Effect of grout W/C ratio and bleed capacity on the permeability of cement grouted sands.

### 5 SHEAR STRENGTH

The shear strength of the grouted sand specimens is expressed in terms of internal friction angle and cohesion, by applying the Mohr-Coulomb failure criterion. As indicated in Figure 4, the internal friction angle ranged from  $40^\circ$  to  $50^\circ$  and the effect of W/C ratio, bleed capacity and cement grain size appear to be insignificant. In general, the internal friction angle of the grouted sands was up to  $5^\circ$  higher than the value obtained for clean sands. The cohesion of the grouted sands is strongly affected both by the W/C ratio and by the bleed capacity of the grouts. As shown in Figure 5, the cohesion values of the grouted sands ranged from 600kPa to 1450kPa, from 300kPa to 500kPa and from 50kPa to 250kPa, for W/C ratios equal to 1, 2 and 3, respectively. Furthermore, grouted sands injected with stable grouts (bleed capacity values less than 5%) obtained the highest cohesion values ranging from 1200kPa to 1450kPa. Increased bleed capacity values (unstable suspensions) in the range of 15% to 65%, leads to an almost linear decrease of the cohesion values from 800kPa to 100kPa. The effect of cement grain size on grouted sand cohesion, as shown in Figure 5, where the microfine cements exhibit higher values of cohesion than the coarse-grained cements, by 40% to 150%, is misleading since the suspensions used had different bleed capacities for the same W/C ratio. For example, at W/C ratio equal to 1, the microfine cement suspensions are stable (bleed capacity < 4%) and fill the sand voids with cement more completely and uniformly than the coarse cement suspensions with W/C=1 (bleed capacity > 16%).

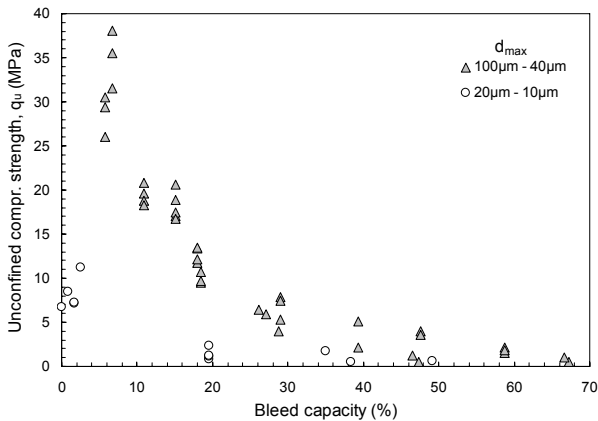
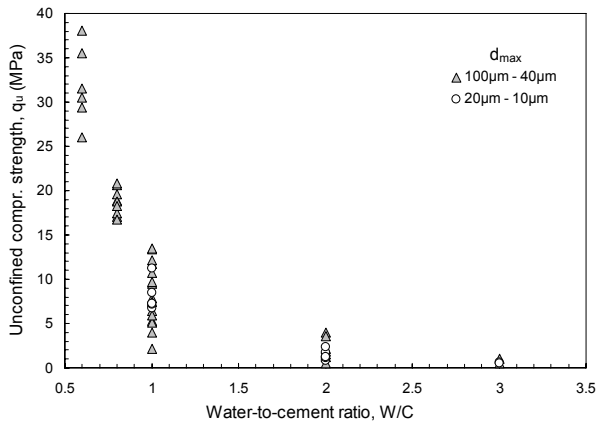


Figure 3. Effect of grout W/C ratio and bleed capacity on the unconfined compression strength of cement grouted sands.

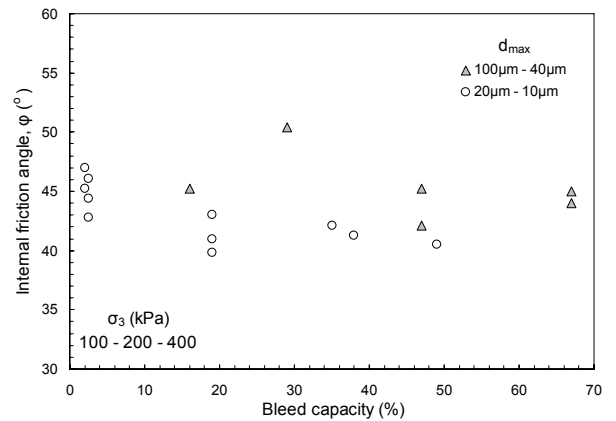
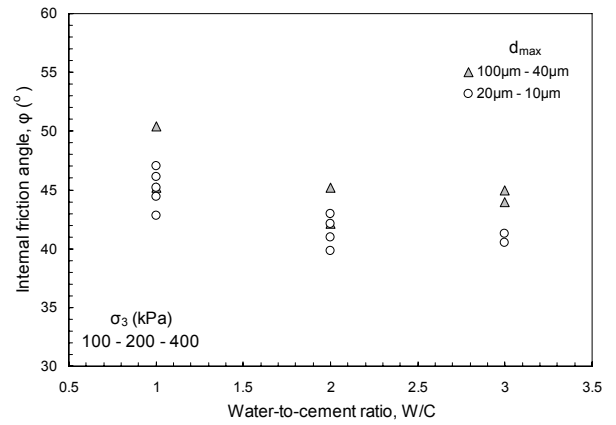


Figure 4. Effect of grout W/C ratio and bleed capacity on the internal friction angle of cement grouted sands.

## 6 SHEAR MODULUS

Presented in Figure 6 are typical results obtained for the shear modulus,  $G$ , of grouted sands at a confining pressure equal to 50kPa and shear strain equal to  $10^{-5}\%$ . The effect of confining pressure is not pronounced for the grouted sands tested (Pantazopoulos and Atmatzidis 2012). As shown in Figure 6, the shear modulus values decrease, from 4.1GPa to 1.5 GPa, with increasing W/C ratio, from 0.6 to 3. The shear modulus values of the clean sands did not exceed 170MPa, indicating an improvement up to 25 times by grouting. The effect of grout bleed capacity on the shear modulus of grouted sand is clearly depicted in Figure 6, where it can be observed that above a bleed capacity value of about 30%, the shear modulus of the grouted sand decreases sharply by about 40%. Cement grain size seems to have a measurable effect on the shear modulus values of the grouted sands. For similar bleed capacity values, the sands grouted with microfine cement grouts have lower shear modulus values, by 15% to 30%, compared to sands grouted with coarse-grained cement grouts.

## 7 DAMPING RATIO

The damping ratio values of the grouted sands are presented in Figure 7 for a confining pressure equal to 50kPa and shear strain equal to  $10^{-3}\%$ . The effect of shear strain and confining pressure on the grouted sand damping ratio has been presented elsewhere (Pantazopoulos and Atmatzidis 2012). In general, the values obtained ranged from 0.5% to 8.0%, increased with increasing shear rate (from  $5 \cdot 10^{-5}\%$  to  $5 \cdot 10^{-2}\%$ ) and decreased with increasing confining pressure (from 50kPa to 400kPa). The grout W/C ratio has a measurable effect on the damping ratio values of the grouted sands, which have a tendency to increase with increasing W/C ratio. The effect of grout bleed capacity on the damping ratio of the grouted sand appears to be less dominant, mainly for coarse-

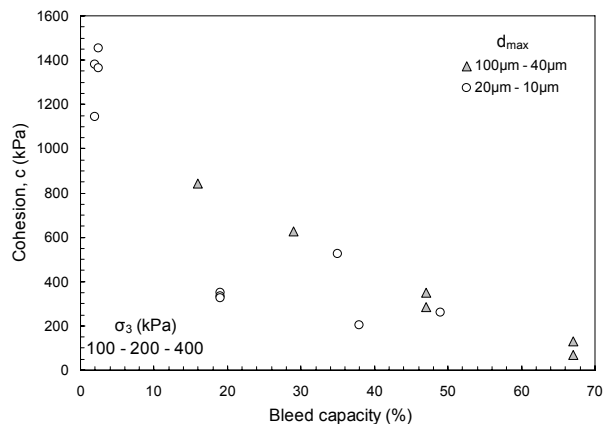
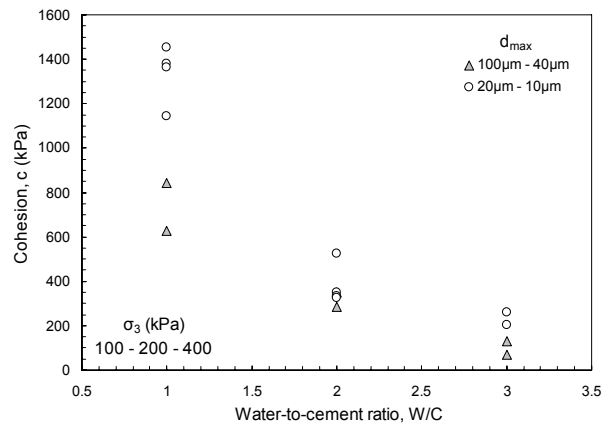


Figure 5. Effect of grout W/C ratio and bleed capacity on the cohesion of cement grouted sands.

grained cements. For microfine cements there is a tendency for the damping ratio of the grouted sands to increase with increasing bleed capacity of the grouts. Even though the

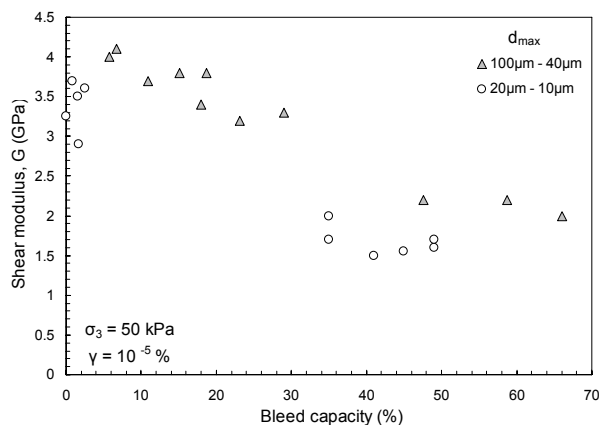
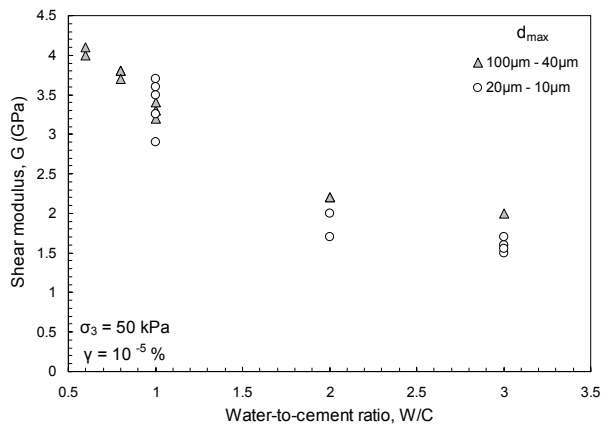


Figure 6. Effect of grout W/C ratio and bleed capacity on the shear modulus of cement grouted sands.

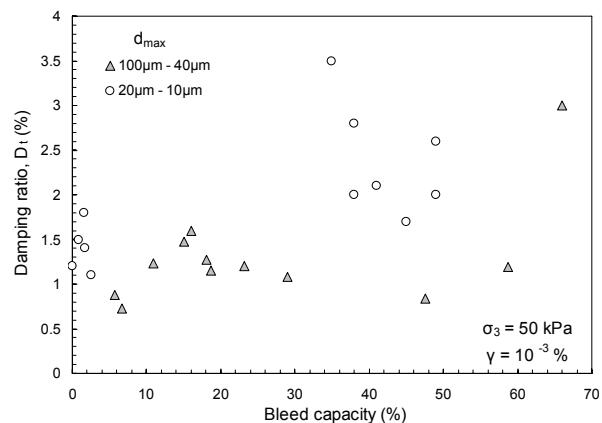
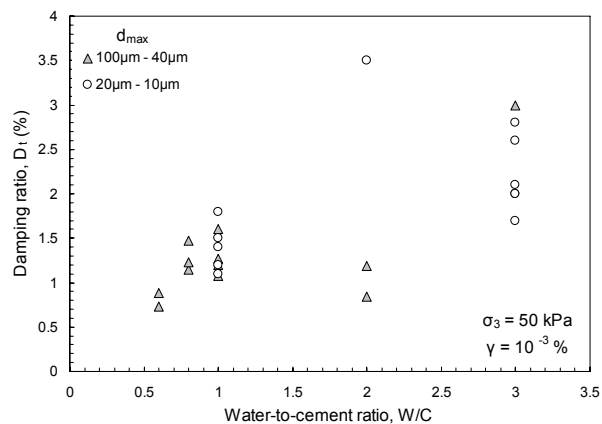


Figure 7. Effect of grout W/C ratio and bleed capacity on the damping ratio of cement grouted sands.

available data are limited, grouted sands injected with stable grouts (bleed capacity less than 5%) of microfine cements indicated damping ratios lower by 50% than those for grouting with unstable grouts. The damping ratios of the clean sands (for confining pressure and shear strain equal to 50kPa and  $10^{-3}\%$ , respectively) did not exceed 0.5%, indicating an improvement up to 10 times by grouting.

## 8 CONCLUSIONS

Based on the results obtained and the observations made, the following major conclusions may be advanced:

- Bleed capacity is an indicator of grout effectiveness, since it is representative of the soil void volume filled by cement.
- The distinction between stable and unstable grouts may not be an indicator of grout effectiveness since similar effects may be produced by both stable and unstable grouts.
- Bleed capacity values correlate very well with some grouted sand properties (i.e. unconfined compression strength, cohesion) and not at all with other properties (i.e. damping ratio, internal friction angle).

## 9 ACKNOWLEDGEMENTS

The information reported herein is part of research project PENED-03ED527, co-financed by the European Social Fund (75%) and the Greek Ministry of Development (25%).

## 10 REFERENCES

- Pantazopoulos I.A., Markou I.N., Christodoulou D.N., Droudakis A.I., Atmatzidis D.K., Antiohos S.K., Chaniotakis E. 2012. Development of microfine cement grouts by pulverizing ordinary cements. *Cement and Concrete Composites* 34, 593-603.
- Head K.H. 1986. *Manual of soil laboratory testing*. vol.3. Pentech Press Ltd, London.
- Pantazopoulos I.A. and Atmatzidis D.K. 2012. Dynamic properties of microfine cement grouted sands. *Soil Dynamics and Earthquake Engineering* 42, 17-31.
- Dano C., Hicher P-Y, Tailliez S. 2004. Engineering properties of grouted sands, *Journal of Geotechnical and Geoenvironmental Engineering* 130, 328-338.

## Effectiveness of In-soil Seismic Isolation taking into account of Soil-Structure Interaction

### Εfficacité d' Isolement sismique dans le Sol tenant compte de l'interaction du Sol avec la Structure

A. K. Tsatsis, I. C. Anastasopoulos, F. L. Gelagoti & R. S. Kourkoulis

Laboratory of Soil Mechanics, National Technical University of Athens

**ABSTRACT:** In the present study an innovative seismic isolation method is proposed that introduces a sliding surface within the foundation soil. The sliding surface comprises of two synthetic liner layers at contact with each other creating an interface of small friction that enfolds the foundation soil. The effectiveness of the isolation system is explored as a function of the earthquake intensity accounting for soil-structure-interaction phenomena. It is shown that the proposed system serves as a fuse mechanism within the soil and substantially reduces the acceleration transmitted onto the structure. The isolated structure may be subjected to increased differential lateral displacement, due to sliding at the isolation interface – something that has to be considered in the design.

**RÉSUMÉ :** Dans cette étude une méthode innovante d'isolement sismique est proposé, composé d'une surface de glissement dans le sol. La surface de glissement se compose de deux couches de revêtement synthétique, caractérisé d'une résistance réduite. L'efficacité du système proposé est explorée en fonction de l'intensité sismique. Il est démontré que le système proposé acte comme un mécanisme fusible dans le sol, réduisant considérablement l'accélération transmise sur la structure. La structure isolée peut être soumise à un déplacement différentiel latérale, en raison de glissement à l'interface d'isolation – quelque chose que doit être pris en compte dans le désign.

**KEYWORDS:** soil-structure interaction; in-soil isolation; synthetic liner

## INTRODUCTION

In the present study an isolation method is proposed that introduces a sliding surface within the foundation soil. The sliding surface comprises two layers of a smooth synthetic liner in contact with each other. Yegian et al. (2004a) were the first to propose the application of synthetic liners just below the foundation with the intention to introduce, an interface of small friction coefficient upon which the structure would slide as a rigid block. To determine the properties of the interface, shaking table tests were conducted, concluding that the static and dynamic friction coefficient is of the order of 0.10 and 0.07, respectively. The same researchers (Yegian et al., 2004b) investigated the idea of such a sliding surface within the foundation soil, forming an isolated soil prism of ellipsoidal shape.

Based on this idea, Georgarakos & Gazetas (2006) parametrically investigated the effect of the sliding surface geometry on the seismic response. Several geometries were investigated, ranging from cylindrical, to basin-shaped, trapezoidal, and trapezoidal with wedges. The latter was found to be the optimum solution, providing the restoring force of the cylindrical surface, while being significantly easier to construct. The systems functionality is based on the ability of the isolated soil to slide on the synthetic liner, while the two wedges offer the necessary restoring force through their weight. The response of this system can be seen as mechanically analogous to a mass sliding on a horizontal surface, being restrained by two springs that work only when compressed.

The investigated system is schematically illustrated in Figure 1. The geometry of the isolation system is trapezoidal, with isolated wedges on the two sides. The synthetic liners are

placed at a depth  $H = 2$  m under the surface. The slope of the excavation trench is assumed equal to 1:1 – a realistic assumption for relatively competent soil. The isolated embankment comprises a dense gravel layer. The latter is modeled with a nonlinear constitutive model, with a Mohr-Coulomb failure criterion and non-associative flow rule. A rather large Young's modulus  $E = 500$  MPa is assumed, while the friction and dilation angles are equal to  $\varphi = 48^\circ$  and  $\psi = 15^\circ$ , respectively. The two wedges are filled with pumice, a light-weight material of density  $\rho = 1$  Mg/m<sup>3</sup> and relatively small stiffness  $E = 10$  MPa, in order to impose the minimum possible resistance to the sliding motion of the embankment.

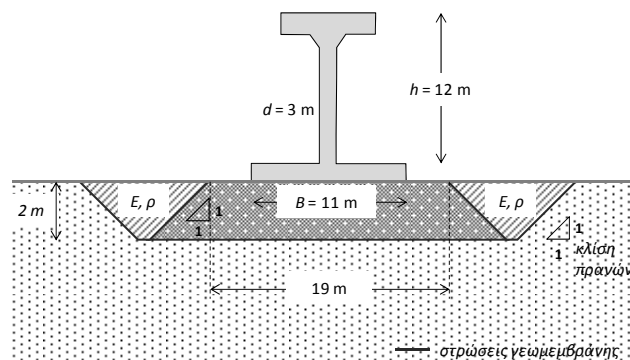


Figure 1. Schematic illustration of the in-soil isolation system under consideration.

The superstructure, an idealized bridge pier (for simplicity), is placed on top of the isolated embankment. The bridge pier is designed according to EC8, assuming a design acceleration  $a_{gr} = 0.24g$  and behavior factor  $q = 2$ . Having an elastic natural period  $T = 0.48$  sec, the design spectral acceleration is equal to  $SA = 0.3g$ . In order to undertake the resulting design bending moment  $M_D = 43$  MNm, a longitudinal reinforcement of  $100\Phi 32$  is required, combined with transversal reinforcement of  $\Phi 32/8$ cm.

## 2 NUMERICAL METHODOLOGY

The problem is analyzed employing the finite element code ABAQUS. The geometry and the key aspects of the model used in the analyses are presented in Figure 2. Assuming plain strain conditions, a representative "slice" of the soil-foundation-structure system is examined, taking account of material (soil and superstructure) and geometric (footing uplift, sliding, and P- $\delta$  effects) nonlinearities.

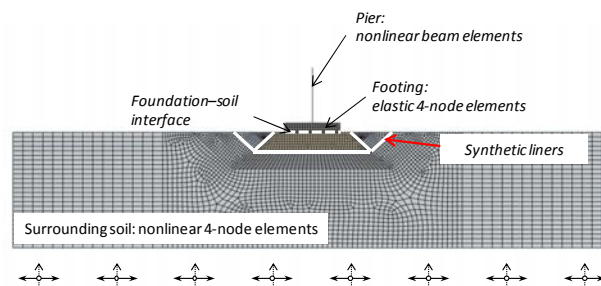


Figure 2. The finite element model used in the analyses: plain strain conditions are assumed, considering material (soil and superstructure) and geometrical (sliding, P- $\Delta$  phenomena) nonlinearities.

The soil is modeled with 4-noded continuum elements. The soil behavior is modeled through a nonlinear constitutive model with Von Mises failure criterion, nonlinear kinematic hardening and associated plastic flow rule. The footing is modeled with elastic 4-noded continuum elements with  $E = 30$  GPa. Beam elements are used for the pier, with their nonlinear behavior being modeled with a kinematic hardening model (Gerolymos et al., 2005), similar to that of the soil.

Model parameters are calibrated against moment–curvature relations of the reinforced concrete pier, computed through section analysis utilizing the XTRACT software (Imbsen & Assoc., 2004). The deck is represented by a mass element, and the contact between the different parts of the model (footing, embankment, wedges, surrounding soil) is modeled with a special interface that allows realistic simulation of possible sliding and detachment.

### 3 DYNAMIC RESPONSE OF THE ISOLATION SYSTEM

Initially, the in-soil isolation system is subjected to idealized Ricker pulses of characteristic frequency  $f = 2$  Hz and gradually increasing maximum acceleration (0.1g to 0.5g). Both the fully SSI problem as well as the free-field problem (i.e., ignoring the presence of the superstructure) are analyzed.

In Figure 3 the response of the isolation system is presented in terms of maximum acceleration at the top of the isolated embankment with respect to the maximum acceleration at the surface of the non isolated free-field (PGA), both in and without the presence of the pier. Evidently, the effectiveness of the in-soil isolation system depends on the presence of the superstructure. Maximum acceleration at the top of the isolated embankment does not exceed 0.2 g without the superstructure on top. On the other hand, the presence of the pier leads to an increase in the acceleration, which in this case ranges between 0.28 g and 0.33 g.

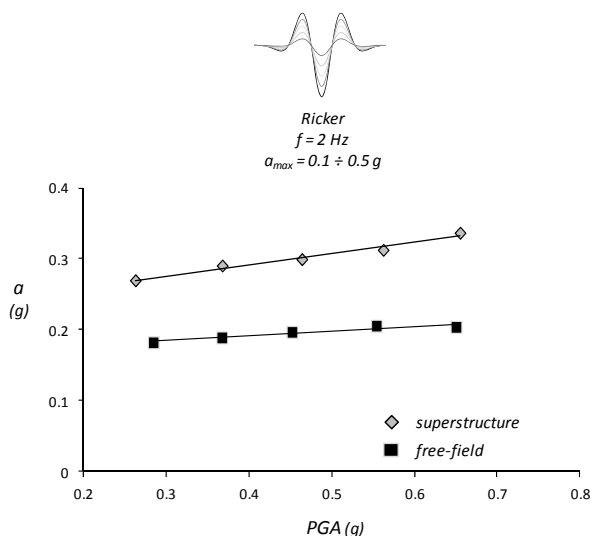


Figure 3. Maximum acceleration at the top of the isolated embankment with respect to the maximum acceleration at the surface of the non isolated free-field (PGA), with and without the presence of the pier. The bedrock excitation is an idealized Ricker wavelet of characteristic frequency  $f = 2$  Hz, and gradually increasing maximum acceleration (from 0.1g to 0.5g).

In Figure 4 the deformed mesh with superimposed displacement contours, showing the deformation of the system when in the presence of the pier and without it. The deformation scale factor applied is deliberately large, in order to highlight the difference between the two cases examined. Observe the aforementioned increase in the acceleration that passes through the isolation layer, which is due to its deformation by the vertical pressures which are imposed by the weight of the pier. As a result, the isolated embankment is forced to slide on a curved surface, rather than a horizontal one. Consequently, the acceleration that is required for slippage is increased substantially, reducing the effectiveness of the isolation system.

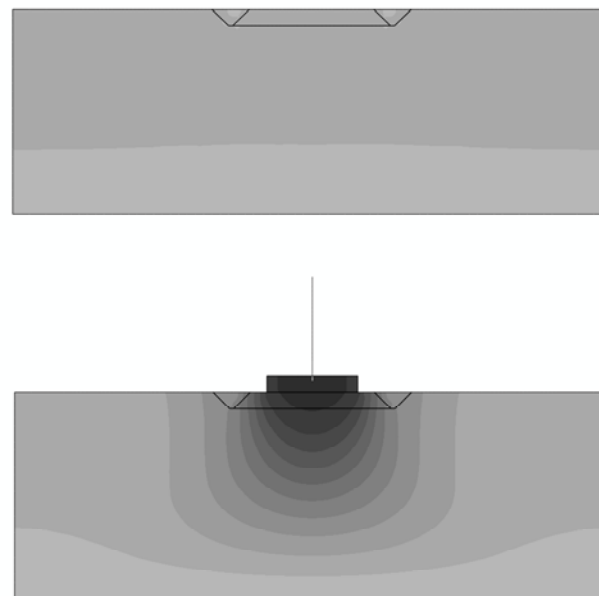
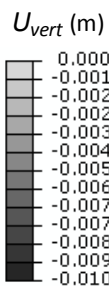


Figure 4. Deformed mesh with superimposed vertical displacement contours considering the superstructure on top of the isolated embankment and without it. (deformation scale factor = 100).

### 4 EFFECTIVENESS OF IN-SOIL SEISMIC ISOLATION SYSTEM SUBJECTED TO REAL RECORDS

The model is subjected to a seismic scenario significantly exceeding the design. The Takatori record (Kobe, Japan 1995) is used as seismic excitation. As seen in Figure 5, the Takatori record is a quite adverse case seismic event: the maximum recorded acceleration was 0.61g, while their spectral values substantially exceed the design accelerations of the pier throughout the entire period range.

In Figure 6a comparison between the response of the isolated pier using the in-soil isolation system and the response of the conventionally designed pier subjected to the Takatori record is presented. Figure 6a compares the acceleration time histories at the base of the pier for each of the two alternatives. Notice that without the proposed seismic isolation, the pier is subjected to a maximum acceleration of almost 1 g. On the other hand, the favorable effect of the application of the in-soil isolation system becomes apparent, since in that case the pier is subjected to maximum acceleration of only 0.35 g at its base. This decrease in the maximum acceleration may not be adequate to reduce the required reinforcement of the pier, yet it proves to be salutary for the survival of the pier.

As depicted in Figure 6b, where the bending moment–curvature response at the base of the pier is presented, plastic hinging quickly forms at the base of the pier, leading to intense accumulation of curvature, than in turn causes the pier to exhaust its ductility capacity and ultimately to collapse. In stark contrast, the seismically isolated pier may reach the moment capacity, yet there is no significant inelastic response, indicating that the pier remains almost intact

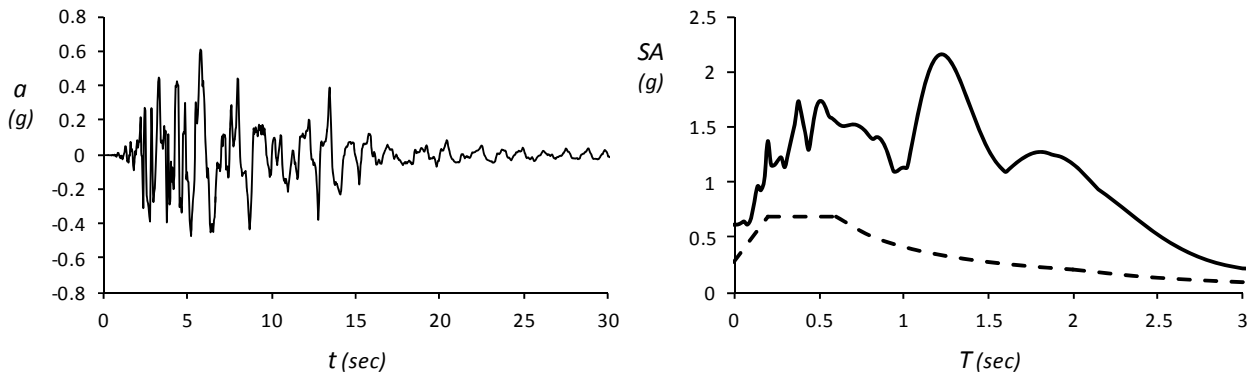


Figure 5. The Takatori record from the Kobe earthquake (Japan 1995) and its elastic response spectrum compared to the pier design spectrum.

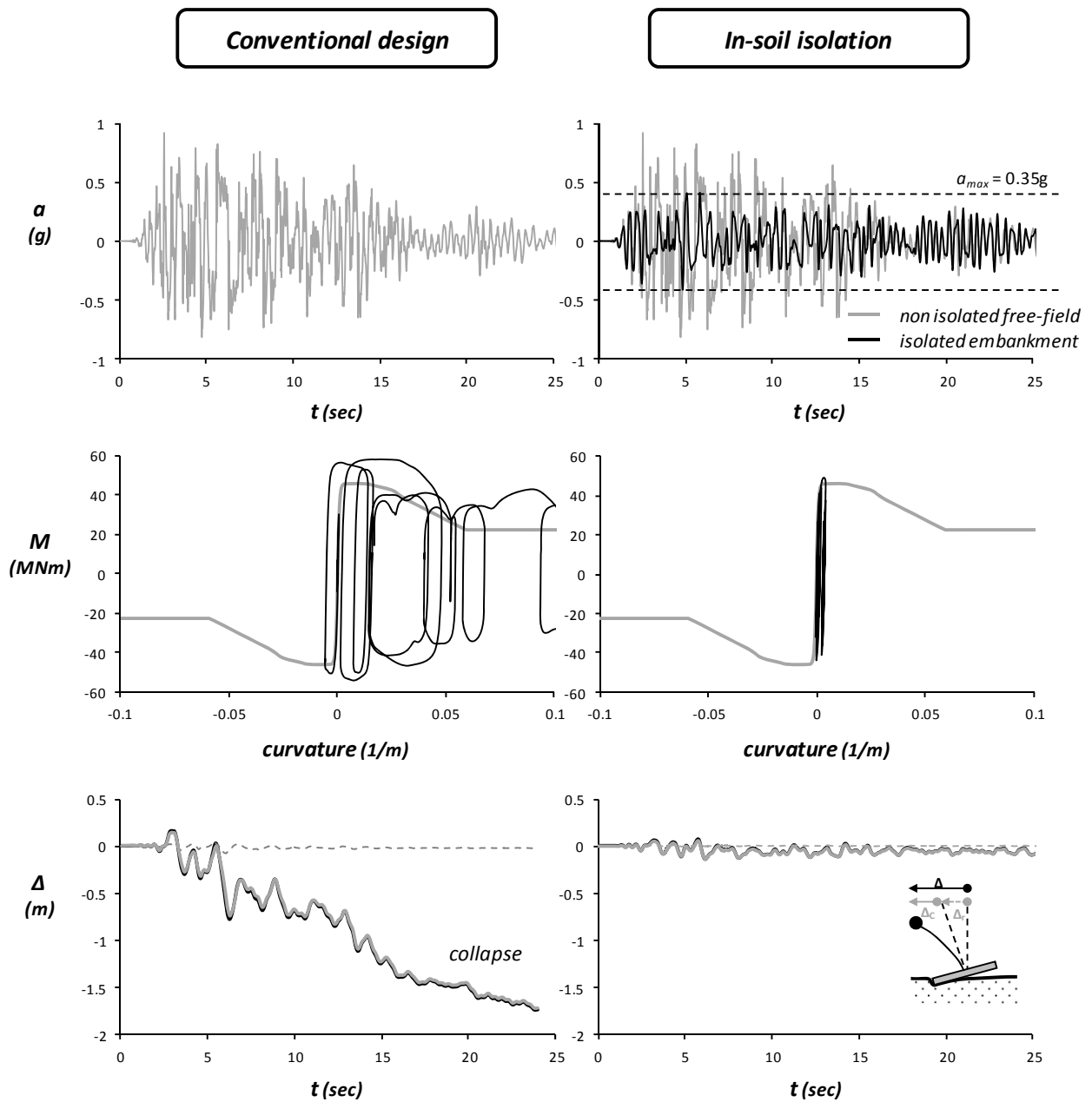


Figure 6. Comparison of the two alternatives: conventionally designed pier response versus pier response with application of the in-soil isolation system (a) Acceleration time histories at the base of the pier. (b) Moment – curvature response at the pier base and (c) time histories of deck drift  $\Delta$ .

after the end of the excitation. Finally, in Figure 6c the time histories of deck drift  $\Delta$  are presented. The conventionally designed pier accumulates horizontal offset towards the one direction and ultimately collapses. On the other hand, the pier founded on the in-soil seismic isolation system survives this extremely strong seismic scenario with maximum drift during the excitation  $\Delta = 0.1$  m, and consequently with limited if any damage. In summary, the in-soil seismic isolation system proves to be an effective measure of fuse mechanism, in case of an extreme seismic loading, preventing pier collapse.

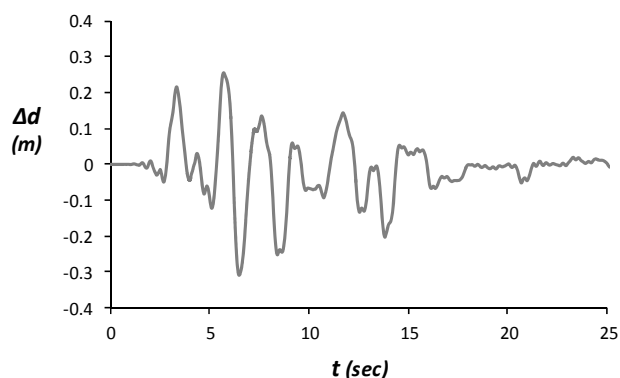


Figure 7. Time history of the relative displacement of the embankment top compared to the non isolated free field.

The beneficial function of the in-soil isolation system comes, however, with a drawback. The system is designed to impose a cut-off at the acceleration that is transmitted to the superstructure, materialized through embankment sliding. This means that excessive slip displacement may occur at the synthetic liner layer that translates to significant relative displacement of the structure compared to the non isolated free-field soil surface. This may be of importance, especially for long structures, such as bridges, where the superstructure is founded on several supports that cannot be isolated at the exactly the same manner. In Figure 7, the time history of the relative displacement of the embankment surface compared to that of free field is presented. During this admittedly excessively strong seismic shaking, the embankment is subjected to a significant relative displacement compared to the non isolated free-field, with a maximum displacement  $\Delta d = 0.3$  m. Although such a differential displacement may be tolerable, it has to be carefully taken into account during design.

#### 4 CONCLUSIONS

The main conclusions of this study can be summarized as follows:

- The application of the in-soil isolation system proves to have a rather beneficial effect on the seismic performance of the superstructure (at least for the idealised bridge pier examined herein). Although the decrease of the maximum acceleration that is transmitted to the superstructure is not adequate to allow the design of the pier for reduced seismic loads, it proves to quite effective in ensuring its survivability.
- The effectiveness of the isolation system depends on the presence of the superstructure. The sliding surface is curved due to the pier imposed additional stresses, demanding in this case from the isolated embankment to slide on an inclined surface rather than a horizontal one. As a result, the acceleration needed for the slip displacement to occur increases, rendering the isolation system less effective
- Since this isolation system relies on slip displacement at the base of the isolated embankment to impose a cut-off at the transmitting onto the superstructure accelerations, significant relative to the non isolated free field should be expected and taken into account during design.

#### 5 REFERENCES

- Georgarakos P., Gazetas G., (2006) "In-soil Seismic Isolation using Synthetic Liners", Proceedings of the 5th Hellenic Conference on Geotechnical and Geoenvironmental Engineering, Xanthi, Greece.
- Anastasopoulos I., Gazetas G., Loli M., Apostolou M., Gerolymos N. (2010), "Soil Failure can be used for Earthquake Protection of Structures", *Bulletin of Earthquake Engineering*, Vol. 8, pp. 309–326.
- Anastasopoulos I., Gelagoti F., Kourkoulis R., Gazetas G. (2011), "Simplified Constitutive Model for Simulation of Cyclic Response of Shallow Foundations : Validation against Laboratory Tests", *Journal of Geotechnical and Geoenvironmental Engineering*, ASCE (in print).
- EC8 (2000), Design provisions for earthquake resistance of structures, part 5: foundations, retaining structures and geotechnical aspects, prEN, 1998-5 European Committee for Standardization, Brussels.
- Imbsen & Associates, Inc. (2004), XTRACT—Cross section analysis program for structural engineer, Ver. 3.0.3, California.
- Yegian, M. and Kadakal, U. (2004). "Foundation Isolation for Seismic Protection Using a Smooth Synthetic Liner." *J. Geotech. Geoenviron. Eng.*, 130(11), 1121–1130.
- Yegian M., Catan M. (2004) Soil Isolation for Seismic Protection Using a Smooth Synthetic Liner. *Journal of Geotechnical and Geoenvironmental Engineering* 130:11, 1131-1139
- Vintzileou E., Tassios T.P., Chronopoulos M. (2007), "Experimental validation of seismic code provisions for RC columns", *Engineering Structures*, 29, pp. 1153-1164.

## Bridge foundation on very soft alluvia with stone column ground improvement

### Fondation de pont sur alluvions très molles et amélioration du sol avec des colonnes ballastées

G. J. Vlavianos Civil Engineer, M.Sc., & A.K. Marinelli Civil Engineer, Ph.D.

Ministry of Development, Competitiveness, Infrastructure, Transport and Networks, Greece

K. Andrianopoulos  
Civil Engineer, Ph.D.

S. Foti  
Geologist, Ph.D.- Civil Engineer, B.Sc., Geosynolo Ltd.

**ABSTRACT:** The present paper proposes technical solutions for a road design project comprising both bridges and high embankments in the Region of Western Greece, where major geotechnical issues had to be dealt with. The very low P-y reaction of the soft silty clays and the eventual liquefaction of the silty sand layers embedded within the foundation soil, the high ground water table and the high seismicity of the area, led to the decision to improve the top part of the natural soil given the necessity for an acceptable solution in terms of both dimensions and cost. Among other possible methods of soil improvement, the application of stone columns followed by preloading was selected. A comparative parametric stability analysis of the bridge embankments and the pile foundations for bridge piers, with or without the presence of stone columns, quantified the benefits from the proposed ground improvement method and verified that the completion of this project is feasible within acceptable performance, safety and cost limits.

**RÉSUMÉ :** La présente communication propose des solutions techniques pour l'élaboration d'un projet des routes qui contient des ponts et des hauts remblais dans la région de la Grèce occidentale où des problèmes géotechniques importants fallait être confrontés. La très basse réaction P-y des argiles limoneuses molles et la liquéfaction éventuelle des couches du terrain formées de sables limoneux qui sont contenues dans le sol de la fondation, la nappe phréatique élevée et la haute séismicité de la région, ont conduit à la décision d'améliorer la partie supérieure du sol naturel en prenant en considération la nécessité de trouver une solution acceptable en ce qui concerne les dimensions et le coût. Permis d'autres méthodes d'amélioration du sol, il a été choisie celle des colonnes ballastées suivie d'un chargement préalable du sol. Une analyse paramétrique comparative de stabilité des remblais des ponts et des fondations sur pieux des piliers des ponts avec ou sans la présence des colonnes ballastées, présente quantitativement des profits obtenus par l'utilisation de la méthode d'amélioration du sol proposée et vérifie que l'achèvement de ce projet est réalisable avec une performance acceptable, sécurité et coût limité.

**KEYWORDS:** road project, bridge foundation, soft alluvia, liquefaction, ground improvement, stone column, preloading.

## 1 INTRODUCTION

A significant project for road infrastructure is currently under way in western Greece, prefecture of Aitolokarnania, concerning the construction of a 13,1km part of a public provincial road connecting the municipality of Astakos to the bridge of Gouria.

Owner of the project is the Greek State and the Supervising Authority is the Directorate of Studies for Road Works, General Directorate of Road Works, Ministry of Development, Competitiveness, Infrastructure, Transport and Networks. Following the necessary competitive procedure, the design of the project was assigned to a joint scheme of

specialized design offices, covering the involved scientific areas.

This paper focuses on the technical solutions proposed for the geotechnical issues that arose with reference to the stability of embankments and bridge foundation.

## 2 PROJECT OVERVIEW

The importance of this project lies in its expected contribution to the improvement of road access towards western Aitolokarnania and mainly the touristic zone of Astakos-Mytikas-Palairios. It is also anticipated to take over some of the traffic load of other local axis and to support the increase in use of an existing tunnel nearby. What is more important though, is the expected traffic load assumption for the shipbuilding and industrial zone of Astakos, which in the future will be the base for development in the whole area.

The realization of the project will improve the accessibility of the area and will facilitate road connection between cities and existing or planned infrastructure, decreasing time demands and improving safety and comfort requirements

This road axis under study forms a part of the connection of Astakos and the port of Platygiali with the major motorway of "Ionia Odos", passing through the bridge of Gouria and the existing tunnel of Saint Elias. The road section is 11,0m wide (1 lane per direction). From geotechnical point of view, it is to be mentioned that the whole project comprises 6 bridges (15-105m long) and a significant length of embankments between 2 and 7 meters high.

Major geological and geotechnical issues that arise for the last 10km of the road are related to the very low altitude of the ground and the lack of inclination, the high ground water table, the insufficient drainage system and the presence of silty clays and sands, often with high content of organics. The whole situation is aggravated by the liquefaction potential of the silty sand layers embedded within the foundation soil, in connection with the high seismicity of the area.

During the preliminary design stages, it became obvious that the most significant geotechnical problems for the realization of the project would be related to the load bearing capacity of the soil, the expected subsidence under static loading and the eventual liquefaction phenomena.

## 3 GEOTECHNICAL CONDITIONS

The area where the bridge foundation will be constructed consists of soft and compressible saturated alluvial soils, while the water table is located at ground level. The prevailing geotechnical conditions at these areas can be simplified in two main profiles.

Soil profile I (Fig. 1) is encountered in the majority of the bridge sites. Its main characteristic is the surficial layer of fine-grained medium plasticity soil. According to the geotechnical exploration results, this soil layer consists mainly of low to medium plasticity silts (ML) and clays (CL), with thin layers of high plasticity silts (MH), fat clays (CH) and organic clays (OL). The thickness of this layer varies between about 22.5 to 35m. Below this layer, to the depth of 40m, either a medium to dense non-cohesive soil unit (SC, SM) or a dense cohesive soil unit (CL) are present. Rock or any other rock-like geological formation was not encountered at any of the locations explored.

Figure 2 presents an estimation of the undrained shear strength of the surficial fine-grained soil unit of Profile I, based on the results of typical CPT & SPT recordings. An estimation of undrained shear strength for normally consolidated clays is also presented, based on Jamiolkowski et al. (1985) (see Eq.1):

$$S_u = 0.25 \sigma'_{vo} \quad (1)$$

where  $\sigma'_{vo}$  is the geostatic effective vertical stress. Comparing these two estimations, it is concluded that the surficial fine-grained layer is normally or even at some depths under-consolidated, with low values of undrained shear strength. Thus, the bearing capacity of this formation is considered low and significant settlements are expected during loading, with the necessary consolidation time to exceed the acceptable time limits (horizontal coefficient of consolidation ranging between  $c_h=7 \times 10^{-7} - 9 \times 10^{-6} \text{ m}^2/\text{sec}$  based on CPTu dissipation tests). The lateral resistance of this layer is also considered very low, leading to large horizontal displacements and structural forces, especially during seismic loading.

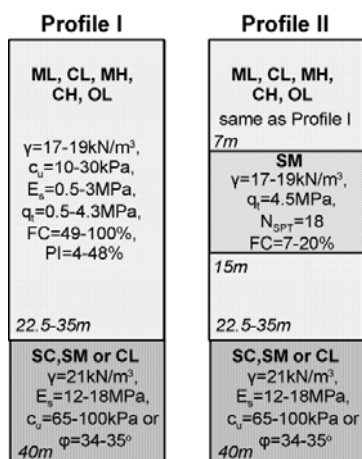


Figure 1: Representative geotechnical profiles

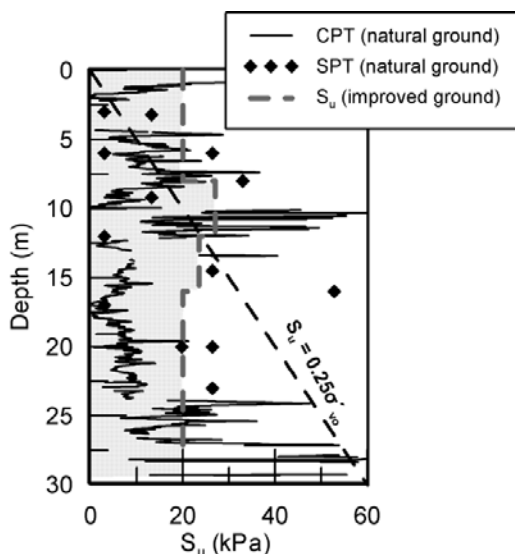


Figure 2: Distribution of undrained shear strength with depth for profile I conditions, before and after the improvement

With regard to the seismic response, profile I belongs to group type S1 according to EC8. The average shear wave velocity  $V_{s,30}$  generally ranges between 85 and 140m/sec, as computed from the CPT recordings:

$$G_{\max,0} = (q_t - \sigma_v) \times 0.0188 \times 10^{0.55I_c + 1.68} \quad (2)$$

where  $I_c$  is a soil behavior type index (Robertson, 2009). Thus, special study is required for the definition of the seismic action, which will take into account the non-linear response of the soil layers and the dependence of soil moduli and internal damping on cyclic strain amplitude.

Profile II (Fig. 1) represents the soil conditions prevailing at one bridge site. The soil conditions resemble those of Profile I, with the exception of an 8m thick layer of loose silty sand that interrupts the surficial fine-grained formation. This non-cohesive formation (SM according to USCS) is relatively close to ground surface (at the depth of 7m), while it is classified as non-plastic, with fines content between 7 and 20% and potentially liquefiable under seismic conditions.

A preliminary liquefaction analysis with NCEER methodology (Youd et al. 2001) for CPT recordings revealed that this non-cohesive formation is liquefiable. As shown in Fig. 4, the factor of safety against liquefaction is well below unity for the silty sand layer, revealing its high liquefaction potential. Hence, although this soil layer presents higher stiffness ( $V_{s,30}=140\text{m/s}$ ) and bearing capacity for static loading, as compared to the clay layer, its liquefaction potential deteriorates its mechanical properties. Thus, during earthquake loading, loss of bearing capacity, lateral stiffness degradation and settlements are expected to occur, increasing this way superstructure displacements and structural forces. Furthermore, Profile II is now characterized as Group type S2 according to EC8 and special study is needed to define the seismic action and the exact liquefaction potential.

#### 4 DESIGN CONCEPT

As a result of the existing poor soil conditions, the foundation of the foreseen bridge piers on surface foundations was excluded and was replaced by a group of piles with a rigid pile cap. However, due to the high seismicity of the area, the very low P-y reaction of the soft silty clays and the eventual liquefaction of the silty sand layer led to extreme internal forces of the piles and increased disproportionately the cost of the project. Hence, the necessity of an acceptable solution in terms of both dimensions and cost, led to the decision to improve the top part of the natural soil.

Among a number of possible methods of soil improvement that were examined, it was decided to proceed with the application of gravel piles followed by preloading. Plastic drains are also prescribed to act as secondary drainage system for greater soil depths.

The main aim of pre-loading was to increase the undrained shear strength of the surficial fine-grained soil unit. The improved undrained shear strength (when the increase of effective stress due to surcharge exceeded 10% of its initial value), was estimated according to Eq. 4:

$$S_{u,f} = S_{u,0} \text{OCR}^{0.8} \quad (3)$$

with  $S_{u,0}$  reflecting the anticipated undrained shear strength for normally consolidated clays (see Eq. 2). The increase of effective vertical stress at each depth was computed according to the well known Westergaard solutions, taking into account the increase of soil stiffness at upper layers, where gravel pile installation accompanies preloading. The effect of pre-loading reduces with depth, while a percentage of the surcharge load is used for the increase of OCR, due to the distribution of the external load between gravel piles and original soil. Despite that, the anticipated increase of undrained shear strength at upper layers (i.e. at layers that are crucial for the overall safety of the bridge embankments) is considered substantial, while its secondary effects such as the acceleration of consolidation at layers that were found under-consolidated and the reduction of downdrag forces at piles (i.e. by allowing the consolidating soil to settle before construction) increase its efficiency. The prescribed pre-loading embankment were wider from the bridge embankment / pile cap by 2.5-3.0m at each side, in order to apply uniform stress at the area of interest, while its height generally varies between 3 and 7m.

Stage construction of pre-loading embankment was decided (with height increments between 1.5-2.0m), due to the poor soil conditions, followed by continuous settlement and pore-pressure dissipation recordings. Figure 2 presents the anticipated final (after improvement) distribution of  $S_u$  with depth for the CPT recording presented in Section 3.

Gravel pile installment is prescribed ahead of preloading, consisting of 0.80m diameter piles in a 1.80 x 1.80m square arrangement (denoting replacement percentage equal to  $a_s = 0.78 \times (0.8/1.8)^2 = 15.4\%$ ). Gravel pile length varies between 8 and 13m, depending on soil conditions.

The installation of gravel piles increased the mechanical properties of the upper cohesive fine-grained layers and subsequently increased the general stability of bridge & preloading embankments. The following equivalent strength parameters were used (Van Impe & De Beer, 1983):

$$c_{eq} = (1-a_s) S_{u,f} \quad (4a)$$

$$\tan\phi_{eq} = [na_s / (na_s + 1 - a_s)] \tan\phi_1 \quad (4b)$$

where  $c_{eq}$  &  $\phi_{eq}$  denote the equivalent cohesion & friction angle of the composite system respectively,  $\phi_1$  denotes the friction angle of gravels (assumed equal to  $42^\circ$ ),  $a_s$  denotes the replacement ratio (equal to 0.154) and  $n$  denotes the ratio of the load taken by the gravel pile versus the surcharge load. The contribution of geostatic stresses is omitted; while outside the embankment limits (where no surcharge is applied)  $n$  equals 1.0. The improved shear strength of the composite system, combined with the increase of the undrained shear strength due to preloading proved adequate for the construction of the bridge embankments with acceptable factor of safety under both static and seismic conditions (e.g. the static F.S. increased from 0.64 to 1.51 for a representative height of 4m).

Note that, besides the improvement of shear strength characteristics, the inclusion of gravel columns combined with pre-loading has altered the seismic ground response relative to free-field. In order to take into account this effect, the shear wave velocity and the spring stiffness in P-y curves of the relevant soil layers were appropriately increased. Namely, the formula presented by Baez & Martin (1993) was used for the estimation of the maximum shear modulus of the composite system:

$$G_{max,eq} = G_{max,i} a_s + G_{max,p} (1-a_s) \quad (5)$$

where  $G_{max,eq}$  is the maximum equivalent shear modulus,  $G_{max,i}$  is the maximum shear modulus of the fine-grained layer after preloading,  $G_{max,p}$  is the maximum shear modulus of the gravel pile and  $a_s$  is the replacement ratio (here 0.154). The maximum shear modulus of the fine-grained layer after pre-loading was computed as follows (Weiler, 1988):

$$G_{max,i} = G_{max,o} OCR^{0.5} \quad (6)$$

where  $G_{max,o}$  is the maximum shear modulus of unimproved soil, as computed by Eq. 2. The maximum shear modulus of the gravel pile was computed assuming a dense configuration ( $e=0.55$ ). Figure 3 presents the shear wave velocity profile of the composite system for the CPT recording of Fig. 1. The average shear wave velocity  $V_{s,30}$  for this profile increased from 86 to 140m/s, reflecting stiffer ground conditions. This increase was also implemented to the P-y curves, by increasing the horizontal subgrade reaction coefficient  $k$ . The increase was assumed proportional to the ratio  $G_{max,eq}/G_{max,o}$ , while for the unimproved soil coefficient  $k$  was computed according to DIN4014 for bored cast-in-place piles.

For the case of Profile II, where a non-cohesive liquefiable layer is present, the gravel piles are expected to act as a countermeasure against liquefaction. The gravel piles will

be constructed via bottom-feed vibro-replacement, while a proper gradation curve range is prescribed in order to ensure the effective drainage of earthquake-induced excess pore-pressures. During vibro-replacement, the non-cohesive layer is expected to be densified and increase its resistance to liquefaction. Based on Mizuno et al. (1987), the average measured tip resistance is expected to increase between gravel piles from 4.5MPa to 9.5MPa, providing an adequate liquefaction resistance. Figure 4 compares results from the preliminary (before improvement) and the detailed (after ground improvement) liquefaction study, which show the minimization of liquefaction potential. The densification of the non-cohesive layer due to pre-loading and the potential dissipation of excess pore pressures were conservatively ignored. It is noted that even if densification was ignored, drainage through gravel piles would retain excess pore pressure ratio  $r_u$  well below 0.5, as computed according to Seed & Booker (1977) and Bouckovalas et al. (2011) for the given characteristics and gravel pile geometry.

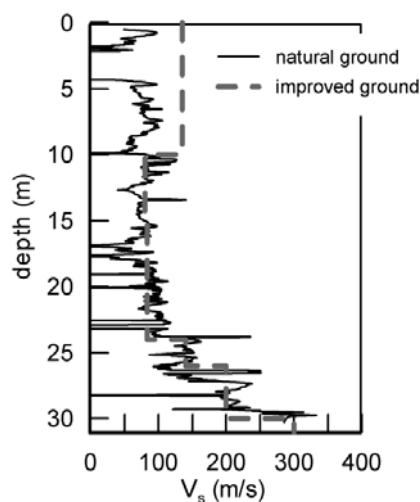


Figure 3: Distribution of shear wave velocity with depth for profile I, before and after the improvement

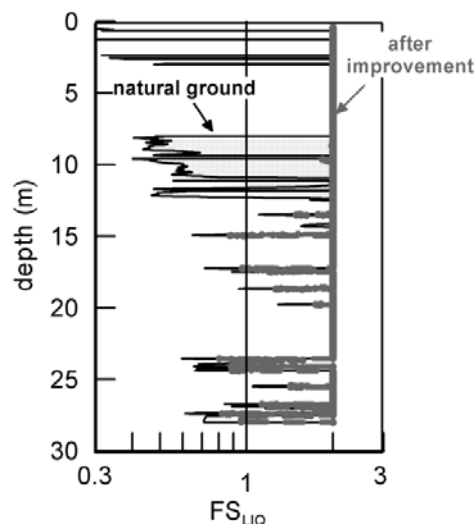


Figure 4: Factor of safety against liquefaction for Profile II, before (preliminary results) and after improvement (detailed study).

Finally, consolidation process is expected to be accelerated with the presence of gravel piles. Excess pore pressures for each loading stage are expected to diminish within 19 days, assuming conservatively only radial flow towards the gravel piles and horizontal coefficient of consolidation equal to  $c_{h1} = 7 \times 10^{-7} m^2/s^2$ . The actual consolidation time is expected to be even lower, considering the actual 2D water flow, the presence of horizontal layers of higher permeability and the

additional discharge from the secondary pipe drains that are prescribed.

## 5 SEISMIC GROUND RESPONSE ANALYSES

Besides ground improvement, detailed ground response analyses were also crucial for the successful completion of the project. Since, both Profile I & II belong to group type S1 & S2 according to EC8, special study was necessary to define the proper seismic action and the exact liquefaction potential. Thus, 1D equivalent linear analyses were performed with the equivalent-linear frequency domain method (e.g. Schnabel et al. 1972). Modulus reduction and hysteretic damping curves were used as a function of cyclic strain amplitude (Vucetic & Dobry, 1991), and introduced the non-linear behavior of soil layers in ground response analyses, according to its layers' plasticity index. According to EC8 provisions, three different accelerograms were used, which cover a wide range of frequencies and are representative of the seismic region.

Shear wave velocities of the improved ground were computed according to Eq. 5, while the peak ground acceleration at bedrock outcrop was calibrated to 0.24g, according to the Greek Annex of EC8 for the area under investigation. Since no bedrock was found, artificial bedrock was used at the end of each borehole, while the bedrock shear wave velocity was assumed to range between 300 and 550m/s, providing a high impedance ratio compared with the soil column characteristics. Thus, radiation damping was conservatively minimized. Fig. 5 shows representative results from ground response analyses conducted in Profile II. Significant de-amplification of the seismic motion is observed, due to the flexibility of the soil column but also due to the non-linearity exhibited by the soil layers. The computed peak ground acceleration at ground surface ranges between 0.20 to 0.24g, significantly lower from the 0.32g required by EC8 for the flexible soil type D. Thus, the structural forces due to seismic loading were significantly reduced, while the factor of safety against liquefaction was substantially increased.

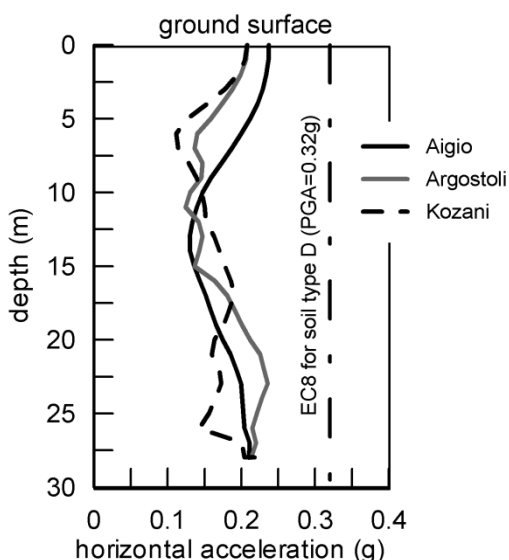


Figure 5: Distribution of peak ground acceleration with depth for Profile II using three different accelerograms.

## 6 CONCLUSION

The present paper presents details of the technical solution proposed for a road design project in Western Greece, where major geotechnical issues had to be dealt with for the foundation of bridges and high embankments. Geotechnical investigations revealed very poor soil conditions consisting of silty clays and sands, often with high content of organics, and high ground water table that locally appeared

on the ground surface. As a result, the foundation of foreseen bridge piers on surface foundations was excluded and was replaced by a group of piles with a rigid pile cap. Among a number of possible methods of soil improvement that were examined, it was finally decided to proceed with the application of stone columns followed by preloading. This way, the following were accomplished:

- increase of the general stability of the bridge embankments
- increase of the bearing capacity of foundation soil layers
- reduction of internal forces of piles
- acceleration of the stage of primary consolidation of silty clay-sands and
- reduction of the liquefaction potential of sandy layers.

All of the above effects were verified by site-specific computations and implemented to the design of the relevant works

## 6 ACKNOWLEDGEMENTS

Authors acknowledge the assistance of Harris Lamaris, Civil Engineer M.Sc. on the geotechnical investigations and the preliminary liquefaction analyses.

## 7 REFERENCES

- Baez J.I., Martin G.R.1993., Advances in the design of vibro systems for the improvement of liquefaction resistance, Symposium on Ground Improvement. Vancouver
- Bouckovalas G., Papadimitriou A., Niarchos D., Tsiapas D. 2011, Sand fabric evolution effects on drain design for liquefaction mitigation, *Soil Dynamics & Earth. Eng.*, 31, 1426-1439
- Jamiolkowski M., Ladd C., Germaine J.T., Lancellota R. 1985. New developments in field and laboratory testing of soils. *IX Intern. Conf. on SMFE*, Vol. 1, 57-154.
- Mizuno Y., Suematsu N. & Okuyama K., 1987. Design method of sand compaction pile for sandy soils containing fines. *Journal of JSSMFE*, 53-56
- Robertson P.K. 2009. Interpretation of cone penetration tests – a unified approach. *Can. Geotech. J.*, 46, 1337-1355
- Schnabel P.B., Lysmer J. and Seed H.B. 1972. SHAKE: a computer program for earthquake response analysis of horizontally layered sites. Report EERC 72-12, Earthquake Engineering Research Center, Univ. of California, Berkeley
- Seed HB, Booker JR. 1977. Stabilization of potentially liquefiable sand deposits using gravel drains. *Journ. of Geotech. Eng., ASCE*, 103 (GT7). 757-768
- Van Impe W., De Beer E. 1983. Improvement of settlement behavior of soft layers by means of stone columns. *Proc. 8<sup>th</sup> European Conf. of SMFE*, Vol. 1, 309-312
- Vucetic M, Dobry R. 1991. Effect of soil plasticity on cyclic response. *Journal of Geotech. Eng. ASCE*, 117 (1), 89-107
- Weiler W.A. 1988. Small strain shear modulus of clay. *Proc. ASCE Conf. on Earth. Eng. & Soil Dyn. II*, New York, 331-335
- Youd et al. 2001. Liquefaction resistance of soils: Summary report from the 1996 NCEER and 1998 NCEER/NSF workshops on evaluation of liquefaction resistance of soils. *Journal of Geotech & Geonv.*, ASCE, 127 (10), 817-833



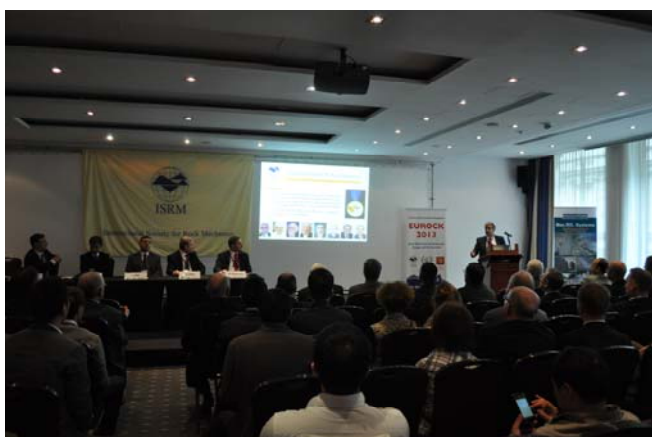
## The 2013 ISRM International Symposium EUROCK 2013

Το συνέδριο πραγματοποιήθηκε από τις 23 έως της 26 Σεπτεμβρίου 2013 στο Βρότσλαβ (Wrocław) της Πολωνίας. Το Βρότσλαβ (Μπρέσλαου μέχρι το 1945) βρίσκεται στις όχθες του ποταμού Οντερ στη νοτιοδυτική Πολωνία, είναι η τέταρτη πληθυσμιακά πόλη και το δεύτερο σημαντικότερο οικονομικό κέντρο της χώρας.

Το συνέδριο διοργανώθηκε από την Πολωνική ένωση Βραχομηχανικής και από το Ινστιτούτο Γεωτεχνικής και Υδραυλικής της σχολής Πολιτικών Μηχανικών του πανεπιστημίου του Βρότσλαβ.



Παρουσιάστηκαν 6 ειδικές ομιλίες από τους καθηγητές: J. Dubinski (PL), P. Berest (FR), J. Hudson (UK), M. Dusseault (CA), X. Li (CN) και H. Konietzky (DE) καθώς και η 2013 ISRM Franklin Lecture από τον Δρ. A. Goricki (AT) και το 2013 Rocha Medal Lecture από τον Δρ. M. Pierce (CN). Επίσης, παρουσιάστηκαν 144 εργασίες προερχόμενες από 33 χώρες, συγκεκριμένα 92 από την Ευρώπη, 27 από την Ασία, 10 από την Β. Αμερική, 8 από την Αυστραλία και 7 από την Ν. Αμερική.



Στις διεργασίες του συνεδρίου συμμετείχαν 268 άτομα από 41 χώρες. Από την Ελλάδα παρευρέθησαν οι: Α. Σοφριανός - Καθηγητής Σχολής Μεταλλειολόγων Μηχανικών ΕΜΠ, Β. Μαρίνος - Επίκουρος Καθηγητής Γεωλογικής Σχολής ΑΠΘ, Δρ. Π. Φορτσάκης, Π. Αστερίου και Κ. Τζιβάκος - Υποψήφιοι

Διδάκτορες Σχολής Πολιτικών Μηχανικών ΕΜΠ και η Α.Μ. Μπαλάση - Όμιλος Τεχνικών Μελετών Α.Ε.

Οι εργασίες με ελληνική συμμετοχή ήταν οι ακόλουθες:

- **Rock engineering design and the evolution of Eurocode 7**, των L. Alejano, A. Bedi, A. Bond, A. Ferrero, J. Harrison, L. Lamas, M. Migliazza, R. Olsson, A. Perucho, Α. Σοφριανός, Η. Stille και D. Virely,
- **Rockfall: Scaling factors for the Coefficient of Restitution**, των Π. Αστερίου, Χ. Σαρόγλου και Γ. Τσιαμπάο
- **Influence of rock mass creep on tunnel loading**, των Π. Φορτσάκη, Α. Καλό, Β. Δεσποτάκη και Μ. Καββαδά,
- **Tunnel behavior and support in molassic rocks. Experience from 12 tunnels in Greece**, των Β. Μαρίνου, Γ. Προυντζόπουλου και Π. Φορτσάκη, και
- **Elastic response of laterally loaded rock sockets using 3D finite element analyses**, των Κ. Τζιβάκου, Μ. Καββαδά και Δ. Καλτσά.



Ο Πέτρος Φορτσάκης κατά την παρουσίαση του άρθρου του

Ο Παύλος Αστερίου, Υποψήφιος Διδάκτορας τομέα Γεωτεχνικής ΕΜΠ, διακρίθηκε μεταξύ των νέων (έως 35 ετών) επιστημόνων και μηχανικών λαμβάνοντας την διάκριση EUROCK Outstanding Paper Award for Young Scientists and Engineers Runner-up, για την εργασία του «Rockfall: Scaling factors for the Coefficient of Restitution».



Ο Παύλος Αστερίου παραλαμβάνει το βραβείο

Στις επόμενες σελίδες παρατίθενται τα προαναφερθέντα άρθρα.

Π. Αστερίου

## Rock engineering design and the evolution of Eurocode 7

L.R. Alejano  
*University of Vigo, Spain*

A. Bedi  
*Imperial College, UK*

A. Bond  
*Geocentrix, UK*

A.M. Ferrero  
*University of Parma, Italy*

J.P. Harrison  
*University of Toronto, Canada*

L. Lamas  
*LNEC, Portugal*

M.R. Migliazza  
*University of Milan, Italy*

R. Olsson  
*NGI, Norway*

Á. Perucho  
*CEDEX, Spain*

A. Sofianos  
*NTUA, Greece*

H. Stille  
*KTH, Sweden*

D. Virely  
*Laboratoire régional des Ponts et chaussées de Toulouse, France*

**ABSTRACT:** The Eurocode for Geotechnical Design, EN-1997-1:2004, informally known as Eurocode 7 or EC7, was fully implemented within the European Union in 2010. This Eurocode is intended to apply to all geotechnical engineering design, including rock engineering. In recognition that all codes must continue to evolve in order to remain applicable, and the long time that such evolution takes, work is already underway under the auspices of the European Committee for Standardisation, CEN, to identify how the code should develop for future revisions. This paper presents a summary of the maintenance procedures for Eurocodes in general and the specific maintenance work currently being undertaken on EC7 in respect of rock engineering design. It also highlights potential future development of EC7, and the need for enthusiastic involvement by the European rock engineering community to direct these developments.

### 1 INTRODUCTION

Standardisation is an integral part of a number of important EU policies that are concerned with better regulation, simplification of legislation, increase in competitiveness and removal of barriers to trade. As a result, the standardisation process is highly developed with the EU.

In the realm of structural engineering, the standardisation process has led to the development of a linked coherent set of standards — the so-called Structural Eurocodes — that govern construction and design.

In this paper we explain the EU's standardisation process, the development and introduction of the standard for Geotechnical Design, EN-1997-1:2004 (CEN, 2004), informally known as Eurocode 7 or EC7, and the manner in which this standard is maintained. We present in detail the maintenance

network that is currently underway, and highlight some issues of long-term, and hence future, importance.

### 2 DEVELOPMENT OF EUROPEAN STANDARDS

Within the EU, the process of standardisation is based on consensus amongst different groups such as industry and public authorities, and is undertaken by independent standards bodies. The development of formal European Standards (EN) is the responsibility of the European Standards Organisations (ESO), of which there are three:

- CEN (Comité Européen de Normalisation/European Committee for Standardisation) which deals with all sectors except electrotechnology and telecommunication;
- CENELEC (Comité Européen de Normalisation Electrotechnique/European Committee for Electrotechnical Standardisation) which deals with electrotechnical standards; and
- ETSI (European Telecommunications Standards Institute) which covers telecommunications and some aspects of broadcasting.

In addition to the formal EN standards, these organisations also produce Technical Specifications, Technical Reports and Guides.

The organisation that has responsibility for standards that apply to rock engineering design and construction is CEN.

#### 2.1 CEN and structural Eurocodes

CEN comprises a number of Technical Committees, of which one—CEN/TC250—is responsible for all of the so-called 'Structural Eurocodes'. These govern all aspects of design and construction related to structural engineering, including geotechnical engineering. The tangible history of the Eurocodes can be traced to 1971, as shown in Table 1.

Table 1. History of Eurocodes.

Year	Event
1971	Public Procurements Directive 1971/305 issued
1975	Eurocode development started
1980	International Inquiry with regard to construction codes performed
1984	First Eurocodes published
1989	Construction Products Directive 1989/106 issued
1990	Work on draft standards (ENVs) started
1992	Publication of ENV Eurocodes commenced
1998	Conversion of ENVs to ENs initiated
2003	EC recommendation on implementation and use of Eurocodes
2004	Directive on Public Works contracts, Public Supply contracts and Public Service contracts issued
2006	Publication of ENs completed
2010	Full EN implementation; conflicting National Standards withdrawn

One aspect of the development shown in Table 1 that is often not grasped is that in 2010 the EN Eurocodes became reference design codes for the purposes of the following: proving compliance with the essential requirements of the Construction Products Directive; offering a basis for specifying contracts; and, giving a framework for drawing up harmonised technical specifications for construction. In As a result, the EN Eurocodes are now the standard technical specification for all European public works contracts, and all designs must demonstrate that they are technically equivalent to an EN Eurocode solution. Taken together, these

statements show that it is critical for designers of rock engineering solutions within the European Union to be fully conversant with the relevant EN Eurocodes.

CEN/TC250 has the responsibility of establishing general policies, programmes and strategies for the Structural Eurocodes, and to oversee their implementation. It also supports and guides its sub-committees in achieving these policies and objectives during any code drafting work.

The membership of CEN/TC250 and its subcommittees comprises delegates of the 29 CEN National Members, together with delegates from the 5 Affiliates (i.e. countries likely to become members of the EU or EFTA) participating as observers. The general structure of CEN/TC250 is shown in Figure 1. In addition to three Horizontal Groups (HG) that work across subject boundaries and a group (WG1) that ensure policy, guidelines and procedures are being followed, there are nine specialist sub-committees each of which is responsible for a particular Eurocode (Table 2). Thus, CEN/TC250/SC7 is responsible for Eurocode 7.

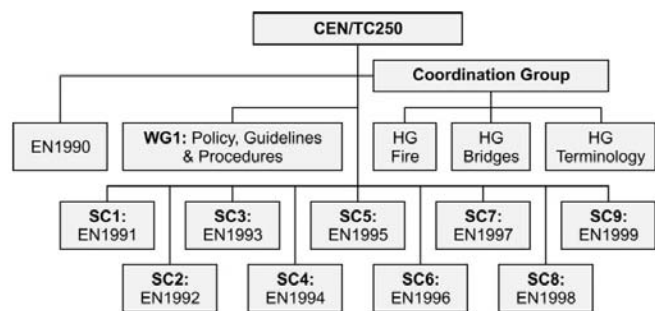


Figure 1. Structure of CEN/TC250 (<http://eurocodes.jrc.ec.europa.eu>).

Table 2. Sub-committees of CEN/TC250 and the Eurocode for which they are responsible.

Sub-committee	Eurocode	Title
SC1	EN1991	Actions on structures
SC2	EN1992	Design of concrete structures
SC3	EN1993	Design of steel structures
SC4	EN1994	Design of composite steel and concrete structures
SC5	EN1995	Design of timber structures
SC6	EN1996	Design of masonry structures
SC7	EN1997	Geotechnical design
SC8	EN1998	Design of structures for earthquake resistance
SC9	EN1999	Design of aluminium structures

### 3 MAINTENANCE OF EUROCODES

In addition to the development of the EN Eurocodes, under the rules governing the operation of CEN, its committees and sub-committees, a critical responsibility is that of code maintenance. This activity is essential in order to preserve the credibility, integrity and relevance of the Eurocodes, as well as to ensure that they do not contain errors.

As a balance between the competing desires of frequent correction and a period of stability that supports industrial implementation, the normal maintenance cycle has been set at five years. Maintenance commences as soon as a draft Eurocode has been accepted (i.e. when an ENV is published as an EN), and comprises all activities connected with the updating of the codes in the light of practical experience of their use. The maintenance process is illustrated in Figure 2 and is arranged as follows:

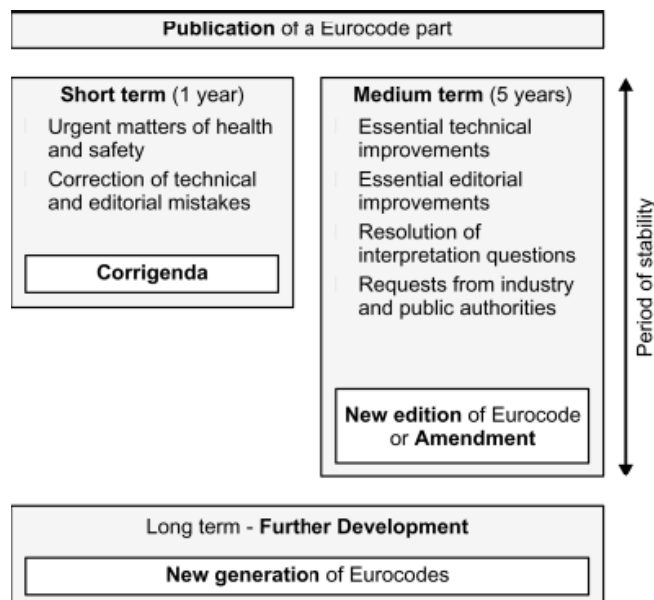


Figure 2. The Eurocode maintenance work programme (<http://eurocodes.jrc.ec.europa.eu>).

- Short term (immediate or within one year). This includes urgent correction of errors, preparation of essential technical amendments with regard to urgent matters of health and safety, essential technical and editorial improvements (e.g. mistakes in symbols, typographical mistakes), elimination of inconsistencies and misleading statements, and resolution of questions of interpretation, resulting from feedback from the use of the Eurocodes.
- Medium term (the normal five-year review cycle). Technical and editorial improvements, the resolution of questions of interpretation, and requests from industrial organisations and public authorities fall into this category. If necessary, a new edition or amendment to the Eurocodes may be published.
- Long term (greater than five years). This contains matters relating to development of new items (e.g. emerging requirements that are not covered by the existing Eurocodes). It includes new material and concepts that require research, and thus may be considered as development.

Thus, CEN/TC250 is now involved in the first of these five-year maintenance cycles, the outline programme for which is shown Table 3.

Table 3. Maintenance programme for the Structural Eurocodes.

Year	Event
2010	March: National Standards withdrawn
2010	May: EU issues programming mandate M/466
2013	October: deadline for receipt of 5-year review comments
2015	October: Draft revisions of Eurocodes available
2018	October: Second generation of Eurocodes available

A key event in this cycle is the publication by the EU of Programming Mandate M/466. Although broad in its content, this specifically asked for the following developments:

- reduction in the number of Nationally Determined Parameters (NDPs);

- incorporation of results from recent international studies, including performance-based and sustainability concepts;
- simplification of rules for limited and well identified fields of application;
- development of auxiliary guidance documents to facilitate implementation

These all support the principles of maintaining credibility, integrity and relevance of the Eurocodes.

#### 4 MAINTENANCE OF EUROCODE 7

In response to Programming Mandate M/466, CEN/TC250/SC7 undertook a survey of National Standards Bodies (NSBs) in order to identify the key maintenance issues regarding EC7. The responses covered the entire range of geotechnical design, but tended to emphasise soil mechanics issues. The ten most popular topics identified for development were:

1. improved guidance on selection of water pressures;
2. simplification/reduction of Design Approaches;
3. guidance on use of numerical modelling;
4. new content regarding reinforced soil;
5. improved general guidance on selecting characteristic soil parameters;
6. improved link to EC8 for seismic design;
7. harmonisation of NDPs;
8. partial factors for different classes of consequence;
9. removal from EC7 Part 2 of material readily found in text books; and
10. improved guidance on buoyancy and hydraulic failure.

Despite the use in item 5 of the word 'soil', items 2, 3, 5, 6, 7, 8 and 9 are directly relevant to rock engineering.

In late 2011 CEN/TC250/SC7 formed a number of Evolution Groups (EGs), shown in Table 4, to further identify both the immediate maintenance requirements and future development of EC7. The membership of the EGs comprises over one hundred experts from industry and academia across the whole of Europe.

Table 4. EC7 Evolution Groups.

Group	Subject	Group	Subject
EG0	Management and oversight	EG1	Anchors
EG2	Maintenance and simplification	EG3	Model solutions
EG4	Numerical methods	EG5	Reinforced soil
EG6	Seismic design	EG7	Pile design
EG8	Harmonisation	EG9	Water pressures
EG10	Calculation models	EG11	Characterisation
EG12	Tunnelling (not convened)	EG13	Rock Mechanics
EG14	Ground improvement		

The subjects represented by these groups clearly correspond with both the wishes of M/466 (e.g. reduction in NDPs, simplification of rules for well identified applications) and the topics identified by the NSBs.

To realise the EGs, in late 2011 SC7 appointed members to EG0, who in turn identified a small number of initial provisional members for each EG. Following this, and with guidance from EG0, each EG revised and expanded its own membership. For each EG, the aim has been to ensure representation from across as much of Europe as possible, subject to the constraint of keeping a modest membership. In accordance with the operating procedures of CEN/TC250/SC7, the membership of all individuals appointed to each EG is required to be ratified by the NSB of the country the individual represents. The current (March 2013) membership of EG 13 is shown in Table 5.

Table 5. Membership of EG13.

Member	Country	Member	Country
L.R. Alejano	Spain	A. Bedi	UK
A. Bond	UK	A.M. Ferrero	Italy
J.P. Harrison	UK	L. Lamas	Portugal
M.R. Migliazza	Italy	R. Olsson	Norway
Á. Perucho	Spain	A. Sofianos	Greece
H. Stille	Sweden	D. Virely	France

As for all EGs, the principal duty of EG13 is to produce by the end of September 2013 a report outlining the medium- and long-term maintenance requirements of EC7.

#### 5 THEWORK OF EG13

In order to develop its work programme and hence the structure its report to EG0, the members of EG 13 sought comments from rock engineering practitioners, held regular teleconferences, and on those occasions when circumstances permitted (e.g. Eurock 2012) small groups of members met in person. In addition, liaison with the other EGs took place both by correspondence and at occasional Convenors' Meetings. The work of EG13 is set out below.

##### 5.1 Interaction with other EGs to improve integration of rock mechanics within EC7

Early in the work of EG13 a general view developed among the members that the integration of rock engineering within EC7 was suboptimal. As a result, it was felt that there was the potential for substantial interaction with the work of the other EGs. The intention was that such interaction would help the other EGs recognise the special design challenges posed by those attributes of fractured rock masses with which rock engineering designers are familiar (e.g. discontinuities, heterogeneity, anisotropy), thereby improving the embodiment of rock engineering requirements within EC7. As a result, interaction took place with EG2, EG3, EG4, EG8, EG10 and EG11.

##### 5.2 Critical review of EC7 with regard to rock mechanics

As written, although many sections of EC7 are directly applicable to rock engineering they either omit to specifically refer to rock engineering or suggest nomenclature, approaches or techniques that are not in general use in rock engineering. This has the effect of making EC7 difficult to apply, or even seemingly inapplicable, to rock engineering. The first of these shortcomings is unintended, and the second manifestly untrue. Thus, a critical review of EC7 was undertaken, specifically to allow identification and suggestions for improvement of those clauses that are deficient with respect to rock engineering practice.

##### 5.3 National Annexes

The detail to which rock mechanics and rock engineering is included within National Annexes varies, possibly as a result of the varying balance of soils to rock engineering within

different countries. Given the deficiencies noted in 5.2 above, a review of all NAs was undertaken to identify those procedures and concepts that could be included within the main body of the code.

#### 5.4 Vocabulary and definitions

In many places, EC7 uses vocabulary and definitions that are inconsistent with those generally encountered in rock engineering. Thus, a thorough review of EC7 was performed in order to identify all vocabulary and definitions that differ from those in customary rock engineering use, and make suggestions for improved wording.

#### 5.5 Design implementation and monitoring

Generally, the rock excavation process (e.g. blasting) leads to an excavation geometry that differs from the one assumed in the design, and may also reduce the strength and stiffness of the surrounding rock mass. Consequently, design implementation is a critical aspect of the rock engineering design process. Associated with this is the issue of monitoring: instrumentation is installed in many rock slopes and most underground openings in order to both guide the construction process and confirm the final performance of the structure. Although both design implementation and monitoring procedures are considered briefly in EC7, they are not covered to the detail required for rock engineering. As such, recommendations are being made regarding improvements to these important aspects.

#### 5.6 Laboratory and field tests

Part 2 of EC7 includes a large number of rock mechanics laboratory and field tests, but the appropriateness of some of these and the comprehensiveness of the list (e.g. there is no guidance on determining the strength of anisotropic rock) is questionable. A list of recommended rock mechanics laboratory and field tests is thus being prepared.

An additional question is whether—as a reference design code—it is necessary for EC7 to refer to other ENs, or whether it can refer to documents such as the ISRM Suggested Methods. This is not a question that EG13 can answer, but it is one that will be presented to SC7.

#### 5.7 Characterisation of rock and rock mass model

Current rock engineering practice is based on the characterisation of rock masses in order to determine appropriate methods of analysis. Unfortunately, EC7 offers insufficient guidance on this critical aspect of engineering practice.

The work of EG13 is to review characterisation philosophies and methods in general rock engineering practice, and identify those that are suitable for inclusion in EC7. In addition, recommendations are being made regarding potential contextual locations (i.e. related to the subject matter, not absolute section numbers) within EC7 for the inclusion of guidance on characterisation methods and their use in rock engineering design.

#### 5.8 Design by prescriptive measures

EC7 suggests that prescriptive measures may be applied in those situations where calculation models are not necessary, and generally 'involve conventional and generally conservative rules in the design, and attention to specification and control of materials, workmanship, protection and maintenance procedures'. Although some countries use prescriptive measures for some rock engineering designs, in general it is not clear to which rock engineering situations this applies or how it connects to the use of empirical or observational approaches, both of which are widely used in rock engineering. These issues are being investigated, and suggestions will be made as to how the concept of prescrip-

tive measures can be clarified and improved with regard to rock engineering.

#### 5.9 Analytical and empirical model

A spectrum of models ranging from the completely analytical through to wholly empirical are used in rock engineering practice, with selection of a particular model for a given project being made by various informal, subjective and *ad hoc* methods. Currently, EC7 gives no guidance on how an appropriate modelling approach should be selected. This is intimately connected with the issue of characterisation described in 5.7 above.

EG13 will make suggestions as to how guidance in respect of model selection could be included in EC7.

#### 5.10 Use of partial factors

As a limit state design code that assumes variability in loads and materials properties is a stochastic phenomenon, EC7 makes extensive use of partial factors to characterise this variability. Although this approach has a long history in structural engineering, and to some extent in soils-related geotechnical engineering, there has been very little development of partial factors in rock engineering. Why this is so is not clear, but it may be due either to a simple lack of the development of such factors by the rock engineering community or the recognition that some characteristic of rock mechanics properties precludes their development. Both of these aspects are being explored by EG13, and the Group's report will offer suggestions as to how the use of partial factors in rock engineering can be clarified.

#### 5.11 Observational method

The observational approach is widely used in rock engineering, and represents a close coupling of the construction and design processes such that both the design and design implementation are continually revised during the construction process. It is not clear that the provisions within EC7 for use of the observational method are properly appropriate for rock engineering works, and so suggestions will be made for improving these provisions.

### 6 FUTURE DEVELOPMENT OF EUROCODE 7

As has been explained above, EC7 is currently undergoing a normal five-year review as part of the standard maintenance cycle. This review will identify medium term revisions. The maintenance cycle also includes long term developments, and it is important that the rock engineering community comes together to identify what is required in this respect. Some required future developments seem clear: for example, EC7 gives no guidance on how to measure and characterise *in situ* stress, nor is it currently applicable to underground excavations (this is one reason why EG12, Tunnelling, was not convened as part of the current five-yearly review). There is also no guidance on the design of rock slopes, which may be the largest single area of work in rock engineering.

The development of EC7 to incorporate these, and other as yet unidentified areas of rock engineering endeavour is a major undertaking that will require many years of dedicated work. By necessity, this work will need to involve the whole rock engineering community of constructors, designers and academics from across the entire EU.

As a first step, and building on the work of EG13, the organisers of Eurock 2014 in Vigo, Spain, are intending to convene a workshop that will hopefully initiate this development. The amount and nature of the work required to develop EC7 for rock engineering means there is the potential for many such meetings in the coming years.

## 7 CONCLUSIONS

The introduction of EC7 will dramatically affect the practice of rock engineering throughout the EU. Although EC7 only became a reference design code in 2010, the first five-yearly cycle of medium term maintenance is now underway. Under the auspices of a CEN Technical Committee, an Evolution Group comprising experts representing a wide number of countries is engaged on identifying those aspects of EC7 that deserve revision. Finally, the long term development of EC7 is yet to be decided, and it seems that the entire rock engineering community within the EU has a critical role to play in this regard.

## ACKNOWLEDGEMENTS

The work undertaken by two earlier members of Evolution Group 13 — namely, Dr Claus Erichsen (Germany) and Dr Tatiani Rotunda (Italy)—is warmly appreciated.

## REFERENCE

CEN (European Committee for Standardisation). 2004. Geotechnical Design: Part 1, General Rules. EN-1997-1. Brussels, Belgium: CEN.

## Rockfall: Scaling factors for the Coefficient of Restitution

P. Asteriou, H. Saroglou & G. Tsiambaos  
Geotechnical Department, School of Civil Engineering, National Technical University of Athens, Greece

**ABSTRACT:** Rockfalls poses a significant hazard on human activities and infrastructure. In order to design remedial measures, simulation programs are used to define the rockfall trajectory. The most significant input parameter is the Coefficient of Restitution which describes the response of the falling block at impact. This parameter is commonly adjusted to the incident velocity with the use of a scaling factor, but the effect of the block mass is usually neglected. A laboratory investigation using artificial materials to account for the influence of the mass and the incident velocity of the falling blocks is presented. Experimental results show that the coefficient values decrease with both the increase of the block mass and the impacting velocity. The various scaling methods in literature are evaluated. Additionally, a momentum based scaling approach was found to be consistent with the present experimental results.

### 1 INTRODUCTION

#### 1.1 Coefficients of Restitution

In general, the coefficient of restitution (COR) is defined as the decimal fractional value representing the ratio of velocities before and after an impact of two colliding entities. Theoretically, a COR that equals one corresponds to a perfect elastic collision, a COR less than unity defines an inelastic collision and a COR that equals zero is obtained when the object instantaneously stops at the surface area without bouncing which corresponds to a perfectly plastic behavior (Goldsmith, 1960).

When in contact with the slope, the block's magnitude of velocity changes according to the COR value. Hence, for rockfall engineering practice, COR is assumed to be an overall value that takes into account all the characteristics of the impact; including deformation, sliding at contact, transformation of rotational moments into translational and vice versa (Giani, 1992).

Various definitions on the coefficients of restitution have been proposed, such as the kinematic, kinetic or energy coefficients of restitution, but it seems that there is no consensus on which of them is more appropriate for rockfall trajectory prediction (Chau et al., 2002).

The kinematic approach, which is derived from the inelastic collision of particles in the Newtonian mechanics, is the most commonly used due to its overall simplicity. The definition of the COR for an object which impacts on a steadfast surface is simplified as:

$$v_{COR} = \frac{v_r}{v_i} \quad (1)$$

where  $v_i$  = incident velocity;  $v_r$  = rebound velocity; and  $v_{COR}$  = kinematic coefficient of restitution.

The most common COR definition is derived from the normal and tangential projections of the velocity vector on the impact surface, according to:

$$n_{COR} = \frac{v_{r,n}}{v_{i,n}} \quad (2)$$

$$t_{COR} = \frac{v_{r,t}}{v_{i,t}} \quad (3)$$

where the subscripts after the comma  $n$ =normal component;  $t$ =tangential component;  $n_{COR}$  =normal coefficient of restitution; and  $t_{COR}$  =tangential coefficient of restitution.

Another COR definition found in literature is given in energy terms:

$$E_{COR} = \frac{0.5(mv_r^2 + I\omega_r^2)}{0.5(mv_i^2 + I\omega_i^2)} \quad (4)$$

where  $I$  =moment of inertia;  $\omega$ =angular velocity; and  $E_{COR}$  =energetic coefficient of restitution.

It can be seen from the aforementioned equations that  $E_{COR}$  yields the square root of the  $v_{COR}$  when angular velocity is zero, which is valid for the case of a free fall impact, while the  $n_{COR}$  is equivalent to  $v_{COR}$ .

However,  $t_{COR}$  cannot be defined according to Equation 4 since the denominator is zero, which results to an undefined expression. Thus, in the present paper  $v_{COR}$  is used and is denoted as COR.

The parameters which influence the bouncing phenomenon, and subsequently the COR values, are summarized in Table 1.

Table 1. Parameters assumed to influence the bouncing phenomenon (Labiouse & Heidenreich, 2009).

Slope characteristics	Block characteristics	Kinematics
Strength	Strength	Translational velocity
Stiffness	Stiffness	Rotational velocity
Roughness	Weight	Collision angle
Inclination	Size	Configuration of block

#### 1.2 Review of scaling factors

COR depends amongst others on incident velocity and mass, as seen in Table 1. Various scaling factors have been proposed in order to take these parameters into account in the analysis of rockfalls with computer codes.

Pfeiffer & Bowen (1989) introduced the CRSP rockfall simulation program, in which both normal and tangential COR values are scaled according to the incident velocity. The scaled normal COR value is calculated by multiplying the literature suggested value by the scaling factor (Eq. 5), while a relevant expression for scaling the tangential COR is also available.

$$B_v = \frac{1}{1 + (v_{i,n} / v_{ref})^2} \quad (5)$$

where  $v_{ref}$  =reference velocity; and  $B_v$  =scaling factor.

According to Equation 5, the scaling factor is equal to 0.5 when incident velocity is equal to the reference velocity, which was defined in CRSP as  $9.14 \text{ ms}^{-1}$ . Richards et al. (2001) suggested a reference velocity equal to  $5 \text{ ms}^{-1}$  based on laboratory investigation. This scaling factor is adopted by many simulation codes. However, very little information is available concerning the calibration of this equation with experiments using blocks of different sizes (Bourrier & Hungry, 2011).

An alternate velocity scaling factor (Eq. 6) was used by Rammer et al. (2010) in which scaling is applied for incident velocities higher than  $10 \text{ ms}^{-1}$ . Since literature sug-

gested values, which are commonly used, originate from testing with lower incident velocities, scaling is included.

$$k = \begin{cases} 1, & v_i \leq 10 \text{ms}^{-1} \\ 10^{0.25} v_i^{-0.25}, & v_i > 10 \text{ms}^{-1} \end{cases} \quad (6)$$

where  $k$  = scaling factor.

This scaling factor originates from an equation proposed by Johnson (1985), according to which COR is proportional to  $v_i^{-0.25}$ . The aforementioned scaling factors, which are all dependent on incident velocity, show a significant variation as presented in Figure 1.

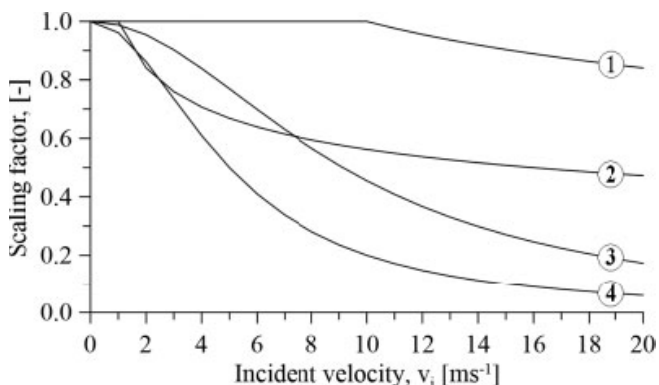


Figure 1. Scaling factors versus incident velocity originating from: 1- Rammer et al. (2010); 2- Johnson (1985); 3- Pfeiffer & Bowen (1989); and 4- Richards et al. (2001).

A momentum based COR definition has recently been proposed by Bourrier & Hungr (2011) based on intuition. COR is represented by a hyperbolic function which yields unity in 'soft' impacts and zero in 'heavy' impacts, where all energy dissipates due plastic deformation.

$$k' = \frac{M_{0.5}}{M_n + M_{0.5}} \quad (7)$$

where  $M_n$  = normal incident momentum;  $M_{0.5}$  = reference momentum; and  $k'$  = scaled coefficient of restitution.

A scaling factor dependent on mass, which presents a similar trend with scaling factor  $B_v$ , is also available in RocFall software (RocScience, 2003). However, no information concerning the definition of this factor is available. According to the software developers, it is not advised to use simultaneously mass and velocity scaling factors, since it results in unrealistic rock paths.

$$B_m = \frac{1}{1 + (m / m_{ref})^2} \quad (8)$$

where  $m_{ref}$  = reference mass; and  $B_m$  = mass scaling factor.

## 2 EXPERIMENTAL SETUP

The rebound angle for a normal and frictionless impact between a sphere and steadfast surface should be theoretically equal to 90 degrees. However, when performing free fall tests with randomly shaped blocks, the rebound trajectory presents a wide deviation from the fall direction. Block shape has been found to pose a significant effect on the rebound angle and subsequently to the obtained COR value (Asteriou et al., 2012). In order eliminate the effect of the block shape effect and the other parameters shown in Table 1; spherical blocks and free fall drops were used in the experiments.

### 2.1 Apparatus

The surface area, upon which the impact of the spherical blocks occurred, was a smooth and planar plate formed by the same material. The plate had a thickness of 5 cm with 15 cm side length, fixed in a massive deadweight base which ensured the preservation of the momentum caused by the impact.

Prior to the experiment, the block was held by suction produced by a vacuum pump and was released to a free fall drop by switching the vacuum pump off. Consequently, the block developed only vertical translational velocity prior to impact. The trajectory of the block was recorded with a digital high-speed video camera, at a capture speed of 500 fps and a resolution of 440X330 pixels, installed 1m away from the impact surface. A high contrast background was installed in order to make the block distinguishable.

### 2.2 Materials

Preparing spheres from natural rock is expensive and time consuming, which are hardly ever perfectly spherical. Thus, artificial materials were chosen, as they present advantages: they can be casted in any shape and size and their mechanical properties can match those of natural materials. For casting the spherical blocks, custom silicon molds were created, able to reproduce boulders with diameters of 3, 4, 5 and 6 cm. The materials chosen were a cement based grout and a high strength epoxy resin. Both materials were stable and cohesive, exhibiting zero segregation and were shrinkage compensating, resulting in uniform samples. The physical and mechanical properties of these materials, presented in Table 2, were determined according to ISRM suggested methods (ISRM, 2007).

Table 2. Properties of used materials.

Material properties	Cement grout	Epoxy resin
Density, $\rho$ (kN/m <sup>3</sup> )	21.9	20.4
Compressive strength, $\sigma_{ci}$ (MPa)	37.4	86.5
Young's modulus, $E_t$ (GPa)	15.7	11.0
Poisson's ratio, $\nu$	0.11	0.38
Tensile strength, $\sigma_t$ (MPa)	7.5	15.6
P-wave velocity, $v_p$ (m/s)	4335	4125
S-wave velocity, $v_s$ (m/s)	2575	2430
Schmidt Hardness, R	33	42

Asteriou et al. (2013) have used these materials for investigating the effect of material properties of free falling blocks with cubical shape along with eight natural rock materials commonly found in Greece.

### 2.3 Data acquisition

A video file is a sequence of still images displayed at a constant rate (fps). A grayscale digital image forms an array of pixels the size of which is described by the image resolution. Each element obtains a numerical value from 0 (black) to 255 (white) representing the intensity of the pixel, which is described by a matrix, easily manipulated within MATLAB environment.

Initially, each frame was converted to a binary image (black-and-white) discretizing the block from the background (Fig. 2a). The near end projection of the block in the capture plan resembles a circular shape. Hereafter, an edge recognition algorithm (Canny, 1986) was used providing the boundary between the circular projection and the background (Fig. 2b). The coordinates of each pixel defining the boundary line were used in order to calculate the center

point and the radius of the boulder using Pratt (1987) least squares method (Fig. 2c). According to this method, the geometric properties of a circle are calculated according to Equation 9.

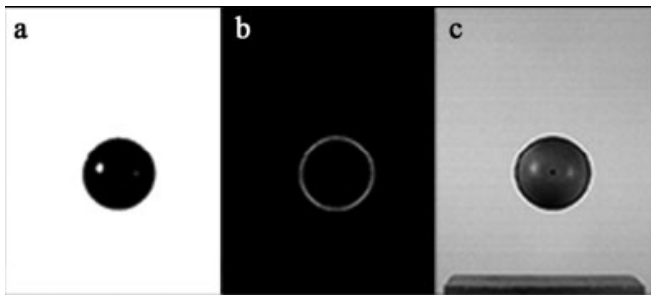


Figure 2. Tracking algorithm stages: a. conversation into a binary image resulting discretization of the block; b. boundary recognition and acquisition of  $x_i, y_i$  coordinates; and c. calculation of block's geometrical properties.

The determination of the trajectory of the block was done by repeating the aforementioned process for all captured frames.

$$SS(X, Y, R) = \sum_{i=1}^n \left( R - \sqrt{(x_i - X)^2 + (y_i - Y)^2} \right)^2 \quad (9)$$

where  $x_i, y_i$  = coordinates of boundary points;  $X, Y$  = coordinates of the center point; and  $R$ =circle radius.

Further on, the trajectory was separated in the pre and post impact stages. For each stage a 2nd degree regression analysis of the  $Y$  coordinates over time was performed, which resulted to a constant acceleration. The impact point and time were calculated as the intersection of the pre and post trajectory curves and the line representing the impact surface.

The points defining block's boundary include a positioning error, due to the finite pixel size. The error in the determination of the center point coordinates was less than the pixel size, due to the large number of boundary points used in Pratt's method.

The error in the measurements of position between frames due to change of velocity caused by the acceleration was diminished by using a high frame rate and a 2nd degree regression. However, the high frame rate increases drastically the velocity error caused by the positioning uncertainty (Feng et al., 2011). When velocity is calculated by the position measurements an uncertainty of  $\delta y$  is included, while the time interval between the two positions is  $\Delta t$ , then the error in velocity is  $2(\delta y/\Delta t)$ . It is apparent that as  $\Delta t$  reduces, when the frame rate increases, the error in velocity determination also increases. In order to increase the time interval and reduce the error, incident velocity was calculated by Equation 10 as the average of the velocities calculated from the impact point and each measured point. A more analytical presentation of the error analysis is beyond the scope of the present paper. However, after implementing this methodology, the relative error in the calculated COR value is less than 5%.

$$v = \frac{1}{n} \sum_{i=1}^n \left[ 0.5g\Delta T + \frac{\Delta Y}{\Delta T} \right] \quad (10)$$

where  $n$ =number of measurements;  $\Delta Y$  =vertical movement of center point between point  $i$  and impact point;  $\Delta T$ =flight time between measurement point  $i$  and impact point; and  $g$  =gravitational constant.

The trajectory of the block in the impacts following the first one deviated from verticality which resulted in horizontal

and angular velocities additional to the vertical. In order to deduct the effect of both horizontal and rotational velocity, only the initial impacts were taken into account. This deviation can be attributed to grain boundaries and micro fissures, since the surfaces of the colliding entities were not perfectly smooth (Imre et al., 2008). The maximum deviation from the vertical was less than 5 degrees, which results in a difference of less than 0.4% between the normal component and the total velocity.

#### 2.4 Experimental program

In order to address the effect of impact velocity and mass of the block on COR values and evaluate the proposed scaling factors, free fall drop tests were conducted with spherical blocks of two artificial materials. Spheres were prepared from the cement grout material with diameters of 3, 4 and 5 cm and from the epoxy resin with diameters of 3, 4, 5, and 6 cm. All spheres were dropped from heights of 0.1, 0.25, 0.5, 1.0, 2.0, 3.0 and 4.5 m. In order to account for the randomness of the impact, each test was repeated five times. Thus, the experimental procedure consisted of 49 series of tests.

### 3 PRESENTATION OF RESULTS

The calculated COR values for epoxy resin and cement grout are presented in figures 3 and 4 respectively. The average value of each test series is presented on the graphs. It becomes evident that COR is dependent on both incident velocity and mass and reduces with increasing incident velocity and mass.

The trend lines presented in figures 3 and 4 are described by multivariate linear regressions. The overall regression coefficients have high values, denoting that the data are well correlated. However, extending those correlations for larger blocks and higher velocities is problematic. Using higher values for mass and velocity, but still low compared to real scale rockfalls, those correlations produce negative COR values, which are unacceptable.

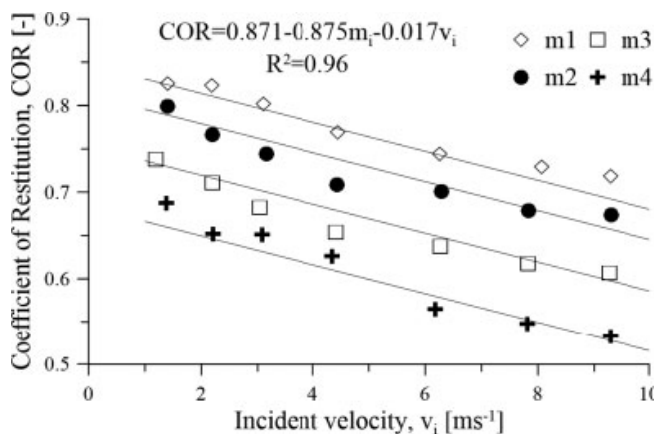


Figure 3. COR values versus incident velocity for the epoxy resin blocks.

Additionally, the presented linear correlations do not predict the COR values for impacts in the elastic regime, where COR should be approximately equal to unity independently of the mass. According to Hertzian theory of collisional impact, a COR value equal to unity is derived when incident velocity is less than the yield velocity, which is defined as the velocity where plastic deformation within the colliding blocks initiates. Johnson (1985) has shown that yield velocity is a function of density, Young's modulus and material's strength. However, even in high strength rock materials, yield velocity is significantly lower than the velocities encountered in real scale rockfalls, which implies that it is practically impossible to observe an impact with COR equal to unity. However, the upper COR boundary

should theoretically approach unity when incident velocity approaches to zero. This demonstrates that COR is connected to the mass and velocity with a nonlinear function.

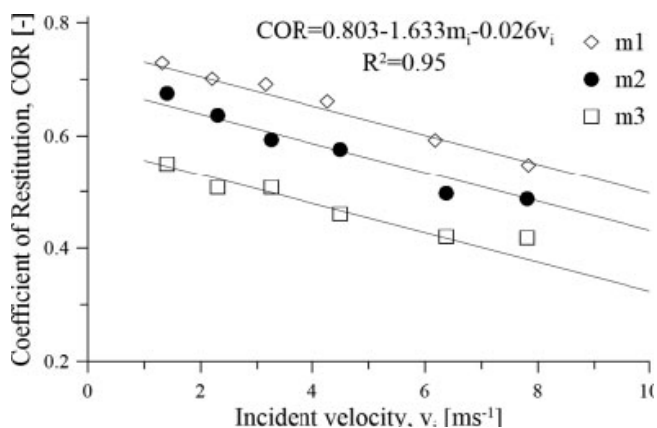


Figure 4. COR values versus incident velocity for the cement grout blocks.

The experimentally derived COR values for both materials are plotted against incident momentum (Fig. 5), which is the product of the mass and incident velocity of the block. A strong correlation between momentum and COR is applicable, which is defined by a non-linear function in the form of:

$$COR = a(mv_i)^{-b} \quad (11)$$

where  $a$  and  $b$  are parameters which are assumed to be controlled by the material properties, such as strength, elastic properties etc. since they were the only parameters that differed between the two tested materials.

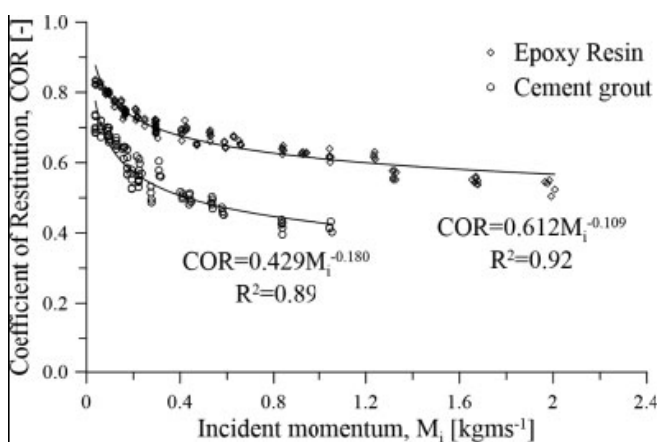


Figure 5. Coefficient of restitution values from all tests versus incident momentum.

However, in order to determine these parameters, additional tests with more materials and larger blocks are required. This forms part of on-going research of the authors.

An interesting observation arises from the tests with cement grout blocks. All blocks were fractured for a release height of 4.5 m, by splitting along the loading direction (fig. 6), which is similar to the failure mode of Brazil test, implying that fracture is controlled by the tensile strength. Moreover, the calculated COR values for these impacts were lower than their prediction obtained by extending the results of tests performed with lower release heights. Fracture of the blocks occurred after 3 to 4 drops and a lower COR value was calculated after each test, denoting that internal cracking developed and propagated. However, until fracture there were no macroscopically visible signs of cracking on the surface of the blocks. These tests were not

included in the present analysis as they concern the fracture phenomenon.

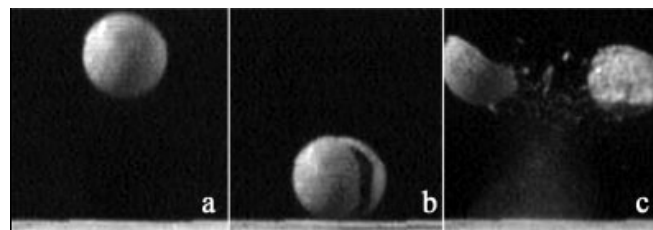


Figure 6. Image sequence of a fracture; 3 cm diameter concrete block released from a height of 4.5 m; a.  $t_a = 0.000$  s; b.  $t_b = 0.008$  s; and c.  $t_c = 0.024$  s.

#### 4 EVALUATION OF RESULTS

The present data are significant for the evaluation of the proposed scaling models and their calibration. The model used in the majority of computer programs is presented by Equation 4 and incorporates incident velocity, reference COR value and reference velocity. However, from figures 3 and 4 it is evident that COR value depends significantly also on the block's mass.

Thus, this model lacks the ability to predict the scaling factor for blocks whose size varies. This is also true with the model proposed by Rammer et al. (2010). Additionally, in this model COR is not scaled for incident velocities less than  $10 \text{ ms}^{-1}$ , due to the fact that COR value is selected by the literature suggested values, which are determined from experimental studies performed within that velocity range, thus already including the scaling factor. However, based on the present study, the velocity effect on the COR value is significant for the range between zero and  $10 \text{ ms}^{-1}$ . Additionally, the model omits the mass dependency for the whole velocity range. Hence, this model cannot be used to describe the trends produced by the presented experimental data.

The momentum based COR definition suggested by Bourrier & Hungr (2011) matches well with trend of the present experimental results. However, the proposed hyperbolic function (Eq. 7) could not be calibrated; the term  $M_0^{0.5}$  presents a wide scatter, although it is defined as a constant parameter. Furthermore, a model defined in terms of incident momentum seems to be appropriate for the simultaneous scaling of COR values according to incident velocity and mass.

#### 5 CONCLUSIONS

In the present paper the COR value dependency on mass and velocity was examined for spherical blocks of various sizes impacting on a horizontal surface. The blocks consisted of two artificial materials and the free fall experiments were conducted from different release heights, up to 4.5 m resulting incident velocities up to  $9.5 \text{ ms}^{-1}$ .

According to the experimental results, it is shown that the COR value reduces by increasing both incident velocity and mass. Additionally, the rate of decrease seems to be a function of the mechanical properties of the blocks. For instance, in the tests conducted with epoxy resin blocks, increasing the incident velocity approximately 10 times COR is reduced by 17%. On the other hand, by increasing mass 8 times, COR is reduced by 20%.

The COR scaling factors found in literature are mainly focused on the effect of incident velocity, and therefore lack the ability to fit to the present data. However, using a momentum based scaling factor, expressed by a power function, seems capable to address both mass and velocity effects. This function could also incorporate parameters connected to material properties, such as strength and Young's modulus.

Besides the uncertainty introduced by the scaling factor, a more important issue is the uncertainty of the reference values. In literature, suggested values are given mostly by the material type, based on laboratory, in situ investigations and back analysis of known rockfall trajectory paths, which present a large scatter. According to present results this scatter can be attributed -beyond other parameters- to the different testing conditions applied, such as incident velocity and mass of the blocks.

Further research on the size and velocity dependency on COR is under progress in the Rock Mechanics laboratory of the School of Civil Engineering at the National Technical University of Athens. Larger blocks and different materials are tested, whereas also shape and incident angle are altered. Additionally research has been recently extended in the field, by conducting tests in real scale, in order to establish sound methods and correlations for predicting rockfall trajectories more accurately.

#### ACKNOWLEDGEMENTS

Authors would like to express their gratitude to Mr. Dario Stefanou, Craftsman-Artist, for the construction of the silicon molds and to Sika Hellas SA for providing the materials used in this research.

#### REFERENCES

Asteriou, P., Saroglou, H. & Tsiambaos, G. 2012. Geotechnical and kinematic parameters affecting the coefficients of restitution for rock fall analysis. *International Journal of Rock Mechanics and Mining Sciences*, 54, 103–113.

Asteriou, P., Saroglou, H. & Tsiambaos, G. 2013. Rockfalls: Influence of Rock Hardness on the Trajectory of Falling Rock Blocks. *Bulletin of the Geological Society of Greece*, XLVII.

Bourrier, F. & Hungr, O. 2011. Rockfall Dynamics: a Critical Review of Collision and Rebound Models. In S. Lambert & F. Nicot (eds), *Rockfall Engineering*: Hoboken, NJ – London: Wiley – ISTE.

Canny, J. 1986. Computational Approach to Edge Detection. *IEEE Transactions on Pattern Analysis and Machine Intelligence*, PAMI-8, 679–698.

Chau, K. T., Wong, R. H. C. & Wu, J. J. 2002. Coefficient of restitution and rotational motions of rockfall impacts. *International Journal of Rock Mechanics and Mining Sciences*, 39, 69–77.

Feng, Y., Goree, J. & Liu, B. 2011. Errors in particle tracking velocimetry with high-speed cameras. *Review of Scientific Instruments*, 82.

Giani, G. P. 1992. *Rock Slope Stability Analysis*. Rotterdam: Balkema.

Goldsmith, W. 1960. Impact: The theory and physical behavior of colliding solids. *Edward Alrnold, London*.

Imre, B., Rábsamen, S. & Springman, S. M. 2008. A coefficient of restitution of rock materials. *Computers & Geosciences*, 34, 339–350.

ISRM2007. *The Complete ISRM Suggested Methods for Rock Characterization, Testing and Monitoring: 1974–2006*.

R. Ulusay & J.A. Hudson (eds) Johnson, k. L. 1985. *Contact Mechanics*, UK, Cambridge University Press.

Labouse, V. & Heidenreich, B. 2009. Half-scale experimental study of rockfall impacts on sandy slopes. *Natural Hazards and Earth System Science*, 9, 1981–1993.

Pfeiffer, T. J. & Bowen, T. D. 1989. Computer simulation of rockfalls. *Bulletin – Association of Engineering Geologists*, 26, 135–146.

Pratt, V. 1987. Direct Least-Squares Fitting Of Algebraic Surface. *Computer Graphics (ACM)*, 21, 145–152.

Rammer, W., Brauner, M., Dorren, L. K. A., Berger, F. & Lexer, M. J. 2010. Evaluation of a 3-D rockfall module within a forest patch model. *Natural Hazards and Earth System Science*, 10, 699–711.

Richards, L. R., Peng, B. & Bell, D. H. 2001. Laboratory and field evaluation of the normal Coefficient of Restitution for rocks. *Proceedings of Proc. ISRM Regional Symposium EUROCK2001*, 149–155.

RocScience. 2003. Advanced Tutorial: Determining Input Parameters for A RocFall Analysis. [www.rocscience.com](http://www.rocscience.com).

## Influence of rock mass creep on tunnel loading

P. Fortsakis, A. Kalos, V. Despotaki & M.J. Kavvasas  
*National Technical University of Athens, Greece*

**ABSTRACT:** Rock mass creep in tunnelling through weak rock masses under high overburden may lead to the potential development of significant convergence. Should this convergence be restrained by a rigid support shell, tunnel loading tends to increase. Although, such increase could be significant, it is often not taken into account in design, due to uncertainties in the calculation procedure. This paper proposes a simplified approach for estimating the additional creep loads on the lining of circular tunnels excavated in one phase. This is achieved by performing a parametric set of 2D numerical analyses with the finite element code ABAQUS. The rock mass is modeled as an elasto-plastic material yielding according to the Drucker-Prager criterion, with time-dependent characteristics described by the Singh-Mitchell creep model. The time-dependent behaviour is initially formulated upon the assumption of a new set of parameters. Typical ranges of these parameters are estimated using creep experiments from the literature.

### 1 INTRODUCTION

In tunnel design and construction through weak rock masses under high overburden the role of rock mass creep may prove important for the final wall convergence and ground loads exerted on temporary support or final lining. However, this time-dependent behaviour is usually not considered in design, due to the large uncertainties of creep and the need for complex laboratory tests and constitutive models.

In tunneling, the time-dependent behaviour of the rock mass is not typical creep, since deformation does not freely develop under constant state of stress. The construction of the support shell restrains the potential creep deformation, leading to increased tunnel loads and rock mass creep evolves with varying stresses. Moreover, the rock mass creep in tunnelling can be separated in two categories (this separation is only in relation to the specific project which determines the time scale):

- Short-term creep. Creep deformation influences the excavation procedure and the temporary support.
- Long-term creep. Creep deformation develops during the tunnel service life leading to increased ground loads on final lining.

There are several case studies in literature, of tunnels that experienced large deformation and in some cases severe failures due to the short-term creep behaviour of the surrounding rock mass (e.g. the Saint Martin La Porte access adit, along the Torino - Lyon Base Tunnel and the Lötschberg Tunnel). Debernardi (2008) describes the case of the Saint Martin La Porte, where up to 2.0m convergence developed during the excavation. Using back analysis the dominant role of the creep of the surrounding rock mass was revealed. Moreover, Barla et al. (2010) presented stress measurements in the final lining, clarifying that the increase of the stresses due to the rock mass creep varied from 70% to 100%. Sandrone et al. (2006) employed three different models to simulate the very large time-dependent convergence (up to 80 cm) developed when the tunnel crossed the base sediments of sandstone and siltstone and up to 1.0m thick beds of carbon and anthracite.

The influence of creep on the surrounding geomaterial has been studied by several researchers in literature using either analytical (e.g. Sulem et al. 1987, Pan & Dong 1991, Nomikos et al. 2011), numerical (e.g. Ghaboussi & Gioda 1977, Boidy et al. 2002, Debernardi 2008, Fortsakis 2012),

statistical (e.g. Sandrone 2006; Kontogianni et al. 2005) or experimental (e.g. Yu 1998) methods.

The present paper investigates the influence of rock mass creep on the final lining loads of circular tunnels. Based on results of viscoplastic 2D numerical analyses a simplified approach is proposed for the estimation of the increased tunnel loads due to rock mass creep.

### 2 ROCK MASS CREEP

Creep is a relatively well defined phenomenon in principle. However, establishing a well-defined constant effective stress to account for the effect of creep deformation is rather illusive. Considering that creep deformation accumulates with evolving time, the pore pressures tend to increase and then dissipate thus leading to a fluctuation of the effective stress.

Throughout the literature creep has been simulated through a series of empirical (e.g. semi-logarithmic law, Singh-Mitchell creep model) or rheological models (e.g. Maxwell, Bingham) and general theories (e.g. Perzyna 1966, Naghdi & Murch 1963). However, the time-dependent mechanical behaviour experienced in oedometer and triaxial or unconfined compression tests tends to describe different aspects of creep.

Oedometer tests activate the volumetric component of creep thus leading to an increase of strength stemming from the chemical bonding experienced. Regardless whether we tend to neglect or silently disregard any significance of the aforementioned creep characteristic, it tends to dominate the overall mechanical behaviour considering the formation of the rock mass throughout the geological history. The only solace we can receive is that the problem at hand is addressing a relatively small time window while the volumetric creep strain effects on rock mass strength become significant only over extensive periods of time.

Triaxial or unconfined compression tests however, reveal the deleterious effects of deviatoric creep strain component on the rock mass strength. Although the primary and secondary creep stages, inherently associated with crystal and microfabric reconstruction, can be described relatively accurately by most empirical and even rheological models under specific loading conditions, they tend to neglect the final primal role of deviatoric creep strain component characterized as tertiary creep. The tertiary creep stage portrays the deleterious effects of deviatoric creep through strength degradation leading ultimately to creep induced failure.

Next, we will be focusing solely on the deviatoric creep strain component and investigate the effect of primary and secondary stages on the overall mechanical behaviour in tunneling by employing a relatively well established empirical relation.

### 3 CREEP MODEL AND PARAMETERS

In the frame of the present paper the rock mass creep behaviour is initially formulated upon the assumption of a new set of parameters ( $\varphi_{cr}$ ,  $t_{50\%}/t_d$ ). These parameters can easily be correlated with most of the widely used creep models and, as it will be shown from the results of the numerical analyses, they can be further employed on the development of a simplified approach for the estimation of creep loads on the tunnel. More specifically these parameters are:

- Creep factor  $\varphi_{cr}$ : This factor represents the magnitude of the potential creep strain for a given stress state ( $q/q_r$ ) in a specific time period ( $t$ ). For instance the time period may correspond to the duration of a laboratory test or the project service life or an arbitrary moment. The creep factor is equal to the ratio of the creep deformation at the specific time and stress state to the elastic deformation

at the same stress state assuming linearly elastic – perfectly plastic behaviour ( $\sigma_c = 2c \cdot \tan(45+\varphi/2)$ ,  $c$ : rock mass cohesion,  $\varphi$ : rock mass friction angle,  $E$ : deformation modulus,  $q$ : deviatoric stress,  $q_f$ : maximum deviatoric stress for a specific value of the mean stress  $p$ ).

$$\varphi_{cr} \left( \frac{q}{q_f}, t \right) = \frac{\varepsilon_{cr}(t=t_d)}{\left( \frac{q}{q_f} \right) \frac{\sigma_c}{E}} \quad (1)$$

– Ratio  $t_{50\%}/t_d$ : This factor determines the rate of increase of the potential creep strain. The parameter  $t_{50\%}$  is the time period required for the 50% of the final creep deformation to be developed according to the creep mode and  $t_d$  is the total time of the analysis.

The following equations illustrate the procedure for the calculation of the Singh-Mitchell (Singh & Mitchell 1968) parameters from the values of the creep factor  $\varphi_{cr}$  and the ratio  $t_{50\%}/t_d$ . The equations for the two time values  $t_d$  and  $t_{50\%}$  are:

$$\varepsilon_{cr}(t=t_d) = \frac{A}{1-m} e^{\alpha \frac{q}{q_f}} \left( \left( \frac{t_d}{t_1} \right)^{1-m} - 1 \right) \quad (2)$$

$$\varepsilon_{cr}(t=t_{50\%}) = \frac{A}{1-m} e^{\alpha \frac{q}{q_f}} \left( \left( \frac{t_{50\%}}{t_1} \right)^{1-m} - 1 \right) \quad (3)$$

The  $m$  parameter of the Singh-Mitchell model is calculated by dividing the two previous equations. It is evident that the  $m$  value is not influenced by the values of the creep factor.

$$\frac{\varepsilon_{cr}(t=t_{50\%})}{\varepsilon_{cr}(t=t_d)} = \frac{1}{2} \Rightarrow \left( \frac{t_d}{t_1} \right)^{1-m} - 2 \left( \frac{t_{50\%}}{t_1} \right)^{1-m} + 1 = 0 \quad (4)$$

By substituting the creep deformation  $\varepsilon_{cr}$  in Eq. 1 the creep factor can be expressed through Eq. 5.

$$\varphi_{cr}(t=t_d, q/q_f) = \frac{\frac{A}{1-m} e^{\alpha \frac{q}{q_f}} \left( \left( \frac{t_d}{t_1} \right)^{1-m} - 1 \right)}{\left( \frac{q}{q_f} \right) \frac{\sigma_c}{E}} \quad (5)$$

Since the creep potential depends significantly on the imposed stress state, two different creep factors should be determined for different values of the  $q/q_f$  ratio (Eqs. 6, 7).

$$\varphi_{cr1}(t=t_d, (q/q_f)_1) = \frac{\frac{A}{1-m} e^{\alpha \left( \frac{q}{q_f} \right)_1} \left( \left( \frac{t_d}{t_1} \right)^{1-m} - 1 \right)}{\left( \frac{q}{q_f} \right)_1 \frac{\sigma_c}{E}} \quad (6)$$

$$\varphi_{cr2}(t=t_d, (q/q_f)_2) = \frac{\frac{A}{1-m} e^{\alpha \left( \frac{q}{q_f} \right)_2} \left( \left( \frac{t_d}{t_1} \right)^{1-m} - 1 \right)}{\left( \frac{q}{q_f} \right)_2 \frac{\sigma_c}{E}} \quad (7)$$

Finally from the above relationships the values of the parameters  $a$ ,  $A$  of the Singh-Mitchell model can be calculated as follows:

$$\alpha = \frac{\ln \left[ \frac{\varphi_{cr2} \left( \frac{q}{q_f} \right)_2}{\varphi_{cr1} \left( \frac{q}{q_f} \right)_1} \right]}{\left( \frac{q}{q_f} \right)_2 - \left( \frac{q}{q_f} \right)_1} \quad (8)$$

$$A = \frac{\sigma_c}{E} \frac{(\varphi_{cr2} - \varphi_{cr1})(1-m)}{\left( \left( \frac{t_d}{t_1} \right)^{1-m} - 1 \right) \left[ \frac{e^{\alpha \left( \frac{q}{q_f} \right)_2}}{\left( \frac{q}{q_f} \right)_2} - \frac{e^{\alpha \left( \frac{q}{q_f} \right)_1}}{\left( \frac{q}{q_f} \right)_1} \right]} \quad (9)$$

#### 4 DESCRIPTION OF NUMERICAL ANALYSES

The problem was investigated via 2D numerical analyses using finite element code ABAQUS. The section of the tunnel was assumed to be circular with diameter  $D=10\text{m}$  and the overburden height equal to  $10D=100\text{m}$  (Fig. 1). The soil was simulated with 4-sided, 4-noded solid elements and the support with linear beam elements.

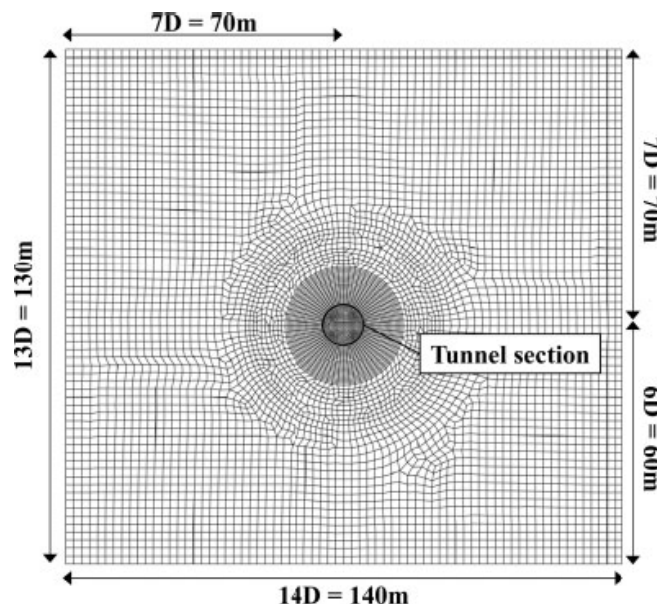


Figure 1. Numerical model.

The surrounding rock mass was modeled as isotropic linearly elastic – perfectly plastic material following the Drucker-Prager failure criterion. The initial selection of the geotechnical parameters was made in terms of the Hoek-Brown failure criterion (Hoek et al. 2002), which better describes rock materials and the rock mass deformation modulus was calculated according to Hoek et al. (2002). The steps of the numerical analyses are:

- Step 1: Geostatic stress state (hydrostatic stress field  $K=1.0$ )
- Step 2: Simulation of the preconvergence development (Chern et al. 1998)
- Step 3: Full face excavation and activation of the temporary support (shotcrete thickness  $d_{sh} = 20\text{ cm}$ ,  $E_{sh} = 20\text{ GPa}$ )
- Step 4: Activation of final lining (thickness  $d_{FL} = 60\text{ cm}$ ,  $E_{FL} = 29\text{ GPa}$ )
- Step 5: Deactivation of temporary support

– Step 6: Simulation of the rock mass creep behaviour

The selection of the  $\varphi_{cr}$  values was mainly based on a large number of creep experiments from the PhD dissertations of Aristorenas (1987) and Debernardi (2008). However, the  $\varphi_{cr}$  values which are calculated from an experimental procedure should be considered as a lower limit of the values that should be adopted in the design since (a) they correspond to the duration of the experiment which is significantly shorter than the tunnel service life and (b) the creep tests are usually carried out using intact rock samples and therefore the role of the discontinuities in the time-dependent deformation is neglected.

Regarding the time-rate parameters ( $t_{50\%}/t_d$  and  $m$  parameter of the Singh-Mitchell model) the selection was based on the co-evaluation of the experimental results and the proposed  $m$  values from the literature that are summarized by Hunaj-Sarihan (2009): 0.70–0.80 (Tavenas et al. 1978), 0.50–1.30 (Lacasse & Berre 2005) and 0.90–1.3 (Mansour et al. 2008). Finally, the value of  $m=0.80$  was chosen for the analyses, which corresponds to  $t_{50\%}/t_d \sim 0.10$  via Eq. (4). All rock mass parameters are summarized in Table 1.

Table 1. Numerical analyses parameters.

Parameter	Range	Units
GSI (Marinos & Hoek 2000, Marinos et al. 2005)	20–30	
$\sigma_{ci}$	4–15	MPa
$m_i$	6	
D	0	
$\gamma$	25	kN/m <sup>3</sup>
$\sigma_o$	2.5	MPa
$\sigma_c/\sigma_o$	0.11–0.30	
$\varphi_{cr}(q/q_f = 30\%)$	0.20–2.00	
$\varphi_{cr}(q/q_f = 70\%)$	0.30–3.00	
$\varphi_{cr}(q/q_f = 70\%)/\varphi_{cr}(q/q_f = 30\%)$	1.25,	1.50
$m$ (Singh-Mitchell model)	0.80	
$t_d$	1200	months
$t_{50\%}/t_d$	0.10	

The range of the rock mass strength and deformability parameters was chosen so as to correspond to weak materials and potentially unfavourable geotechnical conditions for the specific overburden height (low values of  $\sigma_c/\sigma_o$  ratio,  $\sigma_c$ : uniaxial compressive strength of the rock mass,  $\sigma_o$ : geostatic stress). The  $\varphi_{cr}$  values have been set for  $q/q_f = 30\%$  and  $70\%$ , since  $\sigma_{ci}$ : intact rock uniaxial compressive strength,  $m_i$ : geomaterial constant, D: disturbance factor,  $\gamma$ : rock mass unit weight,  $\sigma_c = 2ctan(45+\varphi/2)$ ,  $\sigma_o$ : initial geostatic stress,  $c$ : rock mass cohesion,  $\varphi$ : rock mass friction angle,  $\varphi_{cr}$ : creep factor,  $t_d$ : tunnel service life.

(a) in this range creep experiments can be carried out to study the primary and secondary creep without creep failure (b) the creep potential is considered to be low for  $q/q_f < 30\%$  and (c) this is the range that has been proposed by Singh & Mitchell (1968).

5 RESULTS OF NUMERICAL ANALYSES

The simulation of all the construction stages in the numerical analyses allows for the monitoring of the tunnel loads evolution, from the excavation and temporary support phase to the end of the project service life after the development of the assumed creep deformation. The main symbols which are used for the presentation of the numerical analyses results are summarized here below:

- $p_{sh}$ : average pressure on the shotcrete shell of the temporary support
- $p_{FL}$ : average pressure on the final lining before the rock mass creep simulation
- $p_{cr}$ : average pressure on the final lining after the rock mass creep simulation

Figures 2 and 3 illustrate the distribution of plastic and creep deformation around the tunnel section. The maximum values of the plastic deformation are developed near the tunnel, whereas the maximum values of the creep deformation are developed at the edge of the plastic zone.

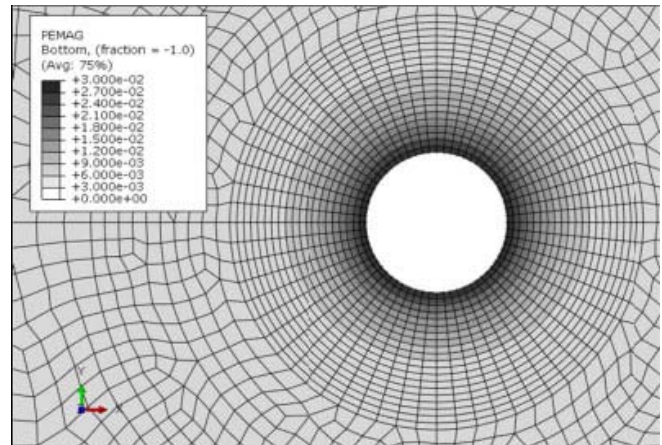


Figure 2. Plastic deformation around the tunnel section. The dark areas correspond to high values of plastic strain (GSI=20,  $\sigma_{ci} = 8\text{MPa}$ ,  $\sigma_c/\sigma_o = 0.14$ ,  $\varphi_{cr1} = 0.60$ ,  $\varphi_{cr2} = 0.75$ ).

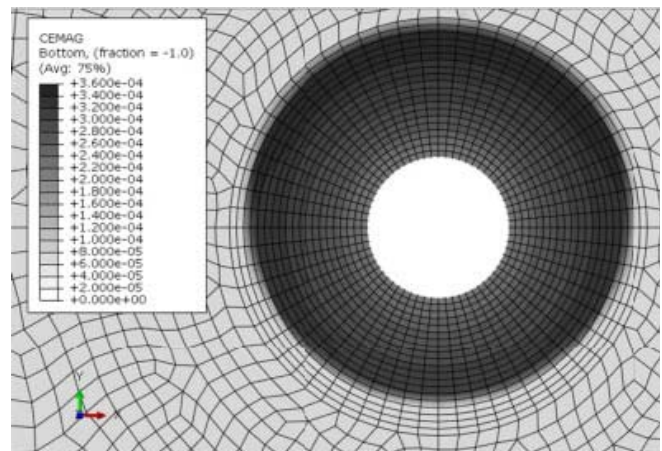


Figure 3. Creep deformation around the tunnel section. The dark areas correspond to high values of creep strain (GSI=20,  $\sigma_{ci} = 8\text{MPa}$ ,  $\sigma_c/\sigma_o = 0.14$ ,  $\varphi_{cr1} = 0.60$ ,  $\varphi_{cr2} = 0.75$ ).

This can be explained via the following diagrams which show the development of the stress component in the rock mass at the tunnel edge. In the beginning of the step of the creep simulation the ratio  $q/q_f$  is equal to 1.0, since the specific finite element is in the plastic zone (Fig. 4). However, the potential creep deformation cannot be freely developed due to the tunnel final lining leading to the increase of the tunnel load, but also to the increase of the mean stress and the decrease of the deviatoric stress in the rock mass (Fig. 5). This decrease of the ratio  $q/q_f$  leads to a decrease of the creep strain rate. As the distance of the tunnel increases and this stress redistribution decreases, the maximum creep strains are developed at the edge of the plastic zone. It is also highlighted that, due to the low  $\sigma_c/\sigma_o$  ratio and the high rigidity of the final lining section in all cases, the percentage of load transfer from the tempo-

rary support to the final lining is higher than 93% ( $p_{FL}/p_{sh} > 0.93$ ).

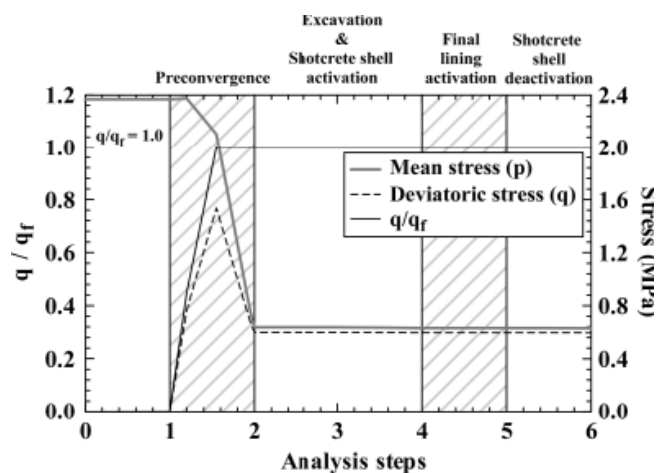


Figure 4. Development of the mean stress ( $p$ ), the deviatoric stress ( $q$ ) and the ratio ( $q/q_f$ ) before the creep simulation in the rock mass at the tunnel edge (GSI=20,  $\sigma_{ci} = 8\text{MPa}$ ,  $\sigma_c/\sigma_o = 0.14$ ,  $\varphi_{cr1} = 0.60$ ,  $\varphi_{cr2} = 0.75$ ).

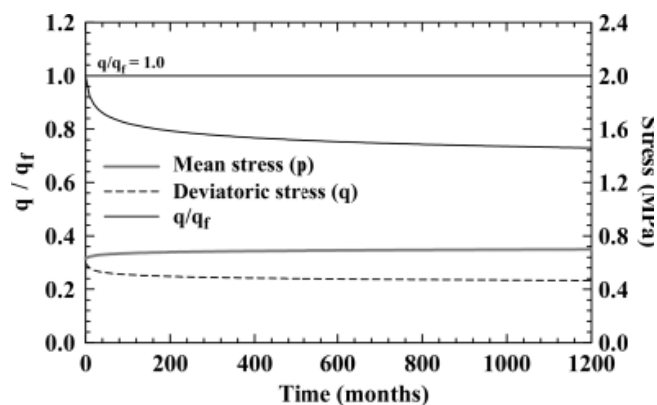


Figure 5. Development of the mean stress ( $p$ ), the deviatoric stress ( $q$ ) and the ratio ( $q/q_f$ ) during the creep simulation in the rock mass at the tunnel edge (GSI=20,  $\sigma_{ci} = 8\text{MPa}$ ,  $\sigma_c/\sigma_o = 0.14$ ,  $\varphi_{cr1} = 0.60$ ,  $\varphi_{cr2} = 0.75$ ).

The ratio  $p_{cr}/p_{FL}$  can be used to quantify the effect of the rock mass creep on the final lining load. The diagrams in Figure 6 portray the distribution of this ratio as a function of the geotechnical conditions ratio  $\sigma_c/\sigma_o$  and the  $\varphi_{cr}$  values. As the rock mass quality improves the  $p_{cr}/p_{FL}$  ratio decreases, considering that the width of the plastic zone is smaller and the values of the stress factor  $q/q_f$  that influences the creep potential are lower. Moreover the increase of the  $\varphi_{cr}$  values tends to reveal an increase of the  $p_{cr}/p_{FL}$ . However, this increase has a decreasing rate, due to the increase of the load and the mean stress, which has already been described. For the range of the geotechnical and creep parameters that has been assumed, the increase of the final lining loads varies from 15% to 70% for  $\varphi_{cr2}/\varphi_{cr1} = 1.25$  and from 20% to 110% for  $\varphi_{cr2}/\varphi_{cr1} = 1.50$ .

In order to investigate the sensitivity of the ratio  $p_{cr}/p_{FL}$  to the rate of increase of the creep deformation a sensitivity analysis was carried out for  $m=0.60-0.90$  that corresponds to  $t_{50\%}/t_d = 0.05-0.20$ . The results illustrated in Figure 7 show that higher  $m$  values – for the same  $\varphi_{cr}$  values – result to higher rate of increase in the beginning of the analysis, but ultimately lower final values. Nevertheless, the maximum difference for the  $p_{cr}/p_{FL}$  ratio at the end of the analysis is 3%.

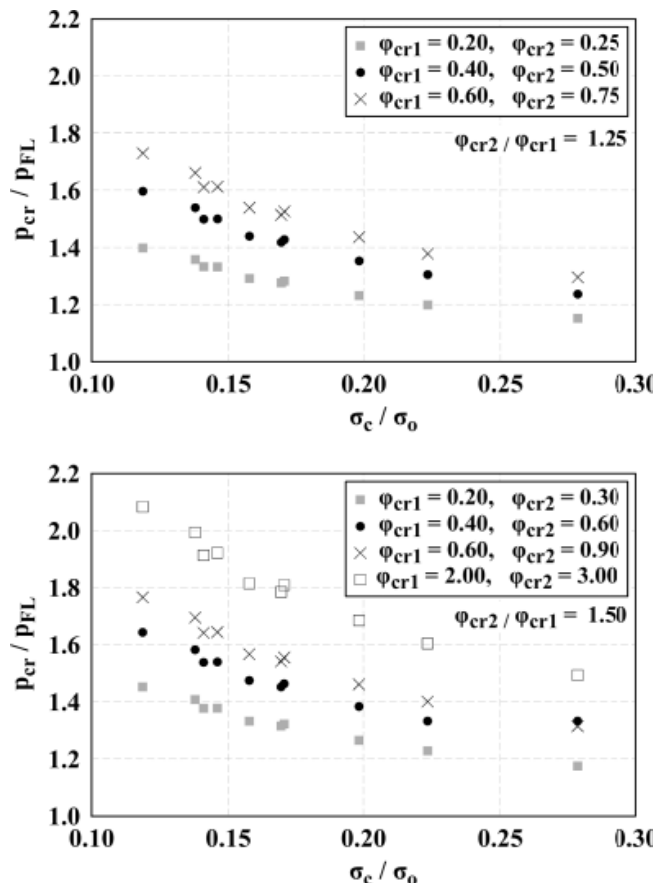


Figure 6. Distribution of the  $p_{cr}/p_{FL}$  ratio as a function of the geotechnical conditions ratio  $\sigma_c/\sigma_o$  for different combinations of the creep factors.

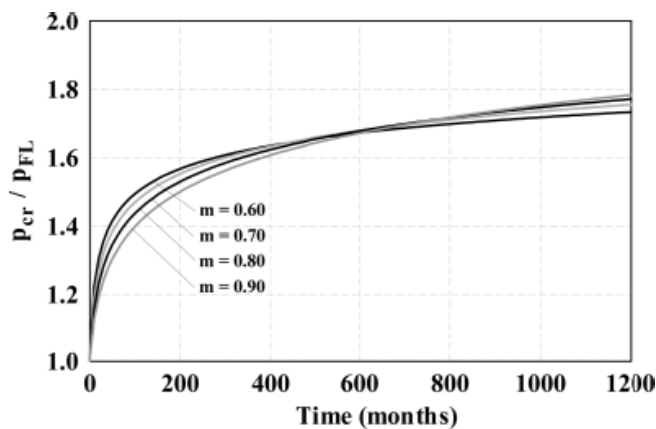


Figure 7. Development of the  $p_{cr}/p_{FL}$  ratio for different values of the  $m$  parameter of the Singh-Mitchell creep model (GSI=25,  $\sigma_{ci} = 4\text{MPa}$ ,  $\sigma_c/\sigma_o = 0.12$ ,  $\varphi_{cr1} = 0.60$ ,  $\varphi_{cr2} = 0.75$ ).

## 6 CONCLUSIONS

The role of rock mass creep can be significant, and sometimes critical, in tunnel analysis, especially in cases of unfavourable geotechnical conditions. However, often it is neglected in the analysis, until it becomes evident from construction monitoring data that there is a significant development of phenomena associated with time-dependent behaviour of the rock mass (e.g. delayed convergence, cracking on the support shell).

Based on the results of numerical analyses, the most critical creep parameter for the estimation of the additional tunnel loads is the potential creep strain that would develop in a tunnel with yielding support during the design life. This parameter also controls the magnitude of the deformation

restrained by the tunnel shell, resulting to the increased tunnel loads. The rate of creep deformation increase proved to be insignificant for the long-term tunnel loads.

In the proposed framework, two parameters were introduced in order to quantify the rock mass creep behaviour ( $\varphi_{cr}$  and  $t_{50\%}/t_d$ ). The ratio of the average final lining load after and before the creep simulation ( $p_{cr}/p_{FL}$ ) can be correlated very well with the values of  $\varphi_{cr}$  and the geotechnical conditions ratio. The resulting normalized diagrams can be used for the estimation of the additional creep loads. For the examined range of geometrical, geotechnical and creep parameters, the long-term increase of loads may reach up to 110% in some cases.

In case of tunnels that exhibit short-term creep phenomena with available pressure cells measurements, these diagrams may also be used to back calculate the rock mass creep parameters, so as to estimate the longterm final lining load and subsequently use it for the dimensioning of the concrete section. It is noted that these diagrams are based on the assumption of elastic behaviour of the temporary support and final lining. In the case of squeezing conditions and temporary support failures the measured loads may be significantly lower due to the increased shotcrete flexibility associated with shell failures.

## REFERENCES

- Aristorenas, G. 1987. *Time dependent behaviour of tunnels excavated in shale*. PhD thesis, Massachusetts Institute of Technology, USA.
- Barla, G., Bonini, M. & Debernardi, D. 2010. Time dependent deformations in squeezing tunnels. *International Journal of Geoengineering Case Histories* 2(1): 40–65.
- Boidy, E., Bouvard, A. & Pellet, F. Back analysis of time dependent behaviour of a test gallery in claystone. *Tunneling and Underground Space Technology* 17(4): 415–424.
- Chern, J.C., Shiao, F.Y. & Yu, C.W. 1998. An empirical safety criterion for tunnel construction. *Proceedings of the Regional Symposium on Sedimentary Rock Engineering, Taipei*: 222–227.
- Debernardi, D. 2008. *Viscoplastic behaviour and design of tunnels*. PhD thesis, Politecnico di Torino, Italy.
- Fortsakis P. 2012. *Investigation of the static interaction of the surrounding soil/rock with the tunnel final lining*. PhD thesis, National Technical University of Athens (NTUA), School of Civil Engineering, Department of Geotechnical Engineering, Athens (in Greek).
- Ghaboussi, J. & Gioda, G. 1977. On the time-dependent effects in advancing tunnels. *International Journal for Numerical and Analytical Methods in Geomechanics* 1: 246–269.
- Hoek, E., Carranza-Torres, C. & Corkum, B. 2002. Hoek-Brown failure criterion. *Proceedings of the 5th North American Rock Mechanics Symposium and 17th Tunnelling Association of Canada, Toronto, Canada*, 1: 267–273.
- Hunaj-Sarihan, N. 2009. Creep movements of reactivated landslides. In Baligh, F., Abdelmohsen, H., Abouseeda, H. & Abdelghani, K. (eds), *Proceedings of the 4iYGEC: 4th International Young Geotechnical Engineers Conference. Alexandria, Egypt, 3–6 October*, 325–328.
- Kontogianni, V., Psimoulis, P. & Stiros, S. 2005. What is the contribution of time-dependent deformation in tunnel convergence? *Engineering Geology* 82: 264–267.
- Lacasse, S. & Berre, T. 2005. Undrained creep susceptibility of clays. *Proceedings of the 16th International Conference on Soil Mechanics and Geotechnical Engineering, Osaka, Japan*: 531–536.
- Mansour, M.F., Martin, C.D. & Morgestern, N.R. 2008. Characterization of creep movements at the Little Chief Slide, BC. *Proceedings of the Canadian Geotechnical Conference & 9th Joint CGS/IAH-CNC Groundwater Conference, Edmonton, Canada, 21–24 September*, 461–468.
- Marinos, P. & Hoek, E. 2000. GSI: a geologically friendly tool for rock mass strength estimation. *Proceedings of the GeoEng2000 at the International Conference on Geotechnical and Geological Engineering, Melbourne, Australia*: 1422–1446. Lancaster: Technomic publishers.
- Marinos, V., Marinos, P. & Hoek, E. 2005. The geological strength index: applications and limitations. *Bulletin of Engineering Geology and the Environment* 64: 55–65.
- Naghdi, P. & Murch, S. 1963. On the mechanical behavior of viscoplastic/plastic solids. *Journal of Applied Mechanics* 30(3): 321–328.
- Nomikos, P., Rahmamejad, R. & Sofianos, A. 2011. Supported axisymmetric tunnels within linear viscoelastic Burgers rocks. *Rock Mechanics and Rock Engineering* 44: 553–564.
- Pan, Y.W. & Dong, J.J. 1991. Time-dependent tunnel convergence – I. Formulation of the model. *International Journal of Rock Mechanics and Mining Sciences & Geomechanical Abstracts* 28(6): 469–475.
- Perzyna, P. 1966. *Fundamental Problems in Viscoplasticity*. Advances in Applied Mechanics 9: 244–377.
- Sandrone, F., Dudt, J.P., Labiouse, V. & Descoeudres, F. 2006. In Van Cotthem, Charlier, Thimus & Tshibangu (eds) *Analysis of delayed convergences in a carbon zone of the Lötschberg Tunnel. Proceedings of the EUROCK 2006 – Multiphysics Coupling and Long Term Behaviour in Rock Mechanics. Liege, Belgium 9–12 May*.
- Singh, A. & Mitchell, J.K. 1968. General stress-strain time functions for soil. *Journal of the Soil Mechanics and Foundations Division*, 94, Proceedings paper 5728, 21–46.
- Sulem, J., Panet, M. & Guenot, A. 1987b. An analytical solution for time-dependent displacements in a circular tunnel. *International Journal of Rock Mechanics and Mining Sciences & Geomechanical Abstracts* 24(3): 155–164.
- Tavenas, F., Leroueil, S., La Rochelle, P. & Roy, M. 1978. Creep behaviour of an undisturbed lightly overconsolidated clay. *Canadian Geotechnical Journal* 15(3): 402–423.
- Yu, C.W. 1998. *Creep characteristics of soft rock and modelling of creep in tunnel*. PhD thesis. University of Bradford, Great Britain.

## Tunnel behaviour and support in molassic rocks. Experience from 12 tunnels in Greece

V. Marinos

*Aristotle University of Thessaloniki, Greece*

G. Prountzopoulos & P. Fortsakis

*National Technical University of Athens, Greece*

**ABSTRACT:** Molasse consists of a series of tectonically undisturbed sediments of sandstones, conglomerates, siltstones and marls, produced by erosion of mountain ranges after the orogenesis. Molassic rock masses may have very different structure close to the surface as compared to those confined in depth, where bedding planes, do not appear as clearly defined discontinuity surfaces. The present paper focuses on the tunnelling experience through molassic formations, based on data from the design and construction of twelve tunnels in Egnatia Highway in northern Greece. The fundamental tool for this research was TIAS database, which has been used for the storage, retrieval and correlation of the available data. The rock mass behaviour that was anticipated during construction is described and the molasse specific GSI chart is validated. In conclusion, a standardization of the geotechnical behaviour of molassic rock mass types and the temporary support categories that have been successfully implemented is presented.

### 1 INTRODUCTION

The present paper addresses the issue of tunnelling through molassic rocks, based on the experience gained from the design and construction of tunnels in Egnatia Highway in northern Greece. The scope of this work is to set a framework concerning the different types of molassic rocks, the geotechnical behaviour of each type in tunnelling and the temporary support philosophy, both for underground construction and portal areas. The main characteristics of the geomaterial in question that cause its particular behaviour are (a) the lithological heterogeneity, as the formation consists of almost uninterrupted series of sandstones, siltstones, marls or claystones and conglomerates, with alternations of layers from just some centimeters to even few meters thick, (b) the low to moderate strength of the intact rock of these alternations, (c) the compact, almost intact structure in depth, even when sandstone beds alternate with siltstones and (d) the problematic behaviour of the formation close to the surface, due to slaking and weathering, especially of the siltstone parts.

A fundamental tool of this research was a database specifically established, where all relevant to investigation, tunnel design and construction data were stored and retrieved, the TIAS database (Tunnel Information and Analysis System, Marinos et al. 2012). The 12 tunnels in the molassic formation of the Panagia – Grevena section of Egnatia Highway are shown in Table 1.

### 2 ENGINEERING GEOLOGICAL FEATURES

#### 2.1 Geological setting

The term molasse comes from a Swiss local name assigned initially to soft sandstones associated with marls and conglomerates belonging to the Tertiary and had a great development in the lowland parts of Switzerland. They have resulted from debris of weathering and erosion of the Alps mountain belt. The term is now used to describe the deposits from the erosion of an entire mountain range, after the final phase of orogenesis behind the mountain building area. The environment is geologically "quiet" and compression effects are mainly confined to the peripheries of new basins.

As molasse characterizes a series of sediments formed and developed after the main orogenesis, it has not suffered

Table 1. Tunnels through molasse in the Egnatia Highway.

Tunnel name	Length (m)	Maximum overburden (m)
Sirtos	1520	112
Ag. Triadas	385	14
Ag. Paraskeuis	500	35
Agnanteros	720	40
Prionia	780	40
Velanidia	640	40
Nika	465	45
Lagadia	425	60
Zigra	385	50
Kiloma	1040	80
Karantza	715	80
Venetikos	700	50

compression, shears and thrusts, thus deterioration of the quality of the rock mass is limited. Only in few cases the molassic formations may be deformed and present thrusts due to the final advance of tectonic napes, but such a decrease of their quality is localized. In such cases, mild folds or minor tectonic slips are present. Gravity faults are common, but their impact in the deterioration of the quality of the rock is limited. Hence, there are no extensively developed poor zones, i.e. fractured, folded or sheared. The inclination of strata is generally low and cases with more than 30° dips are rare.

#### 2.2 Engineering geological characteristics

The particularity of the molassic rock masses focuses on the variable heterogeneity, the presence of low strength geomaterials and the compact structure with depth. The principal engineering geological characteristics of molassic formations are the following:

- Alternations of competent sandstone and/or conglomerate beds and incompetent – generally of low/moderate strength – siltstone or claystone,
- Poor – weak diagenesis in some cases,
- Weathering of siltstone – claystone due to the phenomenon of fission (slaking),
- Detrimental effect of water on the siltstones – clay members and their discontinuities.
- Differentiation of the structure with depth (expressed stratification and discontinuous structure at the surface and close to it, continuous and tight structure in depth).

The various types of molasses, as reported below, mainly concern sandstone and siltstone alternations of different quota and thicknesses. There is also a rather common occurrence of conglomerates that range from very compact (calcitic) to loose (clayey). These rocks can alternate in layers of tens of centimetres to few metres or appear as massive strata. Lateral transitions between layers are common.

#### 2.3 Differences in depth and on surface

Molassic rocks present significant differences between surface and depth. These differences lie on rock mass structure, weathering and permeability and consequently are very important for the rock mass quality and behaviour in tunnelling.

Molassic rocks, particularly with sandstone and well-cemented conglomerates, tend to be highly frictional. Due to the limited deformation to which they have been subjected during deposition, the joints in these rocks are generally

free from the effects of shear movement (slickensides). Siltstone or claystone beds, being confined soon under the surface, are compact enough to form an almost continuous medium. Their presence may however reduce the strength of the overall mass. Yet, in few cases where siltstones are fairly strong and under low stress, their behaviour does not significantly differ from that of sandstones.

The bedding is the essential joint set in a molassic rock mass, but is only expressed on and near the surface. In depth it is mainly concealed. For the cases analysed in this paper, RQD values near the surface range from 0% to 50%. After some metres (~5m) rock masses become medium fractured and weathered, while bedding planes are still evident. In depths larger than 10–15 m, rock masses are usually homogeneous in structure and compact with RQD values >60%.

Weathering alters the rock mass strength significantly. Siltstone (or marly) members are very vulnerable to weathering and fissility may be developed parallel to the bedding when these rocks are exposed to the surface or are very close to it. Siltstone (or marly) members in outcrops appear thinly layered and when they alternate with sandstones, the appearance of the rock mass resembles to flysch. This appearance in outcrops can be misleading when considering the behaviour of molassic rocks in a confined underground environment, in which the process of air slaking is restricted and the rock mass is continuous and massive.

In some cases, sandstones are loose and may be treated as dense sands. In such weak molasses, clays and silts also appear and the material can be treated like a soil. This paper does not address these soil-like molasses that have limited spatial distribution. Yet, it should be noted that molasses near the surface may create a cover with such soil characteristics.

The overall permeability of the molassic formation decreases very rapidly with depth according to the results of in-situ permeability tests presented by Marinos et al. (2008). More specifically, the permeability of sandstone molasse is significantly higher than in the case of the siltstone one. In the case of alternations of the two rock types, permeability approaches the value of the siltstone, since the siltstone layers do not allow the water flow through the rock mass and decrease the overall permeability. Furthermore, the frequent lateral transitions do not permit the development of a uniform aquifer. Fault zones, although more permeable are neither numerous nor wide. Hence, although the water table will usually be above the tunnel elevation, only limited water inflows are anticipated, although in some situations it may be necessary to relieve water pressures by drillholes.

#### 2.4 Molasse rock mass types

The molassic formations are distinguished and classified in rock mass types (I to VI) mainly based on the participation ratio of sandstone and siltstone members (Fig. 1).

#### 2.5 Molasse classification

The GSI classification system for molassic formations was used along the 12 tunnels (Hoek et al. 2005). The use of this GSI chart assisted to the construction of almost all tunnels with much lighter support measures than what was initially foreseen.

The GSI classification for molasses (Hoek et al. 2005) was based on the observations and evaluations from the design of the 12 tunnels along the Egnatia Highway. This approach led to two charts, one for surface and one for depth. The validation of the proposed GSI charts for molasses is hereafter discussed.

Since molassic rock masses are confined in depth and bedding planes do not appear as clearly defined discontinuity surfaces as in flysch and the rock mass is massive, the use of the initial GSI chart (Marinos & Hoek 2000) is recommended and a value of 50–60 or more is to be applied. These values were validated during construction. If no discontinuities are present, GSI is very high (GSI>75) and the rock mass can be treated as intact with engineering parameters given by laboratory testing. When fault zones were encountered in depth, GSI values generally lied in the range of 35–50 (Blocky-Disturbed structure). This is a difference with the original chart (area M2 in Hoek et al. 2005) that suggested more disturbed and disintegrated rocks and accordingly lower GSI values.

On the surface, the heterogeneity of the formation is discernible and similarities exist with the structure of some flysch types. Hence the GSI chart for heterogeneous rock masses (Marinos et al. 2011) can be used. This version of the chart, for fissile molassic rocks had been presented by Hoek et al. (2005). These values were also confirmed during tunnel construction.

#### 2.6 Intact rock properties

A large number of results from laboratory tests regarding the intact rock properties have been presented by Marinos & Tsiambaos (2010). It is evident that the strength and deformability parameters of siltstone are lower than the corresponding values of sandstone, but this difference is not as significant as in the case of flysch ground types (Table 2).

### 3 BEHAVIOUR TYPES

The high strength of the molassic rock mass compared to the in situ stresses at shallow to medium depths, does not qualify serious stress-induced phenomena. The dominant failure mode in tunnels is the gravity driven falls and slides of blocks and wedges defined by intersecting joints and bedding planes. It should be underlined though, that this behaviour has been verified during construction of tunnels under a maximum overburden of 110m and shall not be considered for much greater depths.

Generally, the behaviour of the molassic formations during tunnelling depends on three major parameters. That is (a) the structure, (b) the dominant rock type intact strength and (c) the depth of the tunnel. Therefore the expected behaviour types can be illustrated in Fig. 2. These behaviour types are distinguished in two areas (M1 and M2, see Fig. 2):

- Stable (St), in the case of intact, massive structure and shallow to medium depths. As the tunnel depth increases, stable behaviour with negligible deformation is observed for sandstone or conglomerate dominated formations.
- Stable (St), with only limited deformation (Sh), especially in cases of siltstone dominated formations, under significant overburden. The magnitude of the resulting deformation depends on the strength of the siltstone and the tunnel depth. Serious deformation has not been encountered in the Egnatia tunnels, as the maximum depth was limited to 110 m.
- Wedge failure (Wg), in cases of blocky structures and shallow to medium depths. As the tunnel depth increases, the same behaviour with insignificant deformation is observed for sandstone or conglomerate dominated formations. The increasing confinement with depth may result in less frequent wedge failure incidents (St-Wg). A slightly different failure mechanism can manifest in the case of thin-bedded formations with almost horizontal bedding planes. Failure of rock plates due to selfweight from the crown area may be frequent and intense once their base is exposed, due to deconfinement that may

<p><b>Type I</b> Thick to medium thickness sandstone beds with sporadic thin films of siltstone</p>	<ul style="list-style-type: none"> <li>• Thick sandstone layers (&gt;5m), separated by sparse thin siltstone intercalations (few cm).</li> <li>• Sandstones have generally high strength, which can be lower when they are silty or marly.</li> <li>• Compact in depth, but near the surface silty or marly sandstones may exhibit separation parallel to the bedding.</li> </ul>	
<p><b>Type II</b> Sandstone with siltstone interlayers</p>	<ul style="list-style-type: none"> <li>• Sandstone beds with thickness from 50cm to few meters (~ 5m). They are separated by siltstone intercalations, few cm to 30cm thick.</li> <li>• In depth, though heterogeneous, is uniform and compact. Near the surface may exhibit some separation and loosening with friable parts.</li> </ul>	
<p><b>Type III</b> Rockmass with sandstone and siltstone similar amounts</p>	<ul style="list-style-type: none"> <li>• Systematic alternations of siltstones and sandstones, with beds thickness of few tens of centimeters to few meters (~5m), in similar proportions.</li> <li>• At depths (&gt;~ 6-10m), rock mass is massive and continuous. Near the surface is laminated.</li> <li>• Lithologic heterogeneity and other discontinuities, only at the surface due to splitting.</li> </ul>	
<p><b>Type IV</b> Siltstone with sandstone interlayers</p>	<ul style="list-style-type: none"> <li>• Low degree of weathering in depth but high near the surface.</li> <li>• Siltstone beds are formed by thin to medium thick layers. Sandstone layers are usually thin (~10-20cm).</li> <li>• Main discontinuity is the bedding, showing great persistence (&gt;10m) but is strongly sealed and "virgin".</li> </ul>	
<p><b>Type V</b> Siltstone with sparse sandstone interlayers</p>	<ul style="list-style-type: none"> <li>• Main level of weakness is the bedding.</li> <li>• Large strength variation. Can be fresh to completely weathered.</li> <li>• In the non-weathered nature (depths&gt;~6-10m), formation is massive (the bedding is unnoticeable or "virgin").</li> <li>• In surface, bedding and discontinuities separate the siltstone (air-slaking), resulting in complete collapse of the fabric. May have expandable clay minerals.</li> </ul>	
<p><b>Type VI</b> Conglomerate</p>	<ul style="list-style-type: none"> <li>• Found in intercalations and less as an independent thick horizon.</li> <li>• Cementation may be weak to moderate, when comprised of silty-clayey materials, and strong when matrix is calcitic.</li> </ul>	

Figure 1. Typical types of molassic rock masses on tunnel faces in Egnatia Highway.

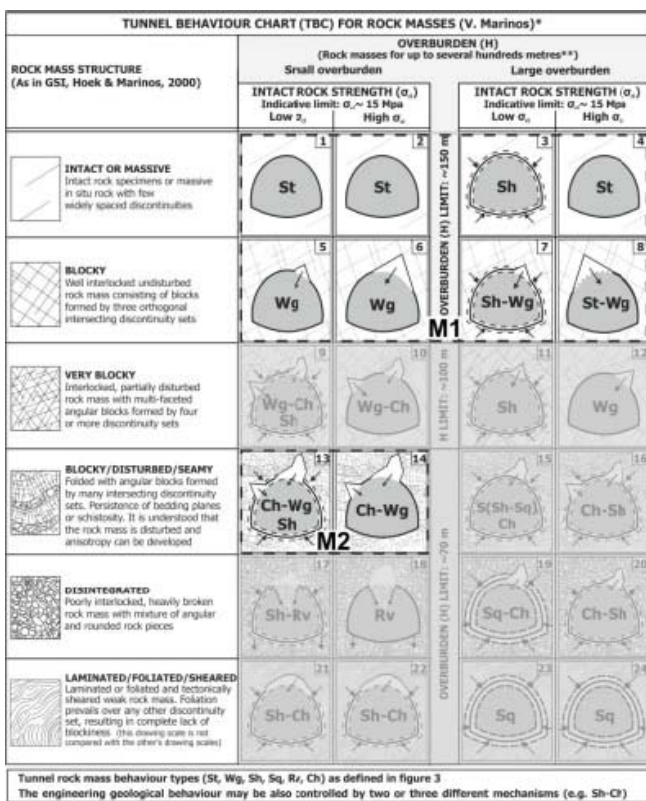
Table 2. Molasse intact rock properties (Marinos & Tsiambaos 2010).

Rock material	$\sigma_{ci}$ (MPa)					$E_i$ (GPa)					$MR = E_i/\sigma_{ci}$			
	n	min	max	$\mu$	$\sigma$	n	min	max	$\mu$	$\sigma$	n	range	$\mu$	$R^2$
Sandstone	238	10.8	116.7	35.1	21.1	132	2.0	31.3	8.8	7.4	123	100–260	170	0.87
Siltstone	152	1.92	51.1	16.9	10.8	58	0.7	9.1	3.0	1.9	58	120–220	160	0.87
Conglomerates	165	5.0	68.2	23.1	13.9	82	1.1	19.4	7.4	5.1	79	180–670	375	0.69

$\sigma_{ci}$ : intact rock uniaxial compressive strength,  $E_i$ : intact rock deformation modulus, MR: Modulus Ratio, n: number of samples, min: minimum values, max: maximum values,  $\mu$ : mean value,  $\sigma$ : standard deviation.

cause subvertical tension cracks. Such unfavourable conditions have to be faced, in order to avoid systematic overbreaks.

- Frequent wedge failure that can evolve into chimney type failure (Wg-Ch), in the case of very blocky rock masses due to faulting. In the case of siltstone dominated formations in medium to large depths, limited deformation (Sh) can occur. It is reminded that serious deformation has not been encountered in the tunnels of the Egnatia Highway, as the maximum depth of the tunnels was 110 m.



Concerning water inflows, limited presence of water has been met in the 12 tunnel projects, which occur mainly in the form of increased moisture to drip. In some rare cases, occasional or continuous low flow at various locations mainly in sandstone-siltstone contact layers and along major discontinuities has been encountered. Nevertheless, this presence degrades the characteristics of the discontinuities and should be taken into account when assessing the geotechnical characteristics of the formation.

The low geotechnical properties of the molassic formations close to the surface have led to several slope failures in the portal areas. These failures were not guided from pre-existing discontinuities such as the bedding planes, but they were associated with the development of a new circular-shaped surface through the weak rock mass. Fig. 3 shows a typical slope failure in conglomerates at the entrance of Karatzas tunnel in Egnatia Highway.



Figure 3. Landslide in molassic formation at the entrance portal of the Karatzas tunnel in Egnatia Odos.

Figure 2. Tunnel behaviour chart for typical molassic rock masses, based on the chart produced by Marinos (2012).

- Wedge failure, with only limited deformation (Sh-Wg), in the case of siltstone dominated formations, under significant overburden. The magnitude of the resulting deformation again depends on the strength of the siltstone and the depth of the tunnel.
- Extensive wedge failure that can evolve into chimney type failure (Ch-Wg), in the case of weathered and disturbed structure, close to the surface (portal areas or tunnelling in shallow depth under streams or gullies), due to slaking of the siltstone parts.

#### 4 TUNNEL SUPPORT

The support philosophy in molassic formations shall take into account the rock mass structure and the observed failure mechanisms, in relation to the tunnel depth as described above. These approaches for the philosophy of temporary support categories have been shaped based on the geotechnical behaviour of the molassic formation, as well as on construction data. In the Egnatia Highway tunnels through molassic formations 54% of the total length has been excavated implementing a support category with shotcrete shell, bolts, steel sets and light spilling. A very

light support category containing a thin shotcrete shell and a sparse grid of bolts has been adopted for the 38% of the total length. Finally a heavy support category with thick shotcrete shell, steel sets, forepolling and fibreglass nails have been implemented in only 6.5% of the total length and mainly at the area of the portals. Therefore, away from the ground surface, where the rock mass is subjective to surface weathering conditions and any possible fault zones, there are two basic types of temporary support sections that could be applied.

The first type concerns stable conditions with only local gravity type failures and small to insignificant deformation (Fig. 4). This is the most common case for all molasse types in depth and shall be applied for low to medium overburden, or even under higher overburden in cases of sandstone or conglomerate domination. The temporary support consists of a thin shotcrete layer and a pattern of rock bolts, whereas the excavation step can be 3–4 m. Additionally, it is proposed to apply wire mesh to avoid small rock falls instead of fibre reinforced shotcrete. The first 3–5 cm thick layer of shotcrete applied on the exposed rock mass surfaces as soon as possible seals and protects the siltstone layers from slaking. The rock bolts pattern strengthens the rock mass, keeps it confined and prevents possible gravity driven falls of relaxed, structurally defined blocks or wedges, or falls due to decompression of the, otherwise, sealed bedding planes. The addition of a second layer of shotcrete, reinforced either by wire mesh or by fibres, creates a complementary shell, incorporating the rock bolts' heads and ensuring overall stability of the excavation.

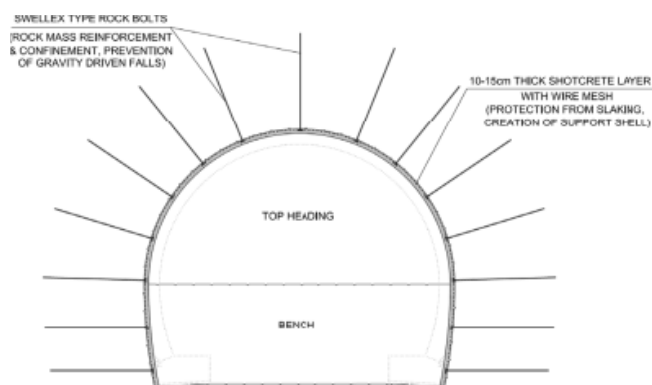


Figure 4. Typical support design for the molassic formations of category M1 (see Fig. 2).

The second support section type (Fig. 5) for sound molasse away from portals or faults refers (a) to conditions with frequent wedge failures due to the geometry of major discontinuities and the conditions already presented (horizontal bedding planes) and/or (b) to cases of weak rock (e.g. siltstone) dominated molassic formations under considerable to high overburden. Additionally to the shotcrete and the rock bolts, light steel sets may be required, whereas the excavation step has to be limited (around 2 m), in order to avoid any wedge formation or significant deformation in the case of large depths.

For the weathered molassic formations close to the tunnel portals or the heavily jointed and weak molassic rock masses within fault zones, there is need for a more stiff support, by means of heavier steel sets and a stronger shotcrete shell. Attention shall be given to cause minimum disturbance to the surrounding geomaterial, by minimizing the excavation step (~1 m). Additionally, it may be necessary to stabilize the tunnel face, using face reinforcement measures (e.g. fibreglass nails) or face protection schemes (e.g. spiles, forepole umbrella), in order to avoid progressive detachment, deconfinement and creation of chimney type failures.

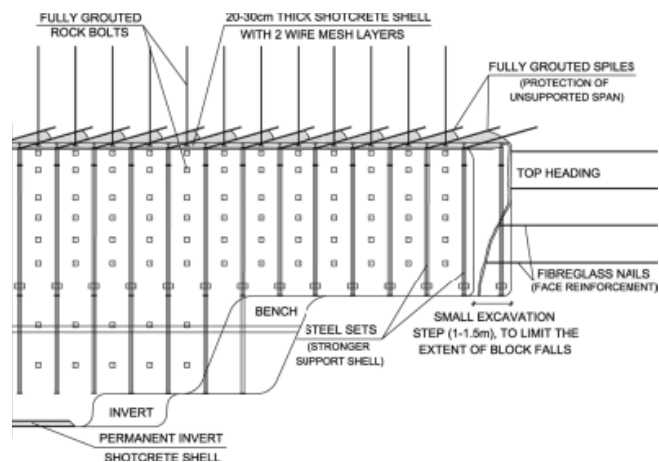


Figure 5. Typical support design for the molassic formations at portal areas, near the surface or in the vicinity of faults/shear zones (Category M2, see Fig. 2).

## 5 CONCLUSIONS

The paper concentrates on the engineering assessment of the molassic formation, on the issues of design parameters and tunnel support. Detailed records from the design and construction of 12 tunnels with lengths of 385m to 1520m and under maximum cover up to 110m were evaluated.

The molasses characterize a sequence of alternations of sandstones, siltstones-mudstones and conglomerates. The molasses form rock masses with dramatically different structure when they outcrop or are close to the surface and when they are confined in depth. In depth they are undisturbed and massive since they have not suffered from compression, shears and thrusts. In outcrops they appear heterogeneous, disturbed and sometimes loose to disintegrate. For the assessment of rock mass properties, GSI charts for molasses (Hoek et. al. 2005) were used. This assisted to the construction of almost all tunnels with lighter support measures. The validation of the proposed GSI charts for molasses is discussed.

The dominant failure mode in the tunnels was wedge falls and slides of blocks. Deformation problems experienced under the maximum overburden of 110m were minor. A medium support class was generally applied and in many cases steel sets have not been applied and the support class has changed to a light category with rock bolts and thin to medium layer of shotcrete. Tunnel face pre-support with spiles was only used when immediate gravity driven failures were anticipated, due to the geometry of formations and the loosening of the rock mass.

## REFERENCES

- Hoek, E., Marinos, P. & Marinos, V. 2005. Characterisation and engineering properties of tectonically undisturbed but lithologically varied sedimentary rock masses. *International Journal of Rock Mechanics and Mining Sciences*, 42(2): 277–285.
- Marinos V. 2012. Assessing rock mass behavior for tunnelling. *Journal of Environmental and Engineering Geoscience*, Vol. XVIII, No. 4, pp. 327–341.
- Marinos, P., Marinos V., Fortsakis, P. & Proutzopoulos G. 2008. Permeability of flysch and mollase. Distribution, comparison and decrease with depth. *Proceedings of the 8th International Hydrogeological Congress, Athens, Greece*, 2: 587–596.
- Marinos, V., Fortsakis, P. & Proutzopoulos, G. 2011. Estimation of geotechnical properties and classification of geotechnical behaviour in tunnelling for flysch rock masses. In

Anagnostopoulos, A. Pachakis, M. & Tsatsanifos, C. (eds), *Geotechnics of Hard Soils – Weak Rocks; Proceedings of the 15th European Conference on Soil Mechanics and Geotechnical Engineering, Athens, Greece, 12–15 September*, 1: 435–440. Amsterdam: IOS Press.

Marinos, P. & Hoek, E. 2000. GSI: a geologically friendly tool for rock mass strength estimation. *Proceedings of the GeoEng2000 at the International Conference on Geotechnical and Geological Engineering, Melbourne, Australia*, 1422–1446. Lancaster: Technomic publishers.

Marinos, V., Proutzopoulos, G., Fortsakis, P., Koumoutsakos, D. & Papouli, D. (2012) Tunnel Information and Analysis System: A geotechnical database for tunnels. *Geotechnical and Geological Engineering*. doi: 10.1007/s10706-012-9570.

Marinos, V. & Tsiambaos, G. 2010. Strength and deformability of specific sedimentary and ophiolitic rocks. In Koukis, G., Zelilidis, A. Koukouvelas, I., Papatheodorou, G., Geraga, M. & Zygouri, V. (eds), *Planet Earth: Geological Processes and Sustainable Development, Bulletin of the Geological Society of Greece and Proceedings of the 12th International Congress. Patras, Greece, 19–22 May, XLIII*, 3:1259–1266.

## Elastic response of laterally loaded rock sockets using 3D finite element analyses

K.P. Tzivakos, M.J. Kavvadas & D.G. Kaltsas  
National Technical University of Athens, Greece

**ABSTRACT:** The paper presents a numerical study of the elastic response of laterally loaded rock sockets. Sockets are loaded at the top with transverse forces and bending moments and the corresponding displacements and rotations are calculated. 3D finite element analyses are carried out to investigate the effects of shaft length, relative stiffness of socket to rockmass and the ratio of the applied moment to shear force. The rockmass is assumed to be linearly elastic, as rock sockets rarely reach the rockmass strength. However, socket-ground interface elements are used along the periphery and at the socket base in order to simulate separation and lift-up effects on the response. The results of the analyses are compiled in semi-empirical dimensionless relationships giving the socket stiffness in terms of the important parameters. The produced results show significant differences compared to the results of numerical analyses reported by Carter & Kulhawey (1992) where separation and lift-up effects were not included.

### 1 INTRODUCTION

Rigid sockets are nowadays an effective foundation type of structures founded with tall piers. The specific foundation undertakes significant horizontal loads and bending moments, thus it undergoes considerable horizontal displacement and rotation on its head.

Two different approaches are met in common engineering practice for the estimation of the aforementioned socket head deformation. One approach involves the subgrade reaction methods, including numerous methodologies of p-y curves for rock that serve the presence of non-linear, horizontal springs along the socket (Reese 1997, Gabr et al. 2002). On the other hand stands the elastic continuum theory, which treats the rigid socket as an equivalent spring with three independent degrees of freedom for the prescribed loading conditions (Douglas & Davis 1964, Carter & Kulhawey 1992).

The scope of the present paper is the evaluation of the socket head deformation predictions proposed by the most recent methodology of the latter approach. Furthermore it is attempted to derive corresponding closed-form equations through 3D finite element analyses, taking into account the frictional behavior and the possible separation between the laterally loaded rock socket and the surrounding rockmass.

### 2 THE CARTER & KULHAWY METHOD

#### 2.1 Assumptions

In the present chapter, a thoroughly determined methodology is described for the calculation of horizontal displacement and rotation of the socket head, namely the Carter & Kulhawey method (1992). The specific methodology has provided the engineering community with closed-form equations for the calculation of the aforementioned deformation, referring to rigid and flexible shafts. The present study investigates the behavior of rigid rock sockets, therefore only the part of the Carter & Kulhawey method with respect to rigid shafts is presented herein.

The socket is simulated by a hollow, cylindrical shaft of effective Young's modulus ( $E_e$ ), Poisson's ratio ( $\nu_e$ ), length ( $L$ ) and diameter ( $D$ ). For a rigid socket with stiffness  $(EI)_e - (E)$  for the Young's modulus of the socket construction material - the effective Young's modulus ( $E_e$ ) is calculated according to Equation 1.

$$E_e = \frac{(EI)_e}{(\pi D^4/64)} \quad (1)$$

The rock socket is considered perfectly elastic, installed in a homogenous, isotropic, elastic rockmass space with Young's elasticity modulus  $E_r$  and Poisson's ratio  $\nu_r$ . Thereafter, the socket head is subjected to prescribed lateral loading ( $H$ ) and bending moment ( $M$ ).

The study of Carter & Kulhawey (1992) uncovered that the effect of the rockmass Poisson's ratio ( $\nu_r$ ) is represented by the secant shear modulus of the rockmass, defined by Equation 2.

$$G^* = G_r \left( 1 + \frac{3\nu_r}{4} \right) \quad (2)$$

where  $G_r$  = the shear modulus of the isotropic rockmass.

For homogenous rockmass, it was determined that the deformation of the shaft head at the level of the rock surface depends on the relative moduli of the shaft and the surrounding rockmass ( $E_e/G^*$ ) and the geometry of the shaft ( $L/D$ ). Especially for rigid shafts, the graphs of Figure 1 were formed from the finite element analyses carried out by Carter & Kulhawey (1992), demonstrating the dimensionless shaft head displacement or rotation against the shaft-rockmass relative stiffness ( $E_e/G^*$ ). The pointed curves indicate that a laterally loaded shaft shall behave as rigid when the condition of the mathematical formulation  $(L/D) \leq 0.05 (E_e/G^*)^{1/2}$  is met.

#### 2.2 Prediction of the response of rigid shafts

Since the rock socket meets the rigidity conditions of Figure 1, it is considered rigid according to the aforementioned methodology. The closed-form solutions for head displacement ( $u$ ) and rotation ( $\theta$ ) of such sockets are described according to Carter & Kulhawey (1992) by Equations 3 and 4 respectively.

$$u = 0.32 \left( \frac{H}{G^*D} \right) \left( \frac{L}{D} \right)^{\frac{1}{3}} + 0.16 \left( \frac{M}{G^*D^2} \right) \left( \frac{L}{D} \right)^{\frac{7}{8}} \quad (3)$$

$$\theta = 0.16 \left( \frac{H}{G^*D^2} \right) \left( \frac{L}{D} \right)^{\frac{7}{8}} + 0.25 \left( \frac{M}{G^*D^3} \right) \left( \frac{L}{D} \right)^{\frac{5}{3}} \quad (4)$$

### 3 THE 3D FINITE ELEMENT SIMULATION

Numerous 3D finite element models of the single, free-head, laterally loaded socket are designed in the commercial code ABAQUS. Solid, 8-node, full integration finite elements are used to model the rockmass and the rock socket. The boundaries of the model are set to 6.5D, 2.5D and 5D from the center of the socket head along x, y and z axis respectively, where D is the socket diameter. At this point, it is important to clarify that the socket is simulated by a solid, elastic, reinforced concrete shaft of diameter  $D=5m$  with Young's modulus  $E=25$  GPa. Therefore, the effective Young's modulus according to Equation 1 is  $E_e = E$ . Various socket-rockmass relative stiffness ratios have been analyzed, namely  $E/G^* = 10, 50, 100, 150, 500, 750, 1000$  in order to examine the rigidity criteria of the sockets involved in the specific analyses. Furthermore, rock sockets with slenderness ratios  $L/D = 1, 1.2, 1.5, 1.8, 2, 3$  are included in the present study. However, not all the combinations of slenderness ratios and relative stiffness ratios refer to rigid sockets. Therefore, a specific procedure is carried out aiming at the determination of cases that shall contribute to the formation of the desired closed-form equations for the response of rigid sockets (see Section 4).

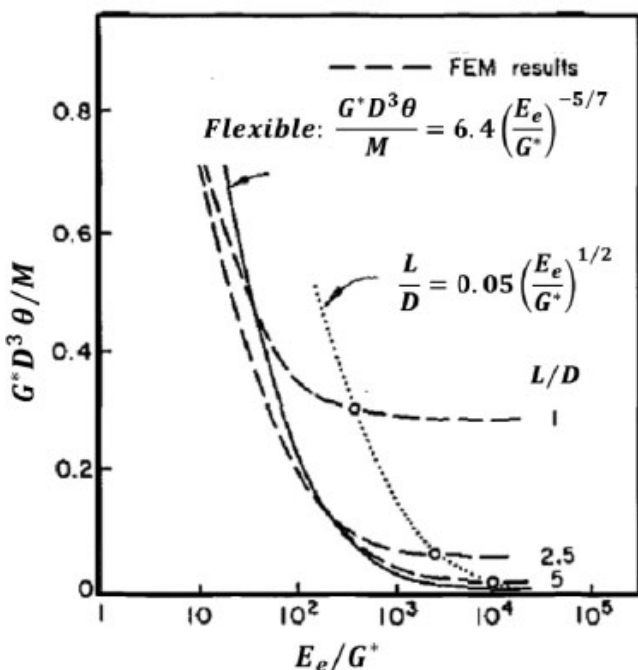
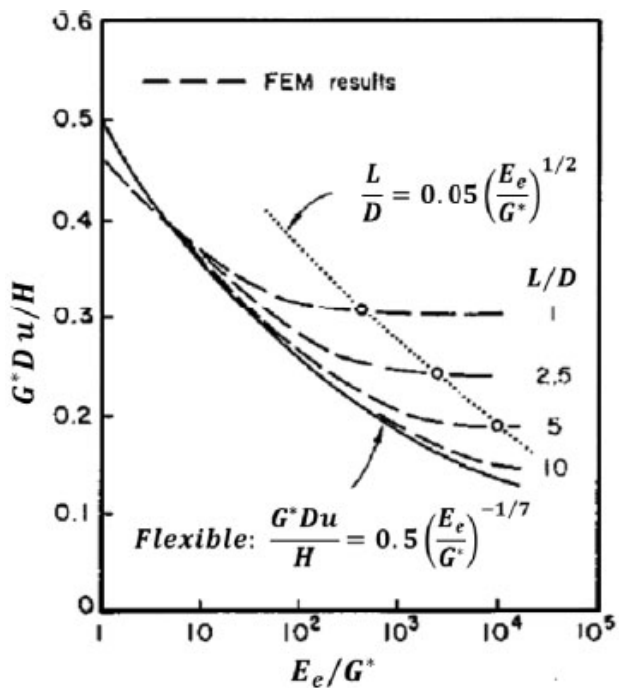


Figure 1. Lateral load-displacement (up) and moment rotation (down) relations according to Carter & Kulhawy (1992).

The rock socket is loaded with a concentrated lateral head load  $H=20\text{ MN}$  – the load is applied in specific load increments. Moreover, concentrated head moment  $M = 0, 300, 600\text{ MNm}$  is applied in equivalent increments, standing for eccentricity values  $e = M/H = 0, 15, 30\text{ m}$  respectively.

With respect to the socket-rockmass interaction, two different approaches are simulated in the finite element code. Initially, a hard contact is modelled between the rock socket and the surrounding rockmass in order to verify the predictions of the Carter & Kulhawy method for the rigid shaft response. The specific simulation is adopted, due to lack of shaft rockmass separation effects in the finite element analyses carried out by Carter & Kulhawy (1992). The second approach involves the simulation of socket-rockmass separation and friction through specially calibrated surface interactions. An exponential clearance pressure law is incorporated for the surface interaction in the normal direction, allowing for the separation of the socket

from the surrounding rockmass and the lift-up effects of the socket base (Fig. 2). The Mohr-Coulomb friction criterion is applied to simulate the shear stresses developed between the rockmass and the socket. The friction angle of the specific interaction is considered  $\delta=(2/3)\phi$ , where  $\phi$ =the internal friction angle of the rockmass with values ranging between  $30^\circ\text{--}45^\circ$ , depending on the rockmass properties.

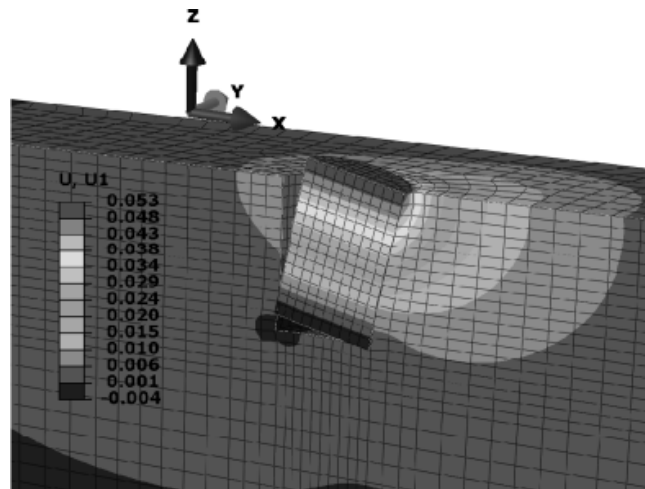


Figure 2. The 3DFEMmodel with socket-rockmass surface interaction (cut along the loading axis of the socket).

#### 4 PREDICTION OF RIGID SOCKET ELASTIC RESPONSE

The predictions of the present study for the elastic response of rigid rock sockets are demonstrated in the current section. Output from both hard contact and friction-separation approaches is presented herein, referring to the socket-rockmass interaction. Thus, the predicted elastic response of rigid sockets for the two aforementioned simulations is available for direct comparison. Furthermore, a comparative depiction of the predictions proposed by the present study against the solutions suggested by Carter & Kulhawy (1992) is attempted.

##### 4.1 The effect of the surface interaction simulation

Although the problem under consideration is linear in terms of materials, certain non-linearity occurs due to the complicated socket-rockmass surface interaction (see Section 3). A parametric study of the eccentricity is carried out in order to determine whether the surface interaction affects the calculated socket head deformation. More specifically, graphs of horizontal socket head displacement ( $u$ ) and rotation ( $\theta$ ) against the eccentricity ( $e$ ) are plotted for certain slenderness ratios ( $L/D$ ) and various socket-rockmass relative stiffness ratios ( $E/G^*$ ) (Fig. 3). A linear distribution of socket head deformation against the load eccentricity is observed. Consequently, the socket-rockmass surface interaction does not affect the linearity of the calculated socket head deformation.

##### 4.2 Determination of rigid sockets

In the following paragraph, all the possible comparisons of socket-rockmass relative stiffness ratios ( $E/G^*$ ) and socket geometries ( $L/D$ ) are taken into account in order to define perfectly rigid sockets, according to the finite element analyses results. In line with the procedure demonstrated by Carter & Kulhawy (1992), the rigid sockets of the present study exhibit head deformation that is independent of the socket-rockmass relative stiffness ( $E/G^*$ ).

Each deformation results from two components: the deformation due to the lateral load ( $H$ ) and the corresponding one due to socket head moment ( $M$ ). The general form of the socket head displacement ( $u$ ) and rotation ( $\theta$ ) is depicted by Equations 5–6 respectively:

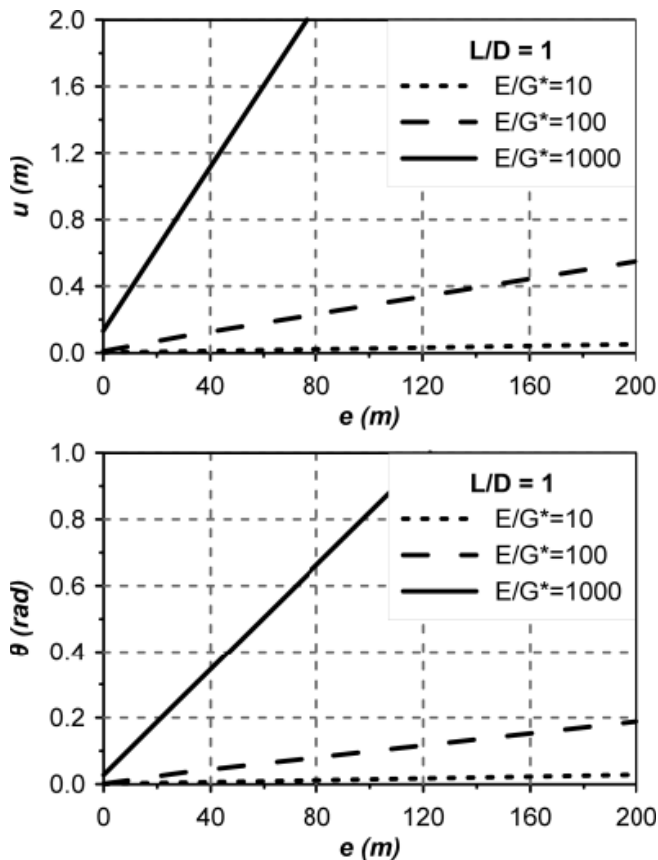


Figure 3. Linear distribution of socket head horizontal displacement (up) and rotation (down) with load eccentricity.

$$|u = u_H + u_M \quad (5)$$

$$|\theta = \theta_H + \theta_M \quad (6)$$

where  $u_H$  and  $\theta_H$  are computed by numerical analyses without the application of any bending moment ( $M=0$ ) on the socket head. On the other side,  $u$  and  $\theta$  are computed by the analyses carried out for any desired eccentricity value ( $e$ ).

Specific graphs are designed, illustrating dimensionless mathematical formulations of the socket head horizontal displacement and rotation against the socket-rockmass relative stiffness ratio ( $E/G^*$ ). Figure 4 depicts that the dimensionless deformation tends to depend less on the stiffness ratio ( $E/G^*$ ) with the increase of the latter.

As a consequence, for each socket slenderness ratio ( $L/D$ ) certain values of stiffness ratio ( $E/G^*$ ) are set as lower boundaries for the characterization of rigid sockets, as demonstrated in Table 1.

Table 1. Lower relative stiffness boundaries for rigid sockets.

Slenderness ratio (L/D)	Relative stiffness Hard contact ( $E/G^*$ )	Relative stiffness Interface ( $E/G^*$ )
1	100	150
1.2	150	150
1.5	750	150
1.8	750	150
2	750	500
3	750	750

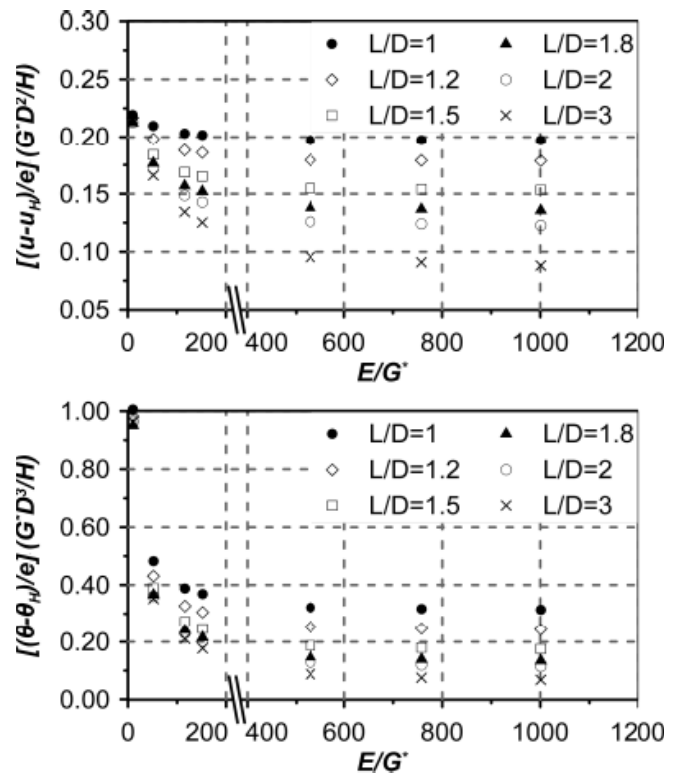


Figure 4. Dimensionless deformation against relative stiffness for the hard contact surface interaction approach.

#### 4.3 Proposed socket head deformation equations

The aforementioned cases of rigid sockets are processed in order to develop closed-form mathematical formulations for the prediction of socket head deformation, assuming either hard contact or sliding and separation effects between the foundation and the surrounding rockmass. The derived equations shall have the general form of Equations 7–8.

$$|u = A \left( \frac{H}{G^* D} \right) \left( \frac{L}{D} \right)^a + B \left( \frac{M}{G^* D^2} \right) \left( \frac{L}{D} \right)^b \quad (7)$$

$$|\theta = B \left( \frac{H}{G^* D^2} \right) \left( \frac{L}{D} \right)^b + C \left( \frac{M}{G^* D^3} \right) \left( \frac{L}{D} \right)^c \quad (8)$$

Consequently, the coefficients **A**, **a**, **B**, **b**, **C**, **c** have to be determined. In the previously presented equations it is obvious that coefficients **B**, **b** are common for displacements and rotations, thus representing the coupled spring stiffness.

Three separate charts are drawn from the finite element analyses output of each socket-rockmass interaction approach (hard contact or separation and sliding) in order to determine these coefficients. The graphs of Figure 5 depict dimensionless forms of  $u_H$ ,  $u$ ,  $\theta_H$ ,  $\theta$  on the vertical axis against the slenderness ratios ( $L/D$ ) of the rigid sockets selected in paragraph 4.2 on the horizontal axis. Thereafter, hyperbolic trendlines are drawn aiming at calculating the aforementioned coefficients. Figure 5 demonstrates the calculation procedure of **A**, **a**, **B**, **b**, **C**, **c** for the friction-separation surface interaction approach.

As a result, the closed-form Equations 9–12 of the present study are derived, referring to rock socket head deformation for:

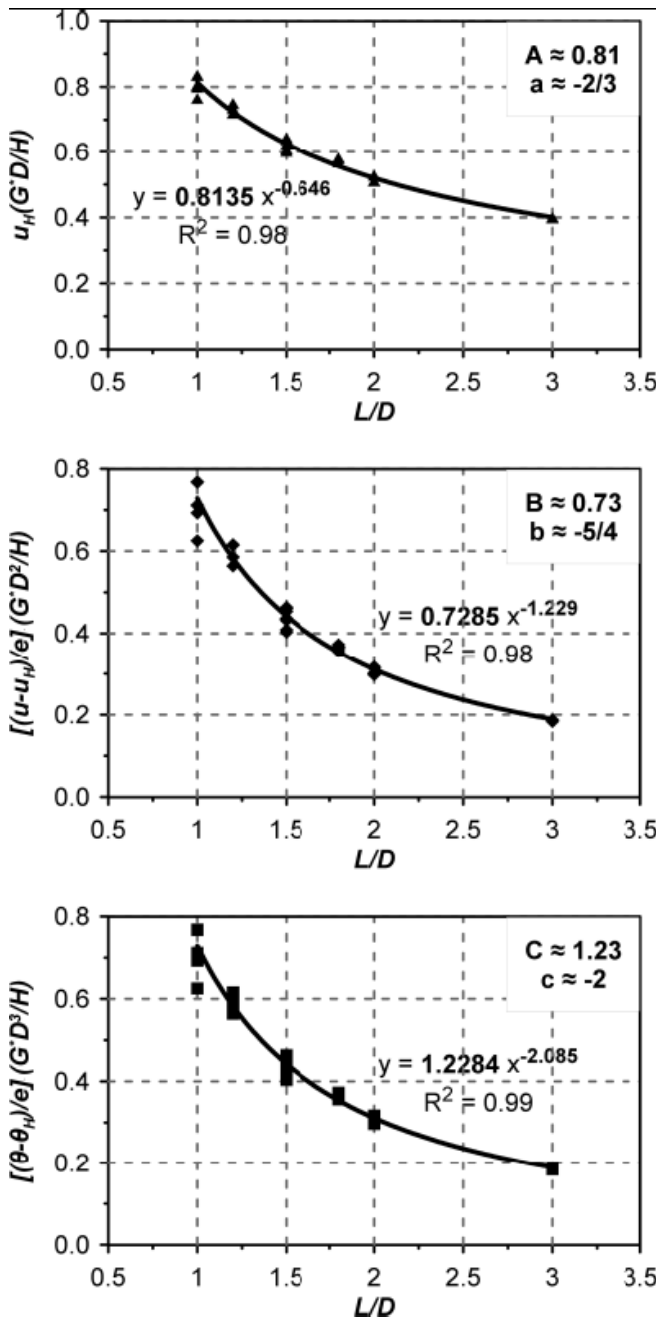


Figure 5. Calculation of the coefficients A, a, B, b, C, c for the friction-separation surface interaction approach.

(I) socket-rockmass hard contact

$$u_I = 0.29 \left( \frac{H}{G^* D} \right) \left( \frac{L}{D} \right)^{-\frac{1}{5}} + 0.20 \left( \frac{M}{G^* D^2} \right) \left( \frac{L}{D} \right)^{-\frac{3}{4}} \quad (9)$$

$$\theta_I = 0.20 \left( \frac{H}{G^* D^2} \right) \left( \frac{L}{D} \right)^{-\frac{3}{4}} + 0.35 \left( \frac{M}{G^* D^3} \right) \left( \frac{L}{D} \right)^{-\frac{3}{2}} \quad (10)$$

(II) socket-rockmass surface interaction

$$u_{II} = 0.81 \left( \frac{H}{G^* D} \right) \left( \frac{L}{D} \right)^{-\frac{2}{3}} + 0.73 \left( \frac{M}{G^* D^2} \right) \left( \frac{L}{D} \right)^{-\frac{3}{4}} \quad (11)$$

$$\theta_{II} = 0.73 \left( \frac{H}{G^* D^2} \right) \left( \frac{L}{D} \right)^{-\frac{3}{4}} + 1.23 \left( \frac{M}{G^* D^3} \right) \left( \frac{L}{D} \right)^{-2} \quad (12)$$

#### 4.4 Verification of the proposed deformation predictions – Rigidity criterion

The derived closed-form predictions of the previous paragraph are verified in the present section. Initially, the fractional difference between the predicted deformation and the one calculated directly through the finite element analysis is investigated. Figure 6 shows that the expected error for the predicted rigid socket head horizontal displacement and rotation is lower than 5% and 15% respectively. For the loading conditions imposed to the sockets of the 3D finite element analyses, the calculated socket head rotations were significantly lower in numerical terms than the horizontal displacements. Therefore, higher numerical errors of the predicted rotation are occasionally expectable and acceptable.

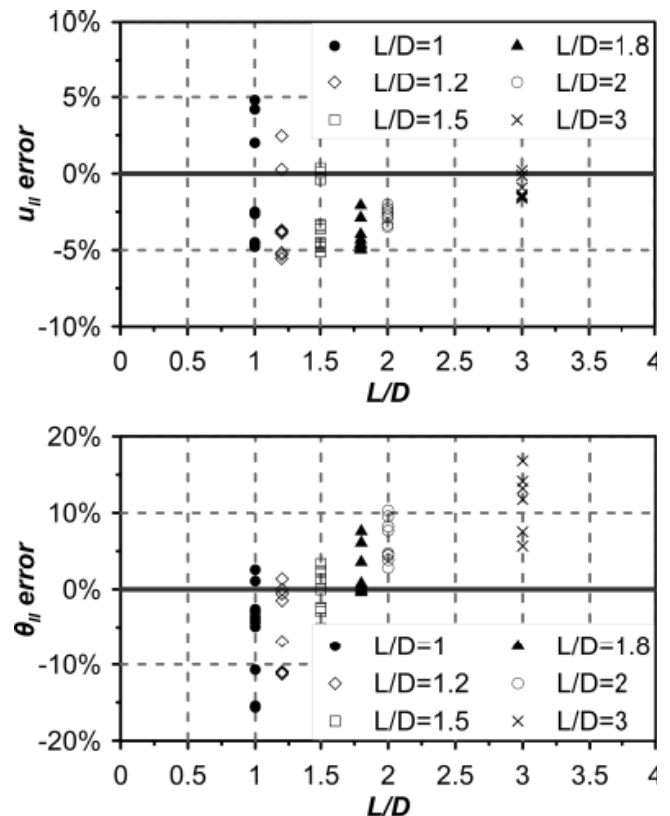


Figure 6. Fractional difference between the proposed displacement (up)/ rotation (down) and the corresponding FEA results.

Subsequently, all the sockets analyzed in the finite element code ABAQUS are incorporated in the graphs of Figure 7 in order to locate cases of sockets that can be characterized as rigid, although they do not meet the conditions of Table 1. Figure 7 depicts the possibility of expanding the rigidity criteria of paragraph 4.2, with an acceptable error  $\pm 10\%$ . An attempt is made to define a numerical formulation of the form  $(L/D) \leq \alpha (E/G^*)^\beta$  between the slenderness ratio  $(L/D)$  and the relative stiffness ratio  $(E/G^*)$  of the socket. The specific procedure involves the determination of coefficients  $\alpha, \beta$  through charts of the variation of the closed-form predictions from the finite element analyses results against the quantity  $\alpha = (L/D)/(E/G^*)^\beta$ , concerning the horizontal displacement.

For the specific graphs, various values of the parameter  $\beta$  are tested, ranging between 0.2–0.5. Finally, aiming at the incorporation of the largest possible amount of  $(L/D)$ - $(E/G^*)$  combinations in the rigidity criterion, Equations 13 and 14 occurred for rigid socket determination of both socket-rockmass interaction approaches (see Section 3).

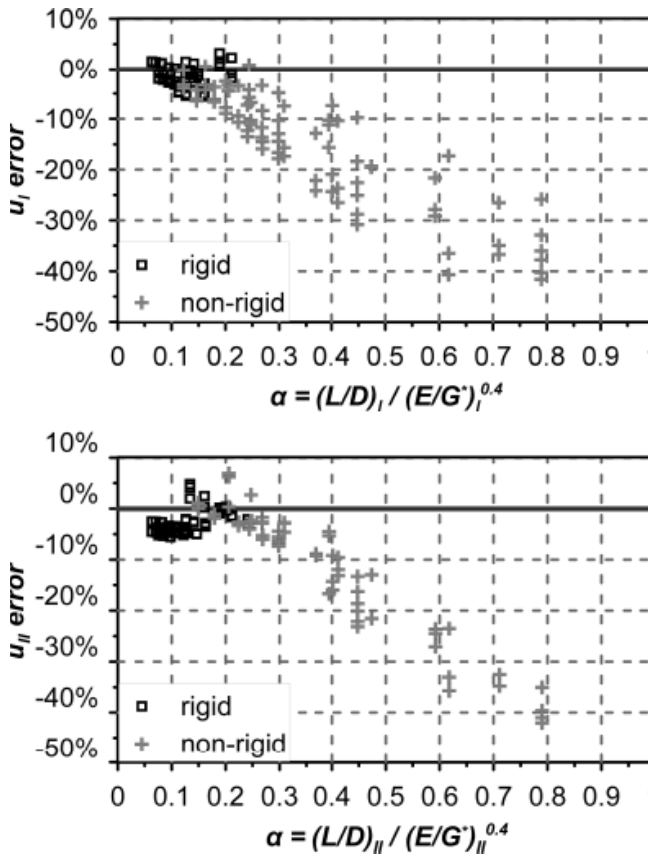


Figure 7. Determination of the criterion for socket rigidity.

$$\left( \frac{L}{D} \right)_I \leq 0.20 \left( \frac{E}{G^*} \right)^{0.4} \quad (13)$$

$$\left( \frac{L}{D} \right)_{II} \leq 0.30 \left( \frac{E}{G^*} \right)^{0.4} \quad (14)$$

#### 4.5 Differences from the Carter & Kulhawy method

The fractional difference between the proposed closed form predictions of the present study and the ones proposed by Carter & Kulhawy (1992) are depicted in the graphs of Figure 8. The specific difference is plotted against the slenderness ratio ( $L/D$ ) for all the cases considered rigid according to Carter & Kulhawy. A peak divergence of 20% is observed between the compared displacements, while the corresponding difference for the rotations is about 40%.

#### 4.6 Differences between the predictions of the hard contact and the friction-separation approach

The fractional difference between the calculated socket head deformation of the hard contact approach and the friction-separation simulation is depicted in Figure 9. Evidently, a divergence is observed, ranging between 40%–80% for the horizontal displacement – similar difference is noticed for the rotation. The aforementioned differences are attributed to the separation and sliding effects simulated by the socket-rockmass surface interaction.

#### 4.7 Prediction of deformation with interface from hard contact output

A final contribution of the present study is to propose a specific numerical procedure for the prediction of socket head deformation by utilizing the output from hard contact finite element analyses and the closed form equations derived from analyses with interface properties on the socket-rockmass surface interaction. Thus, significant computational cost shall be spared. Specific multiplying factors are proposed for each component of Equations 9 and 10 in order to calculate the deformation of the socket head. Equations 15–16 present the aforementioned factors.

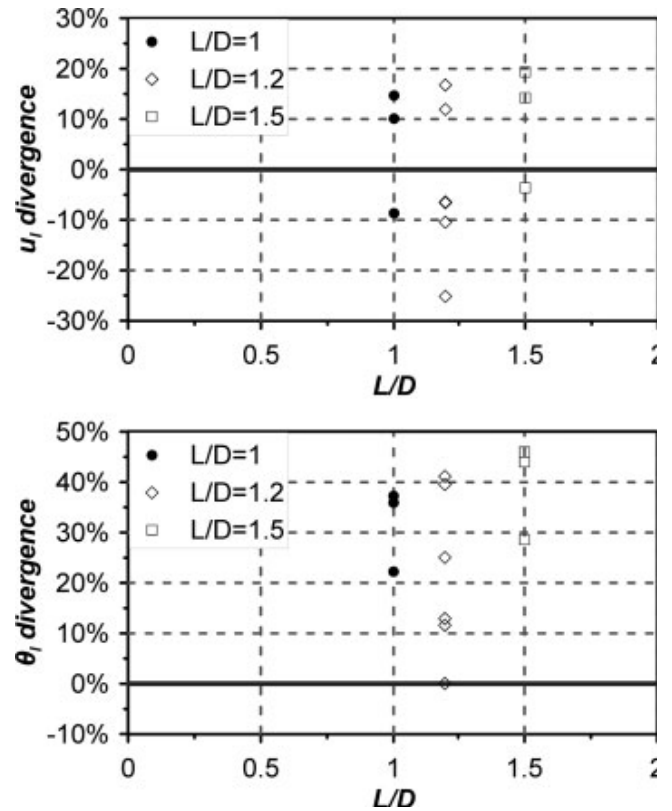


Figure 8. Fractional difference between the proposed predictions of the current methodology and the predictions of Carter & Kulhawy (1992).

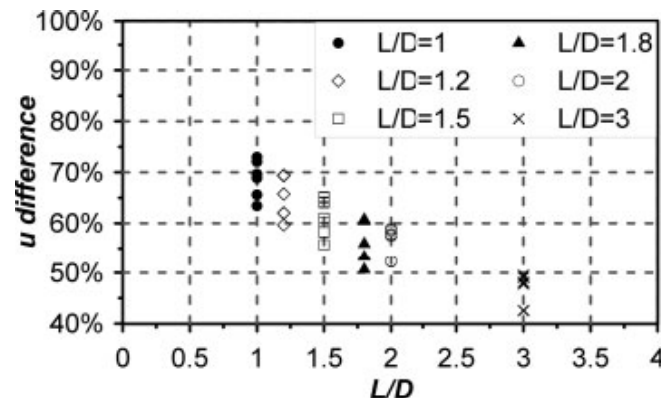


Figure 9. Fractional difference between the socket head horizontal displacement with and without surface interaction.

$$u_{II} \approx 2.8 \left( \frac{L}{D} \right)^{\frac{7}{15}} \cdot (u_H)_I + 3.7 \left( \frac{L}{D} \right)^{\frac{1}{2}} \cdot (u_M)_I \quad (15)$$

$$\theta_{II} \approx 3.7 \left( \frac{L}{D} \right)^{\frac{1}{2}} \cdot (\theta_H)_I + 3.5 \left( \frac{L}{D} \right)^{\frac{1}{2}} \cdot (\theta_M)_I \quad (16)$$

## 5 CONCLUSIONS

A thorough study has been carried out on the elastic response of laterally loaded rigid rock sockets. The deformation of the socket head is investigated and specific closed-form predictions for the respective horizontal displacement and rotation are proposed, derived from 3D finite element analyses of the commercial code ABAQUS. Furthermore, a direct comparison of the aforementioned equations to the predictions of Carter & Kulhawy (1992) for rigid sockets is attempted. The conclusion is drawn that the estimations of

the present method are more conservative. This observation is attributed to the simulation of sliding, separation and lift-up effects of the socket against the surrounding rock-mass in the present study. Finally, a set of multiplying factors are delivered in order to predict the rigid socket head deformation from finite element analyses output without socket-rockmass surface interaction.

#### REFERENCES

Carter, J.P. & Kulhawy, F.H. 1988. Analysis and design of drilled shaft foundations socketed into rock. *Report EL-5918*. Palo Alto, Calif: Electric Power Research Institute.

Carter, J.P. & Kulhawy, F.H. 1992. Analysis of laterally loaded shafts in rock. *Journal of Geotechnical Engineering* 118 (6): 839-855.

Douglas, D.J. & Davis, E.H. 1964. The movements of buried footings due to moment and horizontal load and the movement of anchor plates. *Geotechnique* 14 (2): 115-132.

Gabr, M.A. et al. 2002. *P-y Curves for Laterally Loaded Drilled Shafts Embedded in Weathered Rock*. North Carolina: Department of Civil Engineering, North Carolina State University.

Reese, L.C. 1997. Analysis of laterally loaded piles in weak rock. *Journal of Geotechnical and Geoenvironmental Engineering* 123(11): 1010-1017.

Simulia Abaqus 6.10 Documentation

Zhang, L. 2004. *Drilled Shafts in Rock*. London: Balkema.

## 2ο Πανελλήνιο Συνέδριο Φραγμάτων & Ταμιευτήρων

Σχεδιασμός • Διαχείριση • Περιβάλλον

7-8 Νοεμβρίου 2013, Αθήνα, Αίγλη Ζαππείου

Την έναρξη του Συνεδρίου κήρυξε ο Υπουργός Αγροτικής Ανάπτυξης και Τροφίμων κ. Αθανάσιος Τσαυτάρης. Παρόντες στη ναρκατήρια συνεδρίαση ήταν επίσης οι: ο Γενικός Γραμματέας του ΥΠ.Υ.ΜΕ.ΔΙ. κ. Στράτος Σιμόπουλος, ο Ειδικός Γραμματέας του ΥΠΑΑΤ κ. Δημήτριος Ιατρίδης, ο Διευθύνων Σύμβουλος του Οργανισμού Ανάπτυξης Κρήτης κ. Ελευθέριος Κοπάσης, ο Γενικός Διευθυντής ΕΥΔΑΠ κ. Ιωάννης Πάσιος και ο Διευθυντής της ΔΕΗ ΔΗΥΠ κ. Ιωάννης Αργυράκης

Την Διεθνή Επιτροπή Μεγάλων Φραγμάτων εκπροσώπησαν οι δύο Αντιπρόεδροι για την Ευρώπη κ. Anton Schleiss (Ελβετία) και κ. Jose Polimon (Ισπανία).

Στο συνέδριο συμμετείχαν συνολικά 376 άτομα, εκ των οποίων 229 κανονικοί σύνεδροι, 22 νέοι επιστήμονες, 97 φοιτητές και 28 εκπρόσωποι χορηγών και επίσημοι.

Παρουσιάστηκαν συνολικά 3 προσκεκλημένες ομιλίες, 11 ειδικές ομιλίες και 53 επιστημονικές εργασίες. Οι παρουσιάσεις, οι οποίες θα αναρτηθούν στην ιστοσελίδα της ΕΕΜΦ (<http://www.eeft.gr>), ήταν οι ακόλουθες:

### Εναρκτήρια Συνεδρίαση

**Στόχοι Συνεδρίου – Προοπτικές για Φράγματα και Ταμιευτήρες στην Ελλάδα**, Γεώργιος Ντουινιάς, Δρ., Πολιτικός Μηχανικός, Πρόεδρος Οργανωτικής Επιτροπής ΕΕΜΦ

**Present and future of Dam technology - The importance of training**, Jose Polimon, President of SPANCOLD, Vice President of ICOLD

**Εύηνος – Μόρνος – Υλίκη – Μαραθώνας «Περιβαλλοντικοί προορισμοί»**, Ιωάννης Πάσιος, Γενικός Διευθυντής Ανάπτυξης & Παραγωγής Έργων Ε.ΥΔ.Α.Π. Α.Ε.



Anton Schleiss, Γιώργος Ντουινιάς, Jose Polimon και Μάκης Μπενσασσών

### Γενικές Ομιλίες

**Οι Υδατικοί Πόροι της Ελλάδας: Παρόν και Μέλλον**, Μαρία Μιμίκου, Καθηγήτρια. Σχολή Πολ. Μηχανικών, Τομέας Υδατικών Πόρων και Περιβάλλοντος ΕΜΠ.

**Ταμιευτήρες και ευρωπαϊκή ενεργειακή πολιτική στην προοπτική του 2050**, Κίμων Χατζημπίρος, Καθηγητής ΕΜΠ

**Χάραξη Πολιτικής Προστασίας και Διαχείρισης Υδατικών Πόρων**, Μαρία Γκίνη, Διευθύντρια Προστασίας και Διαχείρισης Υδατικού Περιβάλλοντος, Ειδική Γραμματεία Υδάτων, ΥΠΕΚΑ

**Τα Φράγματα της Κρήτης – Προοπτικές**, Μαμαγκάκης Ευάγγελος, Πολιτικός Μηχανικός, Διευθυντής Διεύθυνσης Ρεθύμνου ΟΑΚ Α.Ε.

**Νέες Τεχνολογίες Κατασκευής Φραγμάτων**, Νικόλαος Μουτάφης, Δρ. Πολιτικός Μηχανικός, Τεχνικός Σύμβουλος

**Raygate technology and recent technical developments**, Sylvain Chevalier, Dam expert, Technical Director, Department of Dams and HPP RAYCAP

**Ελληνικοί Ενεργειακοί Πόροι**, Λουκάς Γ. Χριστοφόρου, Ακαδημία Αθηνών

**The challenge of scour evaluation at high head and high capacity spillways**, Anton J. Schleiss, Laboratory of Hydraulic Constructions (LCH), Ecole Polytechnique Fédérale de Lausanne (EPFL)

**Κατασκευάζοντας το πιο ψηλό φράγμα σε σταυροδρόμιο δύσκολων γεωλογικών καταστάσεων**, Παύλος Μαρίνος, Ομότιμος Καθηγητής, Εθνικό Μετσόβιο Πολυτεχνείο

**Αντισεισμικός σχεδιασμός μεγάλων χωμάτινων φραγμάτων με κριτήρια επιτελεστικότητας**, Γεώργιος Δ. Μπουκοβάλας, Καθηγητής, Εθνικό Μετσόβιο Πολυτεχνείο

**Μια ευκαιρία στην εποχή της κρίσης: Η αιφορική αξιοποίηση του υδατικού δυναμικού της Ελλάδας για την αναγέννηση της αγροτικής οικονομίας και την επανεκκίνηση της υπαίθρου**, Ιωάννης Σακιώτης, Δρ Πολιτικός Επιστήμων - Διεθνολόγος

### Συνεδρία 1: Διαχείριση Υδατικών πόρων

- 1.1 **Οι υδροηλεκτρικοί σταθμοί της ΔΕΗ Α.Ε. και η συμβολή τους στην διαχείριση των υδατικών πόρων**, Ι. Αργυράκης
- 1.2 **Σύστημα υποστήριξης αποφάσεων για τη διαχείριση υδροηλεκτρικών ταμιευτήρων – Εφαρμογή στο υδροσύστημα Αχελώου-Θεσσαλίας**, Ανδρέας Ευστρατιάδης, Δημήτρης Στεφ. Μπουζιώτας, και Δημήτρης Κουτσογιάννης
- 1.3 **Διερεύνηση δημιουργίας ταμιευτήρων στο Δήμο Ιεράπετρας Κρήτης με την κατασκευή μικρών φραγμάτων**, Κ.Δ. Κουλούρης, και Ν.Ι. Μουτάφης
- 1.4 **Υφιστάμενα Φράγματα για την Ύδρευση των Αθηνών**, Μενέλαος Ι. Κωνσταντάκος
- 1.5 **Ενίσχυση της Υδροδότησης της Μείζονος Περιοχής της Πρωτεύουσας και Άλλων Περιοχών με Κατασκευή Νέων Φραγμάτων**, Μενέλαος Ι. Κωνσταντάκος και Δημήτριος Αντ. Νικολάου
- 1.6 **Προσδιορισμός ιδιαίτερος τροποποιημένων και τεχνητών υδατινών σωμάτων (ΙΤΥΣ-ΤΥΣ) από φράγματα και ταμιευτήρες σύμφωνα με την οδηγία 2000/60/ΕΚ και ζητήματα καθορισμού περιβαλλοντικών παροχών**, Ι. Α. Νιάδας, Π. Αντωνάρου και Συνεργάτες Α.Μ.Ε, Π-Σ. Καϊμάκη, Ε. Γκουβάτσου και Σ. Τασόγλου

### Συνεδρία 2: Φράγματα και περιβάλλον

- 2.1 **Αντιμετώπιση περιβαλλοντικών επιπτώσεων ΥΗΕ Ιλαρίωνα και κόστος εφαρμογής περιβαλλοντικών όρων**, Δ. Γεωργιόπουλος, Μ. Νιφάκου, Ε. Γκουβάτσου και Σ. Καϊμάκη

- 2.2 **Στοχαστική ανάλυση και προσομοίωση υδρομετεωρολογικών διεργασιών για τη βελτιστοποίηση ενός υβριδικού συστήματος ανανεώσιμης ενέργειας**, Χρήστος Ιωάννου & Γιώργος Τσεκούρας, Ανδρέας Ευστρατιάδης και Δημήτρης Κουτσογιάννης
- 2.3 **Ανάπτυξη μεθοδολογίας μέτρησης και πρόβλεψη εκπομπής αερίων του θερμοκηπίου από τον ταμιευτήρα του ΥΗΕ Ιλαρίωνα**, Γ. Ι. Πεκρίδης, Ε. Ι. Αμανατίδου, Ι. Ι. Παπαδόπουλος, Ε. Ι. Τρικοιλίδου & Γ. Π. Σαμιώτης και Δ. Ε. Πρίμπα
- 2.4 **Μικρό Υδροηλεκτρικό Έργο Δαφνοζωνάρα-Σανίδι στον π. Αχελώο. Περιβαλλοντικός Σχεδιασμός και Εμπειρία από την μέχρι τώρα Λειτουργία των Ανατρεπόμενων Θυροφραγμάτων (Raygates)**, Ι.Π. Στεφανάκος, Π.Ι. Τσιγκνάκου. S. Chevalier και Ε.Ε. Ράμπιας
- 2.5 **Φυσικοχημικά χαρακτηριστικά νερού τροφοδοσίας του ταμιευτήρα ΥΗΕ Ιλαρίωνα και επίδραση αυτών στην ποιότητα του νερού του**, Ε.Ι. Τρικοιλίδου, Γ. Ι. Πεκρίδης, Γ.Π. Σαμιώτης, Ε.Ι. Αμανατίδου, Ι.Ι. Παπαδόπουλος και Δ. Ε. Πρίμπα

### Συνεδρία 3 : Υδροηλεκτρικά έργα

- 3.1 **Τεχνική παρουσίαση του έργου: Ενεργειακή αξιοποίηση του Φράγματος Ποταμών Ρεθύμνου – Υβριδικός Σταθμός 50 MW**, Τ. Νικολάου και Ε. Μαμαγκάκης
- 3.2 **Δυνατότητες κατασκευής έργων αποταμίευσης μέσω άντλησης σε περιοχές της Ηπειρωτικής Ελλάδας**, Ι.Π. Στεφανάκος
- 3.3 **Δυνατότητες ανάπτυξης μεγάλων Υδροηλεκτρικών Έργων στην Ήπειρο. Σχέδια ανάπτυξης Αώου - Σαραντάπορου – Καλαμά**, Ι.Π. Στεφανάκος
- 3.4 **Υδροηλεκτρικά Έργα - Προοπτική για Ανάπτυξη με Έργα Μεγάλης Εγχώριας Προστιθέμενης Αξίας**, Ι.Π. Στεφανάκος, Π. Τσιγκνάκου και Χ. Παπαχατζάκη
- 3.5 **Υδροηλεκτρικό Έργο Καστρακίου στον ποταμό Αχελώο. Εμπειρία από την εγκατάσταση και την μέχρι τώρα Λειτουργία των Ανατρεπόμενων Θυροφραγμάτων (Raygates)**, Ι.Π. Στεφανάκος, Ι. Α. Μαύρος και S. Chevalier



### Συνεδρία 4 : Ασφάλεια - Μακροχρόνια Συμπεριφορά Φραγμάτων

- 4.1 **Νομοθέτηση της Ασφάλειας των Ταμιευτήρων στη Κύπρο**, Δήμος Αντωνίου
- 4.2 **Φράγματα και Δημόσια Ασφάλεια**, Σ.Ι. Σιάχου, Ι. Θανόπουλος, και Ι. Μπεθάνης

- 4.3 **Σύγκριση μαθηματικών ομοιωμάτων διόδευσης πλημμυρικού κύματος από υποθετική θραύση φράγματος Αγιοκάμπου**, Σ.Ν. Μίχας, Κ.Ι. Νικολάου, Σ.Λ. Λαζαρίδου και Μ.Ν. Πικούνης
- 4.4 **Τα πέντε φράγματα των ΥΗΕ της κοιλάδας 7 πιρουινών στην Κένυα**, Γιώργος Ντουινιάς και Ιωάννης Καραβοκύρης
- 4.5 **Αντιμετώπιση αστοχιών σε φράγματα μικρού ύψους, περίπτωση έργων Λιβαδίου (θέση Κουτη) και Αμπελακίων**, στην Π.Ε. Λάρισας, Ι.Μ. Σίσκος, και Ι. Θανοπουλος
- 4.6 **Γεωλογική και γεωτεχνική αξιολόγηση της συμπεριφοράς του φράγματος Μόρνου μετά την συμπλήρωση 35 ετών από την έναρξη πλήρωσης**, Βασίλειος Ι. Σουλης, Αντώνης Αγγελόπουλος, και Θέκλα Βαρότση



Περίπερα τεχνικής έκθεσης

### Συνεδρία 5 : Σχεδιασμός Φραγμάτων

- 5.1 **Φράγματα Μνημεία - Μνημεία και Φράγματα**, Χ. Τσατσάνιφος
- 5.2 **Μελέτη και σχεδιασμός Φράγματος πολλαπλής σκοπιμότητας Ορεινής Σερρών**, Β.Λ. Μαλιώκας, Σ.Π. Παπαδήμας, και Μ.Β. Μαλιώκα
- 5.3 **Εκτίμηση Στερεοπαροχής και Διαχρονικής Εναπόθεσης Όγκου Φερτών Υλών στον Ταμιευτήρα του ΥΗΕ Ιλαρίωνα**, Μ. Μιμίκου, Ι. Παναγόπουλος και Χ. Μακρόπουλος
- 5.4 **Σχεδιασμός πλευρικού υπερχειλιστή φράγματος Νεστορίου με υδραυλικό ομοίωμα**, Π. Πρίνος και Θ. Κόφτης
- 5.5 **Εκτίμηση συντελεστή ασφαλείας για την καθίζηση της στέψης χωμάτων φραγμάτων**, Σ.Ι. Πυθαρούλη και Σ.Κ. Στείρος
- 5.6 **Υπολογιστική Προσομοίωση ολισθαίνουσας ροής σε βαθμιδωτό υπερχειλιστή**, Μ. Τσακίρη και Π. Πρίνος
- 5.7 **Λιθόρριπα αναχώματα με ανάντη πλάκα σκυροδέματος : προβλήματα και βελτιώσεις στο σχεδιασμό**, Ι. Θανοπουλος
- 5.8 **Βαθιές παλαιές διαπερατές καλυμμένες κοίτες (παλιοκοίτες) ποταμού και ο αντίκτυπός τους στην ανάπτυξη του Σχεδίου Υδροηλεκτρικής Αξιοποίησης του ποταμού Guayllabamba, στο Εκουαδόρ της Νότιας Αμερικής**, Ν. Καζής

- 5.9 **Διερεύνηση και σχεδιασμός σύνδεσης διαφραγματικού τοίχου με πυρήνα γεωφράγματος**, Α. Β. Λύκου, Ν. Ι. Μουτάφης
- 5.10 **Η μελέτη του αρδευτικού φράγματος Σολέας στην Κύπρο**, Νίκος Μαλατέστας, Γιώργος Ντουνιάς, Σ. Σακελλαρίου και Κ. Κατσάβρας
- 5.11 **Επιλογή θέσης και τύπου φράγματος του υδροηλεκτρικού έργου Chontal στο Ecuador**, Ν. Ι. Μουτάφης
- 5.12 **Ο ρόλος και οι ιδιότητες του φίλτρου στην ανάντη παρειά πυρήνα γεωφραγμάτων**, Ν. Ι. Μουτάφης



#### Συνεδρία 6 : Υλικά Κατασκευής - Έλεγχοι

- 6.1 **Προσδιορισμός παραγόντων που επιδρούν στην αντοχή μειγμάτων Σκληρού Επιχώματος. Η εμπειρία του Φράγματος Φιλιατρινού**, Χ. Γκούβας και Χ. Ορφανός.
- 6.2 **Το Φράγμα Βράχου Καστοριάς – Ποιοτικός έλεγχος και συμπεριφορά κατά την διάρκεια της κατασκευής**, Δ.Γ. Κούμουλος, και Θ.Π. Κοργιαλός
- 6.3 **Μια νέα συσκευή άμεσης διάτμησης για χονδρόκοκκα εδάφη και εδάφη με μεγάλα συσσωματώματα. Μετρήσεις διατμητικής αντοχής και μεταβολών όγκου**, Μ. Μπαρδάνης, Σ. Καβουνίδης, και Γ. Ντουνιάς
- 6.4 **Οι έμμεσες μέθοδοι μέτρησης του ογκομετρικού ποσοστού υγρασίας και η δυνατότητα χρήσης τους στον ποιοτικό έλεγχο της κατασκευής χωμάτων φραγμάτων**, Μ. Μπαρδάνης
- 6.5 **Μια νέα εργαστηριακή συσκευή για τη μελέτη της μακροχρόνιας σιμέντωσης φίλτρων φραγμάτων από θραυστά ασβεστολιθικά υλικά**, Μ. Μπαρδάνης Σ. Καβουνίδης και Γ. Ντουνιάς

#### Συνεδρία 7 : Εξελιξεις στον αντισεισμικό σχεδιασμό

- 7.1 **Φράγματα Τελμάτων Μεταλλείων Στρατωνίου υποβαλλόμενα στην Τεκτονική Διάρρηξη του υποκειμένου σεισμογενούς Ρήγματος του Σεισμού της Ιερισσού 1932**, Ι. Αναστασόπουλος, και Γ. Γκαζέτας
- 7.2 **Σεισμική Ανάλυση Χωματινίου Φράγματος Αστερίου**, Ε. Γαρίνη, Φ. Γελαγώτη και Γ. Γκαζέτας
- 7.3 **Υπολογισμός σεισμικής συνίζησης και μόνιμων μετακινήσεων φραγμάτων με ανάντη πλάκα σκυροδέματος**, Δ.Ν. Εγγλέζος.
- 7.4 **Αντισεισμικός σχεδιασμός χωμάτων και λιθόρριπτων φραγμάτων: εμπειρίες από τον Ελληνικό χώ-**

**ρο**, Κ. Μάκρα, Ν. Κλήμης, Α. Αναστασιάδης και Α. Κωμοδρόμος

- 7.5 **Σεισμική ανάλυση φραγμάτων από κυκλώπειο σκυρόδεμα και αντισεισμική ενίσχυση με προενταμένα αγκύρια**, Γ. Χρ. Μαλιτδής
- 7.6 **Αριθμητική ανάλυση της σεισμικής απόκρισης και ρηγμάτωσης φράγματος από κυλινδρούμενο σκυρόδεμα (RCC)**, Γ. Μπουκοβάλας, Κ. Ανδριανόπουλος και Ν. Μουτάφης
- 7.7 **Σεισμική αξιολόγηση του φράγματος Ταυρωπού: Μη-γραμμική δυναμική ανάλυση φράγματος-κοιλιάδας-ύδατος**, Π. Ντακούλας, Γ. Θανόπουλος, .Κ. Αναστασόπουλος και Χ. Δήμου.
- 7.8 **Βελτίωση του αντισεισμικού σχεδιασμού μεγάλων φραγμάτων λιθορριπής με ανάντη πλάκα σκυροδέματος**, Ε. Σταυροθεοδώρου και Π. Ντακούλας

#### Συνεδρία 8 : Κατασκευή Φραγμάτων

- 8.1 **Το Φράγμα Μαραθιάς Μυκόνου – Παρακολούθηση της συμπεριφοράς επί 3 έτη μετά την κατασκευή**, Δ.Γ. Κούμουλος και Θ.Π. Κοργιαλός
- 8.2 **Αποκατάσταση Φράγματος Καμαρών Νήσου Σίφνου**, Ν.Ι. Μουτάφης
- 8.3 **Κατασκευή του αναχώματος του φράγματος Αστερίου στον Ποταμό Παραπείρο**, Γ. Ντουνιάς, Σ. Σακελλαρίου, Π. Διαμαντοπούλου, Ι. Θεοδωρακόπουλος, Γ. Μουλίνος και Ι. Καραβοκύρης
- 8.4 **Φράγμα Σολέας, ποιοτικοί έλεγχοι και παρακολούθηση κατά τη διάρκεια κατασκευής**, Στέλλα Πατσάλη, Γιώργος Ντουνιάς και Χρίστος Μιχαηλίδης
- 8.5 **Τεχνικά και γεωτεχνικά στοιχεία κατασκευής και 1η πλήρωση του Φράγματος Αποσελέμη Κρήτης**, Λ. Σωμάκος, Σ. Λαζαρίδου, Ι. Καραπαναγιώτης, Α. Γκιόλας, Σ. Μίχας, Α. Κοτσώνης, Μ. Καββαδάς και Π. Μαρίνος





**ΕΘΝΙΚΟ ΜΕΤΣΟΒΙΟ ΠΟΛΥΤΕΧΝΕΙΟ  
ΣΧΟΛΗ ΠΟΛΙΤΙΚΩΝ ΜΗΧΑΝΙΚΩΝ  
ΕΡΓΑΣΤΗΡΙΟ ΛΙΜΕΝΙΚΩΝ ΕΡΓΩΝ**

**6° ΠΑΝΕΛΛΗΝΙΟ ΣΥΝΕΔΡΙΟ ΛΙΜΕΝΙΚΩΝ ΕΡΓΩΝ  
Αθήνα 25 - 28 Νοεμβρίου 2013**

Το ΕΚΤΟ ΠΑΝΕΛΛΗΝΙΟ ΣΥΝΕΔΡΙΟ ΛΙΜΕΝΙΚΩΝ ΕΡΓΩΝ, Αθήνα, 11-14 Νοεμβρίου 2013, οργανώθηκε μετά το Πρώτο του 1997, το Δεύτερο του 2000, το Τρίτο του 2003, το Τέταρτο του 2006 και το Πέμπτο του 2010. Στόχουμε στην ανταλλαγή επιστημονικών απόψεων και εμπειριών μεταξύ του ανθρώπινου δυναμικού του απασχολούμενου με την έρευνα, τον σχεδιασμό, την μελέτη, την κατασκευή και τον προγραμματισμό των λιμένων και των λιμενικών έργων. Η πρωτοβουλία, και σε μεγάλο βαθμό η χρηματοδότηση, αναλήφθηκε από το Εργαστήριο Λιμενικών Έργων του Ε.Μ.Π. Στην οικονομική υποστήριξη του συνεδρίου σημαντική ήταν, όπως πάντοτε, η συμμετοχή της Ο.Λ.Π. Α.Ε., προς την οποία εκφράζονται ευχαριστίες.

Οι θεματικές ενότητες, οι οποίες επελέγησαν ήταν οι επόμενες έξι :

(α) Μεγέθη Σχεδιασμού και Κατασκευής Λιμενικών Έργων. (β) Μελέτη Λιμένων σε Φυσικό Προσομοίωμα. (γ) Σχεδιασμός Λιμένων, Μελέτη και Κατασκευή Λιμενικών Έργων, Διαμόρφωση Λιμενικής Ζώνης. (δ) Περιβαλλοντικές επιπτώσεις από την Κατασκευή και Λειτουργία Λιμένων. (ε) Τα Λιμενικά Συστήματα Ελλάδας και Κύπρου. (στ) Θεσμικό πλαίσιο Λειτουργίας Λιμένων – Ιδιωτικοποιήσεις. Επιπλέον υπήρχαν και οι δύο ειδικές συνεδρίες (α) Προγραμματικά Σχέδια (Master Plan) Λιμένων και (β) Περιβαλλοντική Διαχείριση Λιμένων, μια ειδική ομιλία με τίτλο Θεματικά προβλήματα στον Αντισεισμικό Υπολογισμό Λιμενικών Έργων και στον Προσδιορισμό του Μέγιστου Ύψους Κύματος και τέλος η Παρουσίαση Δραστηριοτήτων Διευθύνσεως Λιμενικών Έργων και Έργων Αεροδρομίων Υπουργείου Α.Α.Υ.Μ.Δ.

Παρουσιάστηκαν συνολικά 43 εισηγήσεις, οι οποίες έγιναν δεκτές από την Επιστημονική Επιτροπή του Συνεδρίου μετά από μια αρχική κρίση των περιλήψεων τους.

Εκφράζονται θερμές ευχαριστίες προς όλους, όσους συνέβαλαν στην ετοιμασία του παρόντος τόμου και εν γένει του Συνεδρίου. Η συμβολή των μελών της Επιστημονικής Επιτροπής και των κριτών ήταν ιδιαίτερης σημασίας.

Φεβρουάριος 2014

Ο Πρόεδρος της Οργανωτικής Επιτροπής  
Κ. Ι. Μουτζούρης  
Καθηγητής Ε.Μ.Π.

**Θεματική Ενότητα 1:**

**Μεγέθη Σχεδιασμού και Κατασκευής Λιμενικών Έργων**

- 1 **Το Ελληνικό Λιμενικό Σύστημα στα πλαίσια του νέου χάρτη των Διευρωπαϊκών Δικτύων Μεταφορών : Ρόλος και Προοπτικές**, Γιαννόπουλος Γ.Α. (Προσκεκλημένη Ομιλία)
- 2 **Τρισδιάστατη προσομοίωση κυματογενών ρευμάτων από τη θραύση κυμάτων στην παράκτια ζώνη**, Κολοκούθας Γ.Α., Δήμας Α.Α.
- 3 **Μετρήσεις τυρβώδους ροής υπεράνω πρηνούς ογκολίθων εργασθησιακού ομοιώματος κυματοθραύστη με τη μέθοδο PIV**, Γαλάνη Κ.Α., Δήμου Ι.Δ., Καραγεωργόπουλος Ε.Γ., Δήμας Α.Α.

- 4 **Αριθμητική προσομοίωση ροών με ελεύθερη επιφάνεια κατά τη διάδοση κυμάτων μέσω της μεθόδου εμβαπτισμένου ορίου**, Κουτρουβέλη Θ.Ι., Δήμας Α.Α.
- 5 **Αριθμητική προσομοίωση παλλόμενης ροής γύρω από υποβρύχιο αγωγό κοντά σε πυθμένα με τη μέθοδο εμβαπτισμένου ορίου**, Φονιάς Ε.Ν., Δήμας Α.Α.
- 6 **Προσομοίωση του κυματικού πεδίου πάνω από πυθμένα μεταβαλλόμενου βάθους**, Παπαδόπουλος Κ., Μέμος Κ.Δ.
- 7 **Μαθηματική προσομοίωση των επιπτώσεων της κλιματικής αλλαγής στα λιμενικά έργα – Συμβολή στον επανασχεδιασμό τους**, Καραμπάς Θ., Χριστόπουλος Σ.

**Θεματική Ενότητα 2:**

**Μελέτη Λιμένων σε Φυσικό Προσομοίωμα**

- 8 **Πειραματική διερεύνηση κυματικής υπερπήδησης στο νέο αεροδιάδρομο του αεροδρομίου «ΜΑΚΕΔΟΝΙΑ»**, Γιαντσή Θ., Αζοράκος Σ., Μουτζούρης Κ.Ι.
- 9 **Μελέτη σε φυσικό προσομοίωμα των νέων έργων στον επιβατικό λιμένα Πειραιά για εξυπηρέτηση μεγάλων κρουαζιεροπλοίων**, Γιαντσή Θ., Θεοχάρης Ι., Αζοράκος Σ., Μουτζούρης Κ.Ι.

**Πρώτη Ειδική Συνεδρία**

- 10 **Προγραμματικά Σχέδια (Master Plan) Λιμένων**, Καμαρινάκης Α.

**Θεματική Ενότητα 3:**

**Σχεδιασμός Λιμένων, Μελέτη και Κατασκευή Λιμενικών Έργων, Διαμόρφωση Λιμενικής Ζώνης**

- 11 **Δράσεις και Εμπειρίες : Λιμάνι – Πόλη, Πόλη - Λιμάνι**, Μπράς Ι. (Προσκεκλημένη Ομιλία)
- 12 **Βελτιστοποίηση της απόδοσης διάτρητων caisson για την παραγωγή ενέργειας από κύματα**, Βύζικας Θ.Ι., Greaves D.
- 13 **Διατάξεις εξασφάλισης σιδηροτροχιών γερανών κρηπιδώματος Σταθμού Εμπορευματοκιβωτίων**, Αζοράκος Σ.
- 14 **Λιμενική δραστηριότητα, συγκοινωνιακή υποστήριξη και πιθανές αστικές μεταλλάξεις : Το παράδειγμα της Πάτρας**, Μωραϊτης Κ.
- 15 **Αποθέσεις στην είσοδο μαρίνας και προτάσεις αντιμετώπισης του προβλήματος**, Μαυραντωνάκης Α.Ι., Μέμος Κ.Δ.
- 16 **Υποθαλάσσια σήραγγα Λέοντος στον Λιμένα Πειραιώς**, Τσατσανίφης Χ., Βαντόλας Β., Αστερίου Π.
- 17 **Επιυψωμένα σήραγγα Προλιμένος Πειραιά**, Τσατσανίφης Χ., Βαντόλας Β., Αστερίου Π.
- 18 **Η εφαρμογή συστημάτων λιμενικής κοινότητας (port community systems) στους ελληνικούς λιμένες – Η περίπτωση του Οργανισμού Λιμένος Ηγουμενίτσας**, Μπιζάκης Α., Τσούκος Γ.
- 19 **Επέκταση λιμένα Λαυρίου προς νότο: Βελτιστοποίηση διατομής επεκτάσεως προσήνεμου μώλου**, Σολομωνίδης Χ.Δ., Μπουτάτης Α.Μ., Μαρίνος Μ.
- 20 **Διερεύνηση της εντατικοποίησης της κυματικής δράσης στα κατάντη μώλου λιμένα**, Κούφαλη Μ.,

#### Θεματική Ενότητα 4:

##### Περιβαλλοντικές επιπτώσεις από την κατασκευή και λειτουργία λιμένων

- 21 **Διαχείριση βυθοκορημάτων σε ελληνικούς λιμένες και τρόπος διάθεσής τους**, σέζος Μ., Αναστασάκης Γ., Κασιμάλης Β., Ξηρόκωστας Ν. (Προσκεκλημένη Ομιλία)
- 22 **Σχεδιασμός παράλληλου κυματοθραύστη με χρήση αριθμητικής προσομοίωσης κυμάτων και περιβαλλοντικής βελτιστοποίησής του**, Γουλουμεής Σ., Χωμενίδης Α., Δήμας Α.Α.
- 23 **Σχεδιασμός λιμενικών πυλών διαφυγής – Η περίπτωση της Σαντορίνης**, Σιώρης Ι., Κοκορομύτης Α., Πυρπυλή Κ.
- 24 **Περιβαλλοντική θωράκιση των λιμένων με τη δημιουργία σύγχρονων εγκαταστάσεων υποδοχής αποβλήτων των πλοίων**, Ψαρομιχαλάκης Μ.
- 25 **Αντιμετώπιση των περιβαλλοντικών επιπτώσεων από την κατασκευή και λειτουργία λιμένων με εφαρμογές κατάλληλων τεχνολογιών**, Κόλλιας Π.Σ., Κόλλιας Β.Π., Κόλλιας Σ.

#### Δεύτερη Ειδική Συνεδρία

##### Περιβαλλοντική Διαχείριση Λιμένων

- 26 **Περιβαλλοντική διαχείριση λιμένων. Κύρια επιτεύγματα των ελληνικών λιμένων και προκλήσεις για το μέλλον**, Παλάντζας Γ.Ν., Νανιόπουλος Α.Φ.
- 27 **Βιολογικές παράμετροι και διαχείριση της βιοποικιλότητας στα λιμάνια : Τάσεις, δείκτες, παραδείγματα από την Ελλάδα**, Αντωνιάδου Χ., Τσελέντης Β., Χιντήρογλου Χ.Σ.
- 28 **Η διαχείριση των αποβλήτων σε λιμένες. Διδάγματα από την ελληνική πραγματικότητα**, Παπαχρήστου Ε., Παλάντζας Γ.Ν.
- 29 **Εξοικονόμηση ενέργειας και φυσικών πόρων στα λιμάνια**, Βαγρόπουλος Σ.Ι., Μπακιρτζής Α.Γ.
- 30 **Διαχείριση της κίνησης μέσω λιμενικών εγκαταστάσεων με στόχο τη μείωση της ρύπανσης**, Μποϊλέ Μ.
- 31 **Περιβαλλοντικός σχεδιασμός λιμενικών έργων με χρήση μαθηματικών ομοιωμάτων**, Καραμπάς Θ., Κουτίτας Χ.

#### Θεματική Ενότητα 5:

##### Τα Λιμενικά Συστήματα Ελλάδας και Κύπρου

- 32 **Το Λιμενικό Σύστημα Ελλάδας : Ποσοτικά στοιχεία**, Βαρτελάτου Σ., Καμπουρέλλη Μ., Μουτζούρης Κ.Ι., Σαραντινός Μ.
- 33 **Προβλήματα λιμένων Πελοποννήσου**, Παπαφωτίου Α., Παπαφωτίου Ε.
- 34 **Υποθαλάσσιες αυτοψίες λιμενικών εγκαταστάσεων και αποκατάσταση βλαβών**, Παπαδόπολης - Δετζώρτζης Α.Ν.
- 35 **Μέτρηση αποδοτικότητας των δώδεκα Οργανισμών Λιμένων της Ελλάδας & των δικτύων αυτών : Μια μη παραμετρική προσέγγιση**, Πρίγκος Ι., Μπάρας Χ.

#### Θεματική Ενότητα 6:

##### Θεσμικό Πλαίσιο Λειτουργίας Λιμένων – Ιδιωτικοποιήσεις

- 36 **Αναδιамόρφωση του Διευρωπαϊκού Δικτύου Μεταφορών και ανάπτυξη των ελληνικών λιμένων**, Πλατιάς Χ.
- 37 **Στρατηγική αξιοποίησης υφισταμένων τουριστικών λιμένων της χώρας στα πλαίσια του έργου NEREIDS του Ταμείου Αξιοποίησης Ιδιωτικής Περιουσίας του Δημοσίου (ΤΑΙΠΕΔ)**, Μπουτάτης Α. Μ., Ρογκάν Α. Ι., Σολομωνίδης Χ. Δ., Κρούσκα Δ., Μαθηκολώνης Θ.
- 38 **Αναθεώρηση ευρωπαϊκής λιμενικής πολιτικής – Μοντέλα ανάπτυξης λιμένων – Ιδιωτικοποιήσεις**, Μακρής Δ.
- 39 **Προσδιορισμός σημείων συμφόρησης και ελλείψεις συνδέσεων στους λιμένες της Αδριατικής**, Τσαμπούλας Δ.Α., Zgaljic D., Λέκκα Α.Μ., Ρέντζιου Α.
- 40 **Λιμενικές και τελωνειακές διαδικασίες στην περιοχή της Μεσογείου : Συγκριτική παρουσίαση της υφισταμένης καταστάσεως**, Τσαμπούλας Δ.Α., Λέκκα Α.Μ., Ρέντζιου Α.
- 41 **Η ενιαία ημερησια διαδικασία ΣΥΝΕΛΕΤΑ Λιμένων Αδριατικής**, Τσαμπούλας Δ.Α., Μπαλλής Α.Θ., Καρούσος Ι. Κ.

#### Ειδική Ομιλία

- 42 **Θεματικά προβλήματα στον αντισεισμικό υπολογισμό λιμενικών έργων και στον προσδιορισμό του μεγίστου ύψους κύματος**, Δασκαλάκης Μ.

#### Παρουσίαση Δραστηριοτήτων

- 43 **Παρουσίαση δραστηριοτήτων Διευθύνσεως Λιμενικών Έργων και Έργων Αεροδρομίων Υπουργείου Α.Α.Υ.Μ.Δ.**, Πολιτόπουλος Μ., Καραϊσκού Ε., Τσουρέκης Κ., Ταυλάκης Γ.



ΕΛΛΗΝΙΚΗ  
ΕΠΙΣΤΗΜΟΝΙΚΗ  
ΕΤΑΙΡΕΙΑ  
ΕΔΑΦΟΜΗΧΑΝΙΚΗΣ  
& ΓΕΩΤΕΧΝΙΚΗΣ  
ΜΗΧΑΝΙΚΗΣ

## ENERGY GEOTECHNOLOGY The Role of Geotechnical Engineers in the Energy Challenge

Την Δευτέρα 16 Σεπτεμβρίου 2013 παρουσιάστηκε από τον Carlos J. SANTAMARINA, Δρ. Πολιτικό Μηχανικό, Professor of Civil and Environmental Engineering, Goizueta Foundation Faculty Chair, Georgia Institute of Technology, Atlanta διάλεξη με τίτλο «ENERGY GEOTECHNOLOGY - The Role of Geotechnical Engineers in the Energy Challenge». Η ίδια διάλεξη παρουσιάστηκε την επομένη στην Πολυτεχνική Σχολή του Αριστοτελείου Πανεπιστημίου Θεσσαλονίκης.

Energy and growth are intimately related. There will be a pronounced increase in energy demand in the next decades associated to economical development and population growth worldwide. This situation will exacerbate current issues related to the spatial distributions of supply and demand, the dependency on fossil fuels and its environmental consequences. Geotechnology is at the center of the energy challenge, from production, transportation, consumption and conservation, to waste management and carbon sequestration. Phenomena involved in energy geotechnology often relate to classical topics in our field. Hydraulic fracturing is essentially a geotechnical process. Fines migration and formation damage in oil and gas recovery are akin to filter criteria and clogging, while oil and gas recovery and CO<sub>2</sub> storage are in effect unsaturated soil mechanics and mixed fluid flow problems. Further, hydrate-bearing sediments have many common features with frozen ground engineering, the analysis of geothermal piles must consider thermal consolidation, fly ash impoundments can experience static liquefaction, and reactive fluid transport following CO<sub>2</sub> injection and water acidification parallels karst formation. There are other energy-related geo-phenomena that push our classical boundaries. Typically, they involve coupled hydro-thermo-chemo-bio-mechanical processes such as the design of nuclear waste repositories, emergent phenomena such as various forms of localizations, and spatial variability inherent to large-scale field projects.

### ΣΥΝΤΟΜΟ ΒΙΟΓΡΑΦΙΚΟ ΣΗΜΕΙΩΜΑ ΟΜΙΛΗΤΗ

Santamarina and his team explore the scientific foundations of soil behavior and subsurface processes using innovative particle-level and pore-scale testing methods, combined with numerical methods and high-resolution process monitoring systems. This conceptual and experimental framework is used to advance the study of phenomena and the development of solutions in energy geotechnology with contributions to: efficiency and conservation, resource recovery (petroleum, methane hydrates), energy geostorage, and energy waste (carbon geological storage, fly ash and nuclear waste). Two books and more than 250 publications summarize salient concepts and research results. His former doctoral students are faculty members or lead engineers at foremost universities and organizations worldwide. Dr. Santamarina is a frequent keynote speaker at international events, a member of both Argentinean National Academies, and a member of committees at the USA National Academies. He holds a Ph.D. from Purdue Univer-

sity, M.S. from the University of Maryland and BSc from Universidad de Cordoba.

Η παρουσίαση έχει αναρτηθεί στην ιστοσελίδα της ΕΕΕΕΓΜ.



ΕΛΛΗΝΙΚΗ  
ΕΠΙΣΤΗΜΟΝΙΚΗ  
ΕΤΑΙΡΕΙΑ  
ΕΔΑΦΟΜΗΧΑΝΙΚΗΣ  
& ΓΕΩΤΕΧΝΙΚΗΣ  
ΜΗΧΑΝΙΚΗΣ

## Μελέτη και κατασκευή οπλισμένων επιχώσεων αντιστήριξης

Την Πέμπτη 24 Οκτωβρίου 2013 παρουσιάστηκε από την Χάϊδω Δούλαλα – Rigby, Πολιτικό Μηχανικό, Chief Civil Engineer, Tensar International, διάλεξη με τίτλο «Μελέτη και κατασκευή οπλισμένων επιχώσεων αντιστήριξης».

Η παρουσία της εταιρίας Tensar στα Ηνωμένα Αραβικά Εμιράτα ξεκίνησε στις αρχές του 2000 με την μελέτη και κατασκευή οπλισμένων επιχώσεων αντιστήριξης για τη διάνοιξη του αυτοκινητόδρομου της Dibba. Στο έργο αυτό, το μέγιστο ύψος των οπλισμένων επιχώσεων σε μονή αναβαθμίδα έφτασε μέχρι και τα 19 μέτρα και με κλίση αναβαθμού στους 86° ενώ η συνολική κατακόρυφη πρόσωση των οπλισμένων επιχώσεων που κατασκευάστηκαν για την ολοκλήρωση του έργου ήταν της τάξης των 45.000 m<sup>2</sup>. Η επιτυχής, ταχεία και οικονομική ολοκλήρωση του έργου καθιέρωσε το όνομα της Tensar στον Αραβικό κόλπο συντελώντας στην διαδοχή του επόμενου μεγάλου έργου στην ίδια περιοχή, τη διάνοιξη του καινούριου αυτοκινητόδρομου μεταξύ Fujairah και Dubai, το οποίο ήταν και το αντικείμενο της παρουσίασης. Το έργο περιλαμβάνει την μελέτη και κατασκευή 29 αυτόνομων οπλισμένων επιχώσεων με μέγιστο αριθμό αναβαθμιδών έως 3 και συνολικό ύψος αναβαθμιδών μέχρι και 60 μέτρα ενώ η συνολική κατακόρυφη πρόσωση των τοίχων που κατασκευάστηκαν για την ολοκλήρωση του έργου ήταν της τάξης των 100.000 m<sup>2</sup>. Η παρουσίαση περιελάμβανε την μέθοδο μελέτης, τα υλικά κατασκευής, τον τρόπο κατασκευής καθώς και μετρήσεις μετακινήσεων των πολυμερικά οπλισμένων επιχώσεων τόσο κατά τη διάρκεια κατασκευής καθώς και μετά την ολοκλήρωσή τους.

### ΣΥΝΤΟΜΟ ΒΙΟΓΡΑΦΙΚΟ ΣΗΜΕΙΩΜΑ ΟΜΙΛΗΤΡΙΑΣ

Η Χάϊδω Δούλαλα-Rigby (Γιούλη) είναι Πολιτικός Μηχανικός με εξειδίκευση στα Γεωτεχνικά και εμπειρία 21+ χρόνων. Είναι μέλος του Hong Kong Institution of Engineers (Geotechnical), Chartered (CEng) του UK Engineering Council, Fellow of the Institution of Civil Engineers και μέλος της ΕΕΕΕΓΜ.

Η Γιούλη εργάζεται σαν Chief Civil Engineer στην Tensar International με έδρα τα κεντρικά γραφεία στο Blackburn της Αγγλίας και έχει υπό την εποπτεία της τον τεχνικό έλεγχο των υπόλοιπων γραφείων της Tensar τα οποία βρίσκονται στη Γερμανία, Ολλανδία, Γαλλία, Αφρική, Ρωσία, Ηνωμένα Αραβικά Εμιράτα, Σαουδική Αραβία, Μαλαισία, Ινδονησία, Κίνα, Αυστραλία και Νέα Ζηλανδία.

Πήρε το πρώτο της πτυχίο από το Τεχνολογικό Εκπαιδευτικό Ίδρυμα (ΤΕΙ) Θεσσαλονίκης στα Έργα Υποδομής το 1991. Από εκεί συνέχισε της σπουδές της στην Αγγλία με υποτροφία του «ERASMUS». Πήρε το πτυχίο Bachelor of Engineering με ειδικότητα Πολιτικού Μηχανικού (BEng in Civil Engineering) από το Πανεπιστήμιο του Sunderland και στη συνέχεια έκανε Master of Science με ειδικότητα στη Βραχο-

μηχανική και Θεμελιώσεις (MSc in Rock Mechanics and Foundation Engineering) στο Πανεπιστήμιο του Newcastle upon Tyne. Μετά την αποφοίτησή της εργάστηκε σαν γεωτεχνικός μηχανικός για ένα χρόνο στην διάνοιξη / επέκταση της σήραγγας Jubilee Line του υπόγειου σιδηρόδρομου του Λονδίνου (London Underground). Στη συνέχεια μετέβη στο Χονγκ Κονγκ το 1996, όπου παρέμεινε για τα επόμενα 10 χρόνια. Εκεί εργάστηκε σαν γεωτεχνικός μηχανικός για την Αγγλική μελετητική εταιρεία Mouchel σε διάφορα και πολυποίκιλα έργα γεωτεχνικής φύσης και κυρίως σε έργα σταθεροποίησης ασταθών πρανών. Το 2005 η Γιούλη επέστρεψε στην Αγγλία και συνέχισε την γεωτεχνική της καριέρα πηγαίνοντας στην Tensar σαν εποπτεύων μηχανικός της Αγγλικής μελετητικής ομάδας αρχικά και στη συνέχεια σαν Chief Civil Engineer.

Η Γιούλη είναι ενεργό μέλος της τεχνικής επιτροπής γεωσυνθετικών της Αγγλίας (Committee member of the International Geosynthetics Society, UK Chapter) καθώς επίσης και της οργανωτικής επιτροπής του Ινστιτούτου Πολιτικών Μηχανικών της Βορειοδυτικής Αγγλίας (ICE NW).

Η παρουσίαση έχει αναρτηθεί στην ιστοσελίδα της ΕΕΕΕΓΜ.

## ΕΚΤΕΛΕΣΤΙΚΗ ΕΠΙΤΡΟΠΗ ΕΕΕΕΓΜ (2012 – 2015)

Πρόεδρος	:	Χρήστος ΤΣΑΤΣΑΝΙΦΟΣ, Δρ. Πολιτικός Μηχανικός, ΠΑΝΓΑΙΑ ΣΥΜΒΟΥΛΟΙ ΜΗΧΑΝΙΚΟΙ Ε.Π.Ε. <a href="mailto:president@hssmge.gr">president@hssmge.gr</a> , <a href="mailto:editor@hssmge.gr">editor@hssmge.gr</a> , <a href="mailto:ctsatsanifos@pangaea.gr">ctsatsanifos@pangaea.gr</a>
Α΄ Αντιπρόεδρος	:	Παναγιώτης ΒΕΤΤΑΣ, Πολιτικός Μηχανικός, ΟΜΙΛΟΣ ΤΕΧΝΙΚΩΝ ΜΕΛΕΤΩΝ Α.Ε. <a href="mailto:otmate@otenet.gr">otmate@otenet.gr</a>
Β΄ Αντιπρόεδρος	:	Μιχάλης ΠΑΧΑΚΗΣ, Πολιτικός Μηχανικός <a href="mailto:mpax46@otenet.gr">mpax46@otenet.gr</a>
Γενικός Γραμματέας	:	Μαρίνα ΠΑΝΤΑΖΙΔΟΥ, Δρ. Πολιτικός Μηχανικός, Αναπληρώτρια Καθηγήτρια Ε.Μ.Π. <a href="mailto:secretary@hssmge.gr">secretary@hssmge.gr</a> , <a href="mailto:mpanta@central.ntua.gr">mpanta@central.ntua.gr</a>
Ταμίας	:	Μανώλης ΒΟΥΖΑΡΑΣ, Πολιτικός Μηχανικός <a href="mailto:e.vouzaras@gmail.com">e.vouzaras@gmail.com</a>
Αναπληρωτής Ταμίας	:	Γιώργος ΝΤΟΥΛΗΣ, Πολιτικός Μηχανικός, ΕΔΑΦΟΜΗΧΑΝΙΚΗ Α.Ε. ΓΕΩΤΕΧΝΙΚΕΣ ΜΕΛΕΤΕΣ Α.Ε. <a href="mailto:gdoulis@edafomichaniki.gr">gdoulis@edafomichaniki.gr</a>
Έφορος	:	Γιώργος ΜΠΕΛΟΚΑΣ, Δρ. Πολιτικός Μηχανικός, Κέντρο Δομικών Ερευνών και Προτύπων ΔΕΗ <a href="mailto:gbelokas@gmail.com">gbelokas@gmail.com</a> , <a href="mailto:gbelokas@central.ntua.gr">gbelokas@central.ntua.gr</a>
Μέλη	:	Ανδρέας ΑΝΑΓΝΩΣΤΟΠΟΥΛΟΣ, Δρ. Πολιτικός Μηχανικός, Ομότιμος Καθηγητής ΕΜΠ <a href="mailto:aanagn@central.ntua.gr">aanagn@central.ntua.gr</a> Μιχάλης ΚΑΒΒΑΔΑΣ, Δρ. Πολιτικός Μηχανικός, Αναπληρωτής Καθηγητής ΕΜΠ <a href="mailto:kavvadas@central.ntua.gr">kavvadas@central.ntua.gr</a>
Αναπληρωματικά Μέλη	:	Χρήστος ΑΝΑΓΝΩΣΤΟΠΟΥΛΟΣ, Δρ. Πολιτικός Μηχανικός, Καθηγητής Πολυτεχνικής Σχολής ΑΠΘ <a href="mailto:anag@civil.auth.gr">anag@civil.auth.gr</a> , <a href="mailto:canagnostopoulos778@gmail.com">canagnostopoulos778@gmail.com</a> Σπύρος ΚΑΒΟΥΝΙΔΗΣ, Δρ. Πολιτικός Μηχανικός, ΕΔΑΦΟΣ ΣΥΜΒΟΥΛΟΙ ΜΗΧΑΝΙΚΟΙ Α.Ε. <a href="mailto:scavounidis@edafos.gr">scavounidis@edafos.gr</a> Δημήτρης ΚΟΥΜΟΥΛΟΣ, Δρ. Πολιτικός Μηχανικός, ΚΑΣΤΩΡ Ε.Π.Ε. <a href="mailto:coumoulos@castorltd.gr">coumoulos@castorltd.gr</a> Μιχάλης ΜΠΑΡΔΑΝΗΣ, Πολιτικός Μηχανικός, ΕΔΑΦΟΣ ΣΥΜΒΟΥΛΟΙ ΜΗΧΑΝΙΚΟΙ Α.Ε. <a href="mailto:mbardanis@edafos.gr">mbardanis@edafos.gr</a> , <a href="mailto:lab@edafos.gr">lab@edafos.gr</a>

### ΕΕΕΕΓΜ

Τομέας Γεωτεχνικής  
ΣΧΟΛΗ ΠΟΛΙΤΙΚΩΝ ΜΗΧΑΝΙΚΩΝ  
ΕΘΝΙΚΟΥ ΜΕΤΣΟΒΙΟΥ ΠΟΛΥΤΕΧΝΕΙΟΥ  
Πολυτεχνειούπολη Ζωγράφου  
15780 ΖΩΓΡΑΦΟΥ

Τηλ. 210.7723434  
Τοτ. 210.7723428  
Ηλ-Δι. [secretariat@hssmge.gr](mailto:secretariat@hssmge.gr) ,  
[geotech@central.ntua.gr](mailto:geotech@central.ntua.gr)  
Ιστοσελίδα [www.hssmge.org](http://www.hssmge.org) (υπό κατασκευή)

«ΤΑ ΝΕΑ ΤΗΣ ΕΕΕΕΓΜ» Εκδότης: Χρήστος Τσατσανίφος, τηλ. 210.6929484, τοτ. 210.6928137, ηλ-δι. [pangaea@otenet.gr](mailto:pangaea@otenet.gr), [ctsatsanifos@pangaea.gr](mailto:ctsatsanifos@pangaea.gr), [editor@hssmge.gr](mailto:editor@hssmge.gr)

«ΤΑ ΝΕΑ ΤΗΣ ΕΕΕΕΓΜ» «αναρτώνται» και στην ιστοσελίδα [www.hssmge.gr](http://www.hssmge.gr)